THE DEVELOPMENT OF NOVEL ANTIFOULING MATERIALS:

A MULTI-DISCIPLINARY APPROACH

James Chapman BSc (Hons)

Dublin City University
Ollscoil Chathair Bhaile Átha Cliath

A Thesis presented to Dublin City University for the

Degree of Doctor of Philosophy

Supervisor: Professor Fiona Regan

School of Chemical Sciences

Dublin City University

2011

AUTHORS DECLARATION

I hereby certify that this material, which I now submit for assessment on the programme of study leading to the award of Doctor of Philosophy is entirely my own work, that I have exercised reasonable care to ensure that the work is original, and does not to the best of my knowledge breach any law of copyright, and has not been taken from the work of others save and to the extent that such work has been cited and acknowledged within the text of my work.

Signed:＿＿＿＿＿＿＿＿＿＿＿＿＿＿ (James Chapman)

ID No.: 57115869

Date: 21st September 2011

ACKNOWLEDGEMENTS

How to make this different… It takes a long time to write a PhD thesis but not as long as it will take to remedy the mental torture and pain that has accompanied – and will follow. However, once the step-by-step experience that eventually leads you to the top of this cliff (which invariably you want to throw yourself off by the end) is over, you can enjoy the amazing view around, *and* it is then important to remember that this arduous journey was accomplished through teamwork. Furthermore, it may not be enough to simply express in words the people who have helped and hindered this process along the way – but still, thousands of thanks (or *tanks* - Irish).

So let's get cracking... First and foremost I would like to extend a massive thanks to my supervisor, Professor Fiona Regan, for giving me the opportunity of working in her research group and enabling me to develop into the researcher that I am today. She has been patient and accommodating along every step of the way.

There have also been a mass of other people in this process, the sheer volume of this list would probably extend me into another thesis – and I am most certainly not prepared to go there again… (Well, not for a while anyway!) But, just so everyone knows that they are all loved the same and have given me the same levels of hangovers and guidance I will name the top 14 ;-) Yvonne, Tim, Mark, Aga, Lisa, Mags, Harvey, Spainy, The Hobanator, Rach, Ciprian, Louise, Amy, and the technicians.

ABSTRACT

Biofouling and biofilms exist as ubiquitous, undesirable accumulations of flora and fauna upon a given substrate when immersed into an aquatic medium. Its presence causes a range of deleterious effects for anyone faced in tackling the problem. Generally, the initial biofouling stage is stochastic and the attachment of microorganisms held-fast in biofilm matrices is irreversible. Permanency occurs once exopolymeric substances (EPS) are produced forming a protective surrounding ensuring the adherent microorganisms can colonise and thrive upon the surface. Environmental monitoring is one area that faces this challenge and forms the impetus for the work presented within this thesis.

A considerable focus of this thesis lies in the development of novel antifouling based materials with the incorporation of nanotechnology, with the aim in transferring the developed materials to environmental monitoring devices. The thesis has concentrated, on antifouling agents and materials for the prevention of biofouling in its initial stages. This has been achieved through the investigation and development of novel materials and subsequent biofouling screening assays for this aim, followed by long term field deployment studies.

Chapter 1 introduces the concepts of biofouling and biofilms and in particular, the way in which man has tried to remedy or combat the problem. Specific introductions to the thesis have been included within and a synopsis to the scope of research is detailed.

Chapter 2 is concerned with the practical aspects of the thesis. Experimental techniques employed throughout the thesis are described here, with the methods in the chronology of the thesis – all preparations and deployments have been discussed and included accordingly.

Chapter 3, is concerned with the development of transparent materials, in this case plasticized PVC. The use of PVC as an antifouling material has been overlooked and so the work is novel to the field of antifouling. The materials were developed, characterised and then tested for their efficacy as an antifouling coating and were found to be effective as antifouling transparent materials

Nanotechnology has seen a massive surge of research of late particularly in nanoparticle synthesis. Chapter 4, details the synthetic steps of a series of metal nanoparticles from period four in the periodic table, with significant developments in producing nanoparticles for the polyol method. Chapter 5 details the direct doping and testing of these agents in a series of antifouling assays, some nanoparticles were found to exhibit excellent antifouling responses, where Ga-MNP doped sol-gels have shown best responses and are extremely novel to this research field

Chapter 6 focuses on a series of material developments from earlier stages of research in the thesis. . Here all novel materials are applied to a marine deployment in parallel to the real-time collection of water quality data. The results illustrate the value of the materials developed in this work for application to sensors as part of a strategy for reduction in biofouling on sensors.

Chapter 7 depicts the key findings and overall conclusions of the thesis leading to further recommendations on future developments for this area of research.

GLOSSARY

NOTATION	MEANING
1DGE	1-dimensional polyacrylamide electrophoresis
3D	3-dimensional
AAS	Atomic absorption spectroscopy
AF	Antifouling
AFM	Atomic force microscopy
AHLs	Acylated homoserine lactones
ANOVA	Analysis of variance
APTES	3-aminopropyltriethoxysilane
ATBC	Acetyl tri-n-butyl citrate
ATC	Acetyl triethyl citrate
ATCC	American tissue culture collection
ATP	Adenosine 5'-triphosphate
ATR	Attenuated total reflectance
AU	Arbitrary units
BOP	Butyl octyl phthalate
BSA	Bovine serum albumin
BST	Brine shrimp lethality test
BTX	Benzene, toluene and xylene
CA	Contact angle
CE	Capillary electrophoresis
CFU	Colony forming units
CLP_{40}	Chloroparaffin, 40%
CLP_{50}	Chloroparaffin, 50%
CLP_{60}	Chloroparaffin, 60%
CLP_{70}	Chloroparaffin, 70%
CLSM	Confocal scanning laser microscopy
CTAC	Cetyltrimethylammonium chloride
DBS	Dibutyl sebacate
DCAd	Dicapryl adipate
DCM	Dichloromethane
DEGDB	Diethylene glycol dibenzoate
DEHAd	Di(2-ethylhexyl) adipate
DEHAz	Di(2-ethylhexyl) azelate
DEHP	Di(2-ethylhexyl) phthalate
DEHS	Di(2-ethylhexyl) sebacate
DEP	Diethyl phthalate
DGGE	Denaturing gradient gel electrophoresis
DIBAd	Diisobutyl adipate
DIDAz	Diisodecyl azelate
DINAd	Diisononyl adipate
DIOAz	Diisooctyl azelate

DLS	Dynamic light scattering
DLVO	Derjaguin, Landau, Verwy and Overbeek theory
DMAz	Dimethyl azelate
DMP	Dimethyl phthalate
DMS	Dimethyl sebacate
DNA	deoxyribonucleic acid
DnHAz	Di-n-hexyl azelate
DnHnNAd	Di(n-heptyl, n-nonyl) adipate
DO	Dissolved oxygen
DPGDB	Dipropylene glycol dibenzoate
DTDAd	Di(tridecyl) adipate
EC	Effective concentration
EDX	Energy dispersive X-ray analysis
EG	Ethane-1,2-diol
EGTA	Ethylene glycol tetraacetic acid
EPA	Environmental protection agency
EPS	Exopolymeric substance
ESIMS	Electrospray ionisation mass spectrometry
FDA	3',6' –diacetylfluorescein
FESEM	Field emission scanning electron microscopy
FFF	Field-flow-fractionation
FISH	Fluorescent in-situ hybridisation
FRC	Foul release coating
FT	Fourier transform
GFP	Green fluorescent protein
HAADF	High angle annular dark field
HCl	Hydrochloric acid
HPC	Heterotrophic plate count
ICP	Inductively coupled plasma
IMO	International Maritime Organisation
IPP	Isopropyl palmitate
IR	Infra-red
IUPAC	International Union of Pure and Applied Chemistry
LB	Luria-Bertani
LPR	Localised plasmon resonance
MALDI	Matrix-assisted laser desorption ionisation
MBC	Minimum bactericidal concentration
MIC	Minimum inhibitory concentration
MNP	Metal nanoparticle(s)
MP	Methyl palmitate
NMR	Nuclear magnetic spectroscopy
PAS	Photoacoustic spectroscopy
PBS	Phosphate buffered saline
PCR	Polymerase chain reaction
PDI	Polydispersity index
PDMS	Polydimethylsiloxane

PEG	Polyethylene glycol
PEGDB	Polyethylene glycol 200 dibenzoate
PFGE	Pulsed field gel electrophoresis
PI	Propidium iodide
PSSS	Poly(sodium 4-styrenesulfonate
PVC	Poly (vinylchloride)
PVP	Polyvinyl pyrrolidone
QS	Quorum sensing
QUATs	Quarternary ammonium compounds
RT	Room temperature
SAMs	Self-assembled monolayer
SD	Standard deviation
SE	Secondary electron
SEM	Scanning electron microscopy
SIMS	Secondary-ion mass spectrometry
SN	Sensor network
SP	Surface plasmons
SPM	Scanning probe microscopy
SPM	Scanning probe microscope
SPR	Surface plasmon resonance
SRB	Sulfate reducing bacteria
STEM	Scanning transmission electron microscopy
STXM	Scanning transmission X-ray microscopy
TBT	Tributyltin
TDC	Total direct cell count
TEC	Triethyl citrate
TEM	Transmission electron microscopy
TEOS	Tetraethoxysilane
THF	Tetrahydrofuran
TnBC	Tri-n-butyl citrate
TOF	Time-of-flight
uPVC	Unplasticized PVC
UV-vis	UV-visible
WSN	Wireless sensor network
XPS	X-ray photoelectron spectroscopy

LIST OF FIGURES

LIST OF TABLES

TABLE OF CONTENTS

CHAPTER 1: A REVIEW OF BIOFOULING

CHAPTER 3: PLASTICIZED PVC

CHAPTER 4: THE SYNTHESIS OF PERIOD FOUR METAL NANOPARTICLES

CHAPTER 6: THEORY INTO PRACTICE

1

A Review of Biofouling & Mitigation

1.0 INTRODUCTION

This chapter defines the problem of biofouling and biofilms illustrating the impact they have on everyday life. It reveals the function, need and demand for an antifouling coating in order to preserve material lifetimes without microbial dominance upon a given substrate.

1.1 BIOFOULING: AN AGE OLD PROBLEM

Life has been immersed in bacteria well before the evolution of *Homo sapiens* and indeed can exist in symbiosis or antagonistically throughout. It is only within the last five decades that the scientific world has started to acknowledge that life on earth exists as a multi-facet system consisting of multiple species and microbial communities summarised elegantly by Watnick and Kolter. [1] This trend has developed from a shift in research from pure culture model systems, pioneered through the work of Robert Koch back in the nineteenth century. Only recently, have microorganisms been defined in their communities and are now thought as ubiquitous units as opposed to a single species in existence. This communal network of microorganisms has been termed a biofilm, [2] with the concept of biofilm characterisation accelerating sharply over the past two decades. The earliest report of biofilm characterisation came from Antonie van Leuwenhoek, where teeth scrapings were examined with a very primitive microscope. Today, with significant technological advances in microscopy coupled with biological, physical and chemical testing, researchers are gaining extensive understandings of some of the processes involved in fouling initiated by the likes of Costerton as far back as the 1970s. [3]

1.2 BIOFILMS AND BIOFOULING

In 1999, Costerton *et al.*, suggested that bacteria, amongst other microorganisms, are far more than indiscriminate agglomerations of planktonic forms of organisms at a given interface. They are complex but are able to supersede forces of diffusion, Brownian motion and even electrostatic forces within a system and form aggregated organisations known as biofilms. Recent evidence suggests that biofilm forming microorganisms have been around for a considerable amount of time, as far back as 3.5 billion years ago. [4,5] Biofilms are thought to have evolved from and are key in the lifecycle of prokaryotic cells. The formation of such biofilms represents a protected mode of growth for cells and provides protection and

subsequent survival strategies. The biofilm provides a niche refuge from punishing environmental stresses such as pH, temperature, and light amongst other toxicants. [6]

1.2.1 BIOFILM LIFE-CYCLE

Biofilm formation is an inevitable process provided a source of nutrients and a suitable substratum is provided. Biofilms can occur in a wide variety of environments ranging from industrial, medical, household and even host (i.e. human or animal) sources. The diversity of the environment highlights the capability of adapting and thriving from location to location. Despite this variety they all seem to follow similar characteristic development patterns as shown in Figure 1.1.
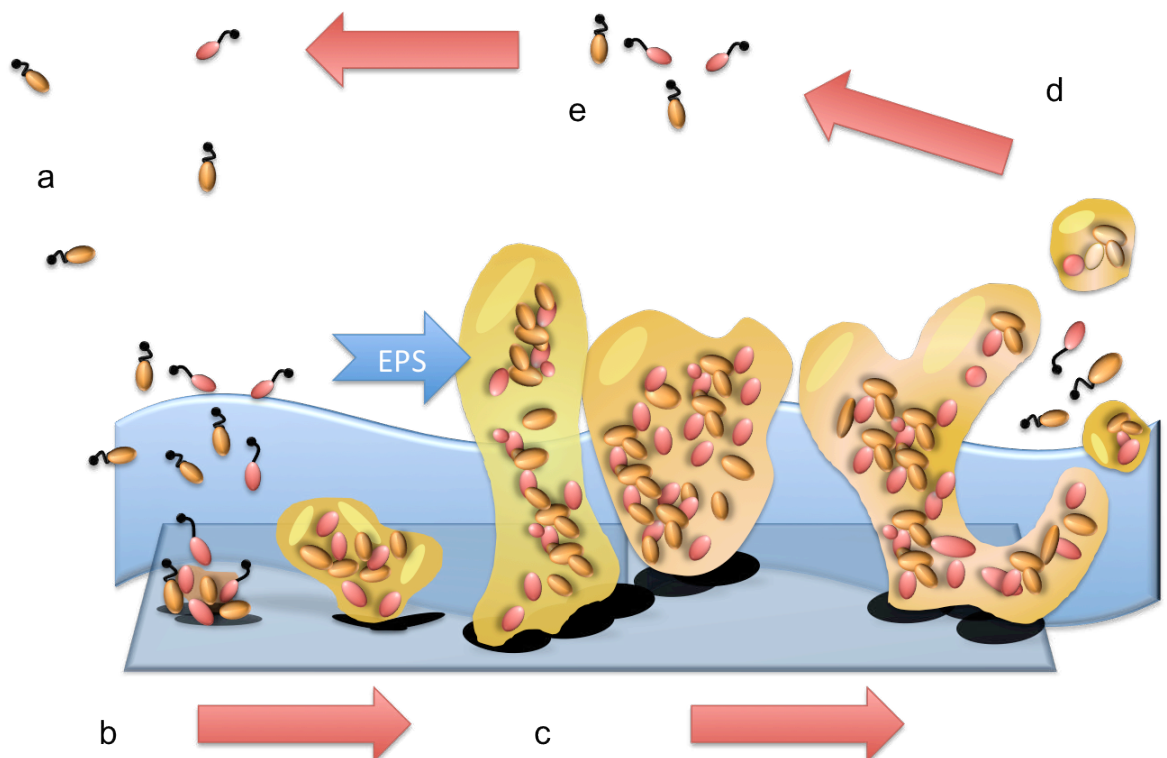
Figure 1.1: Schematic diagram highlighting the biofilm formation sequence. (a) Planktonic bacteria (b) environmental cues (proteins, carbohydrates, humic substances) and initial interactions (c) secretion of exopolymeric substances (EPS) (d) detachment cues (environmental or gene specific) (e) recycled process of planktonic microorganisms. Adapted from Montana State University Centre for Biofilm Engineering. [7]

1.2.2 SURFACE CONDITIONING

Initially, the development of a biofilm commences on the immersion of a substrate into a surrounding medium of water, air or solid. This step is regarded as the precursor to the development of a biofilm, whereby a thin layer is adsorbed. This layer comprises mainly of organic macromolecules such as glycoproteins, humic acids, proteins, amino acids, carbohydrates and uronic acids amongst other unspecified material. [8] The formation of the conditioning layer occurs almost instantly upon the immersion of the substrate into a nutrient rich environment, although the mechanisms by which binding and adsorption occur are still poorly understood. [9] Some authors perceive the conditioning layer as the bond between the surface and the initial adhering organisms, and thus, the resistance of the biofilm is dependent upon the strength of the conditioning layer. [10]

1.2.3 BACTERIAL SETTLEMENT

For the proliferation of biofilm, two events must occur. Firstly, a microorganism must be aligned in proximity (< 1 nm) to a substrate and secondly, the organisms must adhere to the surface. Considerable interest is attributed to the complex processes that influence the proliferation of a microorganism to the substrate, with firm belief that physical-chemical forces further mediate the development of the conditioning layer. Furthermore, the Derjaguin, Landau, Verwy and Overbeek (DLVO) theory of colloidal stability gives further insight into the proliferation of microorganisms towards substrata. [11] However, not all microorganisms behave as impassive colloids, but through evolution have developed mechanisms of movement and motility, for instance the use of a flagella, Figure 1.2

S3400 20.0kV 10.5mm x15.0k SE 9/24/2009   3.00um

Figure 1.2: Scanning electron micrograph of a flagellated zoospore upon a plasticized polymeric membrane taken with working distance 10.5 mm accelerating voltages of 20 kV.

Generally, forces that determine whether a microorganism will contact the surface rely on the system's net electrostatic forces that exist between the organism itself and the substrate it approaches. The exact mechanism is still unclear, but simply, adhesion of a microorganism to a surface can occur in two ways. The first is the initial reversible adhesive contact facilitated by the net electrostatic interaction between the cell and the surface, and the second is the permanent adhesion of the microorganism facilitated through molecular binding and specific adhesions to the substrate. [12] The first of these is usually described as adsorption and the reversible attachment phase is referred to as adhesion; where a plethora of other forces influence this rate of transport of attachment in both categories. [13,14]

A considerable volume of research surrounds the way in which microorganisms sense the suitability of a substrate for proliferation and colonisation. Chemical signalling processes among bacteria, known as quorum sensing (QS), have been shown to play vital roles in cell communications and subsequent formation of a biofilm. It has been shown that this is of particular importance in advanced polymicrobial colonies known as "swarming colonies". QS has been shown to depend on small extracellular molecules called autoinducers or more specifically acylated homoserine lactones (AHLs). QS is also thought to be gene expressive, developed by bacteria to gain and control population density. Autoinducer molecules allow

the microorganisms to process symbiosis, virulence, competence, conjugation, antibiotics, motility, sporulation and exopolymeric substance (EPS) production. [15-18] *N*-AHLs have produced the most results thus far, which is the root of the term "quorum sensing". They consist of five membered homoserine lactone rings with varied termination of amide-linked acyl side chains. Naturally occurring, they range from four to fourteen carbons in length and may be saturated or unsaturated. If quorum sensing is integral to biofilm formation, it is therefore possible to interfere or quench the process that would be inherently beneficial for biofouling-based applications. Unlike antimicrobial agents, quorum-quenching compounds (also known as anti-virulence compounds) are utilised in the disruption of cell communication without affecting growth. QS compounds could potentially offer a viable solution as an antifouling agent, as there should theoretically be less Darwinian selective pressure in their resistance, [19] in disrupting communication, pathogens become more susceptible to the host immune system and build less effective biofilms. Pathogens are notoriously difficult to remove, and in this case, brominated furanones have been used to reduce this biofilm formation especially in *Escherichia coli* forming biofilms. [20]

1.2.4 BIOFILM DEVELOPMENT

Biofilms remain ubiquitous in a collection of locations and in various environmental conditions, but the most widely reported lies in the marine and freshwater environments, and indeed, where biofouling has had the greatest developments. An aqueous environment contains a plethora of other host organisms and an unprotected surface immediately undergoes the colonisation with biofilm development proceeding to a polymicrobial matrix containing; bacteria inclusive of protozoa, molluscs, viruses, algae amongst others. [21-23] Publications on the formation of biofilms and biofouling in marine settings describe sequential successive events (Figure 1.1) with proliferation of higher fouling organisms as a representative model for each element of the process. However, it should be highlighted that this approach is very much a simplified "model" and that every environment where biofilms develop will have differing biofouling precursors that can be seen to be disruptive to this simplified approach.

Following the successful settlement of some prokaryotic species, diatoms are usually a fundamental settling species and quickly form a biofilm like bacteria. [24] They are unicellular algae, consisting of silica, chloroplasts and photosynthetic chemicals. They too, like bacteria, are benthic or planktonic and can excrete EPS of which the composition is similar to bacteria and can consist of bioadhesives and forms the slime matrix in which microorganisms enclose themselves and are generally regarded as a mixture of EPS. [25] The matrix varies in composition, depending on the constituents of the biofilm and the environmental conditions under which

the biofilm matures. [26] The EPS usually fastens the microbial aggregates facilitating the cohesion as well as the adhesion, to the surface of the substrate. [27] Although the EPS gives the biofilm its "slimy" appearance and characteristic, it carries approximately 50 – 80% of the overall biofilm organic matter as suggested by Flemming *et al.*.[28] Costerton *et al.*, defined glycocalyx as the integral element of the outer membrane of Gram-negative cells and the peptidoglycan of the Gram-positive cells. [29] The perception is that this matrix is composed of fibrous polysaccharides, globular proteins, [30] and hydrated material. [27] The attached biofilm species then begin to compete with one another resulting in the biofilm changing and maturing over time shown through its thickness. These colonies grow outward to form the biofilm matrix, secreting more and more EPS acting as a water-retaining matrix and communication network. The composition and structure of EPS as well as the chemical and physical properties can vary widely depending on the microbial community composition and the presence of ions in solution. Charackliss and Marshall describe the biofilm as an organic polymer layer with living microorganisms trapped inside and thus influence the route, penetration and effectiveness of biocides that are used to target the biofilm. [31-34] EPS plays a vital role in bacterial adhesion in general, trapping particles, nutrients and organisms as they encounter the surface and most likely play a role in attracting new species to the "stronghold". EPS has a host of anionic sites, which also facilitates metal binding and has been reviewed in Mayer *et al.*. [35] It has also been shown that biofilms have the capacity to harden under the accumulation of iron and calcium, [36] which also serves as a further protective mechanism and characteristic of the biofilm.

1.3 BIOFILM COMPOSITION

Most microorganisms live, grow and thrive in aggregates and are generally considered sessile. As already discussed, it is broadly described and accepted as the term "biofilm". The biofilm is an intricate and complex structure of numerous colonies of microorganisms surrounded by EPS. It contains hundreds and thousands of different species and possesses specific channels in which nutrients move and circulate. The biofilm itself consists of polymeric compounds and typically the constituents of EPS include: [25,37-41]

- Polysaccharides;
- Proteins;
- Nucleic acids;
- Lipids;
- Humic substances;
- Water.

Each component imposes an effect upon the integrity of the biofilm and the biofilm's lifetime relating to the chemical makeup and properties each molecule possesses. However, biofilm growth is not mediated by covalent C – C bonds between the EPS molecules, but by weak physico – chemical intermolecular interactions. [27,42] Various types of non-covalent interactions favour this, and three types of interaction exist as cohesive forces between components within the EPS and indeed between the microbial communities *viz*. electrostatic interactions, hydrogen bonding and London forces, [35] Figure 1.3.
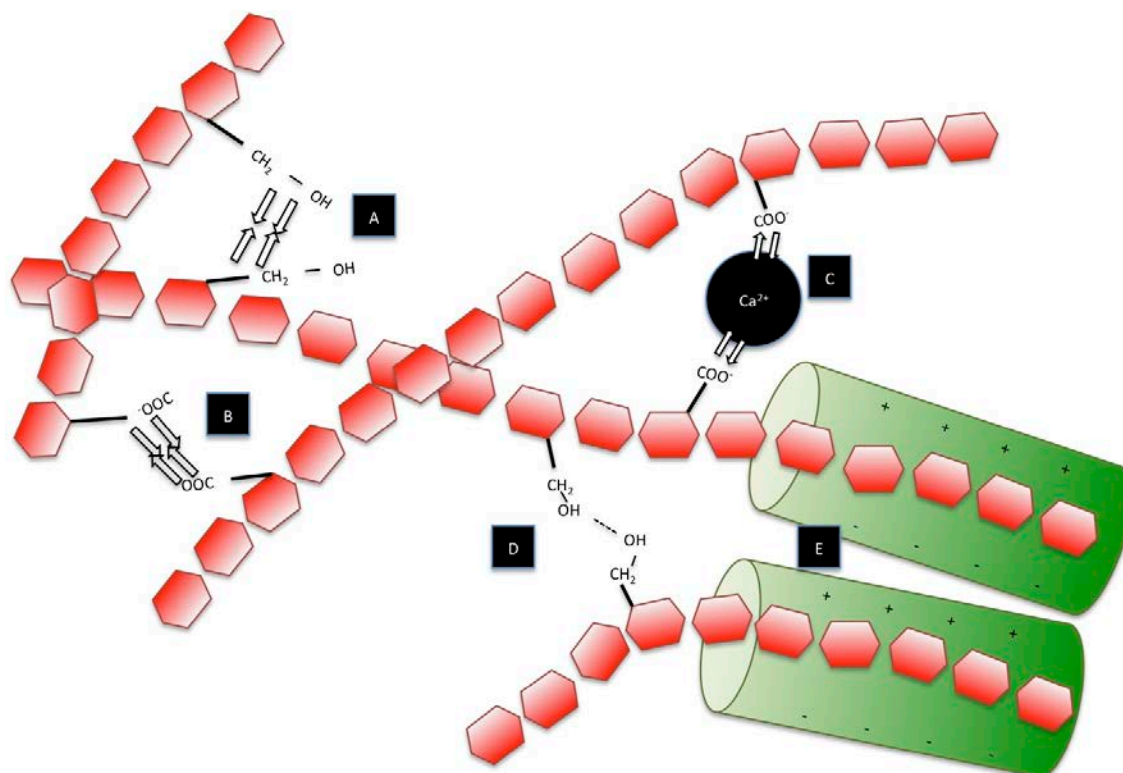
Figure 1.3: Intermolecular interactions contributing to the biofilm integrity. Five phenomena are illustrated: A = electrostatic interactions, B = repulsive electrostatic interactions between ionic species, C = attractive electrostatic, D = hydrogen bonding and E = electrostatic. Hexagonal shapes denote polysaccharides and protein interactions.

Three types of weak interactions theoretically exist within a biofilm matrix, giving rise to its integrity and defining its shape:

- **Hydrogen bonding** – Hydrogen bonding is mainly active between hydroxyl (-OH) moieties in any given molecule and is particularly prevalent in polysaccharides and water molecules. The weak interaction can also act as a supportive measure for the tertiary structure of proteins. A typical bonding energy can range between 10 – 30 KJ/mol. [43] Polysaccharides exhibiting hydrogen bonding can be influenced by chaotropic agents i.e. salt, as they act as a disrupting measure formed by water

molecules surrounding the macromolecule, thus influencing the build-up of biofilms. [44] Mayer *et al.*, have reported that cleaning formulations do not exhibit high levels of hydrogen bonding due to the levels contained within the biofilm matrix but have stated that 'they should not be overlooked as >90% of EPS contains water.' [35]

- **Electrostatic effects** – These forces are mainly active between ions and both permanent and induced dipoles. Ionic interactions are usually strong and individual cations, such as Ca^{2+} account for a considerable amount of binding energy within the EPS matrix. [45] These divalent cations act as bridges contributing significantly to the overall binding force of the matrix. Positively charged groups from amino acids in proteins or polysaccharides can also introduce an interaction with negatively charged groups, providing instantaneous cohesion forces. This type of interaction can be seen in Chen and Stewart, whereby significant decreases in the viscosity of a biofilm were seen when additions of sodium, potassium, magnesium and calcium were added. In comparison, iron cations caused potent effects in increasing the viscosity of the biofilm matrix. [46] The binding energy of a non-ionic electrostatic interaction ranges between 12 – 30 kJ/mol, [47] this would be inherently affected by the distance between the water concentration and neighbouring bonds.

- **London Forces** – These forces act over the whole molecule i.e. the biofilm matrix in an intra- and intermolecular manner and are not dependent on molecular moiety. The source of this type of interaction is the spontaneous formation of transient dipoles due to fluctuations in the electron distribution within the molecule. These temporary dipoles will polarise neighbouring molecules thus creating dipolar attractive forces. This phenomenon can be regarded as an oscillation of induced-dipole dipole interactions. The binding energy related to a London force is usually in the range of 2.5 kJ/mol per carbon on an aliphatic chain and is extremely sensitive to intermolecular distance ($\propto 1/r^{6}$). London forces provide a major contribution to the interaction forces within hydrophobic regions of molecules or between molecules known as 'hydrophobic interactions'. [48]

The binding force of any interaction mentioned remains relatively small compared to a covalent C-C bond (~250 kJ/mol). [47] A theoretical comparison could be denoted; if an EPS molecule possesses 150 functional groups and only 10% of these are involved in bonding, the total binding energy could be in the value of numerous covalent C-C bonds. It is these 3 types of interactions that supply the biofilm its integrity, but also form the basis as to why cleaners and biofilm removing targets cannot readily dissolve the biofilm entirely. [12,49] Mayer *et al.* reported that cleaning formulations mainly address dispersion and electrostatic interactions,

by application of surface activating substances e.g. acids, bases or chelating agents, [35] also reporting that hydrogen bonding is not addressed by typical commercial cleaning products.

1.3.1 BIOFILM SORPTION

Sorption behaviour in biofilms is another key feature in understanding how the mechanics of a biofilm function. [27] Biofilms operate in a sink and source manner attracting and expelling ingredients absorbing water, inorganic and organic solutes and particulate matter. [28] Cell walls, cell membranes, cell cytoplasm and EPS all serve as sorption points. They all display various capacities and preferences to the uptake and expulsion of molecules in the matrix. Additionally, biofilms may respond physiologically to sorbed substances (e.g. uptake of toluene can lead to the formation of uronic acids, leading to increased sorption of cations). [50]

1.3.2 WATER

Commonly EPS has a very high water content in ratio to the biofilm; 1-2% (w/w) EPS and 98% water has been reported extensively. [51-53] A slimy consistency is observed due to the high affinity of water, and thus creating a protective measure against desiccation. [54-56] Ophir and Gutnick identified that colanic acid was associated with the water-binding component for *Escherichia coli, Acinetobacter calcoaceticus* and *Erwinia stewartii.* [57]

1.3.3 ANIONS

Very little information exists concerning the binding of anions to biofilms. The sorption of anions could exist through the various positive charges that exist on amino acids, sugar acids and proteins. [58]

1.3.4 CATIONS

EPS has the potential to contain anionic groups such as carboxyl, phosphoryl and sulfate groups. [37] Bacterial EPS has been shown to contain 20-50% of polysaccharides as uronic acids. [59] Predictions of metal binding capacity, based on estimated numbers of available carboxyl and hydroxyl groups suggest an extremely high capacity in EPS, provided by the acidic polysaccharides. Binding capacity of lead in EPS was investigated by Harvery *et al*., where it was found that if EPS represented a minor fraction of organic material in sediments, then microorganisms could still complex with available Pb^{2+}. [60] Stability constants for Ni^{2+}, Cu^{2+}, Cd^{2+} and Zn^{2+} complexes with EPS in the range of 105 and 109 ppm, [61-63] all depend upon the pH value of the system due to the competition between H^+ and metal ions. Jang *et al.*, proposed

that alginate is an absorbent of dissolved copper from an aquatic matrix, [64] whereby EPS is thought to be composed of 25% of the metal ion.

Additionally, divalent cations are regarded as important components of the microbial agglomerations since they have potential to bind with negatively charged groups present on substrates in EPS molecules, as well as organic particles trapped within the biofilm. Turakhia *et al*., reported that Ca^{2+} present in sludge related biofilms were dependent upon the Ca^{2+} cations to maintain integrity and attachment. The more Ca^{2+} -specific chelant, ethylene glycol tetraacetic acid (EGTA) was used to extract the Ca^{2+} cations resulting in the destabilisation of the biofilm. [65] This observation suggests that divalent cations may be important in the maintenance of the biofilm's structure acting as a bridging component within the matrix. Higgins and Novak, [66] illustrated the role of divalent cations in biofilm formation. Increasing the concentrations of Ca^{2+} and Mg^{2+} resulted in a change in protein binding sites, whereas little effect was witnessed on bound polysaccharides. They also found that adding Na^+ led to a decrease in bound protein.

1.3.5 HYDROPHOBIC AND APOLAR MOLECULES

Some EPS exhibit surface chemistry in particular during growth on hydrophobic nutrients e.g. oils and fats. [67] The level of lipid concentration within EPS would therefore dictate the surrounding interactions. This has the ability to alter the sorption and transport within the biofilm, such as biocides and antimicrobial agents. Prior research with bacterial extracellular polymers produced by soil isolates has shown that they are capable of decreasing the apparent distribution coefficient of phenanthrene onto aquifer sand, and where polymers has been shown to reduce the retardation of phenanthrene transport in column experiments by 39%. [68] The sorption of apolar substances by EPS is unexplored however; this could be considered an important role in both trapping these substances within biofilms but also in the adhesion process of organisms to hydrophobic surfaces. This proves to be an interesting concept as the first cells that are in contact with the surface of the biofilm are hydrated; hydrophilic EPS providing the adhesion force for the cells, of which the nature responsible for this process is still unknown. [69] However, an assumption can be drawn that proteins carrying an apolar region provide suitable bonding sites to facilitate this. Wolfaardt *et al*. were the first to investigate this using confocal scanning laser microscopy (CSLM), whereby they demonstrated that herbicides accumulated in the EPS of the biofilm, [70] and later on chlorinated organics. [71] Following from this work, Spath *et al*., investigated benzene, toluene and xylene (BTX) accumulation in activated sludge, but mention that metal complexation plays an important role in the level of sorption of a biofilm. [72]

1.4 NOVEL APPROACHES TO ANTIFOULING

In order to produce an effective antifouling coating, a range of physiochemical characteristics must be taken into account. We have seen, thus far, that most methods for the prevention of fouling have relied on the biocidal effects upon the surface of the coating. Research into biofilm development and the factors contributing to the formation of biofouling and its removal has been shown that there are other causes and not just those of a chemical nature.

1.4.1 MICROTOPOGRAPHY

Recently, research recognised that the topographical nature of the substrate can influence the settlement of microorganisms and subsequent development of biofilms. This approach has developed from knowledge that cells react with objects in the nanoscale. [73] Consequently, research has moved into pioneering work focussing on cellular attachment to medical devices and the discovery that cells are indeed influenced by micro and nanoscale topography. Furthermore, reports on the effects of settlement and adhesion of cells, bacteria, unicellular algae and invertebrates are all of interest. However, the definition of roughness has created conflicting arguments in roughness scales and subsequent reproducibility. [74,75] Controlling biofouling in the prevention of infections has been known to affect various materials and substrate topographical features. Creating a topography that has the ability to resist biofouling has become an appealing proposition. However, early research into this field has already shown that increasing surface roughness has a positive effect on cellular activity [76] and this so far has been unanswered. A series of hypotheses have proliferated in how these interactions occur; increased surface area, [77] protection from shear forces in fluid systems and chemical changes that cause physicochemical interactions. [78] Furthermore, research on defined substrate topography has shown that cells have the ability to align themselves around boundaries on the topographical features, which is now known as "contact guidance". Initial findings have shown that cells migrate along groves or fibres upon a substrate that possesses them. [79] Curtis and Wilkinson surmise topography and surface chemistry illustrating cell range and topography. [73] The following conclusions can be drawn from the nature of this work in terms of cell response to surfaces:

- Imbalance of the surface forces i.e. degree of attraction and repulsion may or may not be homogenous;
- Strains of cells adhere depending on the conformation to non-planar surfaces;
- Patterns of surface chemistry results in binding sites for specific molecules.

Furthermore, in early research on cellular responses to topography, it was generally believed that settlement of bacteria, algal spores and larvae of invertebrates were enhanced by a rougher topographical surface and inhibited by smooth ones.[80] Similar problems associated with cellular research continued, mainly that the surfaces used were not defined topographically and that protection from hydrodynamic force, increased adhesive contact and protection from grazing, led to favouring of rougher surfaces when introduced to flow.[81] Study into the millimetre and nanoscale gradually increased as techniques for material definition increased and consequently manufactured surfaces have given some promising results in the resistance of biofouling. For example, the barnacle *Semibalanus balanoides* was found to be prevented from attachment at the macro scales of 2 – 4 mm,[82] while *Ulva linza* is inhibited at scales ranging 5 μm to 1 mm.[83]

Biofouling in marine and riverine environments are hugely different to medical implants in terms of cellular biology and the problems they cause in these environments. It was soon realised that many factors that affect the settlement and adhesion in the body or on medical devices are analogous to factors affecting the proliferation of further growth of biofouling. A subtle difference in species in freshwater and marine environments compared to medical environments continues past cellular attachment and increases through diatoms, algae and other further macro fouling organisms. The influence of topographical features on biofouling in fresh and marine water environments has again come under analysis in the medical fields.

Another type of topographical research field for the prevention of fouling lies in the area of biomimetics, whereby the studies of natural surfaces have been used to replicate manufactured surfaces. Biomimetic studies of these patterns from natural surfaces have provided a new-sophisticated technique in the creation of nano and micro scale surface patterns. Consequently, research based on microtopography of scale like placoids present on sharkskin surfaces has an ability to act as a deterrent for marine algae *Ulva linza* and barnacle cyprids *Balanus amphritrite.*[84] So far, the best performing topographical effort was demonstrated when projections of 40 μm heights were shown to reduce barnacle cyprid settlement.

The effect of surface roughness on the function of settlement is still not fully understood. Over time, the artificial surface loses its ability to function.[85,86] Manipulations of surface topographical features have shown that feature widths and spaces between have shown to be a deterrent to microorganism attachment and proliferation in particular, Ulva.[87] In a review by Scardino *et al.*, attachment point theory has been a proposed method of cellular reduction upon topographically engineered surfaces. An organism's attachment increases the fouling

attachment is increased when there are optimal levels of attachment points depending on the size of the settling species from the given micro texture upon the surface. [88]

Superhydrophobicity has also been investigated extensively since the properties of the lotus-effect from the lotus leaf (from the *Nelumbo nucifera* plant), was discovered. Due to the convex microtopography, the plant is able to produce a self-cleaning property. [89] The plant creates a contact angle above 150 degrees while having low contact hysteresis. Surface roughness and wettability was previously addressed, [90] which was not demonstrated until 1997 in the discovery of such a leaf. [91] Marmur presents a review of superhydrophobicity illustrating the mechanism of the Lotus-effect for the prevention of biofouling. This operates through the repulsion of materials by minimising the water-wetted interface, which keeps an air interface between that of the substrate and the liquid. [89]

1.4.2 COATING APPROACH

Three types of antifouling (AF) coatings have been developed, in terms of modern day, AF response to micro and macro-fouling:

1) AF coatings;
2) Fouling release coatings (FRC);
3) Biomimetics.

AF coatings contain biocides that are designed to erode or ablate over a time period. This erosion procedure of the coating allows for the release of the biocide to directly kill the microorganism attached. Presently copper is an antifouling coating used on naval ships. [92] The limitations of this coating selection reside in the effective lifetime of the coating and the overall aggressiveness in toxicity, Figure 1.4.
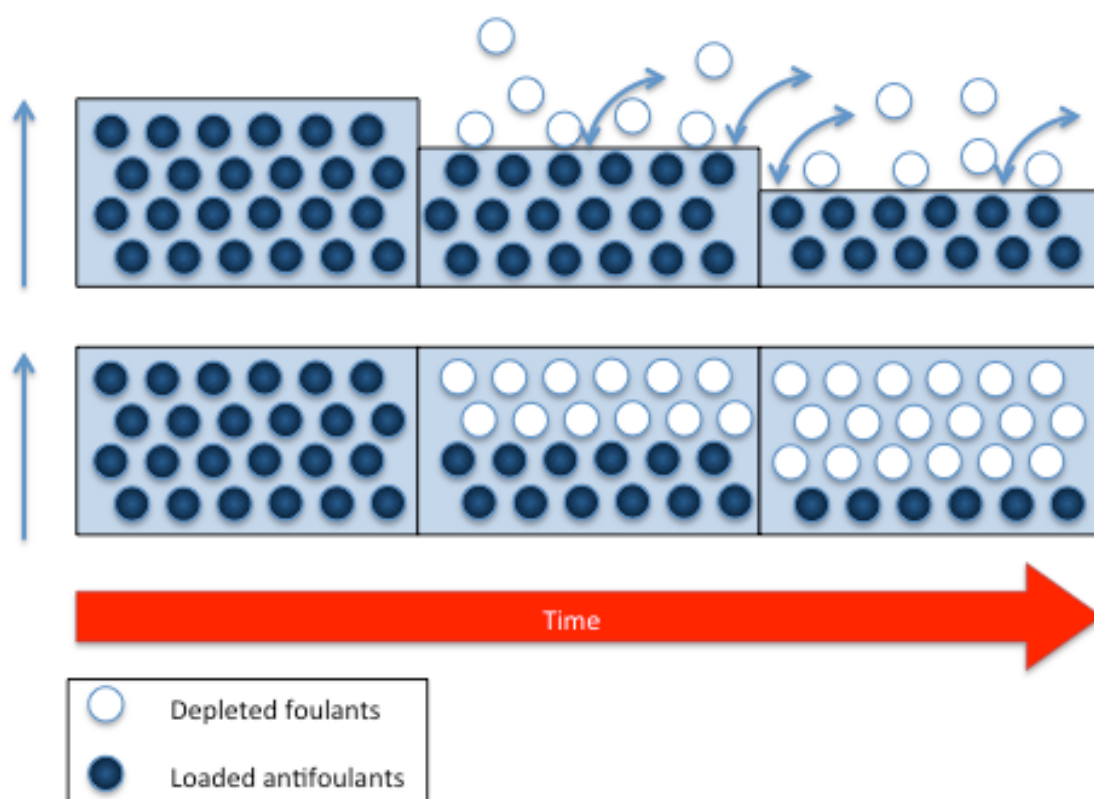
Figure 1.4: Schematic of (top) soluble matrix biocide releasing coating and (bottom) insoluble biocide release coating.

Most new AF coatings are in the form of paints, which is a more general term for enamels, lacquers, varnishes, primers, sealers among others. [93] Antifoulants are the ingredients incorporated into the coating matrix, with the majority of AF coatings being organic and comprising of multiple functions i.e. anticorrosion, [94] or hydrophobic.

FRCs are hydrophobic, low surface energy, non-toxic coatings. Their degree of wetting, i.e. the water on the interface, depends on the relationship between the forces of cohesion and adhesion where wetting refers to the spread of the liquid over the surface. Hydrophobic coatings are often used as they create a larger contact angle between the organism's glue and the surface. This results in less wettability and less fouling due to the adhesive not being able to spread across the surface. The coatings usually have highly flexible backbones affording a low surface energy arrangement. This low surface energy means that an organism's ability to generate strong interfacial bonds with the surface is somewhat impeded. The smoothness of the coating reduces the presence of micro-niches known as the thigmotactic nature of settlement. At a molecular level this allows for organisms to be dislodged once the substrate is moving beyond its critical velocity. This is typified in ships moving at speeds of 10-20 knots, dependent on the fouling community. [95] The nature of the FRC with the hydrodynamic flow

therefore lowers the work of adhesion. [96] There are two types of FRC; fluoropolymer and silicone based polymers an example of which is polydimethylsiloxane (PDMS), Figure 1.5.
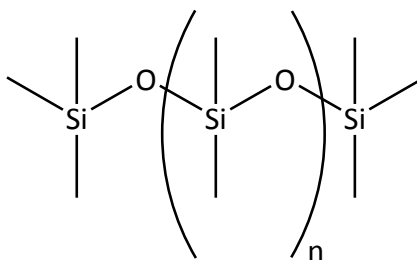
Figure 1.5: Molecular structure of PDMS.

A biomimetic approach deals with designs extracted from the natural environment. It is somewhat bio-inspired rather than directly copied from natural biological function. Biomimetics applies a 'bottom-up' strategy and has a plethora of resources in nature that successfully control levels of fouling. [97] Marine organisms have been researched extensively for the protection of their own surfaces from fouling. [98-101] Many of these have both physical and chemical methods in preventing biofouling. [94,98] Adhesion mechanisms of the mussel *Mytilus edulis*, involves the release of byssal threads composed of collagen and silk-like proteins. The byssus threads are of interest as they can be harnessed as a non-fouling bio-inspired polymer. The byssus is first secreted as a proteinacious liquid that hardens rapidly. [102] Callow *et al.,* used an mPEG-DOPA$_x$ polymer consisting of a linear polyethylene glycol (PEG) monomer to replicate the polymer. The DOPA moiety serves as an adhesive for anchoring the polymer to the substrate, and the mPEG functions as the antifouling polymer. The research found that while the antifouling coating showed good response to the levels of cells being attached, it was susceptible to oxidative cleavage over time, resulting in severe levels of fouling exhibited. [103]

Already, the market yields a range of foul release, protective and antifouling coatings, some of which are listed in Table 1.1.

Table 1.1: Foul release and protective antifouling coatings already available on the market.

Product	Company	Type
Devclear	Devoe Coatings	Silicone Polymer
Sigma LSE	Sigma Shinto Coatings	Silicone Polymer
Nipple Sleek	Nippon Paint Company	Silicone Polymer
Epco-Tek 2000	Hi Tek Company	Epoxy-Cu Powder
Luminore	Luminore	Cold Spray/Metal-Cu
Copper Metal	Multiple companies	Metal
Brass Metal	Multiple companies	Metal
Copper-Nickel Alloy (90:10)	Multiple companies	Metal
Copper Thermal Spray	Multiple companies	Metal
Brass Thermal Spray	Multiple companies	Metal Thermal Spray
Bronze Thermal Spray	Multiple companies	Metal Thermal Spray
Zinc Galvanising	Multiple companies	Metal Thermal Spray
Polyshield Aqualastic	Cynet Enterprises	Hot-Dip or Electrocoat-Zn
SeaLion	Juton Group	Polyurea Elastomer
Rilsan	Arkema Inc	Silicone Foul-Release
Kynar 500	Arkema Inc	PVDF Resin
Fluon ETDE	Asahi Glass	Thermoplastic Fluoropolymer
Neoflon	Daikin Industries	Perfluoroalkoxy Resin
Teflon-FEP	DuPont	Fluorinated Ethylene Propylene
Sylgard 184	DowCorning	Silicone Elastomer
Mille Light	Hempel	Non-Toxic Ablative
Micron Eco	International	Non-Toxic Ablative
SSC-44	US Gloss	Non-Toxic Ablative
Lefant H2000	Lotrec AB	Physical Growth Repellent
Hempasil X3	Hempel	Hydrogel Silicone Foul-Release
Ecolosilk	Nippon Paint	Biocide-free Antifouling
SigmaGlide	Sigma Coatings	Silicone Foul-release

Matsui *et al.,* evaluated the antifouling performance of two silicone polymers; Sigma LSE and Nipple Sleek against *Limnoperna fortunei* in a series of panel based experiments conducted in Japan. They were both found to be effective in preventive mussel attachment and colonisation over a 15-month period. [104] The work carried out in this paper is of value to this field of

research as it implements real environmental testing. Some coatings have also come under scrutiny due to lack of testing pertaining to environmental compliance of its rate of leaching from the matrix. For instance, Epco-Tek manufactures an epoxy primer undercoat and successive layers of epoxy mixed with copper powder. The copper migrates from the surface layers through diffusional leaching. In a 3-year static experiment, copper leached from the matrix at a rate of 1.0-3.0 µg cm^2 per day, indeed this has been found to be adequate to repel sensitive marine organisms by Race *et al.*. [105] Furthermore, LuminOre has also come under review on the leach rates of copper. LuminOre in comparison to Epco-Tek, is a copper composite metal antifouling coating and contains around 75-95% copper metal. Copper particles in LuminOre are surrounded by non-conductive dielectric insulator binder molecules. The mode of which is currently unknown, nevertheless LuminOre is still registered with the US-EPA as an antifoulant. The company claim that leaching is limited to 1.9 µg/cm^2 per day in freshwater systems. Skaja *et al.*, reported that LuminOre was effective against *Dreissena bugensis*, where trails worked better in stagnant flows compared to higher flows. [106]

1.4.3 CHEMICAL APPROACHES

Biocides are chemical agents that are capable of killing an organism in a particular manner. In antifouling, they are usually employed into matrices to prevent or control microbiological attack in a single or cocktail of compounds. Biocides can be inorganic such as chlorine, bromine, ozone etc., or organic including isothiazolones, quaternary ammonium compounds (QUATS) or aldehydes (i.e. gluteraldehyde and acroleine). The action of the biocide used should possess a disinfection property such as bactericidal, fungicidal or algicidal and this presents a need for very broad-spectrum compounds due to their specie specificity properties.

Chlorine has been effectively used as a preventative measure of biological growth for many years. It is an oxidising compound and has been used in the field of water treatment and disinfection, especially in killing *Escherichia coli.* [107] It remains an excellent algicidal and bactericidal agent, and works by absorbing into the EPS. Chlorine's mode of action has been divided into two areas; firstly, disruption of cell permeability and secondly, damage to enzymes and nucleic acids. [108] Verween *et al.*, investigated the use of chlorine with a peracetic acid in measuring toxicities of *Mytilopsis leucophaeata* and *Dreissena polymorpha*. The vulnerability of the species was investigated in terms of cell attachment and corrosion that ensued. [109] Roosenberg *et al.* similarly investigated the effects of chlorine, but in the fouling oyster larvae of *Crossotrea virginica* in a mortality study. [110] It was found that mortality was directly related to increased concentrations of chlorine and exposure time. The authors also

present excellent methods in the calculations for predicting mortality under the varied conditions that were developed as a consequence of their findings.

Ozone has been mentioned as an oxidising biocide as far back as 1886, where it was used as a disinfectant for polluted water by de Meritens. [111] Ozone in comparison to chlorine treatment will kill bacteria on contact with the cell by cellular lysis and cytoplasmic dispersion by directly rupturing the cell wall, whereas chlorine mediates toxicity by diffusing through the cell wall and oxidising any enzymes contained within. The most fundamental advantage of ozone to chlorine is its environmentally friendly property, and although ozone has a relatively short half-life, will breakdown intrinsically to environmental oxygen.

Isothiazolinones are heterocyclic compounds that have various moieties of sulfur, nitrogen and oxygen and are active and efficient biocides. These compounds inhibit the growth of bacteria, fungi and algae by shutting down metabolic pathways, and are frequently used in treating corrosive environments that exhibit populations of sulphate reducing bacteria (SRB) in anaerobic conditions. They are used frequently in waste water systems and environmental water based systems. [112] They have application over a broad pH range and are compatible in multi-chemical treatment platforms. Schmid *et al.*, showed that isothiazolinone biocides inhibited growth and metabolism of microbial cells, achieved by using a photo-acoustic monitoring device. [113] Isothiazolinones are also used in preserving woods as an ingredient preferred to using polyethylene glycol (PEG). PEG alone is a good preservative for wood, but can facilitate metal corrosion, and therefore an additive such as isothiazolinone would prevent this. Rakotonirainy *et al.,* investigated the method for the preservation of artefacts containing both metals and wood fixes in them. However, it was found that isothiazolinones as an additive to PEG was not effective in preventing corrosion. [114]

QUATS are a class of cationic compounds that are used as biocides and mainly corrosion inhibitors. QUATS are detergents, which dissolve lipids, more importantly acting upon the cell wall of an organism, causing a loss of cellular content. Antimicrobial effects are based on the inactivation of proteins and enzymes after the cell wall has been denatured. Their effectiveness is also dependant on the chemical nature of the QUATS, for instance an aromatic ring or radical lengths have different effects upon an organism. Hastrup *et al.,* investigated the use of copper-based wood preservatives encompassing the use of quarternary natured compounds, where they were found to be effective in preventing the fungus *Surpula lacrymus*. They concluded that it was not the copper alone that was effective in preventing the fungus growth, but the QUAT also. [115]

Tiller *et al.,* found the amphiphilic controlled release coating containing QUATS such as cetyltrimethylammonium chloride (CTAC) gave excellent biocidal activity, and would mainly kill bacteria attached to the surface of the polymer. This is of great interest as it does not have an effect on the surrounding media and is only biocidal to contacting, adhering bacteria. The group reports that polymers may be loaded with the QUATs, as a biocide, and prevent a non-toxic route in combating fouling issues. [116] The work shows promise that doped coating methods are applicable to a wide range of conceptual fouling related problems and has scope to be applied to metals, plastics, woods and stones in preventing corrosion. Deng *et al.,* reported the use of vinyl quaternary ammonium salts in preventing microorganism growth in the textile industry. This again shows the versatility of the biocidal compound and how it could potentially be applied to a range of biofouling problems. [117]

Other approaches that have been highlighted in literature lie in multi component matrices such as polyvinyl chloride with the incorporation of plasticizers. Some plasticizers are known to be antimicrobial, and thus their incorporation into a PVC matrix affords different antimicrobial properties. [118]

1.4.4 NANOPARTICLES

Recently, research in the use of nanoparticles in the combating of biofilms and fouling has gained momentum. Nanoparticles are generally no greater than 100 nm in size and have specific properties that are of interest to the research community. [119] They have been used throughout the ages (without the knowledge of their existence) with one of the earliest reports of nano-sized particles in the form of gold. Faraday demonstrated the preparation of colloidal gold, which he named as 'divided metals'. His account dated 2nd April 1856, called the particles he made 'the divided state of gold' of which the solutions can still be found in the Royal Institution in Mayfair, London.

Later in 1890, German bacteriologist Robert Koch proved that compounds with gold incorporated within them inhibited the growth of bacteria for which he was later presented with the Nobel Prize for medicine in 1905. Indeed the use of gold in medicine is not new and has been used throughout history. In India, for example, gold has been prepared for memory prescriptions known as Sarawatharishtam. In China, a gold coin was used in cooking rice in order to help replenish a deficit of gold in the body.

However, the science of nanometre scaled objects was not discussed until much later in the history books. It was not until Richard Feynman gave a talk called "There's plenty of room at the bottom" in 1959 at an American Physical Society lecture. Within his talk he stated, "The

principles of physics, as far as I can see, do not speak against the possibility of manoeuvring things atom by atom..” This, in a way, was the first suggestion of a bottom up synthesis approach. “…it is interesting that it would be, in principle, possible (I think) for a physicist to synthesise any chemical substance that the chemist writes down. Give the orders and the physicist synthesises it. How? Put atoms down where the chemists say, and so you make the substance. The problems of chemistry and biology can be greatly helped if our ability to see what we are doing, and to do the things on an atomic level, is ultimately developed – a development which I think cannot be avoided.” [120] However, it was not until 1981 where tools began to be developed for the probing of such a hypothesis, where the scanning tunnelling microscope was invented. This tool enabled the visualisation and placing of atoms and molecules wherever required. Interestingly, with all these developments, new nano technological products will indeed reach the market place and consumer in the immediate future. However, implications regarding nanotechnology may cause concerns and indeed be significant for governments to discuss, something that needs to be tackled in the future.

1.4.4.1 ANTIMICROBIAL PROPERTIES OF NANOPARTICLES

The use of nanotechnology was unnoticed over the ages due to the distinct lack of understanding of the mode of toxicity towards certain organisms, with the first reports dating back to Cyrus the Great, King of Persia – who established the board of health and medical dispensary for his citizens. [121] This of course has only become possible through the advancement of techniques in the sciences. For instance, silver has been used for centuries to prevent and treat a variety of diseases, and through Davies and Etris it has been suggested that silver may be linked to man's earliest attempt to improve his environment. [122] Only now has it become known that silver has a positive influence towards the reduction of microbial activity. The mechanisms of which are still not fully understood, but are proposed by the following:

- Destruction of the organism by oxidation catalysed by silver;

- Disruption of the electron transfer in bacteria through the monovalent silver species, and preventing the unravelling of DNA in viruses through the substitution of hydrogen ions in the monovalent form;

Silver holds unique properties over all the other metals, especially when introduced to oxygen. Oxygen in the air is adsorbed on to the surface of silver as atomic oxygen, and because atomic oxygen fits into the octahedral holes of silver, oxygen accumulates within the bulk of silver.

This stored octahedral oxygen significantly contributes to the catalytic activity and thus oxidative power of silver. It was not until 1986 that a filed patent in the USA covered the catalytic activity of silver in an aqueous media for sanitation of water, [74] and consequently, this has led to an increase in research and forms part of the impetus of study within this thesis.

1.4.5 NATURAL PRODUCTS

Natural products have been considered as a source of new drugs, antibiotics and biocides. Recently, a large amount of research is being conducted in natural product technology and defence chemical tactics employed by organisms in their own defence of biofilms, these are known as secondary metabolites. Secondary metabolites are compounds that are produced and regarded as non-essential for life to the organism that produces them.
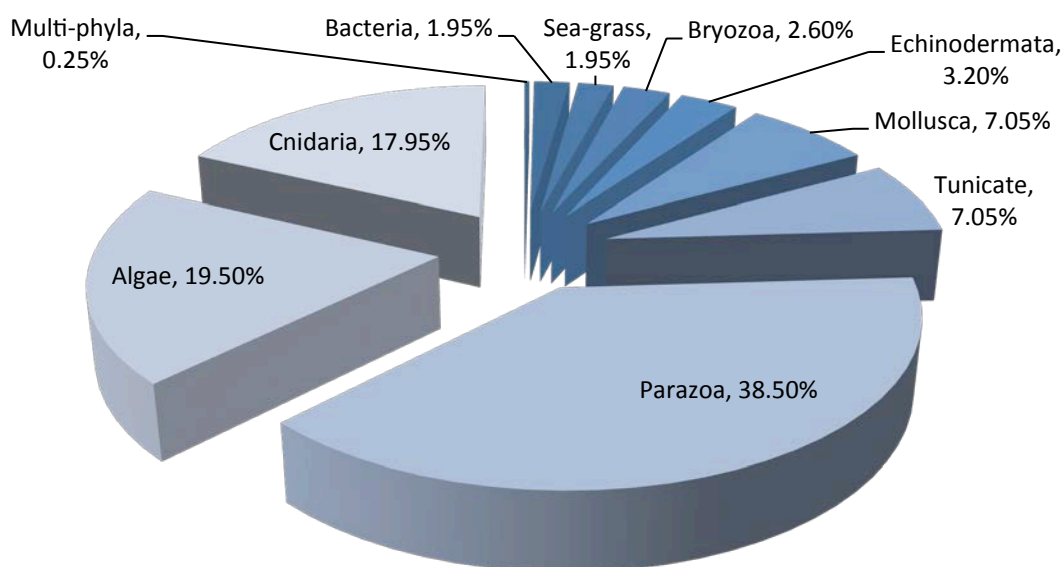
Figure 1.6: Phyletic distribution of marine species which have potential antifouling natural products, taken from Chambers (2006). [94]

Numerous extractions and isolations of natural products from the marine environment have shown response as possible antifouling agents, some of the origins of which have been summarised in Figure 1.6. One compound that has already exhibited good antifouling potential has been derived from the eelgrass, *Zostera marina* in particular zosteric acid. It has been shown to be effective to a broad range of organisms: bacteria, algae, barnacles and tubeworms. One other successful compound that was found to be very effective was extracted from the sea pansy, *Renilla reniformis*, yielding a compound known as renillafoulins – in Hein site of its antifouling nature against the species cypris larvae. [123,124]

Particular success has been achieved with isolation of a range of toxic secondary metabolites from seaweeds. Chemicals known as sesquiterpenes and furanones have shown good antimicrobial properties and thus a good alternative source of non-toxic chemicals. The red algae *Delisea pulchra* produces a brominated furanone that has shown extensively the ability to reduce fouling of both macro and micro fouling organisms. [125-127]

Marine natural product chemistry has had a shorter history than terrestrial counterparts have and the elucidation of such compounds is therefore far less abundant. In recent years, large biomolecules have been found in marine dinoflagellates. [128,129] The metabolites of such marine organisms, with potent bioactivities are often a minor constituent and the source of population is usually extremely limited. Therefore, only minute quantities of the specimen are usually analysed and shows an inherent difficulty in their extraction and elucidation.

Ciguatoxin is a very potent toxin discovered in coral reef fishes. Yasumato's group first elucidated the compound in 1990 and obtained no more than 350 µg illustrating the difficulty of natural product extraction. [130] Dolastatins are also known to possess potent growth inhibitory activity against some cancer cell lines. A clinical trial was attempted for these compounds showing an indication of their potential candidacy as broad-spectrum agents for antifouling.

An investigation by Okana *et al.,* showed that adrenoreceptor molecules have the ability to release cement used in larval attachment in barnacle cyprids exogenously. [131] Consequently, α_2-adrenorecpetor antagonists (metedomine and clonidine) were found to strongly inhibit attachment and subsequent metamorphosis without significant lethal effects to the surrounding environments as published in this work. It was found that doses of 1 nM were significant in cyprid reduction.

1.4.6 ANTIMICROBIAL AGENTS

Aforementioned in this chapter, it has already been established that a range of approaches in creating an effective antifouling product. These have ranged from toxic to antimicrobial or biocidal through natural or synthetic means. This section of the chapter will aim at reviewing current antimicrobial agents that have distinct modes of actions in the antifouling field.

Designing a coating with these specific functions has been reported abundantly. [132-134] Modern day materials often rely on the incorporation of antimicrobial agents and biocides that also serve as antifouling materials, which has already been mentioned in the form nanoparticles, [135,136] plasticizers[137,138] and even natural products. Plasticizers are not reported for their specific antifouling roles and this was work was carried out in Regan *et al.,* showing definite results

where plasticized polymers can produce antifouling effects. Some of these effects could be due to their inherent toxicity to some organisms when they encounter these compounds. Examples of this can be found in Table 1.2

Table 1. 2: Table detailing plasticizer toxicity to organisms when literature search performed.

Plasticizer	Effect	Species or Test-System	Details	Reference:
DEHP	Antibacterial	*Escherichia coli* JM109	Ratio of CFU numbers: CFU was compared for number of control to CFU numbers for DEHP	[139]
	Growth inhibition	*Caenorhabditis elegans* Bristol N2	Worms exposed to DEHP for 24 h @ 20 °C; growth assessed by measuring length of worms killed by heat through microscopy with scaled lens	[140]
DEP	Growth inhibition	*Raphanus sativus*, forty radish	14-day plant growth test, DEP inhibited seedling dry weight by 25%, 92% and 100% at 1, 10 and 100 g/kg	[141]
	Toxicity to bacteria	*Vibrio fischeri*	Flash luminescent bacteria test; BioTox – organisms grown in compost medium containing DEP; Effective Concentration $(EC)_{10}$ values determined EC_{10} of 0.92g/L	[141]
DMP	Phytotoxicity	*Closterium lunula*	Standard bioassay method according to APHA, 1985 for 96 h, EC_{50} determined at 331 mg/L	[142]
	Toxicity to invertebrates	*Hyalella Azteca*, Freshwater benthos	Animals were exposed to primary chambers contained within secondary chambers housed with water bath at 23 °C; mortalities observed, LC50 of 28.1 mg/L determined	[143]
DMAz	Antibacterial	*Escherichia coli*	Serial dilutions in double strength nutrient broth, inoculated and incubated for 24 h at 37 °C, MIC determined 0.78×10^{-2} – 2.5×10^{-2} µg/mL	[144]
DBS	Cytotoxicity	Human KB cells	In-vitro model, dose response curve where an ID-50 of 1549 mg/L was determined	[145]
IPP	Cytotoxicity	Colon HTB-37 Caco-2 cells of human	IPP used in concentrations of 1, 0.1 and 0.01 % w/v, 96-well plate with IPP applied for 30 min, MTT assay performed, toxicity potential of IPP calculated as a fraction of non-viable cells	[146]
MP	Enzyme activity	Liver microsomes of rat	Inhibitory activity related to 5α-reductase in female rats, concentrations of 1.3 mmol/L were used.	[147]
	Enzyme inhibition	Yeast 205 proteasome	Concentrations of 80 µmol/L were used in assay buffer, pH 7.5 37 °C; post acidic activity determined by following hydrolysis of Z-LLE-β-NA (fluorescent substrate) for 30 min.	[148]
DEHA	Growth inhibition	*Rhodococcus rhodochrous* ATCC 13808	Batch experiments were used where DEHA was added to the test system, 30 °C, where microbial growth and biomass were determined using GC-FID	[149]
TEC	Fibril formation	B-amyloid (1-42)	TEC introduced, incubated for 1 h, aggregation of peptide was measured by thioflavin fluorescence assay	[150]
Succinate	Toxicity to bacteria	*Pseudomonas syringae* ATCC	Cultures were incubated at 27 °C, significantly killed bacteria – 20% survived	[151]

Strategies to develop antimicrobial materials [75] involve either release based or contact-active based mechanisms. The disadvantage of release based antimicrobial materials is the loss of antimicrobial activity over time due to the depletion of biocidal agents (silver, plasticizers etc) as well as the release of toxic materials into the environment. The main drawback of contact active antimicrobial materials is the accumulation of dead microorganisms onto the surface of the material.

1.5 ASSESSMENT OF BIOFOULING

Many analytical methods have been developed for the assessment of biofouling and its typical characteristics. The inclusion of nanoparticles into materials has rendered a new challenge in obtaining a good depth and realisation of the level of fouling. This section of the thesis addresses the many methods currently used for determining the chemical and physical compositions of biofilms, fouling and some materials of which they are used in.

1.5.1 PHYSICAL CHARACTERISATION

Ranges of analytical techniques are already present for the assessment of biofilms and biofouling. The research of biofilms has developed into a huge multidisciplinary field, in which scientists from different fields such as microbiology, chemistry, physics, engineering and computer science are all involved. In order to investigate biofilms, focus is generally based on structural, functional and ecological aspects. These all include; biofilm development from the beginning (primary adhesion of organic and inorganic molecules coupled with single microbial organisms attaching to a substratum), through to growth and maturation of the biofilm, biochemical physiology, complex multi-cellular interactions based on cell-to-cell signalling, exchange of genetic material, sorptive and protective properties of EPS, exposure to inorganic and organic pollutants, biocides, detergents, synthetic surfactants, heavy metals, reactive oxygen species followed by detachment processes.

1.5.1.1 CONTACT ANGLE

Contact angle measurements provide an indication of the hydrophobicity or hydrophilicity that a surface possesses. The hydrophobicity or hydrophilicty provides insights for microorganism attachment, particularly in the initial fouling stages. [152] The free energy can be approximated using contact angle measurements as a function of the surface "wettability", whereby the contact angle is the angle at which the drop of water touches the substrate described by Young's equation:

$$\gamma_{lv} \cos \Theta = \gamma_{sv} - \gamma_{sl} \qquad (1)$$

Where γ_{sl}, γ_{sv} and γ_{lv} correspond to the surface tension of solid, liquid and solid-liquid interfaces. Both wetting and adhesion properties can be estimated through calculation of the surface tension induced by the solid-liquid interface, Figure 1.7. Generally, the hydrophobicity of a substrate is determined through multi-solvent analysis
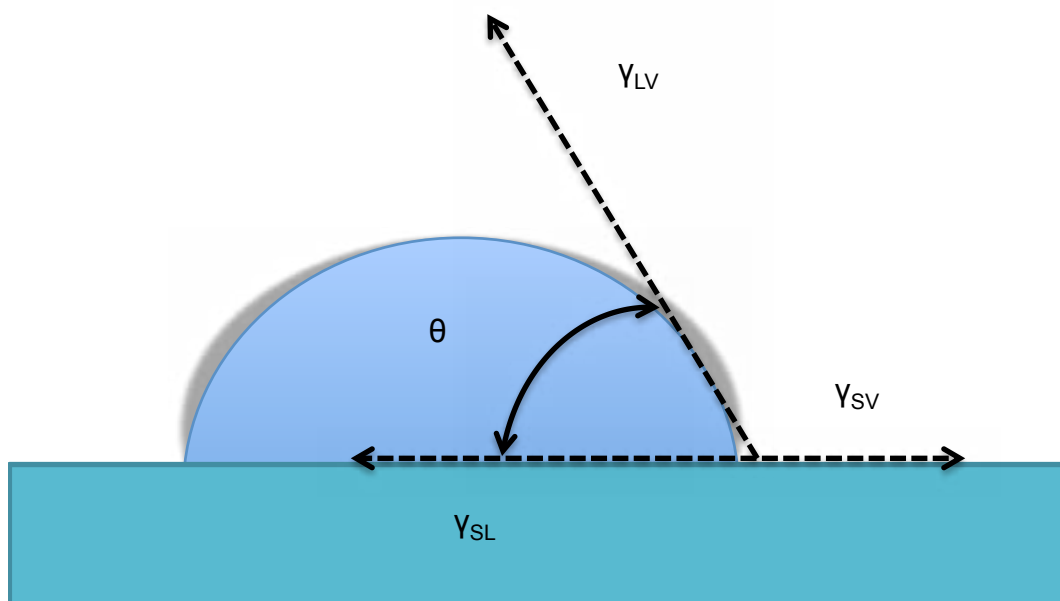
Figure 1.7: An illustration showing the sessile drop technique with a partially wetting liquid droplet on a solid substrate. θ is the contact angle, γ_{sl} , γ_{sv} and γ_{lv} correspond to the surface tension of solid, liquid and solid-liquid interfaces.

Polymers do not tend to adhere to this equation as they are regarded as non-ideal due to liquid penetration into the matrix causing swelling phenomena. Low contact angle measurements (<90 °) have been considered a positive factor in designing materials as antifoulants. [120,153-155]

One of the most common methods for contact angle analysis is using the sessile drop method. Images are taken on a side profile and the data for advancing and receding measurements are collected. Zhao *et al.* investigated the surface free energy of PTFE coatings using a sessile drop contact angle approach. The authors found that varying PTFE content influenced the level of microbial adhesion and subsequent fouling.

An advantage of this method, aside from its relatively straightforward nature, is the fact that with substrates with large enough surface areas, multiple droplets can be deposited in various locations upon the sample thus determining heterogeneity. Some disadvantages include the converse to the aforementioned, therefore with fewer samples, heterogeneity cannot be determined and is sometimes therefore assumed. Contrastingly, the sample spotting of water droplets does not reflect the 'true' environment the substrate/material is being subjected to, as more than often samples are completely submerged.

Some researchers define the contact angle in terms of surface energy, [156] given the sessile drop technique this is not always well defined. The values obtained using the sessile drop

depend not only on the solid substrate but equally the liquid (probe) being used. However, some researchers simplify the system by 'lumping' surface energy into one number when, realistically a system has multiple components such as molecular interactions (van der Waals), polar and acid/base interactions and solvent properties, some of these theories have been listed below.

1.5.1.2 MASS DETERMINATION

Mass determination involves, simply, the weighing of the substrate both before and after a study thus ascertaining any mass increments due to activity upon (if any) the substrata's surface. Generally, a sample will be dry weighed in order to remove water content, thus giving an indication of some of the biological and chemical material that is pertaining to fouling. More than often this is reported as a %mass increase: [135,138,157]

$$\left(\frac{f-i}{i}\right) \times 100 = \%biomass \qquad (2)$$

Where f is the final weight, i the initial weight, both before and after the drying step (or where weight remained constant). Vrouwenvelder *et al.,* reported biomass analysis on membranes used in drinking water production, which were then viewed using scanning electron microscopy (SEM), thus determining mass increase attributed to microorganisms attachment. [158] Other researchers have used a scraping method, for instance, in Chandra *et al.,* the biofilm was removed in this manner from the substrate and then transferred to centrifuge tubes with phosphate buffered saline (PBS). [159] However, this method should be proceeded with caution as the material requires a certain level of robustness to remove the biofilm in the first instance to perform such a physical procedure. Lee and Kim recommend performing a range of characteristic assays in tandem with biomass analysis. They state that in order to analyse biomass accumulation, Adenosine 5'-triphosphate (ATP), total direct cell count (TDC) and heterotrophic plate count (HPC) should be used to probe the makeup of biomass. [160] ATP gives an indication of the total amount of active biomass whereas the TDC value can be determined via fluorescence microscopy, of which will be discussed further in this section of the thesis. In other work, biomass has been determined with components of the biofilm makeup quantified using a range of biochemical techniques. For instance, biological mass can be scraped or sonicated, depending on the nature of the substrate, and then the biofilm material gets centrifuged and analysed for components such as: protein, carbohydrates, uronic acids, and deoxyribonucleic acid (DNA). [42,135] Both methods quantify the level of mass attributed to fouling in general, with further investigation into the nature of what is composed in the material adhered to the substrate's surface.

1.5.1.3 SCANNING ELECTRON MICROSCOPY

Scanning electron microscopy (SEM) can be used to investigate a fouled sample for levels of biofouling upon a substrate. It remains a fundamental technique in assessing levels of fouling and has been used extensively throughout many areas of biofouling research. [161-165] Lazarova *et al.,* reported that a more in-depth micrograph image could be achieved by omitting a gold sputter coating step and then using a low emission current. [166] An obvious downside to this method is that transparent surfaces would not be able to be characterised due to the inferior electron detection from the instrument.

It is not only the surfaces that require analysis but also the adherent bacteria that have presented attachment to the surface. This enables the characterisation of microorganisms attaching to the substratum and whatever secretions they deposit. Azevedo *et al.*, have used SEM to characterise settlement and colonisation that had occurred on poly (vinylchloride) (PVC) coated glass membranes, giving clear topographic images, inclusive of 3D colonies of bacteria *Helicobacter pylori.* [13]

Lee and Tsao demonstrated that SEM could be used to characterise silver nanoparticle doped hydrogels, although the resolution was not able to fully characterise the nanoparticles in the composite material. However, it has been shown that if a treatment of 6 M HNO_3 was applied to the nano-composite material, then the embedded nanoparticles could be visualized, depending on the resolving power of the microscope. [167]

Stewart *et al.*, have shown structural heterogeneity of microbial consortia attached to substrata through SEM and CLSM. They used a cryoembedding technique followed by the tandem microscopy techniques. [168] The authors compare three different microscopy methods illustrating differences in the information they provide especially in biofouling research.

SEM is a viable counting method for visual enumeration of bacteria adhered to a substrate. It would give clear accounts of the morphology of the bacteria and the material surface and in some cases the relationships they have between each other. [169] The limitation to this method is it's time consuming nature and only the small fields of view under focus.

1.5.1.4 TRANSMISSION ELECTRON MICROSCOPY (TEM)

TEM is a useful tool in the determination of sizes, shapes and orientations of biological and physical samples. TEM using high angle annular dark field (HAADF) detection in scanning transmission microscopy (STEM) mode can be used to visualise biological systems and has

been done successfully by Shrivasta *et al..*[170] TEM was used to probe the internal biofilm structure the contained bacterial cells and the metal nanoparticles that were contained within. From these findings, they found that gram-positive bacteria had a reduced response to silver nanoparticles when compared to gram negative.

Morones *et al.* used TEM in STEM mode to confirm the presence of metal nanoparticles within the bacterial cell membrane following exposure to the bacteria. The method implicitly analysed the cell morphology and interactions with the metal nanoparticle. [171] Dynes *et al.*, presented a method for the detailed quantitative analysis of ferrous and ferric iron in a river biofilm mapping both Ni and Mn ionic species within the same regions. [172]

1.5.1.5 X-RAY SPECTROSCOPY

X-ray spectroscopy and scattering techniques have been found to be particularly useful in the study of biofouling and interfacial phenomena surrounding the subject. [173] Inherent molecular scale sensitivity and the ability to penetrate large depths render X-rays an ideal tool for the investigation of structural details of environmental materials under in-situ conditions. An excellent review from Trainor *et al.,* shows the application of X-ray fluorescence techniques to investigate the distributions and speciation of heavy elements at environmental interfaces. [174] Immobilisation of furanones (a natural product antifouling compound) was investigated using X-ray photoelectron spectroscopy (XPS) and tapping mode AFM was administered after each immobilisation step. [175]

1.5.1.6 ATOMIC FORCE MICROSCOPY (AFM)

AFM has become one of the most widely used, and indeed, one of the most important tools of the scanning probe microscopy (SPM) techniques. AFM has the ability to provide a high level of resolution in surface topography, but also in measuring atomic forces between surfaces and adhered cells. Its other uses include, measuring the surface roughness of a substrate, whereby testing its effectiveness as an antifouling surface or coating: the technique also provides clear resolved images of, for example, microorganisms.

Hansma *et al.,* reviewed AFM of biopolymers with some specific examples including: EPS, condensed DNA, DNA constructs and even DNA-protein interaction. [176] Van der Aa and Dufrene investigated bacterial adhesion to polystyrene under aqueous conditions, cell morphologies and cell interactions across the surfaces were realised. [177] Furthermore, Whitehead *et al.,* report that AFM can be used to investigate the strength of adhesion between organisms and a substrate highlighting the instruments broad use. [178]

Some fundamental differences between AFM and SEM is that AFM is capable of measuring samples in air and aqueous environments. SEM requires a small sample preparation in order to mount the sample within the instrument's analysis chamber that can often be subjective in sample analysis. Beech *et al.,* have reported that daughter cell division in a time period of 100 min was witnessed showing the versatility of surface topography and interaction analysed simultaneously. [169] AFM requires very little sample preparation, but has some limitations to the degree of surface height when placing a sample in the instrument, usually in the range of ±6 μm. Depending on the level of resolution required and depth of image, the instrument can render lengthy and time-consuming analysis compared to SEM which is a downside to the instrument.

1.5.1.7 COMBINATION SURFACE CHARACTERISATION

Techniques and instrumentation can often be combined with one another to increase the level of knowledge and depth to a system. Microbe surface interactions upon substrata were reviewed by Beech *et al.*, where an understanding of mechanistic perspectives on biofouling and biocorrosion using Atomic force spectroscopy (AFS) was explored. The technique enabled the elucidation of cell adhesion to substrata and using modern mass spectroscopy methods biofilm populations could be characterised within the matrix of the biofilm. [179] Another example of combinational instrumentation for the improved investigation of biofilms is given in Pradier *et al..* [180] Within this work, FT-IR, XPS and time-of-flight (TOF) secondary-ion mass spectrometry (SIMS) was used to characterise the topmost cellular layer of microorganisms in the biofilm matrix.

1.5.2 BIOLOGICAL CHARACTERISATION

As previously discussed, the main components of biofilm are water, microbial cells, EPS and organic particulates. As such, there is a need for separation processes to identify and quantify each component of the biofouling problem. The choice of a suitable separation method links to the analytical and microbiological problem and will form this section of the thesis.

1.5.2.1 BIOCHEMICAL DETECTION

It is already accepted that EPS comprises of carbohydrates, proteins, water and organic particulates. Therefore, the detection of such molecules allows the assessment of the degree of biofouling upon a substrate.

Carbohydrates within a biofilm matrix have been reviewed in Christensen (1989). [181] Proteins, and in particular, proteomics and metaproteomic analysis is of interest to biofilm research. Normally, a restriction in biomass of the biofilm does not allow sufficient proteome analysis. This restriction often causes enrichment features in biofilm generation. Consequently, alternative biofilm systems were developed for increasing biofilm mass, with some of the best results coming from using glass wool as a substrate support for biofilm maturation.[182]

Interestingly, proteins in biofilm research are linked to cell-to-cell communication, with certain proteins being attributed to specific signalling pathways. [183] In order to investigate microbial metabolic activity attributed to protein adsorption it is necessary to divide proteins into two parts: intracellular and extracellular protein expressions. A summary of which can be found in Wells and Weil, where protein has been separated into procedures and methods of detection. [184]

A range of methods exist for protein detection in biofouling ranging from simple detections such as:

- Spectrophotometric, where protein adsorption can be found using the Lowry (alkaline copper) assay; [185]

- 1-dimensional polyacrylamide gel electrophoresis (1DGE) where only a few proteins can be viewed at any one time owing to the lack of standards;

- 2-dimensional gel electrophoresis (2DGE), where a hundred to a thousand proteins can be realised; [186]

- Mass spectrometric analysis can be carried out using matrix-assisted laser desorption ionisation or electrospray ionisation mass spectrometry (MALDI-MS and ESI-MS). For example, [187] present the application of mass spectrometry for protein analysis by gels. This occurs due to the gel separated proteins by the generation of peptide fragments from an electro elution technique, the identification of peptides for mass fingerprinting can then be realised and it was reported that there is potential to analyse peptides in the sub-p mol concentrations was capable. [188]

1.5.2.2 MINIMUM INHIBITORY CONCENTRATION

The minimum inhibitory concentration (MIC) shows the lowest concentration at which an antimicrobial agent will inhibit the growth of a microorganism. [189] The method is well established for the investigation of future antimicrobial agents such as metal nanoparticles. [190,191] Typically, the antimicrobial agent is diluted in a liquid solution where a series of concentrations are made. The series of concentrations are then inoculated with a standard

number of known organisms. The lowest concentration that inhibits growth represents the MIC. Numerous authors have used this method in screening novel antimicrobial agents inclusive of: Zeng *et al.,* [192] Qi *et al.,* [193] and Pal *et al..* [194]

One method that is closely linked to MIC is the minimum bactericidal concentration (MBC). This method indicates the lowest concentration by which 99.9% of microorganisms are killed by the investigated compound. The MBC is defined as the lowest concentration of the antimicrobial agent that restricts the growth of the organism when subcultured into antibiotic free media. Qi *et al.* performed an MBC on copper coated nanoparticles against chitosan coated nanoparticles and found that chitosan coated copper nanoparticles were more effective than copper alone. [193]

1.6 THE SCOPE OF RESEARCH

At the interface of a material, when introduced into any aqueous system (such as water or indeed the human body in the form of blood plasma) the process of biofouling and biofilm development begins to transpire. Consequently, biofouling remains to be persistent for any user faced with the problem. The biofouling problem is one that has been tenacious throughout the ages and as research evolves, a better understanding of the multi-facets to the problem can be better understood. For instance, it is already known that organisms proliferate on a given substratum in order to continue life and evolve in a natural fashion. But, how organisms achieve this and what defines a suitable surface for enticing this settlement and proliferation is still very much unknown. More importantly, how can these effects be prevented in the initial phases and the subsequent developments not be encountered – these are defining topics the thesis aims to answer.

Consequently, the aim of this thesis is to develop a novel antifouling material suitable for the prevention of biofouling in the initial stages. With the objective of reducing the cost of ownership of sensor systems in the environment this thesis seeks to study a variety of materials that could be applied to sensors in a variety of applications.

The Objectives of the thesis are to:

- Deliver an antifouling material suitable for coating a range of substrates or systems when introduced into an aqueous interface.
- Study the factors that affect the anti-fouling characteristics of plasticisers from different chemical groups;
- Study the doping of polymer and sol-gel substrates with anti-fouling agents;
- Design and characterise Nanoparticle-based anti-fouling agents;
- Test and characterise the antifouling materials in the natural environment.

2

Materials &

Methods

2.0 INTRODUCTION

This thesis has been based on the development of materials suitable for the resistance of fouling in the initial stages in prevention of the subsequent proliferation of more advanced stages of biofouling. Consequently, the studies carried out within this chapter detail the experimental stages used throughout the thesis concerned with material development and analysis.

2.1 PLASTICIZED PVC

All PVC polymer preparations and techniques involving the screening of the plasticized PVC thin films for evidence of biofouling have been detailed.

2.1.1 MATERIALS AND CHEMICALS

Plasticizers listed in Table 2.1 used throughout, were all obtained from Scientific Polymer Products Inc ©, Ontario, New York. Poly (vinyl chloride) (PVC) M_w80,000, tetrahydrofuran (THF), sterile phosphate buffer (pH 7.2) and acridine orange were all purchased from Sigma-Aldrich. Water (HPLC >98%) was obtained from Labscan, Ireland, absolute ethanol (>98%) from Cooley Distillery, Co. Louth, Ireland, chloroform (>99%) from Fisher Scientific, Ireland, glacial acetic acid (>99%) from AGB Scientific, Ireland, toluidine blue from Avonchem LTD, UK and sterile nutrient broth from Oxoid, UK. All chemicals were used as received without further processing. All aqueous solutions were prepared from Milli-Q reagent water (Millipore Corp), 18 MΩcm.

2.1.1.1 PVC THIN FILMS
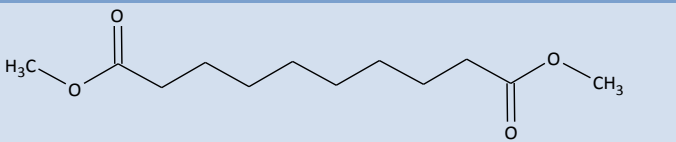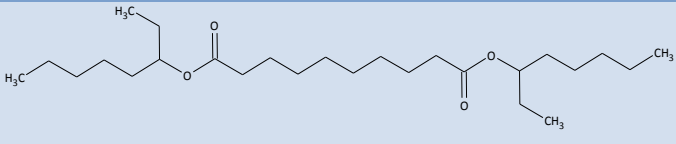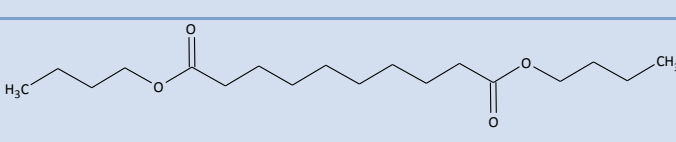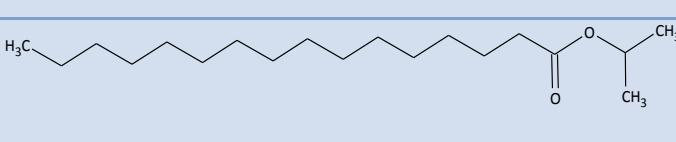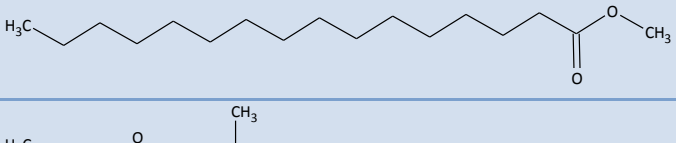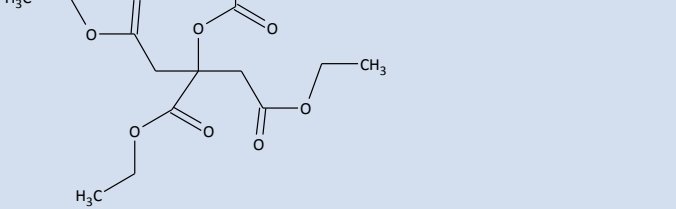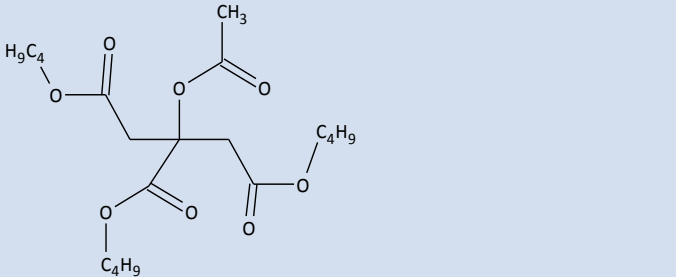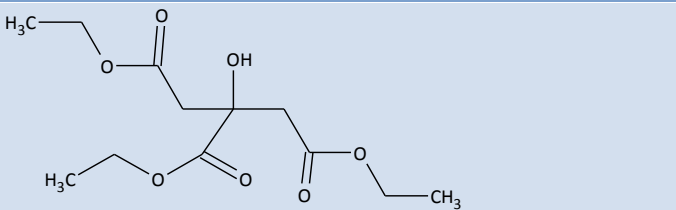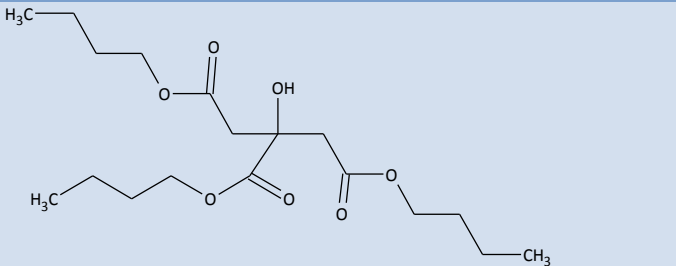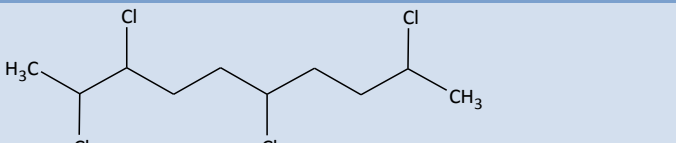
A polymeric solution containing PVC was prepared for the different groups of plasticizers used within the study. This was achieved by adding 5% w/v PVC and 5% w/v of each plasticizer to each PVC polymeric solution dissolved in THF. The polymeric solutions were stirred in sealed sample jars until all components had fully dissolved.

The polymeric solutions were then individually coated on to pre-cleaned glass substrates (75 mm x 25 mm), using a spin coating method described herein. The glass substrates were pre-cleaned with acetone submerged in an ultrasonic bath for 15 min. They were then wiped clean with fibre-free wipes (Kimcare medical wipes, UK) that had been previously soaked in the same solvent. [138]

Using a spin coater (Chemat Technology, Europe), the plasticized PVC polymeric solutions were spin coated on to the pre-cleaned glass substrates using a 1000 rpm for 3 s gradient ramp and then ramped to 3500 rpm for 15 s programme. All polymer thin films were optically clear when measured using UV-visible spectrophotometry (UV-vis, Cary-50, UK) in the range of 200 – 800 nm, using air as a reference, Table 2.1.

Table 2.1: Showing plasticizer name, abbreviations used throughout the chapter, CAS numbers, molecular weight (M_w) and boiling point (BP).

Name and abv	Structure	CAS	M_w	BP (°C)
Di(2-ethylhexyl) adipate (DEHAd)		103-23-1	371	224
Diisobutyl adipate (DIBAd)		141-04-8	258	154
Di(n-heptyl, n-nonyl) adipate (DnHnNAd)		68515-75-3	370	224
Dicapryl adipate (DCAd)		108-63-4	371	211
Diisononyl adipate (DINAd)		33703-08-1	399	233
Di(tridecyl) adipate (DTDAd)		16958-92-2	511	282
Diisooctyl azelate (DIOAz)		26544-17-2	413	235
Diisodecyl azelate (DIDAz)		28472-97-1	327	225
Dimethyl azelate (DMAz)		1732-10-1	216	156
Di(2-ethylhexyl) azelate (DEHAz)		103-24-2	413	282
Di-n-hexyl azelate (DnHAz)		109-31-9	356	282

Name	Structure			
Dimethyl sebacate (DMS)		106-79-6	230	142
Di(2-ethylhexyl) sebacate (DEHS)		122-62-3	427	248
Dibutyl sebacate (DBS)		109-43-3	314	186
Isopropyl palmitate (IPP)		142-91-6	299	160
Methyl palmitate (MP)		112-39-0	270	137
Acetyl triethyl citrate (ATC)		318	318	297
Acetyl tri-n-butyl citrate (ATBC)		77-90-7	402	327
Triethyl citrate (TEC)		77-93-0	276	294
Tri-n-butyl citrate (TnBC)		77-94-1	360	325
Chloroparaffin, 40% Cl (CLP$_{40}$)		63449-39-8	N/A	N/A
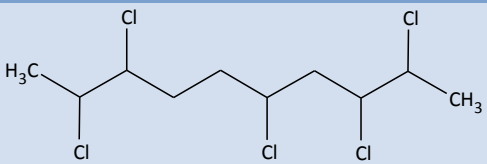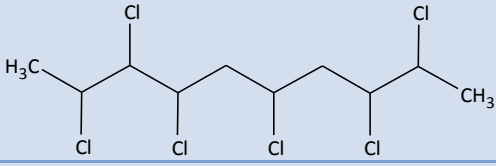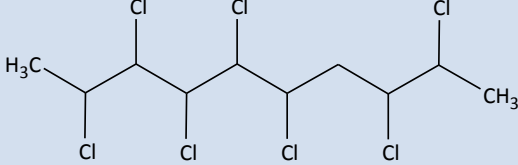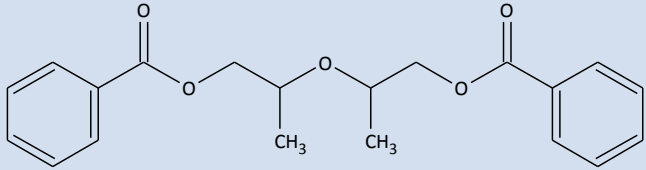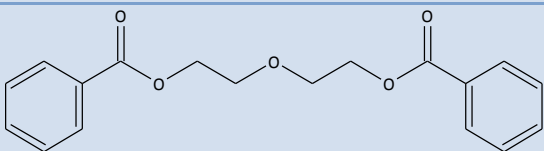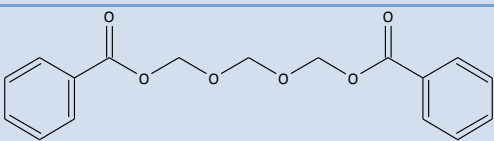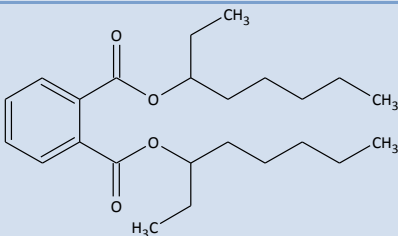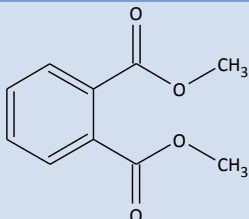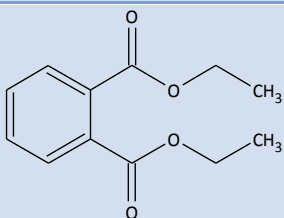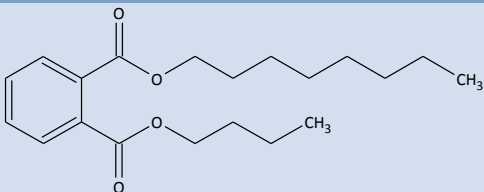
Chloroparaffin, 50% Cl (CLP$_{50}$)				
Chloroparaffin, 60% Cl (CLP$_{60}$)		108171-26-2	N/A	N/A
Chloroparaffin, 70% Cl (CLP$_{70}$)		63449-39-8	1000	N/A
Dipropylene glycol dibenzoate (DPGDB)		27138-31-4	342	232
Diethylene glycol dibenzoate (DEGDB)		120-55-8	314	240
Polyethylene glycol 200 dibenzoate (PEGDB)		9004-86-8	408	217
Di(2-ethylhexyl) phthalate (DEHP)		117-81-7	390	350
Dimethyl phthalate (DMP)		113-11-3	194	284
Diethyl phthalate (DEP)		84-66-2	222	302
Butyl octyl phthalate (BOP)		84-78-6	334	210

Figure 2.1 demonstrates the steps involved in the preparation of the plasticized PVC thin films. The spin-coated PVC glass substrates were introduced into a substrate holder and then transferred to a laboratory based freshwater tank for a 7 d test.

Figure 2.1: Schematic showing the plasticized thin film process from polymeric solutions toward final thin film membranes.

2.1.1.2 LABORATORY TANK SETUP

An environmental flow-through tank system with 240 L/min water exchange was setup in order to deploy and test developed materials as shown in Figure 2.2. The system was aerated constantly with access to natural light and ambient temperatures. Both pH (Carl Stuart Limited, Advanced Applied Tech, Ireland) and dissolved oxygen (DO; YSI ProPlus, UK) measurements were recorded by direct immersion in each of the tanks, where an average was calculated over the duration of the test for pH and DO.
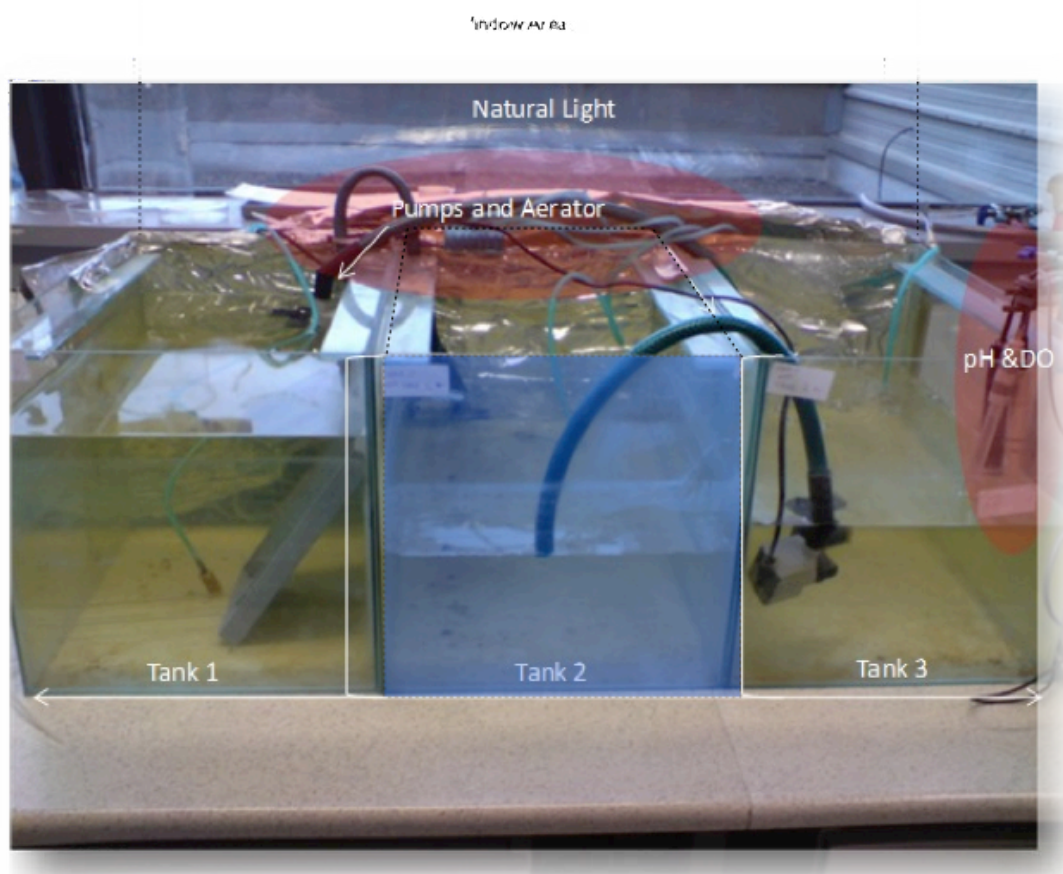
Figure 2.2: Photograph showing 240 L flow through tank system used throughout the laboratory tank studies exchange of 8 L / min exchange between each tank.

Three 80 L standard fish tanks (Aquatics online, UK) of rectangular dimension (640 x 1664 x 500 mm) were situated side by side. Water pumps (Eheim, UK) with tubing (diameter 15 mm x length 50 mm) were positioned in each tank to create an exchange feature through the whole system. Aeration was created through the use of an air pump (Rena Air Pump, UK) with airstone attachments (Biorb, UK) in each tank that was balanced to achieve a DO reading representative of the environmental sampling site it was taken from. The tanks were left to condition for a 4 d period and were stabilised for flow and DO before the introduction of any test substrates.

2.1.1.3 ENVIRONMENTAL SAMPLING SITE

The test tanks were filled with a representative sample of freshwater sampled from a freshwater river source in Dublin, Ireland. The water sample (b) was taken at the river Tolka, Griffith Park, Dublin, Ireland. The site has been displayed in Figure 2.3.

**Figure 2.3: Satellite map of Griffith Park, Dublin, Ireland of (a) glass deployment site [53°22'23.68",
-6°15'42.25"] and (b) water sampling site [53°22'11.59", -6°16'5.47"] with the arrow indicating river
Tolka into Dublin Bay.**

The site is described as clear flowing with a pH of 8.3 and dissolved oxygen content of 10.5 mg/L and these rates were mimicked in the laboratory tanks where possible (pH 8.1 and DO 11.0 mg/L) where the study continued until these parameters were lost. The sample site was then used as a dedicated deployment site shown in Section 2.5.1, which was used to deploy the glass panel developed later in the thesis.

2.1.2 PHYSICAL CHARACTERISATION OF MATERIALS

Characterisation of the materials was performed in order to determine surface properties and differences each plasticized PVC thin film exhibited. A series of measurements were performed using scanning electron microscopy (SEM), atomic force microscopy (AFM) and contact angle measurements (CA).

2.1.2.1 SEM

Surface morphological measurements were taken using a Hitachi S3400 scanning electron microscope (Hitachi, Global), where plasticized PVC thin films were detached from the glass substrate and reattached to 22 mm carbon SEM tabs. Analysis was performed varying working

distances from 5 – 25 mm utilising accelerating voltages from 5 – 20 kV working variable pressures.

2.1.2.2 AFM

AFM examinations were performed with a commercial AFM (Dimension 3100 AFM, UK using a Nanoscope IIIa controller, equipped with a phase imaging extender Digital Instruments); this was operated in tapping-mode atomic force microscope (TM-AFM), using standard silicon tips (Tap300, Budget Sensors, Romania) with 42 N/m nominal spring constant and 330 kHz nominal resonance frequency. All images were recorded in air at room temperature at a scan speed of 1–2 Hz. The background slope was resolved using first or second order polynomial functions. No further filtering was performed. Roughness measurements were taken across the plasticizer groups of the highest and lowest branched molecules within each group.

2.1.2.3 CONTACT ANGLE

Contact angle measurements were taken using a sessile drop method (Artray and Navitar camera with FTA32 video 2.0 data log software, UK). Measurements were taken through the analysis of sitting drops upon the plasticizer doped PVC thin films through automatic drops of HPLC grade water ($n = 10$), with a range of 10–2000 mN/m, resolution 0.2%. The drop was released from a 25-gauge 10 mL hypodermic needle where all contact angles are quoted in degrees (°) and each sample was photographed for each polymer treatment at room temperature.

2.1.2.4 SURFACE ACTIVITY STUDIES

Determination of plasticizer availability and thus the surface activity of each thin film was carried out using a Perkin-Elmer FTIR (GX-FTIR, UK) instrument. The plasticised PVC samples were scanned (16 scans/min at 0.5^{-1}) with a reference background of PVC in order to isolate the plasticizer characteristic bands. Samples were immersed in ultra-pure water over a 1-week period thus ascertaining the plasticizer leaching effects from the internal PVC thin film matrix. This was achieved by monitoring the characteristic IR-bands linked to the plasticizers, which are depicted in the figures accordingly. Temperatures remained constant (20 °C) and were representative to the laboratory tank study as possible. A weight study was performed in tandem observing the level of weight attributed to total plasticizer loss, which was then deducted from the overall mass.

2.1.3 BIOLOGICAL ASSESSMENT OF MATERIALS

A biological assay was devised and used to quantify the level of bacterial adhesion upon one group of plasticized PVC thin films. Minimum inhibitory concentration measurements were performed by Noeleen Loughran and Amy Harrington, DCU.

2.1.3.1 RETENTION ASSAY OF GRAM NEGATIVE AND GRAM POSITIVE MICROORGANISMS

A retention assay was used to investigate the level of microorganism stability on a given substrate. This was achieved through the use of a gram negative and gram positive bacterial strain.

Sterile nutrient broth (Oxoid) was inoculated with a single colony of either *Escherichia coli* (ATCC 25925) or *Staphylococcus aureus* sp. (ATCC 25923) and incubated at 37 °C overnight in an orbital shaker (Gallenkamp). The culture was then placed in sterile centrifuge tubes and centrifuged (Eppendorf 5810R) at 5000 rpm for 10 min at 25 °C. The supernatant was removed and the cell pellet resuspended in sterile Ringers solution (Oxoid) and centrifuged at 5000 rpm for 10 min at 25 °C, and repeated to remove any remaining broth. The cell pellet was finally suspended in Ringers solution and adjusted until an optical density of 0.1 absorbance units (AU) at 600 nm was achieved – giving a cell suspension of approximately 10^8 colony forming units per mL.

S. aureus (Gram positive) and *E. coli* (Gram negative) were chosen to conduct the pure culture studies as they are typically used to assess bacterial adhesion on modified polymeric surfaces. [195,196] [197] The test materials were sterilized (germicidal Ultra-Violet light, 1 h) in order to prevent side polymerisation and degradation reactions, after which levels of bacterial retention were evaluated.

The test materials were removed by sterile forceps from culture and rinsed twice with sterile phosphate buffer pH 7.2 (Sigma Aldrich, Ireland), then stained with 0.1% (w/v) acridine orange (Sigma Aldrich, Ireland) for 2 min and rinsed with the buffer when complete. Imaging was performed on a Leica microscope with magnifications of 63 X. The images were analysed using Image J software and plugins. [198] To analyse the images, random grid reference numbers were obtained and using 10 grid references, cells contained in each reference were then counted and recorded.

2.1.3.2 STATISTICAL ANALYSIS OF PURE CULTURE ASSAY

Images were processed by Image J software, [198] where bacterial cells were counted from randomly chosen grid positions. The averages were obtained and processed. Statistical analysis was conducted on the values obtained for the retention of bacterial cell counts upon a surface. Analysis was performed with SPSS (version 15) statistical software. The non-parametric Kruskal–Wallis test was used to assess the data obtained from both bacterial species. This type of statistical test allows the group of means of the retention of bacteria to be analysed for their ranking of group means. The Kruskal-Wallis test was performed on the ranked data where ANOVA could not be used due to the data sometimes being very far from normally distributed.

2.1.4 BIOFOULING CHARACTERISATION

Within this work, a series of biofouling-based assays were developed to assess the overall performance of the test materials. These tests were all conducted following a 7 d exposure to freshwater and then assessed accordingly.

2.1.4.1 SCANNING ELECTRON MICROSCOPY

Surface analysis of adhered microorganisms and cells of the washed thin film samples was carried out using a Hitachi S3400 SEM. Accelerating voltages of 5–15 keV with secondary electron (SE) detection was used, varying the working distances from 5 to 10 mm under variable pressure vacuum. Samples were prepared ($n = 9$), by cutting 2 mm × 2 mm samples, peeling them from the glass substrates and then attaching them to carbon SEM tabs. Analysis was then performed detailing the build-up of residual material adhered to the surface of the thin films.

2.1.4.2 MASS ASSESSMENT

Each polymer sample was weighed before and after immersion into the tanks to ascertain any changes in mass (% mass change). Samples, following exposure, were rinsed with Milli-Q water (15 mL x 3) to ensure un-adhered material was removed, such as particulate matter, and allowed to dry in air (covered from airflow) where the weight remained constant at room temperature. A subtraction of weight of the glass slide with phthalic ester doped PVC thin film per sample before and after was carried out and then a subtraction of plasticizer loss (where data was obtained from the IR leaching data) was factored giving a mean mass increase result.

2.1.4.3 GLYCOCALYX (SLIME TEST)

Glycocalyx production was evaluated using a series of fixation and staining techniques. Slime production was measured on the test material that was attached to the sol-gel surface only. The slides were washed twice using a Pasteur pipette with 1 mL of sterile Milli-Q water prior to staining. The slime was initially exposed to Carnoy's solution (absolute ethanol, chloroform and glacial acetic acid in a 6:3:1 v/v ratio) for a 30 min period. The solution was then decanted and a 0.1% v/v toluidine blue was added to stain the biofilm present on the polymers for 1 h. The excess stain was decanted off and the polymers were rinsed twice with Milli-Q water (3 mL) using a Pasteur pipette. NaOH (0.2 M) was added and heated to 85 °C for 1 h. Each sample was allowed to cool to room temperature and optical density was measured at 590 nm (Cary 50 UV-visible spectrophotometer, UK). [199]

2.2 NANOPARTICLE SYNTHESIS

The work contained within this section details the chemical synthesis techniques required for the nanoparticle synthesis shown in Chapter 4. The initial focus of nanoparticle synthesis relates to an optimisation method, investigating reagents and their effects within a reaction. After, a method was developed (using ethylene glycol) creating a range of metal nanoparticles across period four of the periodic table, details of which are described here.

2.2.1 MATERIALS AND CHEMICALS

Sodium borohydride ($NaBH_4$), ethane-1,2-diol (EG), polyvinyl pyrrolidone (PVP), metal salts (Table 2.2), poly(sodium 4-styrenesulfonate) (PSSS), trisodium citrate, ascorbic acid and were all obtained from Sigma Aldrich and were used without further purification. A modified reflux with injection port was used as an experimental setup. Milli-Q reagent water (Millipore Corp), 18M Ω cm was used and has been highlighted where appropriate. Metal salts used throughout the thesis are shown in Table 2.2, each was purchased from Sigma Aldrich, Ireland and used without further purification.

Table 2.2: Table showing metal salts used throughout the nanoparticle synthesis with CAS numbers, order numbers and prices from Sigma Aldrich, Ireland.

Metal Salt and Chemical Name	CAS number
Scandium Chloride	10361-84-9
Titanium Chloride	7705-07-9
Vanadium Chloride	7718-98-1
Chromium Chloride	10025-73-7
Manganese Chloride	7773-01-5
Iron Chloride	7705-08-0
Cobalt Chloride	7646-79-9
Nickel Chloride	7718-54-9
Copper Chloride	7447-39-4
Zinc Chloride	7646-85-7
Gallium Chloride	13450-90-3
Germanium Chloride	10038-98-9
Selenium Chloride	7791-23-3
Silver Nitrate	7761-88-8
Gold Chloride	27988-77-8

2.2.1.1 INITIAL SILVER NANOPARTICLE STUDIES

A synthesis was adapted from a procedure developed by Aherne *et al.*, it was found that a rapid and reproducible seed-based method could be obtained. The procedure begins with the use of PSSS seed solution containing silver seeds. The seed solutions allow the rapid growth of crystal surfaces and are used as a shape to template particles. The "seed-mediated" growth pathway allows for a much slower nucleation process, whereby they can be grown into larger particles of a particular morphology or habit. Aqueous trisodium citrate (5 mL, 2.5 mM), aqueous PVP (0.25 mL, 200 mg/L), and aqueous $NaBH_4$ (0.3 mL, 10 mM – requires fresh solutions) were all mixed and stirred constantly at a rate of 300 RPM. An aqueous solution of silver nitrate (5 mL, 0.5 mM) was dropped into the stirring solution at a rate of 1 mL/min. The solution remained a bright yellow colour and was stable with no aggregation throughout the synthesis.

A beaker equipped with magnetic stirring bar was used where moderate stirring was applied (150 rpm). A 5 mL Milli-Q water was added to the beaker, followed by ascorbic acid (100 µL, 10 mM) and various quantities of seed solution, followed by aqueous $AgNO_3$ (3 mL, 0.5 mM) at a rate of 0.5 mL/min. Following the reaction, of which various colours were produced, a stabilisation agent was added which could then be diluted as required.

2.2.1.2 AGGREGATION STUDIES

Aggregation studies were carried out on the samples of silver nanoparticles in order to quantify a suitable level of protecting agent to be used throughout the synthesis. Silver nanoparticles were synthesised as given in Section 2.2.1.1. PVP was made up in the following concentrations: 0.3, 0.1, 0.05, 0.04, 0.03, 0.02% w/v and a NaCl (0.5 M, 1 mL) was added to each and shaken for 1 min. Following this, an observed effective limit of aggregation proceeded using NaCl, the results of which can be found in Chapter 4, Section 4.2.1.3.

2.2.1.3 NANOPARTICLE SYNTHESIS IN ETHYLENE GLYCOL

Following initial studies with the use of silver nitrate as a precursor for the formation of nanoparticles, a reproducible method was performed using ethylene glycol as a joint solvent and protecting agent against aggregation.

MNPs were synthesised using a modified polyol reduction method,[200] where a 10 mM solution of $NaBH_4$ was made up in ethane-1,2-diol (pH 7.0) as a stock reducing agent, all at ambient temperature. A 0.5 mM solution of metal salt was prepared with ethane-1,2-diol prior to any reflux synthesis, and each can be found in Table 2.2

A protecting agent of PVP was made up to 0.1% w/v concentration. All reactants were introduced in the following order drop-wise and refluxed at 160 °C for a 24 h period; metal salt (15 mL), $NaBH_4$ (2.5 mL), PVP (2.5 mL). Colour changes were observed across each MNP solution indicating a reaction had taken place, Table 2.3.

Table 2.3: Relative colour changes exhibited from each metal nanoparticle synthesis using the ethylene glycol method.

Metal Nanoparticle	Colour observed in solution
Sc	Green
Ti	White
V	Light Green
Cr	Blue
Mn	Pink
Fe	Brown
Co	Red
Ni	Blue/Green
Cu	Red
Zn	White
Ga	White
Ge	Red
Se	Yellow

2.2.2 NANOPARTICLE CHARACTERISATION

This section of the thesis deals with the methods involved with the characterisation of synthesised metal nanoparticles. A series of microscopic and spectroscopic techniques are described here.

2.2.2.1 UV-VISIBLE SPECTROSCOPY

To study the optical properties of the nanoparticles, a series of UV-vis measurements were taken across each of the colloidal nanoparticle solutions. A 2 mL aliquot of the MNP solution was added to a 1 cm path-length quartz cuvette and scanned at wavelengths from 200-800 nm (Cary 50 UV-visible spectrophotometer). Examples of nanoparticle spectra can be found in

Figure 4.3, *vide infra* (Section 4.2.1.2) where the colour of solution was compared to the absorption spectrum obtained.

2.2.2.2 MICROSCOPY OF METAL NANOPARTICLES

The morphology pertaining to nanoparticle shapes was studied by FESEM in TEM mode using a Hitachi S5500 system. One droplet of the aqueous phase containing MNPs was placed on a copper grid of 400 mesh with carbon film. The sample excess was removed by blotting with a filter paper until all residues had been removed.

2.2.2.3 PARTICLE SIZE DISTRIBUTIONS (DYNAMIC LIGHT SCATTERING – (DLS))

Nanoparticles were characterised in terms of size and their size distribution by DLS using the Malvern Zetasizer Nano ZS (Malvern Instruments Inc., Southborough, MA, USA). Measurements of size and polydispersity index (PDI) were made for freshly synthesized MNPs (prior to purification), for purified nanoparticles, and for resuspended nanoparticles. In all cases, a volume of 1.3 mL of each sample at a concentration of 0.3 mg/mL was placed in a polystyrene cuvette and the measurements were performed at 25 °C. The viscosity and refraction index was set to those specific to water (Dispersant RI:1.330 and Viscosity cP:0.8872). Following MNP characterisation, the MNPs were isolated from solution by centrifugation (Ependorf), performed at 13000 rpm for 30 min at 4 °C. The MNPs could then be doped into a polymer solution, before being spin-coating onto glass test substrates.

2.2.2.4 ENERGY DISPERSIVE X-RAY ANALYSIS (EDX)

Elemental composition measurements of the metal nanoparticles were achieved using an EDX analyser (IncaEnergy, Oxford Instruments, UK) A series of measurements were taken as spot target measurements with the following conditions: Working distance 10 mm, accelerating voltage of 20 kV and beam current of 35-50 uA, sensitivity values >0.1% were achieved for elements heavier than carbon.

2.3 NANOPARTICLE DOPED SOL-GELS

This work pertains to the descriptions in Chapter 5 of this thesis. Following the completion of the synthesis of metal nanoparticles, a sol-gel material was made to support the nanoparticles for antifouling testing.

2.3.1 MATERIALS AND CHEMICALS

Tetraethoxysilane (TEOS), 3-aminopropyltriethoxysilane (APTES), acridine orange, Luria-Bertani broth, phenol, Lowry reagent powder, Folin-Ciocalteu, bovine serum albumin (BSA), glucose and glucuronic acid were all obtained from Sigma Aldrich, Dublin, Ireland. Hydrochloric acid (HCl) was obtained from Labscan, Ireland, Ethanol from Cooley Distillery, Ireland and Milli-Q water (18Ω) was used throughout. For the biological analysis, *Escherichia coli* (E. *coli*) was obtained from the American Tissue Culture Collection (ATCC), ATC25922.

2.3.1.1 PREPARATION OF SOL-GELS

The sol-gel used within this study contained TEOS and APTES. A 12 mL aliquot of 2-ethoxyethanol was mixed with 12 mL TEOS. A 600 μL quantity of APTES was then added. Following this, 400 μL of concentrated HCl followed by 4 mL of Milli-Q water was added and left stirring for a 2 h period in ambient RT. Condensation was allowed to progress at 80 degrees for 16 h and then 3 d at ambient laboratory temperatures (22.8 °C). When the solution had formed a clear liquid, and the consistency remained constant, the reaction had ceased and was ready to be doped with the already synthesised metal nanoparticles.

2.3.1.2 NANOPARTICLE DOPING

Each of the metal nanoparticles underwent a series of washing steps using clean EG (10 mL) prior to re-suspension in the doping matrix, the sol-gel. The nanoparticles were each centrifuged (Heltich zentrifugen (Universal 320)) at 13000 rpm for 25 min at 15 °C. The supernatant was removed and the nanoparticles were washed with EG repeating this for a minimum of five times. The pellet was then extracted and re-suspended in a suitable aliquot of sol-gel already previously synthesised. This was then mixed vigorously under sonication (Clifton Sonic Bath, UK; 42000 Hz for 10 min) prior to spin coating on to glass substrates.

2.3.1.3 SPIN COATING OF METAL NANOPARTICLE SOL-GELS

The metal nanoparticle doped sol-gels underwent a coating programme suitably conveyed through the use of a spincoater (Chemat Technology); a 2 mL aliquot of each doped sol-gel was spread on to a glass substrate and spin coated using the following program; 1000 rpm for 3 s gradient ramp and then ramped to 3500 rpm for 15 s programme. The samples were then air dried (22.8 °C) and stored in microscope box holders (Kartell, Italy) until required.

2.3.1.4 SOL-GEL CHARACTERISATION

The metal nanoparticle doped sol-gels underwent a series of physical characterisations using contact angle, SEM and EDX, which have been detailed within.

2.3.1.4.1 SEM ANALYSIS

Surface morphology was carried out in triplicate using scanning electron microscopy (SEM) using a Hitachi S-3400 instrument. Samples were prepared by spin coating a 2 mL aliquot of the sol-gel solution directly to carbon SEM tab. Accelerating voltages of 5-20 keV was applied to the surface, varying the working distances from 5 – 10 mm. Samples were sputter coated in gold, energising for 2 min intervals prior to any analysis.

In order to determine the size distributions, Image J was used to characterise the nanoparticle sizes. The program enables thresholding of images, with an array of plug-ins for size determination. The watershed plug-in was used occasionally to separate close nanoparticles prior to any analysis. Histograms of the average diameter were obtained and fit into Gaussian distributions, for three separate spots on each FESEM grid, with fits performed for each sample. Minima of 50 particles were counted for each different metal nanoparticle and the data are included in Chapter 4, Figure 4.7, *vide infra*.

2.3.1.4.2 CONTACT ANGLE ANALYSIS

Contact angle analysis was performed on each of the metal nanoparticle doped sol-gels, thus determining the wettability of each of the substrates. The advancing contact angle was measured using a sessile drop technique with an Artray and Navitar camera with FTA32 video 2.0 Data Log Software. A 10 mL syringe with 25-gauge hypodermic needle was used. 2.7 µL of ultra-pure water was used. Three drops of HPLC grade water (LabScan) were photographed for each treatment of the sol-gel at ambient temperature (22 °C), which were then repeated in triplicate.

2.3.1.4.3 EDX ANALYSIS

Identification and characterisation of the sol-gel surface was carried out using EDX (Inca Energy, Oxford Instruments, UK) was carried out in triplicate. A series of measurements were taken as spot target measurements with the following conditions: working distance 10 mm, accelerating voltage of 20 kV and beam current of 35-50 uA, sensitivity values >0.1% was achieved for elements heavier than carbon.

The assessment of the concentration of nanoparticles throughout the sol-gel matrix was investigated using freeze fracturing of the sample by liquid nitrogen. The spin-coated sol-gels were frozen with liquid nitrogen, by immersion for 30 s. The sample was then fractured and positioned on an SEM stub in order to analyse a cross section of the sample. Shots of the sample were then analysed through EDX, with parameters given above.

2.3.2 BIOLOGICAL ASSESSMENT OF MATERIALS

A series of biological assays were carried out to investigate the relative toxicities and efficacy as antifouling materials. Biochemical assays of protein and carbohydrate adsorption with mass and slime studies were also used.

2.3.2.1 MINIMUM INHIBITORY CONCENTRATION

Pure metal nanoparticle samples were tested against a strain of *E. coli* (ATC 25922 - Performed by Noeleen Loughran, DCU). This bacterial strain is rare and was used as an indicator tool for the level of toxicity pertaining to the material. If repeated in future, a more relevant organism should be selected for this type of experiment. A glycerol stock of *E. coli* XL10 Gold containing pGP plasmid was streaked on selective media and incubated overnight at 37 °C. A single colony was picked and 10 mL of fresh Luria-Bertani (LB) broth containing 100 µg/mL ampicillin was inoculated and incubated overnight at 37 °C with shaking at 220 rpm. 100 µL of this overnight culture was plated on appropriate selective media and 100 µL of the compound of interest was spotted and incubated at 37 °C overnight.

MNPs were centrifuged at 12,000 rpm and resuspended in pure water thus eliminating any contamination. The MNPs were then dropped at 50 µL on to the petri-dish, incubated overnight at 37 °C and then analysed using photography.

2.3.2.2 ENVIRONMENTAL BACTERIAL ENUMERATION

Before exposing the MNP doped sol-gels to the environmental freshwater sample it was important to ensure that no bacterial contamination existed upon the test substrates. The spin coated glass surfaces were subjected to a sterilisation method where germicidal ultraviolet light (254 nm) (NuAire, UK) was applied for a 24 hr period. Following sterilisation, the glass substrates were suspended in holders (in triplicate) and left in a freshwater sample (river Tolka, Dublin) for 3 days.

The test substrates were prepared for fluorescence imaging using a modified method by Peltonen *et al.,* [201] the test substrates were removed from the environmental tanks and rinsed with (2 x 5 mL) of sterile water and then stained with 0.1% (w/v) acridine orange for 2 min and rinsed again with 5 mL of sterile water. Imaging was performed using a Leica microscope with 63X magnification by Emma Weir.

Epifluorescence images of adhered bacterial cells to the test materials were analysed and counted using Image J software. [198] Obtained images were input into the Image J application and using the image analysis accessories a grid of 9 cm x 7 cm was overlaid to enumerate bacterial retention to the substrates of the outermost surface.

2.3.3 BIOFOULING CHARACTERISATION

Biofouling based assays were used to investigate the metal nanoparticle doped sol-gels in the same manner as was already developed in Section 2.1.4. Each of the metal nanoparticle doped sol-gels was screened for mass, slime, protein and carbohydrate adsorption after a 7 d freshwater environmental laboratory tank study.

2.3.3.1 MASS ASSESSMENT

Mass analysis for the nanoparticle-doped sol gels was carried out in the same manner as described in Section 2.1.4.2, *vide supra*.

2.3.3.2 GLYCOCALYX (SLIME TEST)

Glycocalyx production was evaluated as described in Section 2.1.4.3, *vide supra* and was performed on the nanoparticle-doped sol-gels in the same manner.

2.3.3.3 PROTEIN ADSORPTION ASSAY

Protein determination was performed with a modified Lowry assay, [185] using commercial reagents as specified in Section 2.1. 40 mL of modified Lowry reagent powder was made up in Milli-Q water in a separate manner. Folin-Ciocalteu's phenol solution was diluted in Milli-Q water (1:5) and remained stored until required at room temperature (RT). The glass-coated substrates were rinsed with Milli-Q water prior to analysis and then added to a 50 mL sample tube. The tubes were then filled with ultra-pure water and sonicated for 5 min (which was found to give a maximum protein extraction from the slide). Following this, centrifugation was applied at 3000 rpm for 5 min at RT (again this was optimised for a maximum extraction of protein) to remove particulates that might have been suspended in the solution following sonication. An aliquot of the sample (0.5 mL) was taken and added to a 7 mL sample tube, where 0.50 mL of Lowry reagent solution was added; this was mixed and incubated for 20 min at room temperature. Following this, 0.25 mL of Folin-Ciocalteu's phenol solution was added to the sample tube and was shaken with incubation for 30 min at room temperature. The absorbance was measured using UV-vis at 750 nm (n=3).

2.3.3.4 CARBOHYDRATE ADSORPTION ASSAY

Determination of total carbohydrate content was carried out according to a modified method first prepared by Dubois *et al..* [202] A 5% w/v phenol solution was made up in Milli-Q water and sulfuric acid (95-97%) was prepared and stored until required. The glass-coated substrates were rinsed with Milli-Q water prior to analysis and then added to a 50 mL sample tube. The tubes were then filled with ultra-pure water and sonicated for 5 min. Following this; centrifugation was applied at 3000 rpm for 5 min at RT to remove particulates that might have been suspended in the solution following sonication. An aliquot of the sample (0.5 mL) was taken and added to a 7 mL sample tube where 0.5 mL phenol solution, and 2.5 mL sulfuric acid, was added and mixed immediately. The sample tube was then incubated for 10 min at room temperature and following this for 15 min at 30 °C. After 5 min at room temperature, the absorbance was measured at 480 nm.

2.4 SUPERHYDROPHOBIC COPPER COATINGS

The work contained within this section of this material development chapter deals with the synthesis and development of superhydrophobic coatings for application to sensor.

2.4.1 SYNTHESIS OF COATING

Copper sheets (Sigma, 99.9% purity, R_a=0.3 μm) were cut into substrates of dimension 30 x 10 x 0.5 mm. The substrates were polished with a series of emery papers (Halfords, UK P2500 grit size) followed by ultrasonic degreasing in acetone (15 min) and then dried in air (overnight, (22 °C). Gold and silver chlorides were both obtained from Sigma Aldrich, Ireland.

2.4.1.1 GOLD SUPERHYDROPHOBIC COATINGS

A gold layered superhydrophobic coating was synthesised using the following details as set out by Larmour *et al.* [203] A galvanic reaction was established for gold chloride (0.05 mM) with the copper substrates and was immersed in the solution for 20 s. The substrates were then removed, washed with water using a pipette (10 x 10 mL) and blown dry with nitrogen for 2 min using a modified pipette tube. The superhydrophobic surface was then created by immersing the coated copper coupon in a 1 mM solution of $CF_3(CF_2)7CH_2CH_2SH$ in dichloromethane (DCM) for 5 min. The substrates were then allowed to air dry (in a microscope holder at 22.0 °C for 2 hr and then tested by applying Milli-Q water to the superhydrophobic surfaces using a pipette.

2.4.1.2 SILVER SUPERHYDROPHOBIC COATINGS

A silver layered superhydrophobic coating was synthesised using the following details as set out by Larmour *et al.* [203] A galvanic reaction was established for silver chloride (0.05 mM) with the copper substrates and was immersed in the solution for 20 s. The substrates were then removed, washed with water using a pipette (10 x 10 mL) and blown dry with nitrogen for 2 min using a modified pipette tube. The superhydrophobic surface was then created by immersing the coated copper coupon in a 1 mM solution of $CF_3(CF_2)7CH_2CH_2SH$ in dichloromethane (DCM; 15 mL) for 5 min. The substrates were then allowed to air dry in a microscope holder at 22.0 °C and then tested by applying Milli-Q water to the superhydrophobic surfaces

2.4.1.3 TRANSFER TO SENSOR HOUSES

The above synthesis was not practical for the application to sensor houses, and so, copper tape was purchased (3M, UK) where the tape (10.5 mm width) was applied in a series of bands around a sensor housing, which can be seen in Figure 2.4. This represents a novel feature to the work as the concept of superhydrophobic coatings has already been detailed in literature.
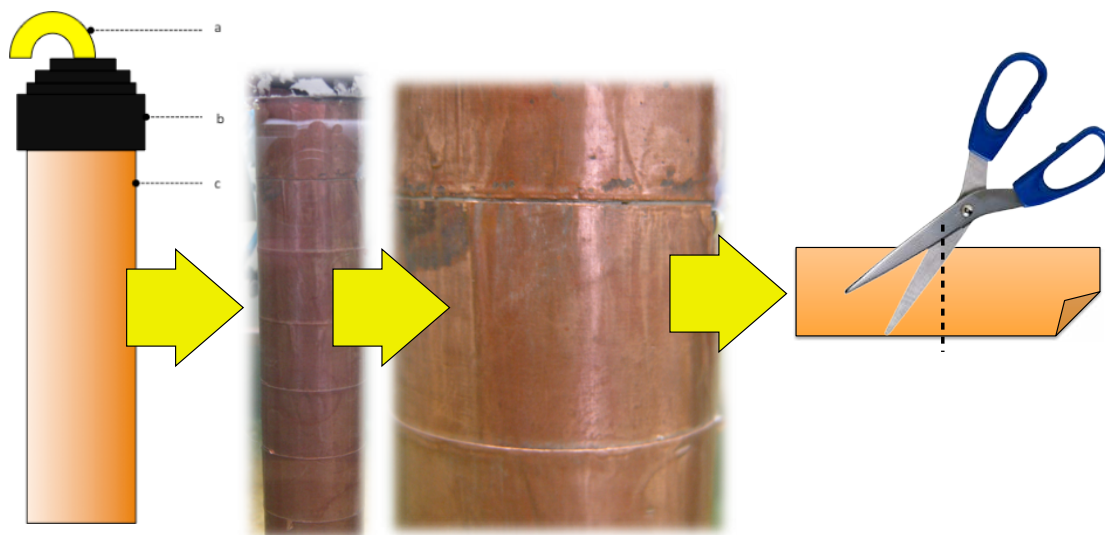
Figure 2.4: Showing sensor scheme of (a) cable, (b) head and (c) copper coated sensor housing with inset photograph showing the copper coating bands over the sensor house. Middle: whole sensor house and Right: close up of copper tape and finally, sample preparation.

The same coating procedure could then be applied for the gold and silver coated copper sensor houses. This was achieved using a measuring cylinder serving as the synthesis chamber for the superhydrophobic sensor house. Once the deployment period time expired the sensors were removed and a layer of the superhydrophobic tape was removed, cut into strips and then analysed accordingly.

2.4.2 CHARACTERISATION OF COATING

A series of characterisation techniques was carried out upon the superhydrophobic coatings. This would therefore afford the hydrophobicity and physical character of each of the coatings to be determined before any laboratory and field-testing were carried out.

2.4.2.1 SCANNING ELECTRON MICROSCOPY

Scanning electron microscopy was carried out on each of the substrates previously described. Sample preparation involved a hole punch of each substrate (solid superhydrophobic copper, and tape superhydrophobic copper) being measured. The punched samples were then attached directly to carbon SEM tabs and analysed using a Hitachi S3400 instrument.

2.4.2.2. CONTACT ANGLE ANALYSIS

Contact angle measurements were carried out on the superhydrophobic copper coated surfaces using the method described in Section 2.1.2.3, *vide supra*. The instrument software was setup to capture images over a 10 s time frame; this was due to the extreme hydrophobic nature of the material, making it difficult to capture the contact angle of the water droplet. By imposing a timeframe the user is able to capture an image of this contact point.

2.5 ENVIRONMENTAL DEPLOYMENTS OF TEST MATERIALS

Described within this section of the thesis are details of how the developed and best performing coatings underwent real environmental challenges in both fresh and marine water environments. The chapter will first introduce the methods used to test the best performing plasticized and nanoparticle materials challenged in a fresh water environment. The last part of the chapter will challenge the superhydrophobic materials that were applied to sensors and investigated for their potential as antifouling coatings.

2.5.1 DEPLOYMENT SITE (GRIFFITH PARK, RIVER TOLKA, DUBLIN, IRELAND)

A freshwater test site was picked to coincide with the previous work already performed in fresh water tank studies. Here the best performing materials were selected and doped into a PVC matrix which was then deployed for 28 d in the river Tolka, Dublin, Ireland.

2.5.1.1 TEST PANEL

An engineered glass test panel was created for the deployment of the materials described herein. A toughened glass panel (70 cm x 70 cm) was deployed in the river Tolka for a 28 d study in a region of flow shown in.

Figure 2.5: Photograph showing deployment regime where glass test panel containing the materials was put in to the freshwater environment.

2.5.1.2 MATERIALS

The test panel was coated in a range of materials that had seen good laboratory test successes. All the successful materials were based on a PVC matrix and were doped accordingly in the following concentrations, Figure 2.6.

Dopant	Concentration
DEHP	10% (w/v)
DTDAz	10% (w/v)
CLP$_{70}$	10% (w/v)
Gallium NPs	10 mg/ 100 mL
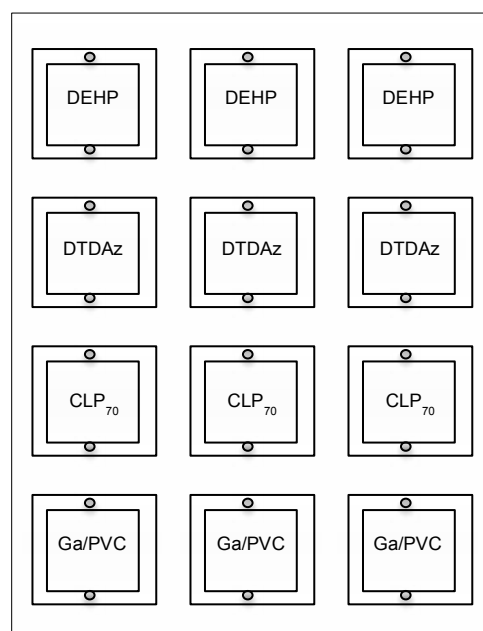
Figure 2.6: Glass panel material arrangement and table showing concentrations of dopant used in each panel square. PVC was used as the material-doping matrix in 10% w/v.

2.5.1.3 BIOFOULING ASSESSMENT

A series of biofouling assays were performed on the materials that were deployed in the freshwater system as shown in Figure 2.6. The same assays developed in Section 2.1.4 were performed without mass determination explained for mass, slime, protein and carbohydrate adsorption in Section 2.5.2.1, *vide infra*.

2.5.2 DEPLOYMENT SITE (POOLBEG DUBLIN, IRELAND)

A brackish test water site was chosen in Dublin, Ireland. Here a freshwater mouth emanating from the river Liffey, (Dublin Ireland), meets the Irish Sea. Figure 2.6 depicts the satellite image of the site where the sensor suite was deployed.

Figure 2.6: Satellite map showing (a) Poolbeg Marina deployment site [53°20'38.72, , -6°13'3.62"] above highlighted by the green arrow is the river Tolka used in previous fresh water sampling in the thesis.

Here, the samples were attached to a coupon frame (X12 slides) where the samples were deployed in the water for 2 weeks in tandem with a sensor sonde (YSI, UK) containing the following measurement parameters (conductivity, salinity, depth, temperature and turbidity). These measurements were taken alongside the study in order to measure environmental fluctuations that could influence the rates of fouling.

2.5.2.1 SENSOR SONDE PARAMETERS

A sensor sonde unit (YSI, 6920, UK, Figure 2.7) was deployed in Poolbeg Marina, Dublin, Ireland over the months of February to April 2011. The sonde was equipped with temperature, turbidity, conductivity and depth sensors. The sonde was set to take readings every 15 min over the 1-month period to compare environmental changes in the study of fouling in its initial stages.

Figure 2.7: Photograph showing YSI 6920 Sonde (a) sonde housing, (b) sensors and (c) mechanical wipers.

2.5.2.2 DEPLOYMENT OF MATERIALS

On the same test site, a substrate frame containing the superhydrophobic samples was deployed adjacently to the sonde that would measure the water readings over the same test time. Periodically, samples were taken out of the test system every two days, which were then stored in Milli-Q water in 50 mL centrifuge tubes (Sarstedt, Ireland). The samples were then measured for slime, overall mass, protein and carbohydrate adsorption as previous described in Section 2.3.2.3 and 2.3.2.4 of this chapter. Blank copper, superhydrophobic copper with silver and gold base metals were put into an engineered frame (n=9) and then suspended at a depth of 1 m, Figure 2.8.

Track of engineered Perspex plastic. Hole sizes were 5 mm for plastic screw inserts

Copper, gold and silver superhydrophobic copper randomly inserted through the engineered track held in place by plastic screws.
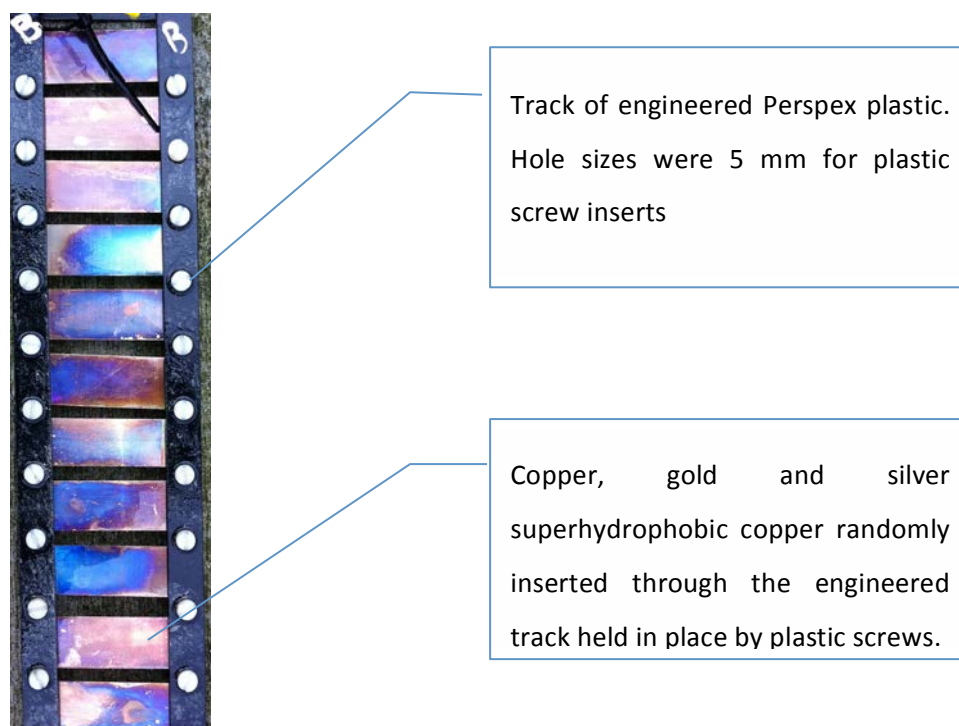
Figure 2.8: Engineered track containing superhydrophobic copper and copper blank samples.

3

Plasticized

PVC

3.0 INTRODUCTION

The use of surface coatings in the prevention of fouling dates as far back to the Phoenicians. [204] The progression of increasingly more complex antifouling coatings has been proceeded by an advance in coating design, such as foul release, insoluble biocide release, and also biomimetic design. [205] The work presented in this chapter illustrates the use of a modern everyday polymer that, in the field of biofouling, appears to have been overlooked for application in an antifouling capacity.

3.1 COATINGS

A coating is defined as a covering that is applied to a surface, usually referred to as the substrate.[206] In most cases, coatings are applied in order to improve surface characteristics such as appearance, adhesion, wettability, corrosion resistance, scratch resistance, wear resistance or fouling. Coatings involve the application of thin films of functional material and are usually applied as; solids, gases, or more commonly, as liquids.

In 1870 there were more than 300 antifouling paints registered on the market, with most of the formulations containing biocides to kill organisms via a leaching process. This was attributed to the introduction of iron ships on which copper coating caused corrosion of the iron. Following this, heavy metals were added into marine antifouling paints forming both antifouling and anti-corrosive properties. Copper is currently the most widely used biocide in antifouling paints, concentrations of which have been reported to be 10-30%, but as much as 50% has been used. Cu_2O is used at the biocide but also CuSCN and copper metal are also in use. [207] Mercury and lead have also featured as metals used in antifouling paints, both in their inorganic and organic forms. Following the second world war, the introduction of petroleum-based resins and health and safety concerns relating to organo-arsenicals and mercurial meant that copper based paints became more prevalent. Following this, chemical advances allowed future coatings to be made, one of which is well known in the modern world, as PVC.

3.1.1 PVC

PVC was discovered in the late nineteenth century, where scientists had observed the creation of a chemical gas, vinyl chloride which, when it was exposed to sunlight underwent a polymerisation reaction. It remains one of the oldest synthetic materials with the longest history in industrial production. The two most notable reports of early PVC were in 1838, by

the French physicist and chemist Henri Victor Regnault and the second was in 1872 by German Eugen Baumann. It was not until 1913, German inventor Fredrich Heinrich August Klatte took out a patent on PVC, polymerising vinyl chloride in light. It was during the 1950s companies began to produce PVC in increasing volumes and thus methods were refined for its production. Today PVC is the third largest selling commodity plastic in the world, owing to its low cost, durability and processability. [208]

PVC's uses stretch across many industrial fields ranging from construction, healthcare, automotive and packaging. The material has served as a coating material since 1932 where the first pipe coatings were introduced. This led to subsequent further developments ranging from packaging to coating medical devices with this versatile and almost chemically inert material. It remains low-cost, robust and malleable and therefore has a potential to coat most modern interfaces that are subject to fouling. Despite this, literature does not report extensive use of PVC as an antifouling matrix and therefore forms a novel impetus for this chapter of research.

In its raw form, PVC is a very brittle material and, as such, 'peels' when the adherent polymer is coated to a substrate. In order to overcome this, compounds known as plasticizers are used, improving the polymer matrix by interrupting polymer links within the network as depicted in Figure 3.1. The novel aspect of this work is governed by doping a variety of agents into the PVC matrix. Again, the question is asked whether PVC is a suitable material for this development. PVC has a plethora of suitable characteristics making it a very versatile material for the purpose of this project. It is an optically clear platform, cheaper than other polymers and can be doped with suitable agents for investigation. The novelty of this work stems from an overlooked issue, where plasticizers are almost taken for granted when incorporated within a PVC polymer matrix.

3.1.2 PLASTICIZERS

As stated in the International Union of Pure and Applied Chemistry (IUPAC) in 1951, "a plasticizer is a substance or material that is incorporated in a material, usually a plastic or elastomer, to increase its flexibility, workability or extensibility". A plasticizer may reduce the melt viscosity, lower the temperature of the second order transition, or lower the elastic modulus of the product. [209] The first recorded use of a plasticizer dates back to 1862, [210] and since then plasticizers have become an inherent part of the polymer industry. In 2003, the plasticizer market was valued at around 10 million pounds sterling (€11 million euro), with ~90% dedicated to the PVC markets. [211] Phthalates make up the dominant class of plasticizers comprising 87% of the plasticizer industry, [212] with di-2-ethylhexyl phthalate (DEHP) accounting for more than 50% of this total. [213]

Within a polymer matrix plasticizers act by interrupting the primary bonds holding the polymer together, thus forming secondary plasticizer-polymer bonds. Since these bonds are weak, so there exists a dynamic whereby the molecule attached to one site of the polymer network may be dislodged and replaced by another, Figure 3.1.
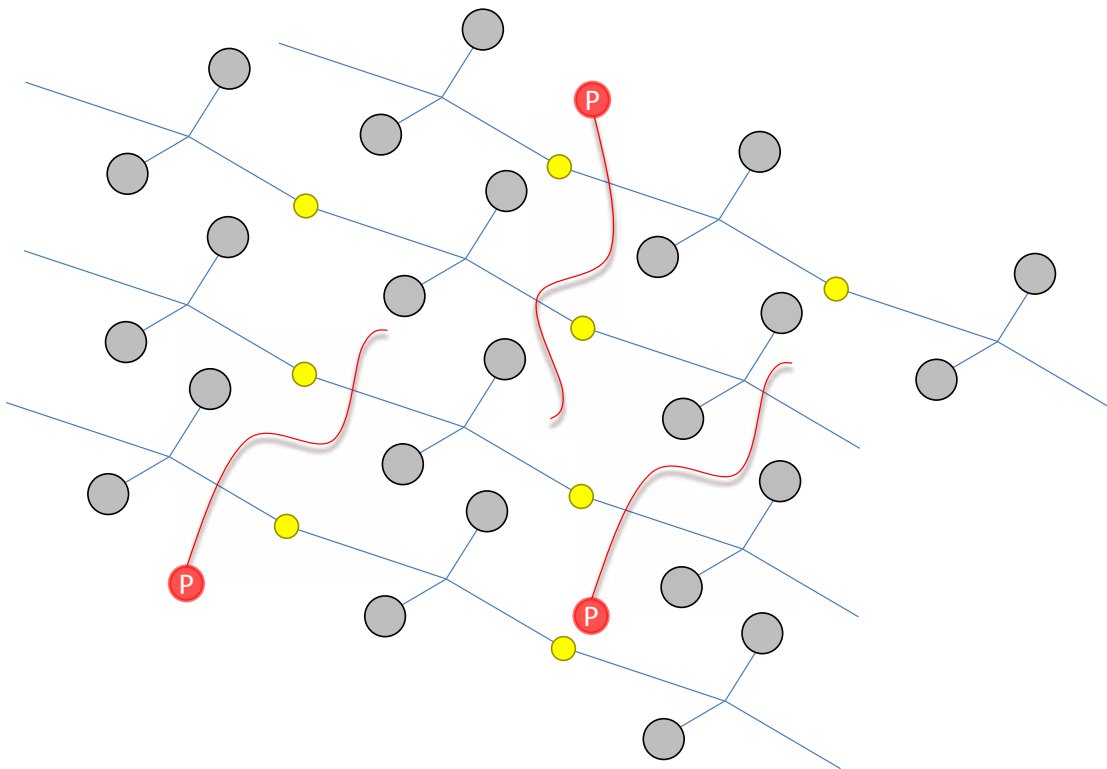
Figure 3.1: Schematic showing polymer chain links with plasticizers (P) within the polymer network an example of which is plasticized PVC.

The plasticizing efficiency of various plasticizers is thought to be a function of the organic/inorganic moiety and functional groups present in particular molecules with a bearing on chain length, molecular weight and molecule branching all change the functionability of the polymer they are contained within. [211] It is therefore known that different plasticizers will generate different plasticization effects owing to this difference in interaction with the plasticizer-polymer bonding.

The use of plasticizers in PVC could therefore be an excellent route for investigating whether the molecule improves the functionability of PVC, but forms an antimicrobial protection for the polymer coating. This forms another reason for the investigations carried out in this chapter of work.

3.1.3 AIMS AND OBJECTIVES

The purpose of this chapter is to develop a material that is optically clear i.e. suitable for transmittance but also possess antifouling protection potential, which is a directive of the project.

One way of achieving this is using plasticized PVC, which has been largely overlooked in this topic of research rendering a gap in the knowledge. Consequently, a number of research questions will be focussed on within this body of work:

1) What is the function of the plasticizer when introduced into the PVC matrix;

2) Can PVC be utilised to render a substrate fouling resistant;

3) Does the plasticizer structure afford different properties in PVC and will these properties proliferate as different antifouling responses;

4) Can a plasticizer be used to create an antifouling effect when incorporated into a PVC matrix;

5) Is the plasticizer capable of producing a toxicity factor in order to prevent biofouling and biofilm proliferation upon a given substrate?

3.2 RESULTS AND DISCUSSION

The results presented herein will address the materials in a physical characterisation section where all plasticizers are analysed for contact angle, surface roughness and morphology. Plasticizer migration studies were also performed, thus, ascertaining the surface activity that each plasticized PVC membrane might exhibit. Following this, a series of biofouling assays were performed, screening and interrogating the materials for their potential use as an antifouling material, representing substantial novelty to the field of biofouling research.

3.2.1 MATERIAL CHARACTERISATION

Each of the materials underwent a series of SEM topographical scans thus obtaining the morphological data of the plasticized PVC thin films as presented in Section 3.2.1.1, *vide infra*. Contact angle analyses were then performed to investigate the wettability of the films when introduced into a water interface, Section 3.2.1.2, *vide infra*.

3.2.1.1 SURFACE MORPHOLOGY

A series of surface morphological measurements were performed using scanning electron microscopy across each of the membranes of which has been detailed in Section 2.1.2.1. Nominal thickness was also obtained using a scratch method as described in Maata *et al.*.[214] Figure 3.2 illustrates some of the pitting behaviour that occurs when plasticizers leach from the membranes, and this has been detailed extensively in Wilkes.[208]
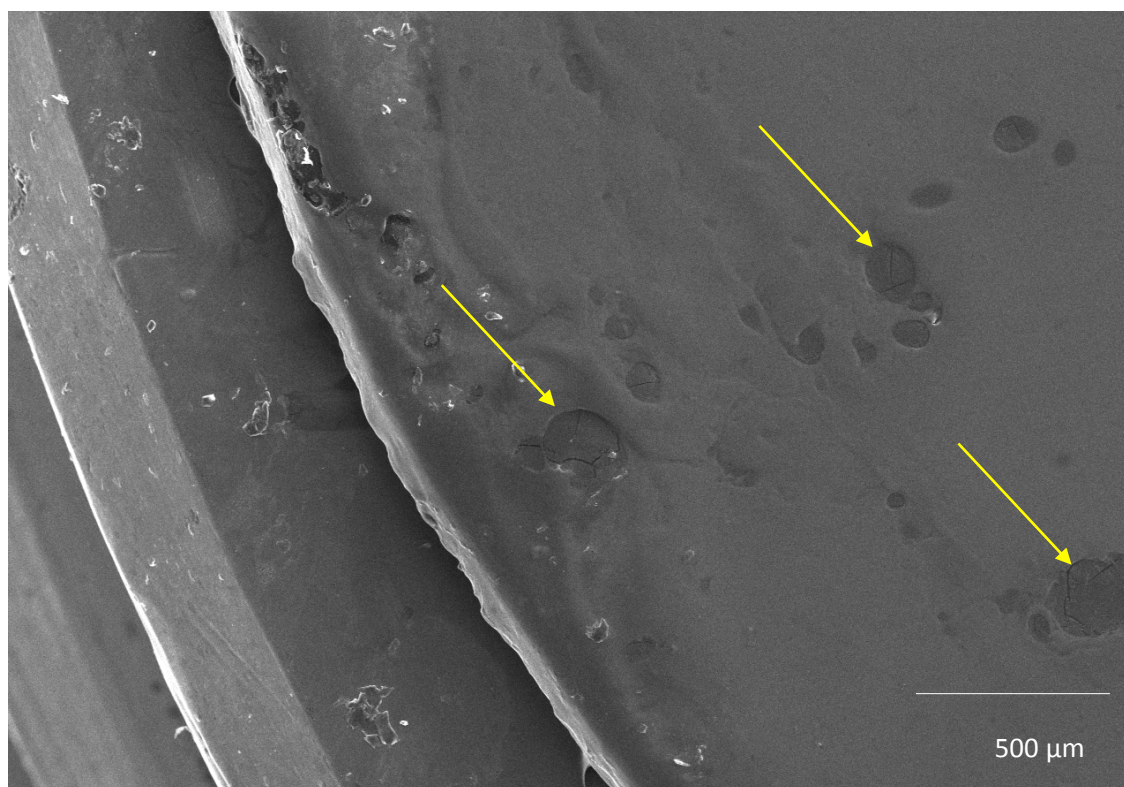
Figure 3.2: Scanning electron micrograph illustrating pitting behaviour of leached plasticized PVC, arrows indicate region of pitting.

Each of the plasticized PVC thin films showed similar surface morphologies with 'smooth' topography exemplified throughout when examined under the naked eye. However, when examined under the electron microscope there is evidence of micro topographies that present as roughness. SEM is used as a technique in this level of determination for surface morphology and topography throughout literature and the technique remains pioneering. [138] [216]

An example of smooth and pitted plasticized PVC thin films, obtained in this body of work, can be seen in Figure 3.3. In most cases, the surfaces were 'smooth' natured with similar characteristics of rippling on the surface or pitting. This has been reported to indicate that good dispersion of the plasticizer within the PVC matrix has occurred. [215] Some authors report that particles appear on the surface of plasticized PVC, owing to plasticizer migration from the matrix, [215] contrastingly, most artefacts on a given polymer surface are due to contaminants, examples of which can be seen in Figure 3.3 where the highlighted area depicts this. Other authors have reported SEM's ability to resolve molecular fillers within a PVC matrix, [217] but due to limitations in some instruments, this is not always possible unless spectroscopic techniques were to be employed.
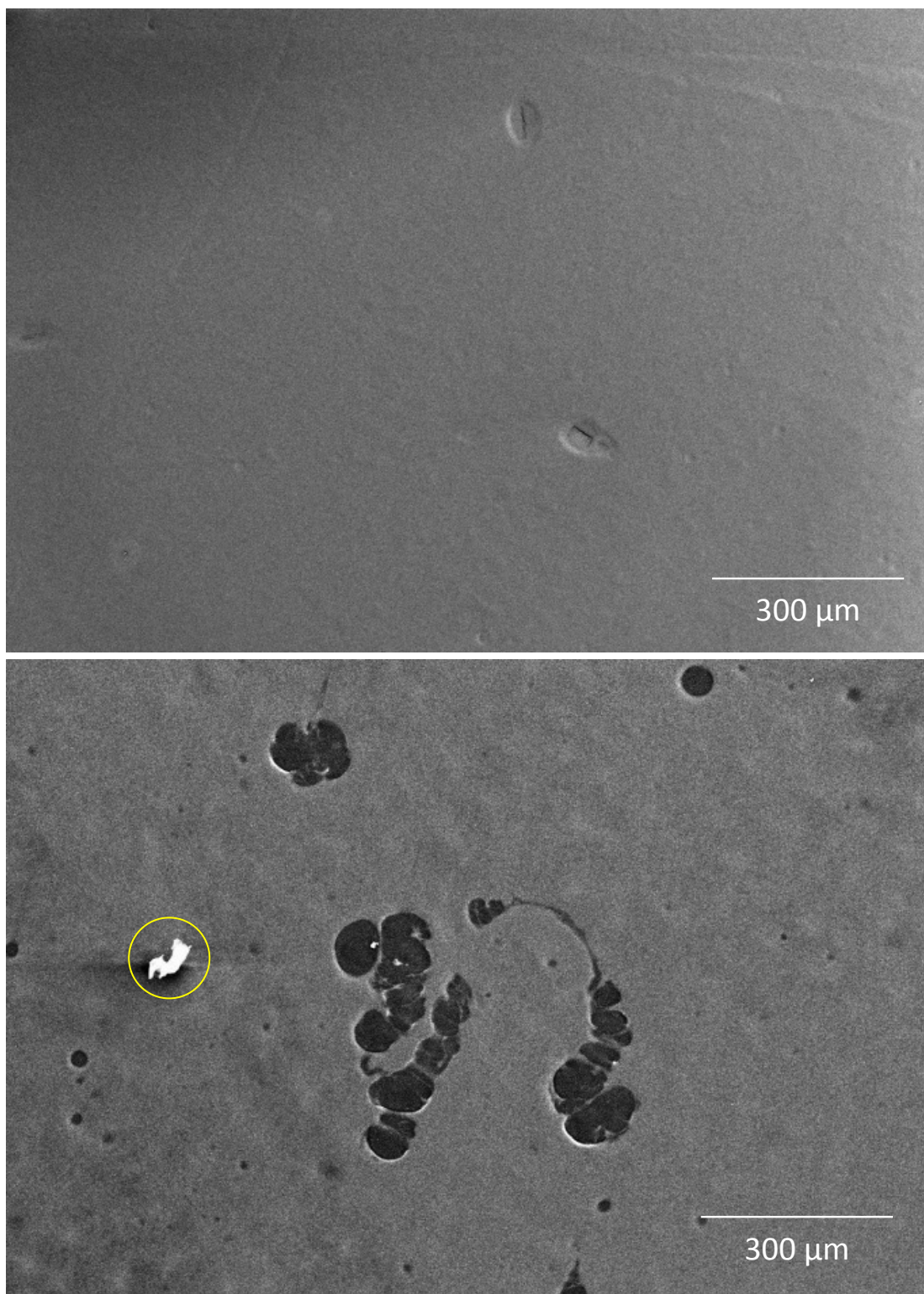
Figure 3.3: Typical scanning electron micrographs depicting surface morphology; smoothness and pitting (top) DIBAd and (bottom) DEHP, where the circle identifies the artefact upon the surface.

3.2.1.2 EFFECT OF PLASTICIZER ON WETTABILITY

Contact angle analysis was carried out on each of the plasticized PVC coatings in order to determine relative wettability, as depicted in Figure 3.4.
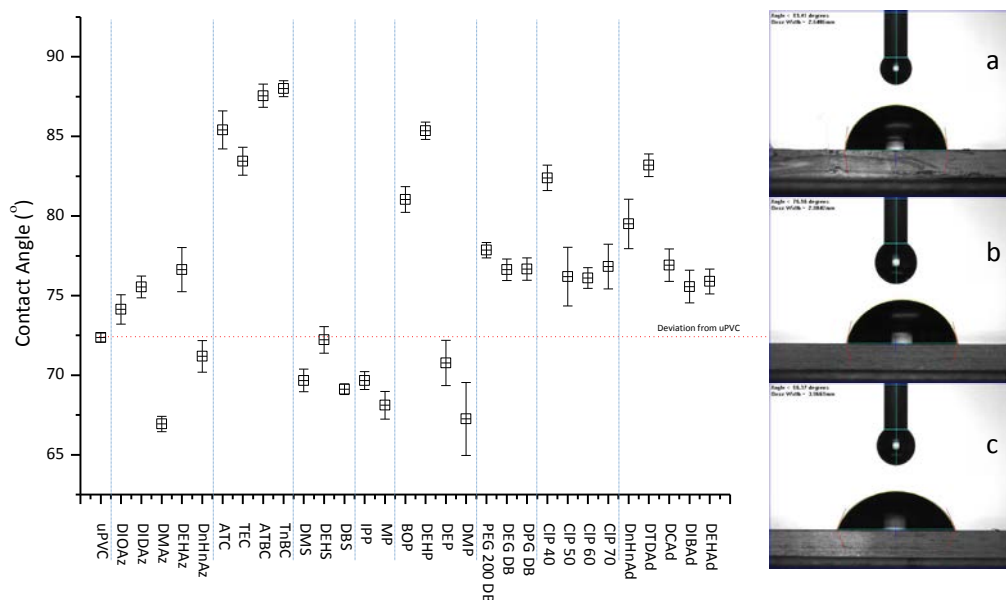
Figure 3.4: Contact angles of all plasticized PVC samples with some examples of typical contact angle photographs (a) TEC, (b) CLP$_{50}$ and (c) DMAz (n=9, ±1SD).

It was found that plasticizer concentration in PVC had an overall effect on the wettability of the solvent, in this case, water. Many authors report that for PVC without plasticization, values of ~80° can be achieved; [214,218] indeed, this is a result reflected in this body of work. Notably, most of the plasticizer groups have a decrease in wettability compared to the uPVC blank displayed in the following groups; adipates, chloroparaffins, dibenzoates and the citrate plasticizers. On closer examination, plasticized PVC samples with decreased wettability have similar underlying molecular attributes. For instance, the increased branching and longer alkyl chain substitution on the terminal plasticizer groups have, in most cases, shown decreased wettability and thus hydrophobic response to the solvent. The azelate group demonstrates clearly that higher alkyl branched plasticizers have decreased wettability: DIOAz (74°), DIDAz (75°), DEHAz (76°) where all have larger branching and side chain substitution when compared to DMAz (66°) seen in Chapter 2, Table 2.1 which possesses smaller alkyl substitution on the azelate functional group. Sanchez *et al.*, reported that contact angle increased when different glycol plasticizers were introduced in a polymer matrix. They found that low molecular weight plasticizers produced a decrease in wettability when compared to higher molecular weight

plasticizers wettability decreased.. The authors however, did not report any increase to be attributed to plasticizer branching upon the molecule. [219]

In each of the plasticizers under investigation a common C=O functional group exists with varying alkyl termination and substitution comparatively. A common property of a $C = O$ is a strong region of electronegativity within the molecule. Oxygen is considerably more electronegative than carbon resulting in a pull of electron density away from the carbon causing an increase in the bond's polarity. Authors have reported these surface phenomena abundantly. [220,221] In particular, Giovambattista *et al.*, address the dichotomy between macroscopic and molecular descriptions using a model. The authors reported that when a surface contained polar regions at the interface, a hydrophobic surface prevails (therefore decreased wettability) in contrast to an apolar surface which brought about a minimal net solvent polarisation at the interface. [221] This is the same for the plasticizers used in this body of work. For instance, the phthalate group demonstrates some differences in polarity across each of the molecules. Figure 3.5 illustrates the common regions of polarity exhibited by the di-substitution of oxygen on the molecule as highlighted.
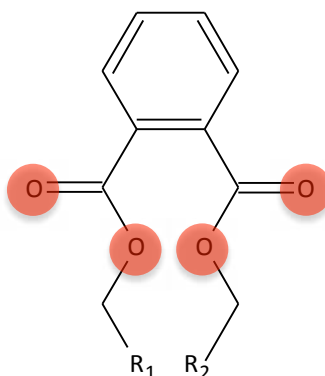
Figure 3.5: Molecular structure of phthalic acid ester moiety with highlighted regions of electronegativity.

Further consideration of alkyl directing groups substituted in the R_1 and R_2 positions are also contributing further electron density effects. In the case of DEHP (85.36°) a higher degree of branching with subsequent alkylated substitution has given larger contact angle values especially when compared to DMP (67.3°), which possesses neither. The actual mechanism can be addressed through inductive effects caused by the groups attached in the R_1 and R_2 position. For example in DEHP, di-2-ethylhexyl is substituted in the R_1 and R_2 positions. These groups direct charge in the form of electron density across the molecule, which is causing higher polarity and furthermore higher wettability exemplified in the contact angle results. When comparing DMP or DEP a dimethyl and diethyl substitution in the R_1 and R_2 positions is

causing less inductive effect and subsequently exhibits lower contact angle values. In the same way Kiso *et al.*, observed increased wettability in larger alkylated phthalates in filtration membranes, [222] this too has been demonstrated in this work where branched molecule plasticizers showed the same hydrophobic effect.

In the azelate plasticizer group a similar trend to the phthalic acid esters was observed. The common functional group was identified and shown in Figure 3.6, where a common C_7 aliphatic chain exists in the centre.
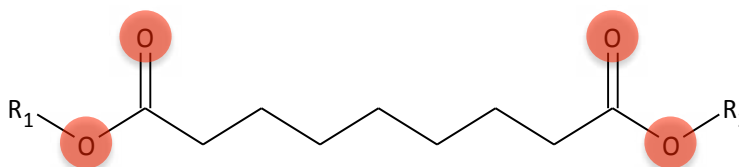
Figure 3.6: Molecular structure of azelaic acid ester derived plasticizer with highlighted regions of electronegativity.

In the same manner as the phthalate plasticizers the longer, branched azelate plasticizers (DEHAz; 76°, DIDAz, 75°, and DIOAz, 74°) showed increased wettability when compared to the shorter ones (DMAz; 66° and DnHnAz; 71°). Another approach in the explanation of wettability differences have been observed in some plasticizers has been addressed by Marchal *et al.,* where azelate plasticizers were described as having a rougher micelle formation owing to the orientation and folding because of the distance between the oxygen substituted regions upon the molecule. [223] Additionally, Tsao *et al.*, report that attractive forces exhibited by molecules with higher branching or alkylation results in increased wettability. [224] As with the phthalate plasticizers this is true of the azelate plasticizers, where longer alkylated azelaic acid esters were found to have higher wettability when incorporated into PVC.

Furthermore, other plasticizer groups have also demonstrated that differences in molecular branching and alkyl termination impose varied wettability. This can also be found in the adipaic acid esters, succinic acid esters and palmitate acid esters plasticizer groups, where higher branching and alkyl termination have all resulted in higher wettability compared to those without these molecular attributes.

The paraffin-derived plasticizers showed similar contact angles throughout the group. In this case, the substitution of chlorine on the aliphatic molecule has given a range of contact angles as depicted in Figure 3.7.
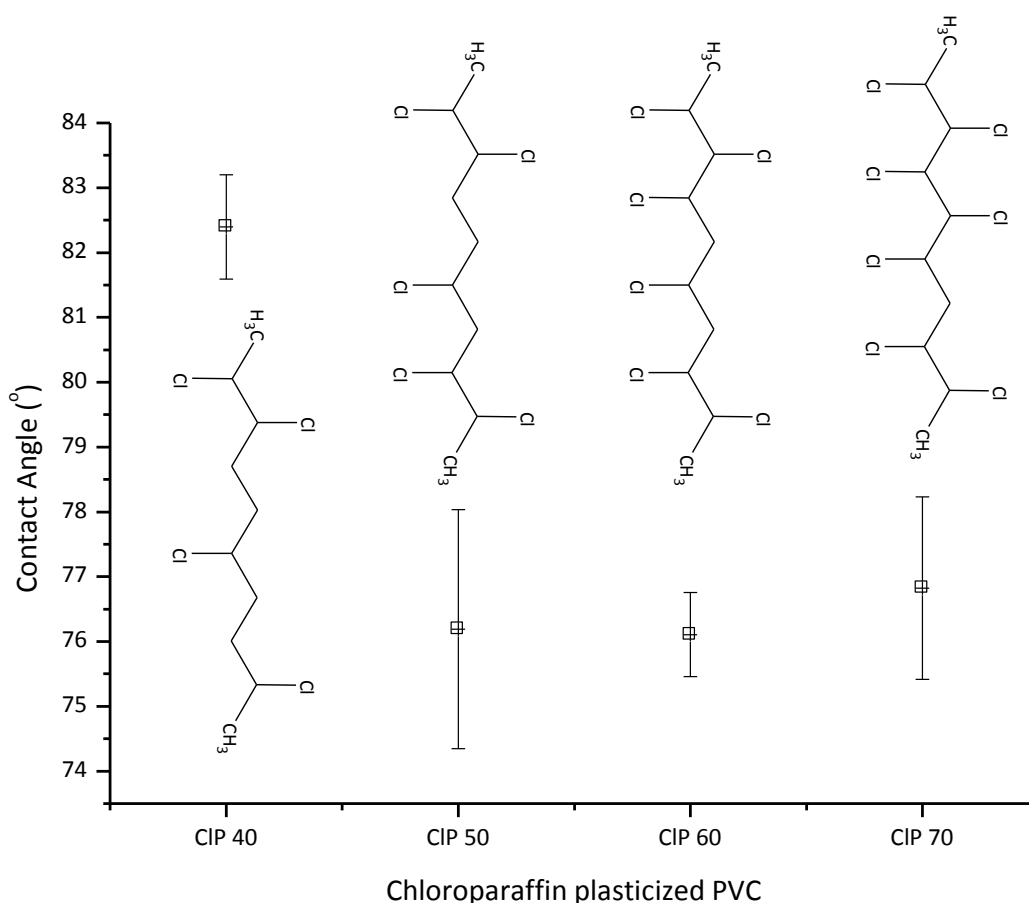
Figure 3.7: Contact angle measurements of the paraffin derived plasticizer group.

CLP$_{40}$ (82.39°) showed the least wettability in this group when compared with the other plasticizers. This plasticizer has less chlorine substitution upon the aliphatic molecule and as a result decreases the wettability of the solvent. As chlorine by nature is electronegative this has caused wettability to be reduced and has been reported by Seguchi *et al.*, [225] where substitution of additional chlorine on glass beads caused a hydrophilic response. CLP$_{70}$ has on average 7 atoms of chlorine substituted per paraffin molecule, which has exhibited higher degrees of wettability as observed in Figure 3.7. This has been explained in Ellison *et al.*, [226] where although wettability of PVC was unchanged with a range of solvents, the introduction of anions such as Cl$^-$ decreases the contact angle, reflected herein. The attractive forces present between the solvent and the polymer interface simulate this. The results demonstrate this phenomenon where larger chlorine substitutions on paraffin molecules, CLP$_{70}$ have produced increased hydrophilic tendencies when compared to the smaller chlorine substituted paraffin molecules.

For the citric acid derived plasticizer group, the contact angles have remained similar, which have been shown in Figure 3.8.
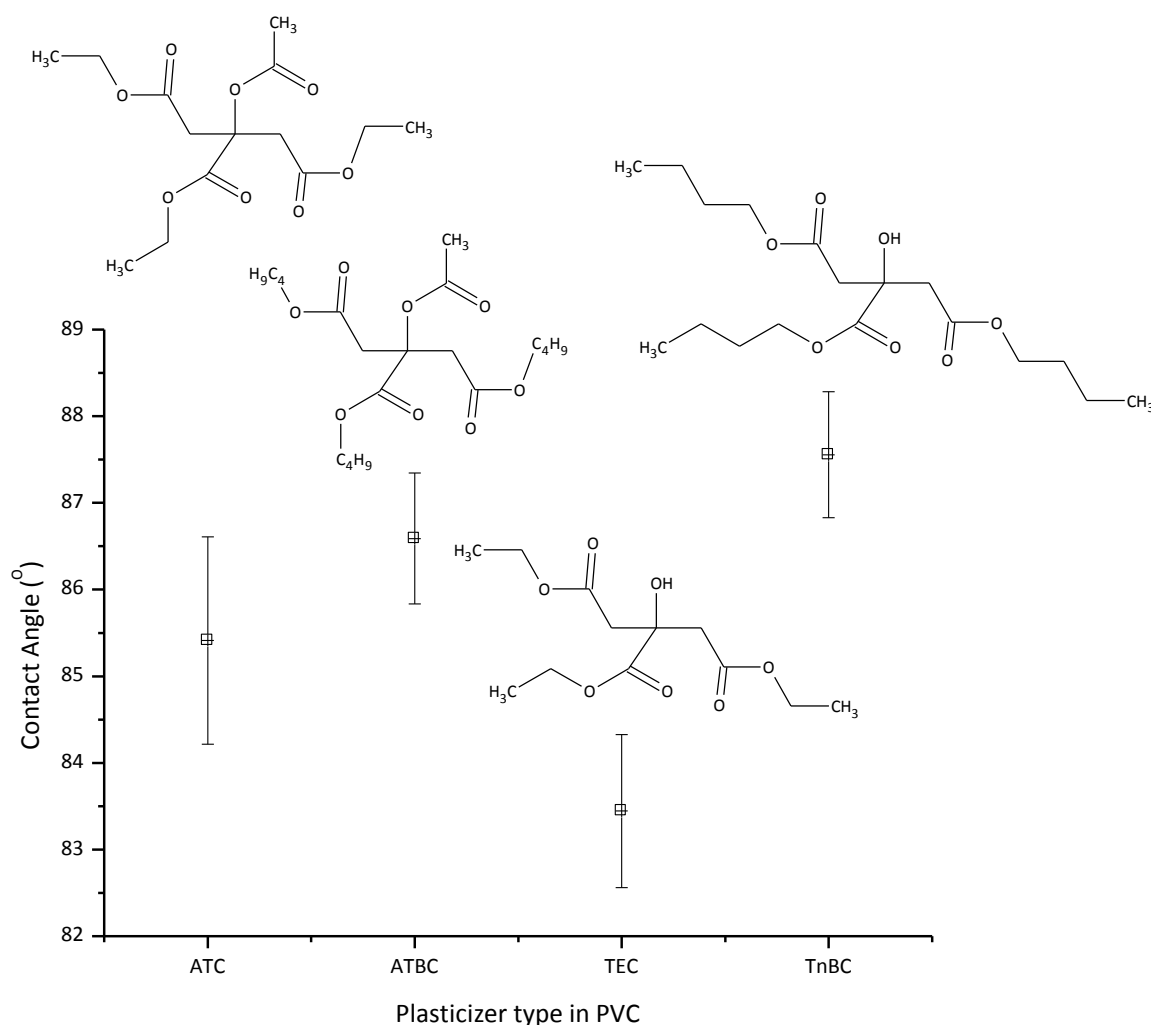
Figure 3.8: Contact angle measurements of the citric acid derived plasticizer group.

Noticeably, TEC (83°) is producing smaller contact angle values and therefore increased wettability when compared to ATBC, ATC and TnBC. These values could therefore relate to the molecular structure of the plasticizer as displayed in other work and could be related to the electronegative groups that a plasticizer possesses. [223] TnBC has a molecular formula of $C_{18}H_{32}O_7$ when compared to ATBC, which has the molecular formula $C_{20}H_{34}O_8$. As an illustration, ATBC contains more substituent oxygen on the molecule and observed higher contact angle values. ATC has less substituent oxygen on the molecule and so a lower contact angle value has been observed relating to the polarity of the molecule.

In summary, when a plasticizer molecule is introduced into a PVC matrix the contact angle value indeed changes. In most cases, an electrostatic effect is observed through the use of certain plasticizers thus giving rise to the varied wettability observed in this work which has also been reported by other authors. Contact angle analysis investigates the initial contact of a solvent with a given substrate - this would be likened to that of a microorganism experiences in the first instance. Although wettability is driven by molecular level attractions between

water and the substrate, surface topography governs another facet to this phenomenon and this is reported abundantly. [89,227,228] Surface roughness of the plasticized PVC polymers that could also cause the wettability of a material to alter is also an important factor. This next body of work investigates whether the incorporated plasticizers are changing the surface roughness and therefore induce any changes in wettability.

3.2.1.3 SURFACE ROUGHNESS

The roughness of the material's surface was determined using a Scanning Probe Microscope (SPM). The purpose was to investigate whether the plasticizers of long branched and those of short, unbranched in nature differ greatly in surface roughness measurements, which may or may not affect the wettability of the material.

Many authors report that surface roughness causes either a hydrophobic or hydrophilic response depending on the topographical nature of the surface, this has been extensively reviewed by numerous authors. [214,229,230178] This was reported to be caused by microstructuring across the surface of the coating. [231] If a surface has many microstructures the wettability is generally increased. [228,232,233] This has been suggested to be caused by the interfacial wetting energy of the solid-liquid interface resulting in a repellent force across the surface, from the individual micro-niches explained as heterogeneous or homogenous wetting, [89] illustrated in Figure 3.9.
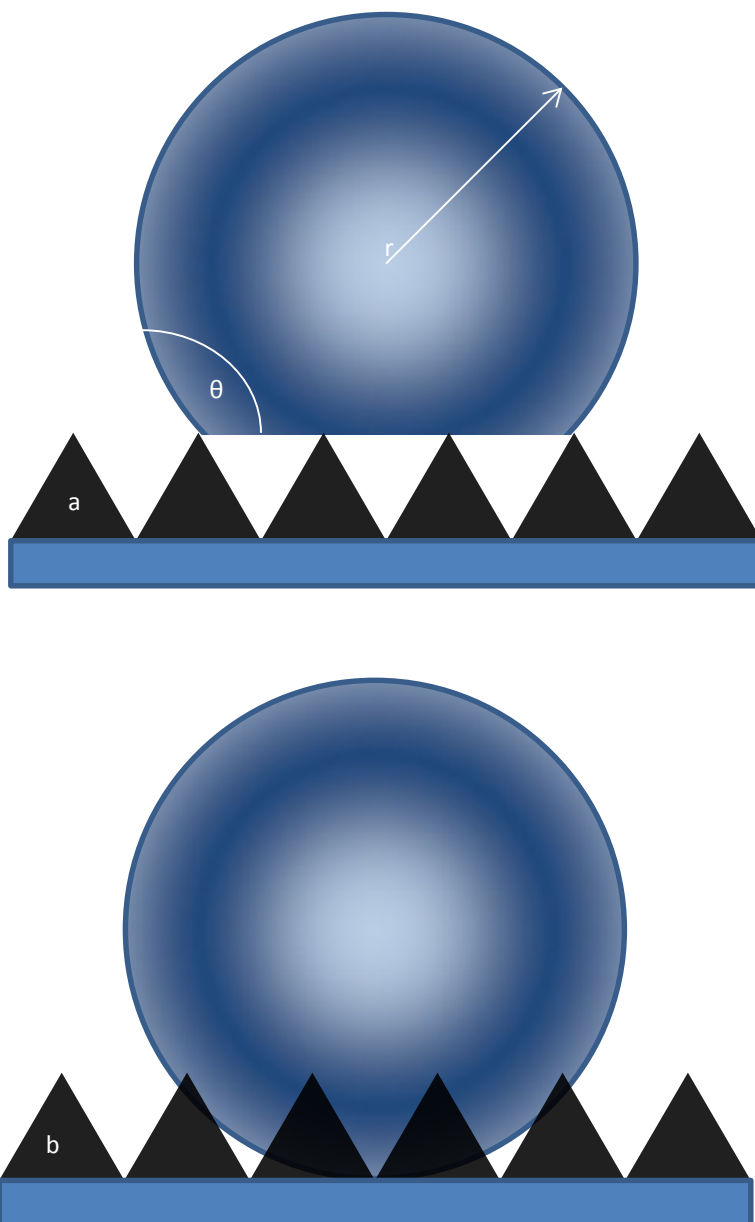
Figure 3.9: Schematic showing how different wetting regimes may exist on rough substrates (a) heterogeneous wetting on rough surface, described as Cassie-Baxter wetting and (b) homogenous wetting on rough surfaces described as Wenzel wetting of a substrate.

The roughness measurements were obtained for a select few plasticized PVC polymers, listed in Chapter 2, Section 2.1.1.1: Table 2.1, as an example of branched and longer alkyl termination compared with shorter or no branching or alkyl termination on the plasticizer molecules.

Table 3.1 depicts the average roughness data obtained for a selection of these plasticizers. The roughness average, R_a, is defined as the arithmetical mean roughness of a surface that can be expressed in nm.

Table 3.1: Mean surface roughness measurements of different plasticizer groups depicting opposite molecular attributes.

	Polymer	Mean roughness, R_a, (nm ± 1 SD)
Blank	uPVC	37.69 ± 1.66
Phthalic acid esters	DMP	35.139 ± 2.93
	DEHP	154.32 ± 3.21
Paraffins	CLP40	95.61 ± 1.64
	CLP70	93.72 ± 1.38
Benzoic acid esters	DEGDB	74.91 ± 0.74
	PEGDB	73.29 ± 1.83
Azelaic acid esters	DMAz	45.60 ± 2.06
	DIDAz	137.11 ± 1.32
Adapic acid esters	DIBAd	39.31 ± 1.96
	DTDAd	149.65 ± 2.11

The phthalate doped PVC films show distinct differences in mean roughness values between the higher alkylated, branched plasticizer, DEHP (154 ± 3.21 nm) when compared to the lesser branched, alkylated phthalate, DMP (35 ± 2.93 nm). This has already been reported by other authors, [138][214] where plasticizers do indeed cause roughness changes and different wettability across the materials. Rahmawan *et al.*, showed that higher surface roughness pertains decreased wettability, something that was observed in this study, Figure 3.10, *vide infra*.

For the chloroparaffin plasticizers, average roughness did not change significantly between the two un-similar plasticizers, CLP_{40} and CLP_{70} showing differences of ~2 nm. The chlorinated paraffin plasticizers, although heavily reported in the literature, are not discussed readily for their use as a matrix additive in changing topographical features and so no comparison can be made. [234-239] Although this is not a surprising result as the chloroparaffin molecule possesses the same size aliphatic chain and the difference between each is the chlorine termination on each of the molecules, thus very similar surface roughness was observed.
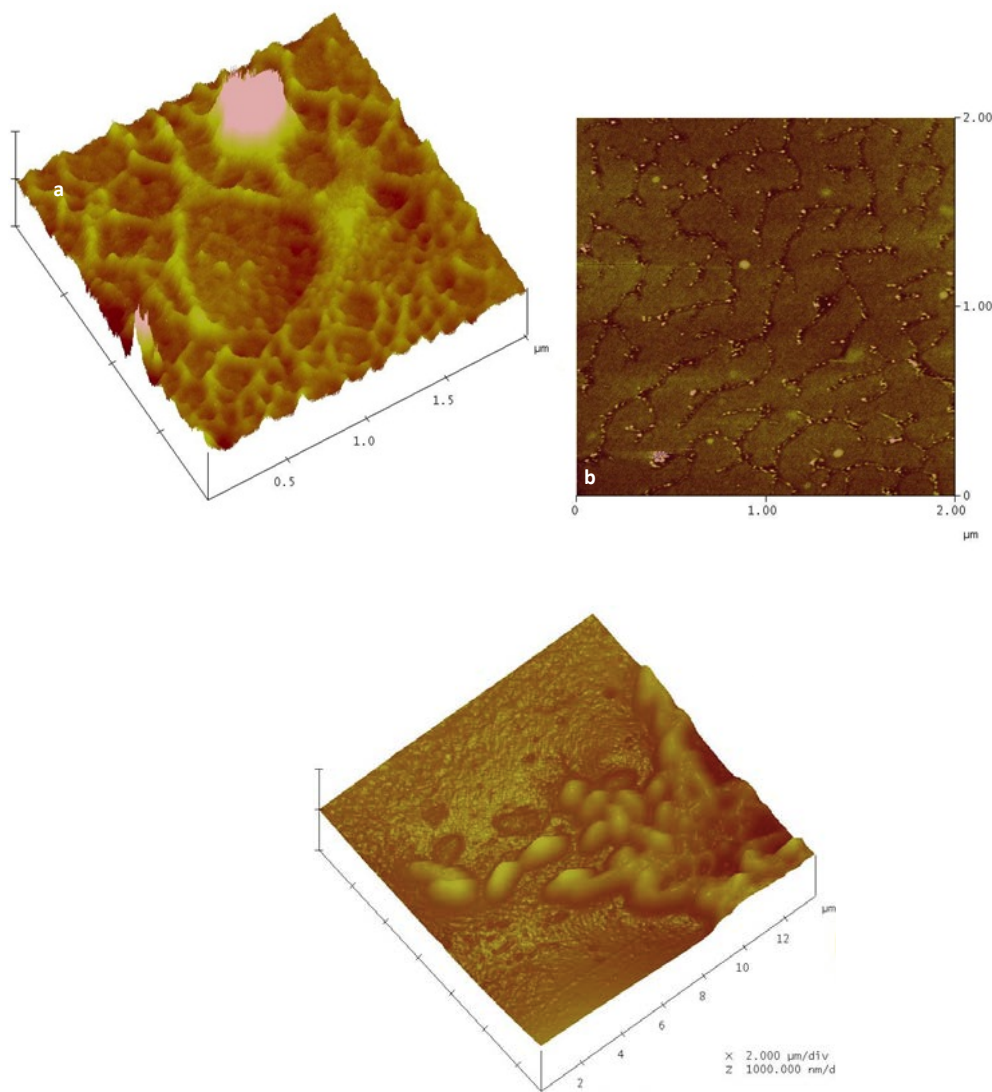
Figure 3.10: AFM micrographs showing (a) profilometric micrograph of plasticized PVC with DEGDB and (b) blank uPVC and (c) micrograph showing an example of rod-like microbe retention upon the surface of the substrate.

The benzoic acid derived plasticizers have also shown similar average roughness values when compared with each other displaying differences of ~1 nm in the R_a value. When compared to the paraffin-derived plasticizer group this is a similar response, and as such, both plasticizer molecules in this group are alike in structure. Maata *et al.*, reported a method using AFM, where surface roughness values of 1.1-4.2 μm were achieved when incorporating benzoic acid derived plasticizers in PVC illustrating the relevance of this technique for this type of characterisation. Although the author reports an R_a value which is an order of magnitude higher to what is reported in this work, the plasticizer concentration were higher, which could be a contributing factor to this elevated value. [214]

Similarities were observed in the adipate group where average roughness values exhibited were likened to the phthalic acid esters whereby increased branching and alkyl chain length on

the plasticizer molecule produced higher surface roughness values. The increase in surface roughness has also presented larger hydrophobic values as seen in Figure 3.4, *vide supra*. Lastly, the azelaic acid ester derived plasticizers have also shown that a more branched, alkyl chain molecule exhibits higher surface roughness values and decreased wettability compared to the least branched or alkylated ones.

Analysis of the contact angle values and observed average roughness values have been compared in Figure 3.11.
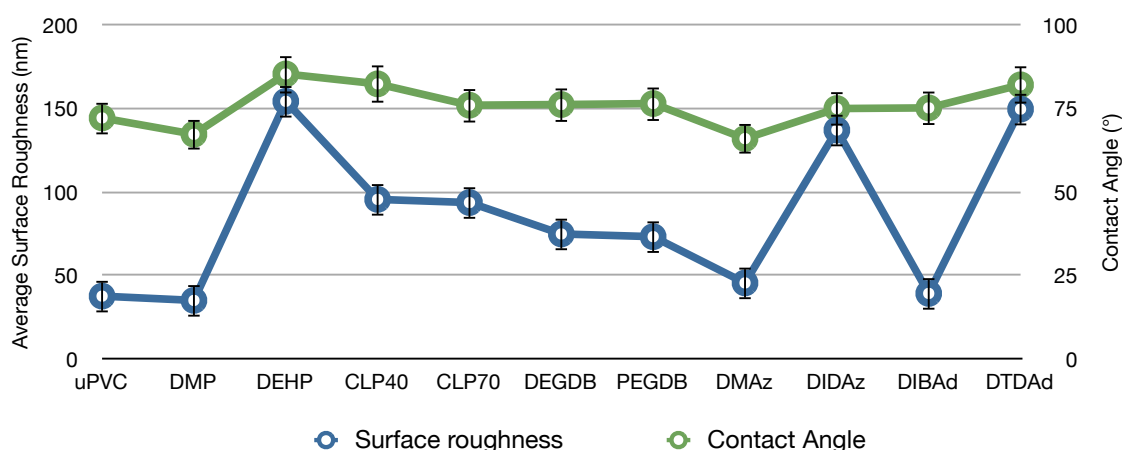
Figure 3. 11: Double line plot showing average surface roughness and wettability. The graph depicts similar trends for roughness and wettability for the plasticized PVC films.

Contact angle values monotonically increases from plasticizer to plasticizer depending on the average roughness value obtained. Since the roughness decreases in, for example DMP (35 nm) the contact angle value decreased (67.3 °), indicating that the wettability of the material has increased. The data was then subjected to one way ANOVA where *P* <0 .01, suggested that there is direct correlation between surface roughness and wettability. Rosales-Leal *et al.* have performed similar studies, where the authors found that surface roughness of dentin surfaces influenced the wettability of the material. This work differs from the work presented herein, whereby the authors are not using polymeric materials, and note that chemical changes and indeed morphological changes induce variable wetness values.

In conclusion, assessment of each plasticizer group demonstrates that surface roughness affects the wettability of the surface. The adipates, azelates and phthalates have clear structural differences between the two opposite choices in their respective plasticizer groups. Thus, observed changes in the wettability have occurred. In the cases of the benzoic acid and paraffin-derived plasticizers, the molecular structure remains similar and therefore negligible

differences in microtopography in the form of surface roughness and subsequent contact angles were observed. [240]

3.2.2. AN ASSESSMENT OF FOULING

Assessment of biofouling was made using a series of analytical techniques for each of the plasticized polymer coatings. A series of experiments were devised to probe the level of fouling on each of the surfaces, in particular it is the initial attachment and interactions of fouling organisms of biofouling that are of relevance to this thesis.

The following measurements were performed and were developed as laboratory-based assays in the determination of the level of fouling (as already discussed in Chapter 2, Section 2.1.3):

- Mass: Here a change in mass across each of the plasticized PVC test coatings over a 7-day laboratory tank test was observed. This period of time was selected, as it is the initial stage of fouling that governs the subsequent, heavier fouling processes.

- Glycocalyx: Measurement of glycocalyx (slime) upon each of the plasticized samples was measured. This was achieved through a series of fixation and staining steps, and was performed on the same samples used in the mass analysis assay. The same samples for mass were used in order to ascertain depth to the composition of what is labelled 'mass' in this work. Glycocalyx has been described as consisting of proteogylcans, glycoproteins and glycoaminoglycans. [241] Luft originally described the thickness of a glycocalyx layer to be 20 nm, but the work of Vink and Duling and Smith *et al.,* revealed the core proteins, which provided the first direct estimation of glycocalyx thickness *in vivo* as closer to 0.4 – 0.5 µm. [242,243] Electron microscopy enabled the distinction between protein structures as described Squire *et al.*, showing the underlying structural properties. [244]

- Protein and carbohydrate adsorption: Here protein and carbohydrate adsorption across the plasticized polymers was observed, quantifying the level of biochemical involvement expected from microorganisms. A series of measurements were obtained for protein and carbohydrate adsorption across each of the plasticized PVC thin films; absorbance measurements indicated the quantity of protein or carbohydrates that adhered to the polymer thin films only, as given in Chapter 2, Section 2.3.2.3, *vide supra*. Similar work by Lazarova and Manem also showed that the Lowry protein adsorption assay gave reproducible and sensitive results. [166]

- Plasticizer leaching: This investigation was carried out determining the level of migration of the plasticizer from the PVC matrix.

3.2.2.1 ADIPATE PLASTICIZERS

For the adipate plasticizers, a series of laboratory-based assays were developed for the screening of the plasticized PVC thin films. The tests included: mass, slime and protein and carbohydrate adsorption. Following this, a leaching study was performed for each thus ascertaining the surface activity of films.

3.2.2.1.1 MASS AND SLIME

The best performing adipate plasticized PVC thin films in this group were found to be DCAd and DEHAd for the mass and slime results. Mass and slime were measured for the adipate plasticized PVC thin films. The two tests were administered together thus investigating the level of slime contributing to the overall mass that may have adhered to the films, Figure 3.12.
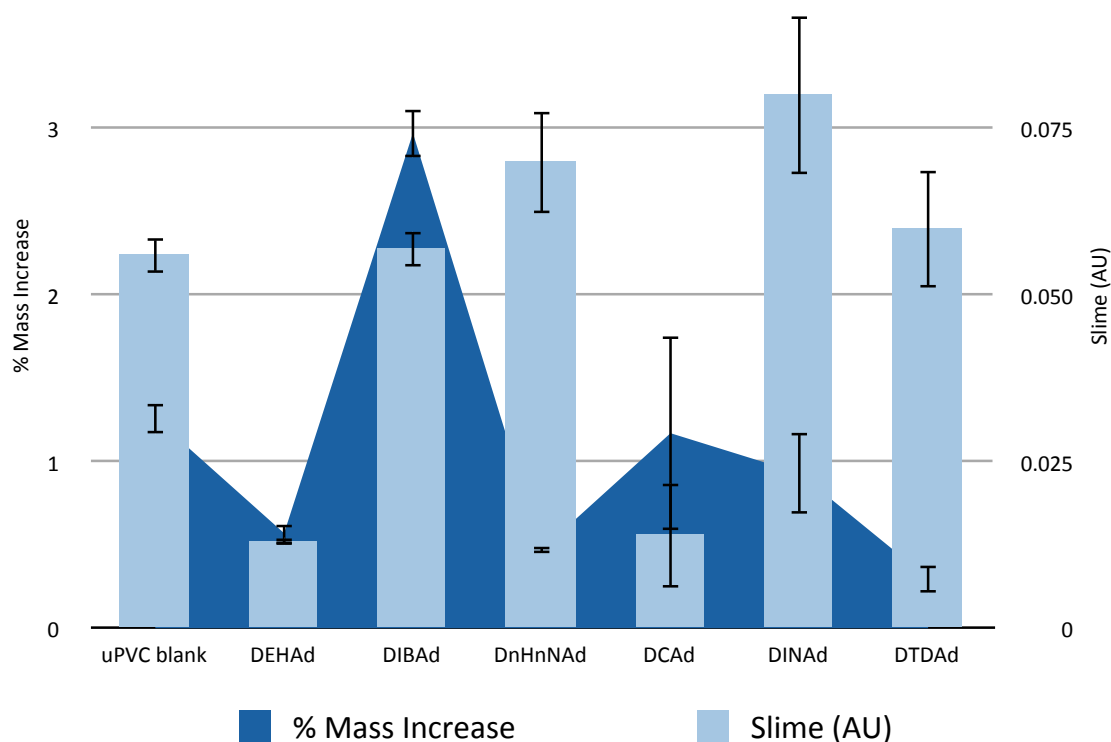
Figure 3.12: Double axis plot showing slime and mass for the adipate plasticized PVC films following a 7 d freshwater laboratory assay (n=9 ± 1SD).

The adipate plasticizers showed broad results following the assessment of mass with a range of percentage results; 0.30% to 2.97%. DTDAd displayed the greatest reduction to mass across the adipate thin films. Naruhashi *et al.* explain that adipate derivatives with less molecular branching, have little to no effect on toxicity of mammalian cells, and although this is not the target cell types, this indication provides another possible facet to the behaviour of this

plasticizer group. [245] In other studies by Bhasin *et al.*, toxicity of adipic acid was assessed using Bacillus subtilis, in one study and *Salmonella typhi* in another, where antibacterial studies proved that adipic acid was ~10% effective as an antibacterial agent. [246] As the plasticizers are all derivatives of adipic acid, it is important to note that varying the degree of alkylation and branching produces varied mass responses as observed. Furthermore, adipic acid in its pure form, as depicted in Figure 3.13, has been found to be non-toxic to *Rhodococcus rhodochrous* in concentrations of up to 1 g/L. [149] This suggests that perhaps the shorter alkyl chain plasticizers used in this study; DIBAd and DCAd showed higher percentage mass gain owing to these results.
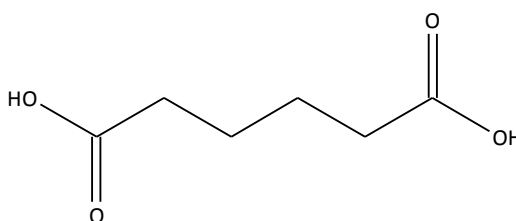
Figure 3.13: Molecular structure of adipic acid.

DnHnNAd (0.07 ± 0.01 AU) has less slime when compared to the uPVC blank (0.056 ± 0.04 AU) some 8 times improved. The remaining adipate doped plasticized PVC membranes; DEHAd (0.013 ± 0.04 AU), DCAd (0.013 ± 0.01 AU), DINAd (0.08 ± 0.01 AU) and DTDAd (0.06 ± 0.01 AU) have all shown similar levels of slime adsorption across this group. Additionally, DIBAd (0.057 ± 0.02 AU) showed an elevated level of slime when compared to the rest of the adipate doped PVC coatings. This is also true of the mass result obtained. This suggests that the slime produced is contributing to the overall mass increase exhibited by each of the different plasticized PVC membranes, which after performing a 'student' t-test (unpaired) of slime related to mass increase, showed statistical significance with $p < 0.0001$. This reinforces that slime is thus related to a mass increase and contributes to these values. Elevated levels of glycocalyx suggest that increased levels of mechanotransduction of fluid shear stress and cell signalling could be occurring across the DIBAd plasticized PVC coatings, this phenomenon has been reported in Tarbell and Pahakis. [247]
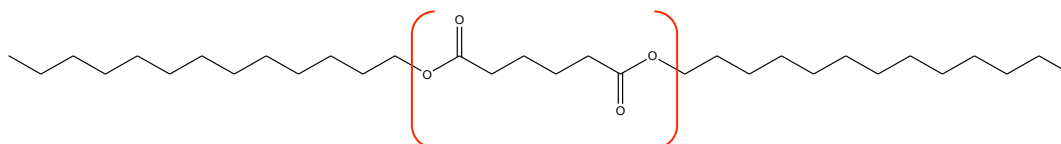
Figure 3.14: Molecular structure of DTDAd with highlighted area showing common moiety.

Figure 3.14 depicts the molecular structure of DTDAd with the di-alkylated C_{10} chains on the terminal adipic acid moiety. The long alkylated chained plasticizers showed reduction to mass and slime adsorption on the adipate plasticized coatings, when compared to the shorter DIBAd

plasticized PVC. In other studies, Novak *et al.* showed longer terminal alkylation of N,N-substituted amines exhibit antimicrobial activity. It was also found that chain branching causes antimicrobial activity to be reduced, [248] an observation has been supported in this body of work where slime adsorption increased on the branched plasticizer PVC coatings; DeHAd and DCAd.

3.2.2.1.2 PROTEIN AND CARBOHYDRATE ADSORPTION

A series of measurements were obtained for each of the adipate plasticized PVC thin films for protein and carbohydrate adsorption, Figure 3.15.
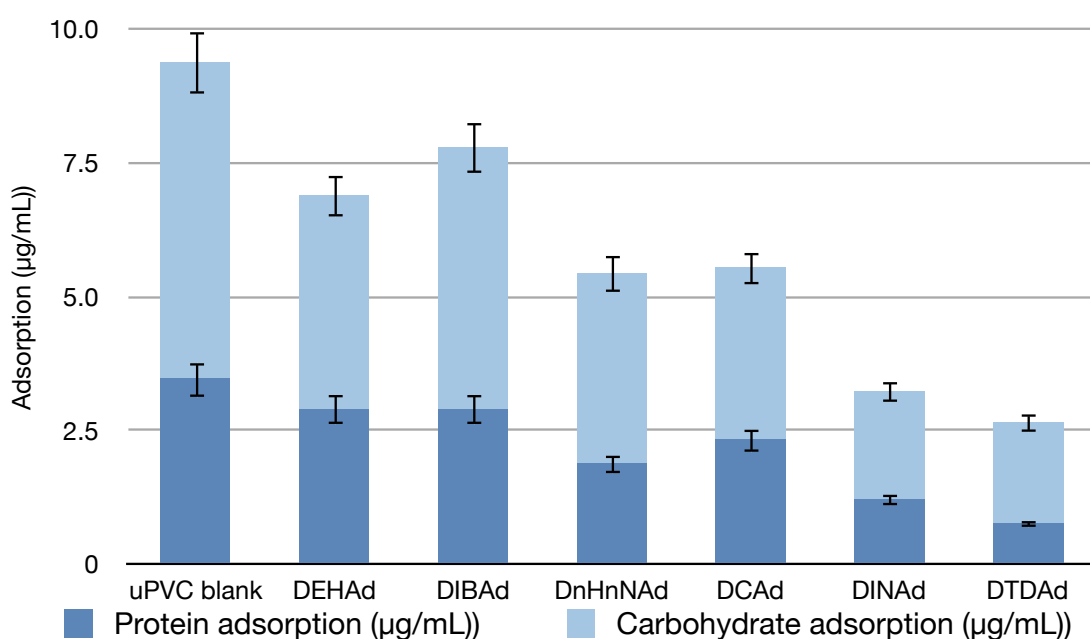
Figure 3.15: Protein and carbohydrate adsorption for adipate plasticized PVC thin films, following a 7-d freshwater tank study n=3 ± 1 SD.

All of the plasticized PVC thin films within this group showed lower concentrations of both protein and carbohydrates when compared to the uPVC blank (3.46 ± 0.12 µg/mL). DTDAd (0.76 ± 0.32 µg/mL) showed the least protein adsorption when compared to the uPVC blank which is ~4.5 times less.

Carbohydrate adsorption was also quantified for the adipate doped PVC thin films. As in the protein results these plasticizers have all shown lower carbohydrate concentrations when compared to the uPVC blank (5.91 ± 0.21 32 µg/mL). Furthermore, the best performing plasticized thin film was DTDAd (1.89 ± 0.32 32 µg/mL) a result that has been observed in all assays explored. No recent literature has been published on the adsorption behaviours of

carbohydrates to plasticized PVC, which shows the distinct novelty to this work in the biofouling area.

3.2.2.1.3 LEACHING AND PLASTICIZER AVAILABILITY

Owing to the nature of the PVC matrix, plasticizers are able to move freely from within and thus introduce a leaching property to the makeup of the plasticized PVC. The surface activity can therefore change over a given time and when introduced into a given interface. A leaching study was employed to investigate migration of plasticizer through the PVC matrix.

Total plasticizer loss was then calculated according to the absorbance changes in typical plasticizer bands as depicted within the data. PVC belongs to a group of polymers that enable incorporated dopants to slowly release from the polymeric matrix. Therefore, if antimicrobial agents are incorporated within a PVC matrix, they are almost certain to leach into a surrounding interface, shown is this study as the plasticizer compound. This proves to be a desirable characteristic regarding its antifouling capacity, [249] and has been probed herein using FTIR analysis.
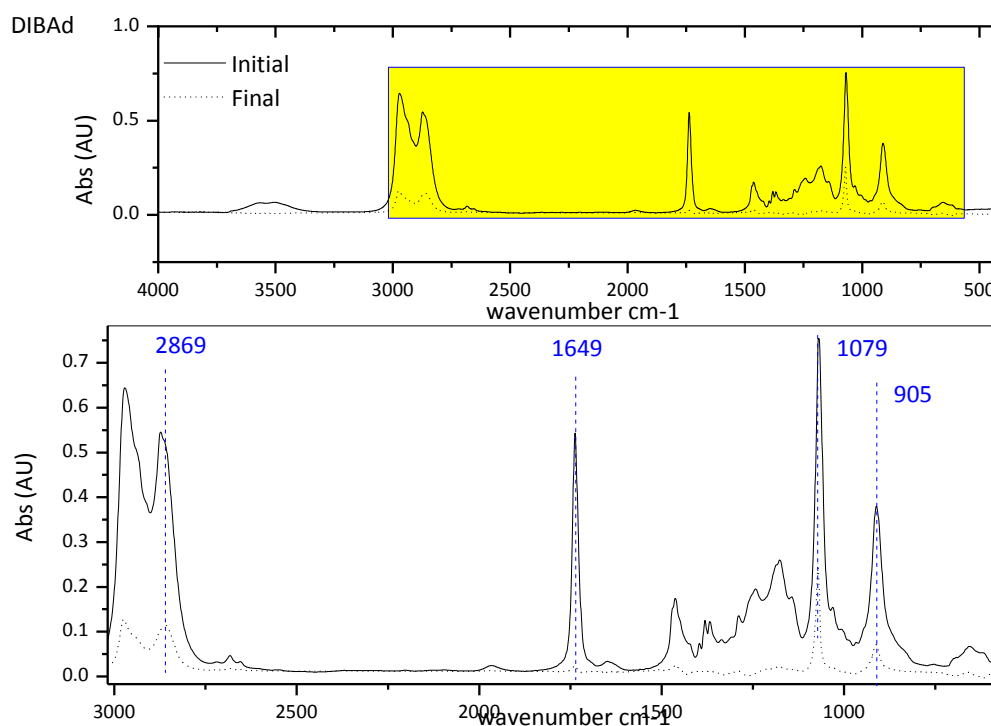
Figure 3.16: FTIR absorbance measurements illustrating plasticizer migration from the PVC matrix example given by DIBAd. (Top) Whole spectra, (bottom) zoom of spectral region 2800 – 1000 cm⁻¹ showing 4 bands of interest.

Each of the plasticizers used have characteristic bands and are shown in Figure 3.16 where, changes in absorbance were related to the level of leachate and thus surface activity of each of the adipate doped PVC thin films was determined. Each adipate had the following IR bands monitored: ϑCOC (2869 cm^{-1}), stretching $C = O$ (1649 cm^{-1}), CH_2CH_3 vibration (1079 cm^{-1}), asymmetric symmetric CH$_2$CH3 (905 cm^{-1}), which relate to adipic acid esters within the PVC matrix. [250,251] DnHnAd (0.6 %) leached at a significantly lower rate than the other adipate plasticizers investigated in this group. The plasticizer exhibits high levels of branching upon the molecule, thus affording significantly slower rates of leaching across the polymer-water interface. The leaching process relies on plasticizers moving through the polymer links of PVC and has been reported in Faouzi *et al.*. Here they report that as molecule links are increased, manoeuvrability of the plasticizer contained within a polymer matrix is made inherently more difficult through the polymer links and thus leaches at a slower rate. [252] DIBAd (32.25 X) leached at a higher rate within this group of plasticizers (Table 3.2), and indeed, the molecule is of shorter alkyl length that in turn migrates through the polymeric PVC links at a faster rate.

Table 3.2: Tabulated plasticizer migration data for the adipate plasticizers. Absorbance measurements were obtained both before and after a pure water study, where change in absorbance and %RSD were calculated (n=3 ± 1SD).

IR band analysed	DTDAd		DEHAd		DnHnAd		DCAd		DIBAd	
2869 cm^{-1}	Initial	Final	Initial	Final	Initial	Final	Initial	Final	Initial	Final
	6.423	6.421	0.87	0.73	0.056	0.054	0.45	0.42	0.54	0.11
Change in Absorbance	0.002		0.14		0.02		0.03		0.43	
% RSD	2.81		0.34		0.56		1.21		1.54	
1649 cm^{-1}	Initial	Final	Initial	Final	Initial	Final	Initial	Final	Initial	Final
	0.695	0.647	0.22	0.21	0.043	0.043	0.095	0.091	0.18	0.12
Change in Absorbance	0.048		0.01		0		0.04		0.06	
% RSD	1.02		4.32		0.76		0.44		1.32	
1079 cm^{-1}	Initial	Final	Initial	Final	Initial	Final	Initial	Final	Initial	Final
	6.423	6.421	0.87	0.73	0.056	0.054	0.45	0.42	0.54	0.11
Change in Absorbance	0.04		0.3		0.009		0.04		0.49	
% RSD	4.21		3.21		1.09		1.32		0.35	
905 cm^{-1}	Initial	Final	Initial	Final	Initial	Final	Initial	Final	Initial	Final
	6.79	6.75	1.62	1.32	0.01	0.001	0.78	0.74	0.74	0.25
Change in Absorbance	0.07		0.1		0.001		0.09		0.31	
% RSD	3.21		0.23		0.53		1.43		1.69	
Total Plasticizer Loss (%)	**3.95**		**13.75**		**0.6**		**5**		**32.25**	

3.2.2.1.5 SUMMARY FOR ADIPATE PLASTICIZERS

The adipate plasticized PVC thin films displayed a range of results pertaining to each assay. The plasticizers in this group that had slower leaching rates DnHnNAd (0.6 %), DCAd (5 %) and DTDAd (3.95 %) have the greatest molecular branching and alkyl termination per molecule.

DEHAd (0.057 ± 0.02 AU) had least glycocalyx adsorbed to the plasticized PVC film, where elevated levels of protein and carbohydrate adsorption were found to exist for this particular plasticizer.

DTDAd was the best performing plasticizer for this group and demonstrated the least mass, protein and carbohydrate production when compared to the rest of the adipates.

3.2.2.2 AZELATE PLASTICIZED PVC

As in Section 3.2.2.1, the azelate plasticized PVC thin films were taken through the same series of tests. For conciseness, the data has been tabulated as shown in Table 3.4 and the results are discussed accordingly.

3.2.2.2.1 AZELATE FOULING RESULTS

The table presented, Table 3.3 shows the whole data set observed for slime, mass and protein and carbohydrate adsorption.

Table 3.3: Table showing data observed for each of the fouling assays performed on the azelate plasticized PVC thin films.

	% Mass Increase	(SD)	Slime (AU)	(SD)	Protein adsorption (µg/mL)	(SD)	Carbohydrate adsorption (µg/mL)
uPVC blank	1.26	0.095	0.056	0.0028	3.46	0.1231	5.912
DIOAz	0.96	0.19	0.25	0.06	1.076	0.122	1.8553
DIDAz	0.27	0.12	0.02	0.07	0.89	0.212	1.323
DMAz	1.83	0.18	0.33	0.07	4.12	0.206	6.221
DEHAz	0.82	0.31	0.22	0.08	2.12	0.106	2.321
DnHnAz	0.92	0.16	0.29	0.06	1.99	0.311	1.986

The best performing azelate plasticizer when doped into PVC was DIDAz (0.27 ± 0.12%) which showed improved antifouling response when compared to the uPVC blank of up to 4.7 X. As with the adipate plasticizers, extensive literature is not prevalent as antifoulants, representing the novelty in this work. However, there are reports of literature detailing their use as an antimicrobial agent in the azelaic acid form. [253] Thiboutot *et al.,* show the use of azelaic acid as

a topical cream to prevent acne, caused by bacteria upon the surface of the skin, highlighting a potential toxic characteristic for this plasticizer. Interestingly, DMAZ (1.83 ± 0.83 X) produced a result of increased mass greater than that observed with the uPVC blank (1.26 ± 0.36%) indicating this could be due to preferential microorganism settlement upon these polymer surfaces.

This can be explained by the mode of breakdown of the plasticizers by microorganisms. It was shown in Matthies and Schink that long chain alkylated azelates were metabolised at a much slower rate by fermenting bacteria, [254] indicating a possible reason why the mass observed did not change for longer alkylated plasticizers seen herein.

In other work, Narasimhan report that dimethyl azelate displayed excellent antimicrobial property when tested against Gram-negative *Escherichia coli* than Gram-positive *Staphylococcus aureus* and *Bacillus subtilis*. This contradicts the findings of this study, as the shorter alkylated plasticizers have produced more mass adhesion to the dimethyl azelate plasticized polymer, thus indicating that microorganism interaction is in abundance. Although mass is an indication of what has adhered to the surface of the polymers, further testing was carried out to investigate the actual composition of the mass and slime measured herein.

DIDAz (0.02 ± 0.01 AU) showed the least level of slime adsorption on the PVC coatings. Additionally, DMAz (0.33 ± 0.01 AU), has adsorbed slime some three times more than the uPVC blank (0.056 ± 0.04 AU) suggesting microorganisms prefer these plasticized polymers. Tsai *et al.,* report that higher absorbance relates to higher concentrations of slime production. [199] Furthermore, Sivakumare *et al.*, have similarly modified the 'slime-test' using safranin as the selected stain, [255] where absorbance also increased when concentration of glycocalyx increased.

Charnock *et al.* report that Skinoren © containing 20% azelaic acid was effective against *S. aureus* when incorporated into topical creams. Although the azelaic acid showed most promise in preventing antibacterial activity, [256] it is not conclusive in literature to the actual mode of breakdown when it has entered the bacterial cell. As with the adipate plasticizers, the most effective plasticizer possesses long alkyl termination or branching on the molecule, Figure 3.17.
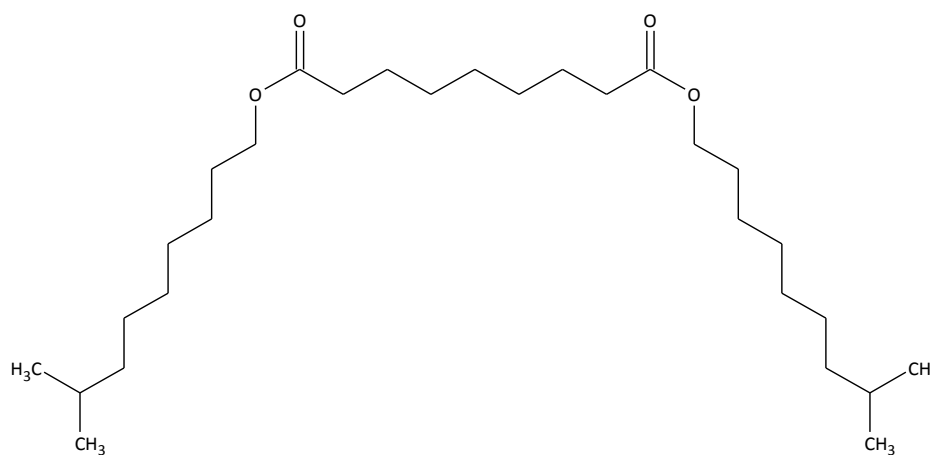
Figure 3.17: Molecular structure of DIDAz.

The DIDAz structure possesses a C_{10} di-alkyl termination chain on the azelate moiety and has exhibited the best response to slime and mass adsorption as previously discussed. The results presented show a dual role for the compounds as, (a) a source of carbon and (b) as a toxic agent. This has also been shown in Janota and Wright, where it was found that the concentration of low amounts of azelate and prolonged action of azelaic acid is produced phenotypic changes. Similarly, the level of release from the PVC matrix of each of the plasticizers would contribute to this phenomena, something that will be discussed in Section 2.1.2.4, *vide infra*.

Protein adsorption within this group has also demonstrated varied results. Interestingly, DMAz (4.12 ± 0.21 32 µg/mL) has seen elevated levels of protein concentration exceeding the uPVC blank (3.46 ± 0.12 32 µg/mL). The best performing plasticizer in the azelate group was DIDAz (0.89 ± 0.21 32 µg/mL), averting some 3 times more protein adhesion than the uPVC blank. It has been reported that protein adsorption infers a greater level of fouling exhibited on a system, [257] this phenomena has been observed, where higher levels of protein adsorption appear to produce higher levels of fouling exhibited in the mass and slime results, *vide supra.* This is true of the plasticized thin films where carbohydrate adsorption is somewhat higher than the proteins. Strathmann *et al.*, have also reported this phenomena where carbohydrates were in excess to proteins in a fouling system. [258] Microorganisms require carbohydrates for metabolism and survival and therefore it seems feasible to suggest that this rate of adsorption is higher for this reason. [259]

The adipic acid ester derived plasticizers have followed a similar trend where the level of leachability was governed by the molecular characteristics of the plasticizer, Figure 3.18. Evidently, DMAz (47%) has leached the greatest from the PVC matrix, with DEHAz (4.58 %) leaching the least. Similarly, Gamez found that DIOAz leached from PVC in hexane when

performing a solvent extraction at a rate that was similar to that of DEHAd, [260] this was reflected in this chapter of work (Table 3.4), where they have leached at similar rates in a water extraction. The use of FTIR to assess the migration of plasticizers is seldom reported, and has been shown to be a viable method for this type of analysis.

Table 3.4: Tabulated plasticizer migration data of azelate plasticizers from PVC, absorbance measurements were obtained both before and after a pure water study, where change in absorbance and %RSD were calculated (n=3 ± 1SD).

IR band analysed	DEHAz		DIDAz		DIOAz		DMAz		DnHnAz	
$2856\ cm^{-1}$	Initial	Final	Initial	Final	Initial	Final	Initial	Final	Initial	Final
	0.523	0.454	0.51	0.44	0.059	0.037	1.77	0.21	0.301	0.09
Change in Absorbance	0.069		0.07		0.022		1.56		0.211	
% RSD	1.56		1.22		1.97		3.01		0.84	
$1454\ cm^{-1}$	Initial	Final	Initial	Final	Initial	Final	Initial	Final	Initial	Final
	0.125	0.121	0.13	0.12	0.179	0.01	0.53	0.18	0.112	0.04
Change in Absorbance	0.004		0.01		0.169		0.35		0.072	
% RSD	1.91		0.33		6.32		1.02		1.32	
$1062\ cm^{-1}$	Initial	Final	Initial	Final	Initial	Final	Initial	Final	Initial	Final
	0.78	0.612	0.68	0.4	0.67	0.56	1.74	0.2	0.32	0.103
Change in Absorbance	0.04		0.3		0.11		1.54		0.217	
% RSD	3.01		1.72		0.51		4.68		0.35	
$909\ cm^{-1}$	Initial	Final	Initial	Final	Initial	Final	Initial	Final	Initial	Final
	0.395	0.328	0.38	0.26	0.44	0.27	1.39	0.14	0.23	0.09
Change in Absorbance	0.07		0.1		0.17		1.25		0.14	
% RSD	4.65		4.92		3.21		3.14		0.34	
Total Plasticizer Loss (%)	4.58		12		11.78		47		16	
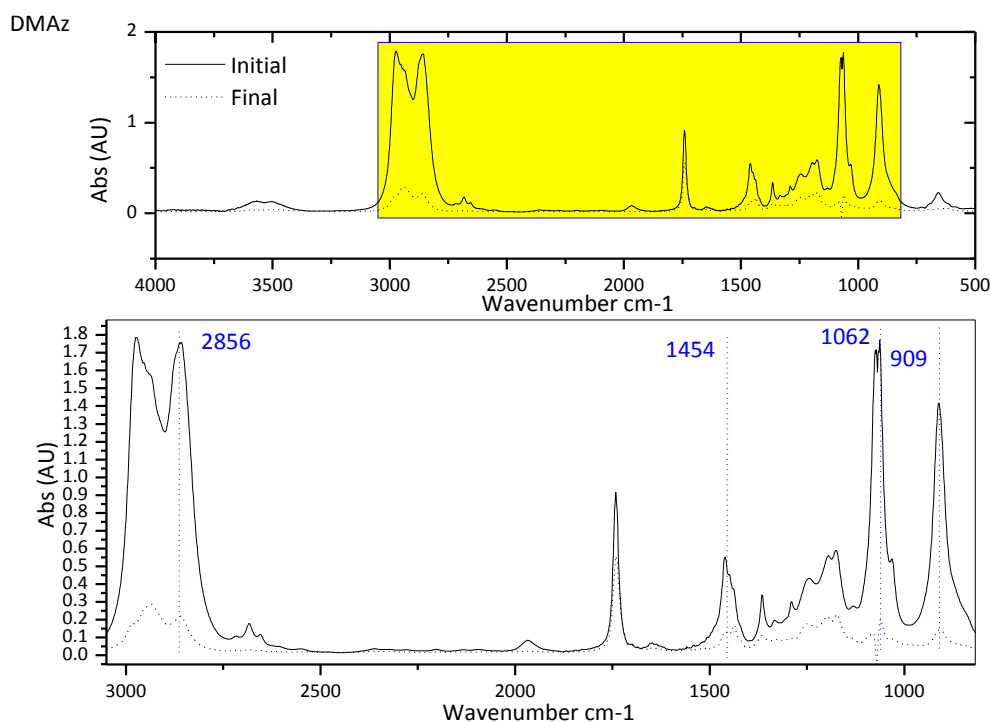
Figure 3.18: FTIR absorbance measurements illustrating plasticizer migration from the PVC matrix example data of DMAz. (Top) Whole spectra, (bottom) zoom of spectral region 3000 – 1000 cm⁻¹ showing 4 bands of interest.

3.2.2.2.2 SUMMARY FOR AZELATE PLASTICIZERS

The results for this group of plasticizers, thus far, present a range of interesting findings. The plasticizers that have leached at slower rates DEHAz (4.5%), DIOAz (11.7%) and DIDAz (12%) in a 7 d period showed the least levels of mass and slime adsorption across the group. This trend could possibly be explained as follows:

If plasticizer leach rate is slower, the rate of biocide release is therefore equivalent;

If the higher alkyl chain and branched plasticizer molecules are more toxic to microorganisms within this system, then the slower leach rate could be aiding a more continuous long term leach rate through the PVC matrix seen in DEHAz, DIOAz and DIDAz;

If the shorter alkyl chain plasticizer molecules leach at a faster rate, we no longer see a biocidal effect but merely a surface that is more suitable for settlement and colonisation and could go as far as postulating that the shorter chained plasticizers are creating a food-source at the surface as seen in DMAz. This has been further explained in Nalli *et al.,* where shorter alkyl diester plasticizers are metabolised by *Rhodococcus rhodochrous* [149] something that has been reflected herein.

3.2.2.3 CITRATE PLASTICIZED PVC

The citrate plasticizers have also been analysed as previously demonstrated for mass, slime and protein and carbohydrate adsorption across the thin films, Figure 3.19. A table has been presented showing the total observations for each of the assays as seen in Table 3.5, where pie charts of the total data have been demonstrated. The best performing citrate plasticized PVC film in this group was ATBC, and this has been observed for all the biofouling results.

Table 3.5: Tabulated results for citrate plasticizers of mass, slime, protein and carbohydrate assays.

	% Mass Increase	(SD)	Slime (AU)	(SD)	Protein adsorption (µg/mL)	(SD)	Carbohydrate adsorption (µg/mL)	(SD)
uPVC blank	1.26	0.095	0.056	0.0028	3.46	0.1231	5.912	0.213
ATC	0.35	0.09	0.034	0.034	0.98	0.134	2.34	0.222
ATBC	0.31	0.01	0.035	0.035	1.01	0.0454	2.519	0.145
TEC	0.35	0.12	0.047	0.047	1.45	0.1212	3.21	0.522
TnBC	0.37	0.15	0.0339	0.0339	1.32	0.9333	3.33	0.232
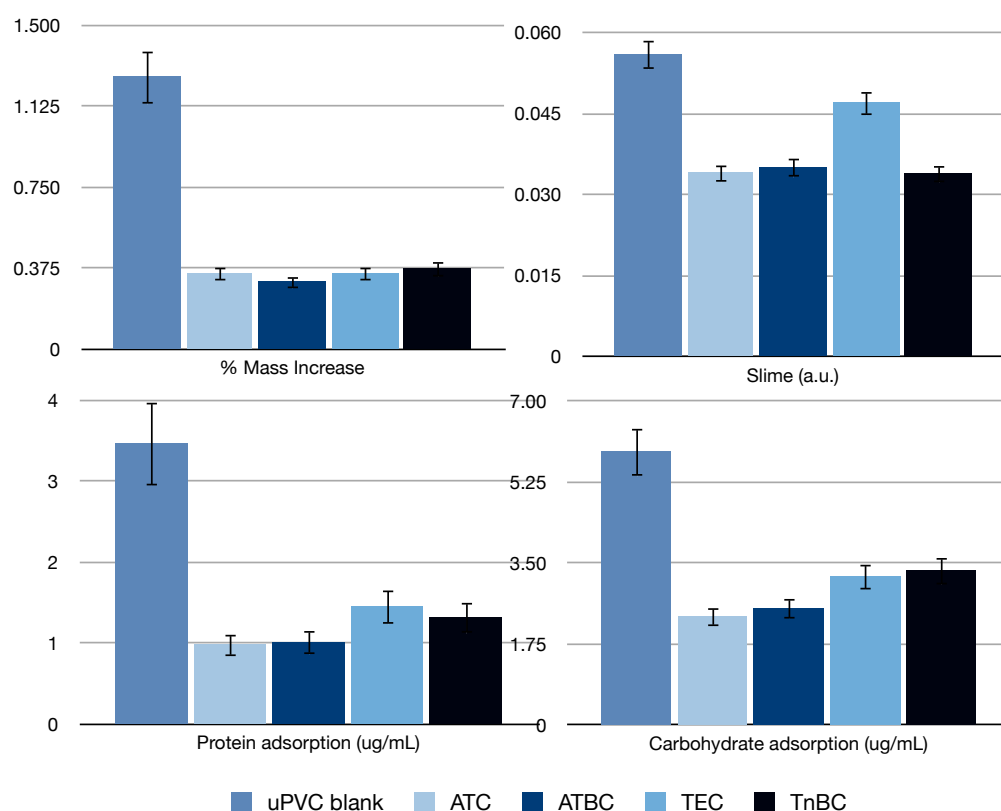
Figure 3.19: Bar charts for mass adsorption, slime adhesion along with protein and carbohydrate adsorption showing the performance of each plasticizer within the group.

The citrate plasticizer group showed lower mass adhesion when compared to the uPVC blank, possibly showing more toxicity to microorganisms and subsequent growth. Toxicity by citrate related plasticizers have been demonstrated by Mochida and Fujita, where ATBC was noted to cause cell death in human, monkey and dog cells in concentrations up to 44.7 µg/mL in human cells for ID_{50},[145] indicating possible reasoning why improved response for mass adsorption occurred. Additionally, it was found that acetyltriethyl citrate could be effective to the bacteria *Bacillus thuringiensis* var. *israelensis*, reported to be a prolonged bioactive agent. It was found that 100% control of multiple infantile species could be obtained for at least 21 or 30 days in fresh and brackish water, respectively. [261] Again, this reflects the mass result observed showing a small change in mass for these plasticized PVC coatings.

Evidently, the citrate plasticized PVC coatings were found to have similar levels of slime adsorption on their surfaces, but have all outperformed the uPVC blank. ATC (0.034 ± 0.004 AU) showed least slime adsorption with TnBC (0.0339 ± 0.002 AU) and ATBC (0.035 ± 0.004 AU) closely matching these results, overlap has occurred statistically from the standard deviation of data points. Upon performing an unpaired 'student' t-test all plasticizers showed statistical significance where $p < 0.0001$, illustrating that slime is conferring mass increase for each of the plasticized PVC membranes. Slime is therefore contributing to mass levels and shows the relationship between adherent mass to the substrates.

Although mass analysis is performed in many biofouling-based studies, [40,262,262] it remains a crude analytical tool for assessing of the level of the overall problem that exists. The slime test is reported heavily as an effective tool in measuring biofouling experiments performed in a laboratory. [24,252] Encompassing the two assays measuring the slime and mass, provides a reinforced knowledge of the level of fouling upon a substrate.

Protein adsorption within the citrate plasticized group demonstrated that all have outperformed the uPVC blank (3.46 ± 0.12 32 µg/mL). The best performing plasticizer, ATC (0.98 ± 0.14 µg/mL), has observed less protein adsorption, and showed the most promise within this body of work.

The observed carbohydrate adsorption shows the citrate group affording less carbohydrate adsorption and in the case of ATC (2.34 ± 0.21 µg/mL) has outperformed the uPVC blank (5.91 ± 0.21 µg/mL) by up to 2.5 times.

A series of leaching measurements were performed for the citrate doped plasticized PVC thin films after a 7-d pure study tabulated in Table 3.6. Figure 3.20 illustrates that ATBC (9.8%) has the least plasticizer loss from its PVC matrix and therefore has the slowest rate of migration,

compared to TBC (34.45%). The citrate plasticizer molecules all possess the same common citric acid derived moiety with differences in alkylation and branch termination on each plasticizer. The degree of branching and alkylation upon the molecule causes characteristic changes in the surface and thus offers different physical challenges for microorganisms to colonise and thrive upon the surfaces of each of these plasticized PVC coatings. Within the citrate group the plasticizers have leached from the PVC matrix at different rates. ATBC was the slowest plasticizer to leach from the PVC matrix, and overall less mass adsorption was observed. TEC leached fastest from the PVC matrix, where increased mass adhesion was also observed. Therefore, if leaching is faster, the level of antifouling effectiveness is also reduced. However, this would require further experimental work and is a hypothesis.

Table 3.6: Tabulated plasticizer migration data of citrate plasticizers from PVC, absorbance measurements were obtained both before and after a pure water study, change in absorbance and %RSD were calculated (n=3 ± 1SD).

IR band analysed	ATC		ATBC		TEC		TnBC	
2975 cm^{-1}	Initial	Final	Initial	Final	Initial	Final	Initial	Final
	0.83	0.180	0.29	0.11	0.75	0.23	0.73	0.27
Change in Absorbance	0.65		0.18		0.52		0.46	
% RSD	1.37		1.09		3.11		0.83	
2864 cm^{-1}	Initial	Final	Initial	Final	Initial	Final	Initial	Final
	0.76	0.14	0.242	0.09	0.67	0.18	0.68	0.20
Change in Absorbance	0.01		0.052		0.43		0.48	
% RSD	0.44		0.50		1.59		1.89	
1449 cm^{-1}	Initial	Final	Initial	Final	Initial	Final	Initial	Final
	0.18	0.05	0.08	0.04	0.121	0.053	0.43	0.21
Change in Absorbance	0.13		0.04		0.068		0.217	
% RSD	1.76		1.83		3.21		0.65	
765 cm^{-1}	Initial	Final	Initial	Final	Initial	Final	Initial	Final
	0.571	0.08	0.17	0.05	0.48	0.12	0.07	0.027
Change in Absorbance	0.491		0.12		0.36		0.043	
% RSD	1.83		4.01		4.99		3.23	
Total Plasticizer Loss (%)	**32.1**		**9.8**		**34.45**		**30**	
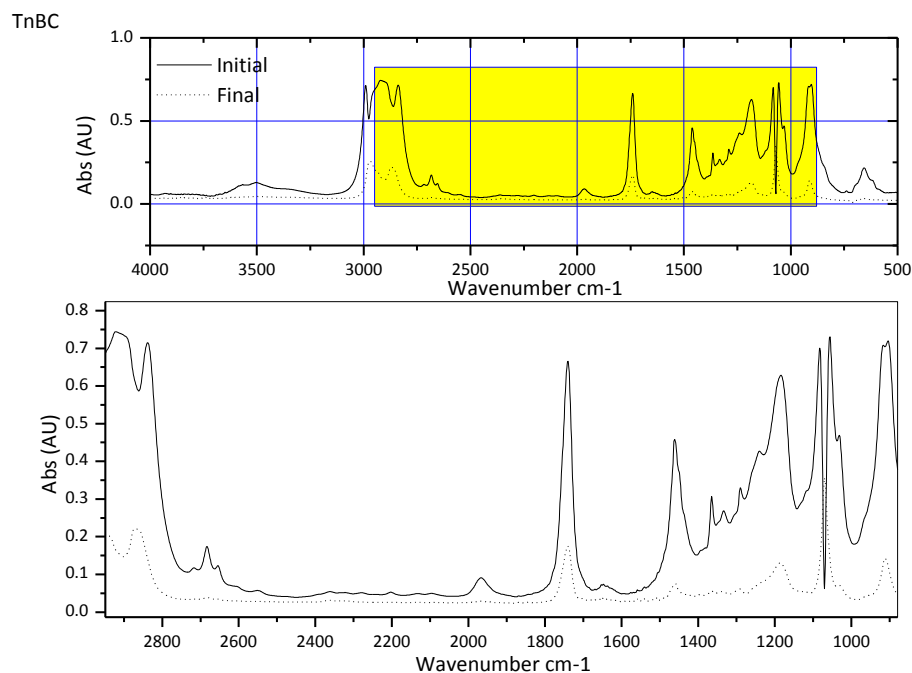
Figure 3.20: FTIR absorbance measurements illustrating plasticizer migration from the PVC matrix example data of TnBC. (Top) Whole spectra, (bottom) zoom of spectral region 2900 – 1000 cm^{-1} showing 4 bands of interest.

Gruetzman and Wagner reported that TEC leached at a faster rate owing to its ability to readily dissolve in water. [263] As with the mentioned author's work, TEC exhibited faster leaching rates showed similar results in this work. In other work, Bando and McGinity showed that drug dissolution was affected through the rate of TEC leaching from the polymer. [264] They found that as TEC was increased within a storage polymer, the rate of drug dissolution decreased, owing to TEC's ability to readily dissolve in water and thus migrate through out of the polymer, further reinforcing the FTIR absorbance measurements demonstrated in this work.

The citrate plasticized PVC thin films have demonstrated a range of responses when compared to the uPVC blank. This represents, for the first time, the way in which these plasticizers have been used to produce an antifouling response to the material. The novelty of the work highlights that plasticized PVC is an overlooked material for this type of application.

3.2.2.3.1 SUMMARY OF CITRATE PLASTICIZERS

The results for the citrate plasticziers show that ATBC across the group was the best performing plasticizer in this group for the biofouling assays administered. The plasticizer has also shown the slowest leach rate, due to its ability to move through the polymeric chains in PVC at a much slower rate. Consequently, this plasticizer has shown the best responses for protein, carbohydrate and mass adsorption.

3.2.2.4 CHLOROPARAFFIN PLASTICIZED PVC

This section details observed results for chloroparaffin plasticized PVC thin films. As with previous sections, for brevity, the data has been tabulated as displayed in Table 3.7. These chloroparaffin plasticizers have all demonstrated promise as an antifouling plasticized PVC material. CLP_{70} demonstrated the best antifouling responses in the group in all assays performed.

Table 3.7: Table of results for the chloroparaffin doped PVC thin films for all assays administered .

	% Mass Increase	(SD)	Slime (AU)	(SD)	Protein adsorption (µg/mL)	(SD)	Carbohydrate adsorption (µg/mL)	(SD)
uPVC	1.26	0.095	0.056	0.0028	3.46	0.1231	5.912	0.213
CLP40	1.12	0.056	0.048	0.00526	2.91	0.0921	3.98	0.162
CLP50	1.01	0.0505	0.053	0.00665	2.76	0.0832	3.87	0.330
CLP60	1.05	0.0525	0.051	0.00555	2.83	0.0545	4.81	0.251
CLP70	0.69	0.0345	0.043	0.00327	2.84	0.2313	3.66	0.332
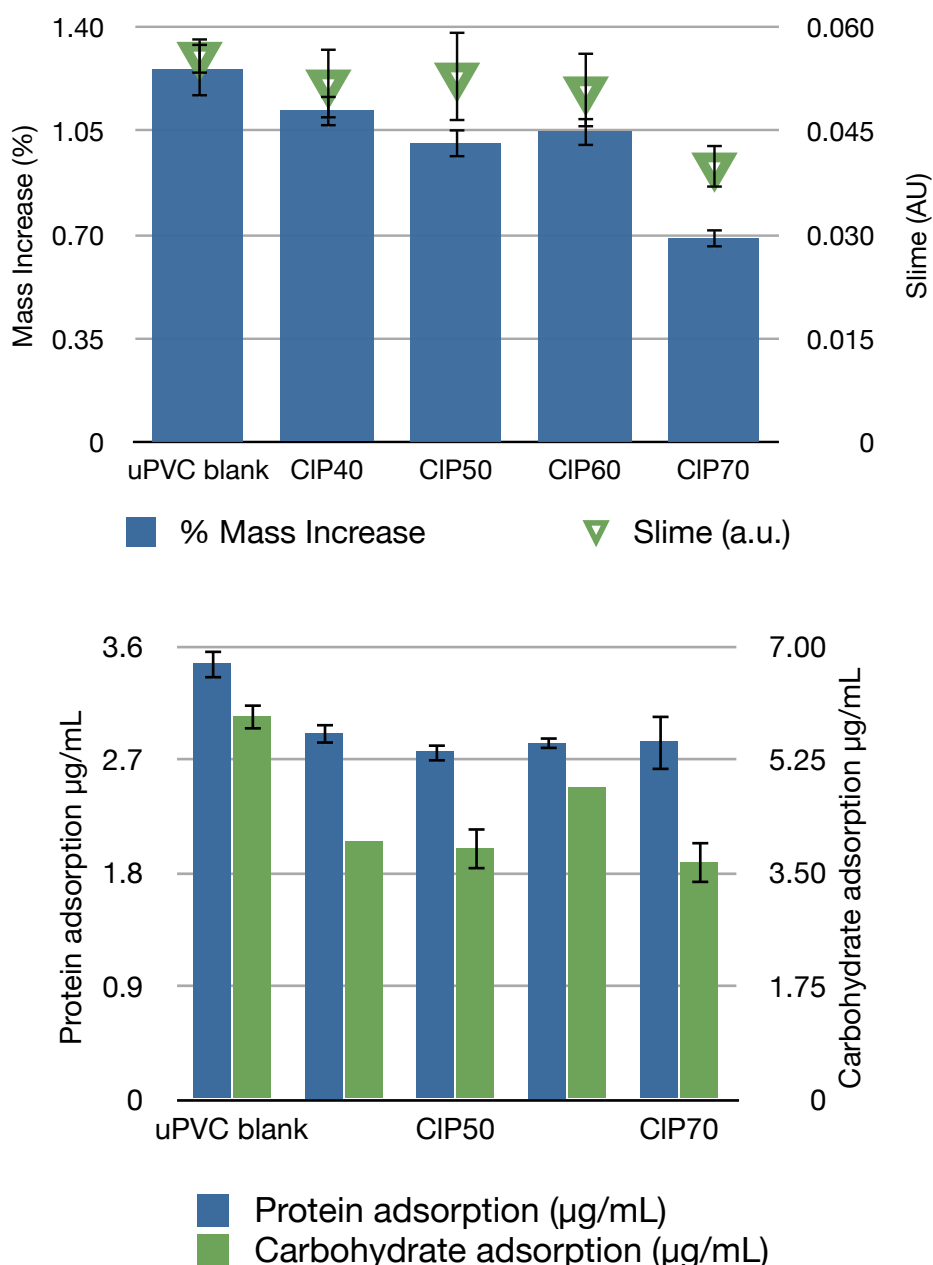
Figure 3.21: Showing all data for mass, slime, protein and carbohydrates for the chloroparaffin doped PVC thin films. Top chart shows mass and slime and the bottom chart shows protein and carbohydrate adsorption for the chloroparaffin plasticizer group.

Literature is scarce on overall toxicity of polychlorinated alkanes (PCA). However, Fisk *et al.*, showed that chlorine substitution did not greatly increase or decrease the toxicity of C_{10} and C_{14}- PCAs. Indeed, this result from Fisk *et al.*, conflicts with the results that were found in this work, where differences in fouling has been observed. [265]

Within the literature, chloroparaffin plasticizers are used as flame-retardants when incorporated into a PVC matrix, [234-236,238] with the last publication of chloroparaffin doped in PVC used as a chemical catcher (a polymer capable of absorbing analytes) being reported in

1996. [239] Thus far, no reports of chloroparaffin doped with a PVC matrix as an antifouling based coating has been reported and therefore presents novelty to this work, along with other plasticizers aforementioned.

Across the group considerable differences in slime adsorption were observed for the plasticized PVC polymers compared to the blank, with CLP_{70} showing the best response overall. CLP_{70} (0.04 ± 0.03 AU) demonstrated least slime adsorption (x 1.4) more effective than the uPVC blank (0.056 ± 0.003 AU). The remaining plasticizers remained relatively similar to the uPVC blank indicating the efficacy of these plasticizers not as effective. Chloroparaffin has been discussed with specific mention of toxicity to microorganisms in Sverdrup's work, toxicity was studied using nitrifying bacteria. [266] It was found that short chain chloroparaffins, such as the ones used in this study, were not effective and often needed concentrations of up to EC_{10} = 570 mg kg^{-1} in order to be toxic to these bacterial strains. This result has been reflected, where there has been least slime produced across the chloroparaffin plasticized PVC compared to the uPVC blank. However, it should not be ignored that CLP_{70} showed a decrease in slime adsorption when compared to the other chloroparaffin plasticizers as well as in the mass result. Tang and Wang report the quantitative structure activity relationship (QSAR) in chlorinated alkanes is increased and indeed relates to the level of substitution of chlorine atoms on the alkane molecule. [267]

The carbohydrate adsorption data demonstrates that CLP_{70} (3.66 ± 0.332 μg/mL) demonstrated least carbohydrate adsorption in this group. CLP_{40}, CLP_{50}, and CLP_{60}, have all demonstrated similar levels of carbohydrate adsorption, illustrating that these surfaces may be experiencing similar fouling responses owing to possible microorganism involvement especially when compared to the uPVC blank.

Protein adsorption again was reduced in the PVC films containing chloroparaffin plasticizers, showing repeatedly that chloroparaffins are successful antifouling materials. In a study by Wang *et al.,* it was found that the introduction of a non-ionic surfactant into a PVC system would reduce the adsorption of proteins by up to 15 μg/mL in the first hour of use. [268] Although, this is not something which is applicable to this work, but highlights another concept that could be considered when using and designing chloroparaffin plasticized PVC.

3.2.2.4.1 LEACHING AND SURFACE ACTIVITY

As with previous plasticizer groups, the chloroparaffin plasticized PVC thin films were analysed for their surface activities investigated through the leaching of the plasticizer from the polymer

matrix. In a paper by Kang and Meyerhof, chloroparaffin plasticizers were incorporated into ion-gas polymer sensors to prevent further leaching of film components, they anticipated that their detection limits would improve since the use of chloroparaffin plasticizers are non-volatile under ambient conditions. However, the authors found that the addition of chloroparaffins increased the rate of migration of film components because the level of plasticizer loss exacerbated this phenomenon. [269] In another study, Ertan-Lamontagne *et al.*, used 60 & 70% chloro-substituted chloroparaffin plasticizers to investigate concentrations of surrounding analytes when incorporated in PVC. [270] They found that as PVC was doped with CLP_{60} and CLP_{70} the level of uptake for PVC in adsorbing nitrobenzene increased. This could be due to CLP_{60} and CLP_{70} leaching from their PVC matrices and therefore facilitating nitrobenzene adsorption on the polymer, thus increasing analyte enrichment. Leaching studies were not performed in their work, which could resolve their closing conclusion of polymer thickness having an overall effect on the level of enrichment.

Table 3.8 summarises the leaching rates of the four chloroparaffin plasticizers doped into PVC; CLP_{40} , $CLP_{50,}$ CLP_{60} and CLP_{70} in PVC (5% w/v). Interestingly, the chloroparaffin-doped plasticizers have leached in accordance with the level of chlorinated substitution on each.

Table 3.8: Table showing total plasticizer loss for the chloroparaffin doped PVC thin films.

Plasticizer Type	CLP_{40}	CLP_{50}	CLP_{60}	CLP_{70}
Total Plasticizer Loss (%)	**22.53**	**14.55**	**13.7**	**7.76**

The level of plasticizer migration shows → CLP_{40} , $CLP_{50,}$ CLP_{60} to CLP_{70} lowest to highest indicating that the level of chlorine substitution on each C_{10} paraffin molecule is causing the migration rate to change in each PVC matrix. Consequently, fouling has been reduced on the materials which have had slower migration. This could be due to extended surface activity on the slower leaching plasticizers shown within. This highlights that plasticizer loss is linked to the antimicrobial effectiveness of the polymer over time. Fankhauser and Grobb approached a plasticizer migration problem by analysing leachate from PVC gaskets for food storage items. They discovered that temperatures above 40 °C would impose further migration of plasticizers to leach from the PVC matrix. [271] Temperatures within this study were maintained at 20 °C throughout and thus migration levels were not elevated.

3.2.2.4.2 SUMMARY OF CHLOROPARAFFIN PLASTICIZERS

The most interesting result of the chloroparaffin plasticized PVC thin films was demonstrated by $CLP_{70.}$ This plasticizer leached the slowest from the PVC matrix and demonstrated this as a

loss of 7.76 x. Consequently, mass adhesion was less when compared to the remainder of this group.

3.2.2.5 DIBENZOATE PLASTICIZED PVC

Figure 3.22 details results for mass, slime, protein and carbohydrate all displayed on the same chart. This data set enables the observation of how the plasticized thin films are performing as an overall material. Within the dibenzoate plasticizer group, noticeably, PEGDB demonstrated the best antifouling responses where least slime, mass protein and carbohydrate adsorption have been detected – all of which are attributed to the overall biofouling problem.
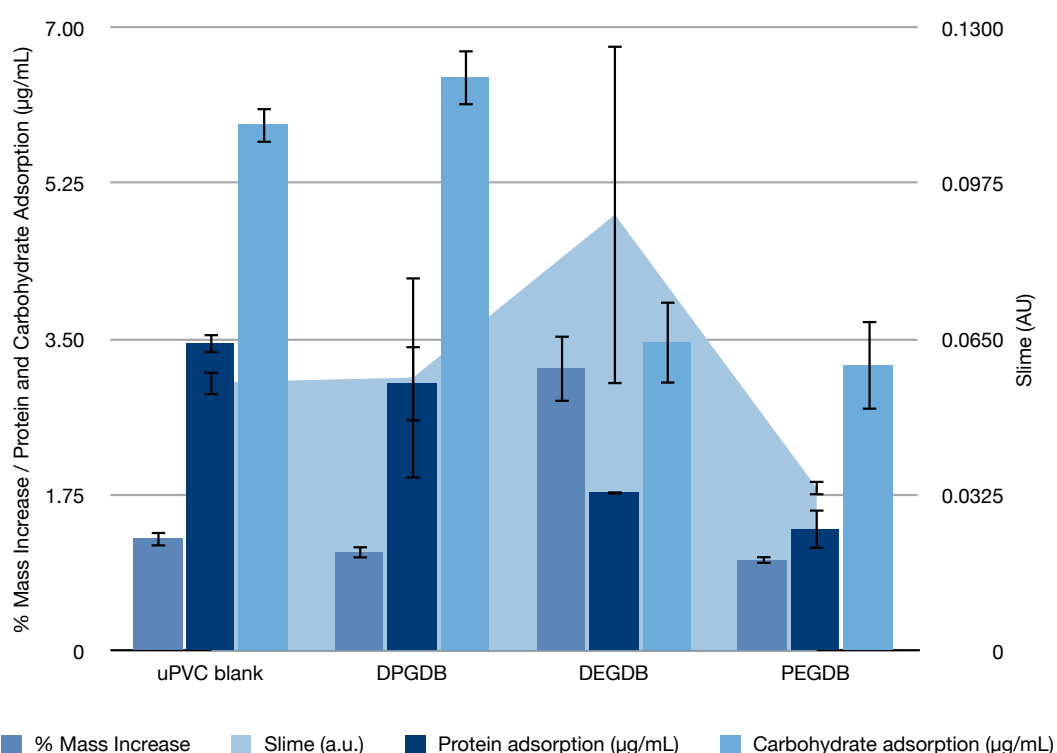
Figure 3.22: Chart showing all data series for mass, slime protein and carbohydrates for the dibenzoate doped PVC thin films.

The data demonstrates similar mass increases for the uPVC blank (1.26 ± 0.36%), DPGDB (1.11 ± 0.08%) and PEGDB (1.02 ± 0.39%), with DEGDB (3.179 ± 0.051%) displaying some 2% higher mass adhesion. The effectiveness of the plasticizers from this group as an antifouling material is somewhat different to other groups described as they are performing similarly to the uPVC blank. It can be concluded, from the results in Figure 3.21, that the dibenzoate plasticizers present little efficacy as an antifouling material. Within the last ten years, Demssie *et al.*, filed a patent for the use of DEGDB as a potential compound for the prophylaxis or treatment of an immunodeficiency condition highlighting a potential use in the prevention of diseases. [272] The

use of this type of plasticizer in other fields highlights a potential candidacy for a broad range of practical applications. Figure 3.23 shows the general structure of the dibenzoate plasticizers where the benzoic acid moiety has been identified on the molecule by the blue arrows.
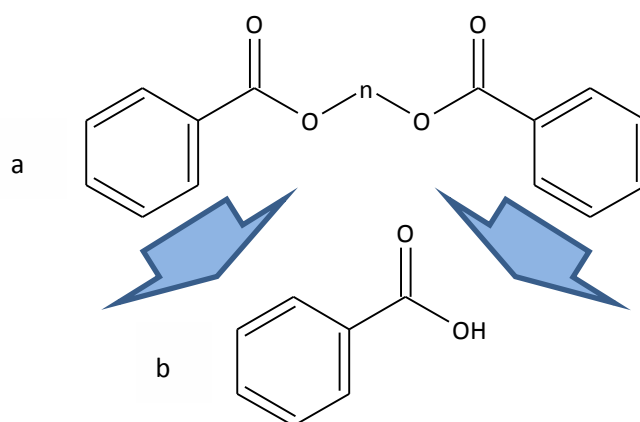
Figure 3.23: Molecular structure of (a) benzoate derived plasticizer, where n is the substituted structural difference between the plasticizers in the group and (b) molecular structure of benzoic acid.

The 'n' represents the structural differences between each of the plasticizers contained in this group; two benzoic acid derived terminated moieties on the molecule are highlighted.

Slime adsorption measurements of dibenzoate plasticized PVC were obtained for DPGDB, DEGDB and PEGDB. PEGDB (0.034 ± 0.0017 AU) resisted slime adsorption by up to 40% when compared to the uPVC blank (0.056 ± 0.0003 AU). The distinct lack of literature on the slime adsorption to plasticized PVC again highlights the need to investigate the level of biochemical interaction with such a material, illustrating the novelty of this type of work.

DEGDB (0.091 ± 0.0212 AU) produced an increased slime adsorption when comparing the whole group, suggesting that preferential settlement and slime excretion occurred. The plasticizers within this group all consist of the same dibenzoate moiety as depicted in Figure 3.24. The structural differences between each of the dibenzoate plasticizers are seen within the centre of the molecule and have thus possibly brought about various differences seen in the slime result, but also that of the overall mass adsorption. It can be seen that ether substitutions and branching of alkyl moieties are what separates the three molecularly.
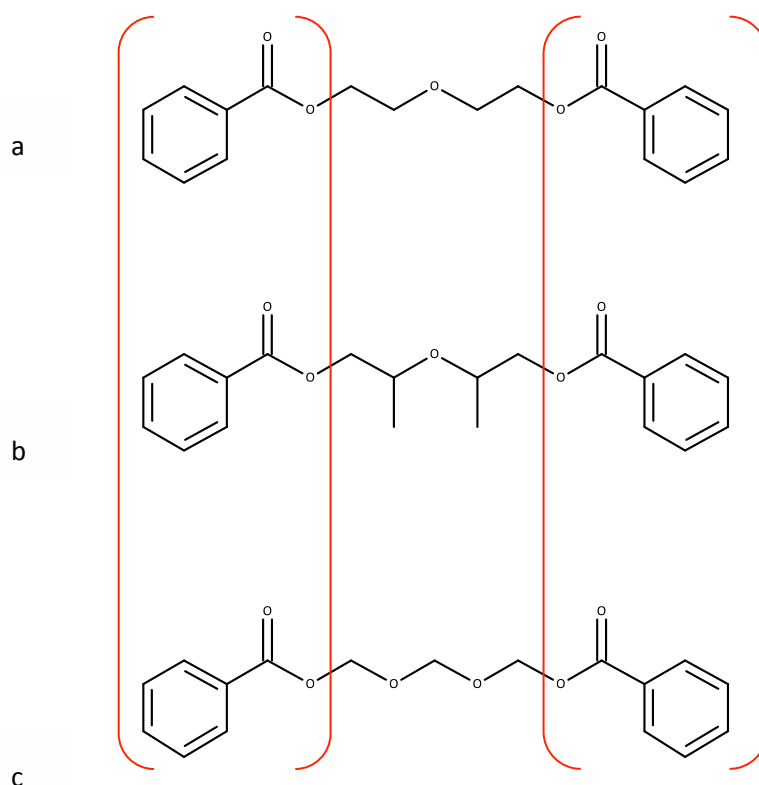
Figure 3.24: Molecular structures of (a) DEGDB, (b) DPGDB and (c) PEGDB, with highlighted dibenzoate moieties.

Ether is known to inhibit the binding of certain enzymes necessary for metabolic functions in some bacteria. [273] For instance in Jennings *et al.*, it was found for 81 compounds tested in triplicate assay systems containing luminescent bacteria, ether required 5623 ppm to produce a 50% effective concentration (EC). [274] This shows the potency of the moiety depicted in PEGDB, compared to the others suggesting possible validity for its display in minimising slime and mass adsorption. Benzoic acid, and in particular, dibenzoate derivatives, are known to have antimicrobial attributes, [275] showing that each of these plasticizers could have potential in preventing microbial attachment. Contrastingly, DEGDB (0.091 ± 0.033 AU) displayed greatest slime adsorption of the plasticized PVC coatings suggesting otherwise to this statement. For instance, Kermanshahi *et al.*, showed the degradation of DEGDB by microorganisms, simpler than that of propyl or polyethyl plasticizers, [275] and thus could be a reason for elevated slime adhesion observed comprehensively in this body of work. The authors showed that DEGDB degrading bacteria were faster at degrading DEGDB than that of DPGDB, thus detailing a feasible explanation in why slime adsorption was elevated, and mass, on this plasticized PVC coating alone.

The dibenzoate plasticized PVC thin films have displayed varied results in each assay within this group. The carbohydrate adsorption assay, quantified PEGDB (3.21 ± 0.51 µg/mL) having the least concentration of adsorbed total carbohydrates to each of the thin films, and

outperformed the uPVC blank (5.91 ± 0.21 µg/mL) by up to 1.8 times. Interestingly, DPGDB (6.44 ± 0.322 µg/mL) displayed higher carbohydrate concentrations within the group, this could be due to the faster plasticizer migration where microbial activity increased. Molecularly this molecule has more glycol substituted moieties and thus could also be attractive to some microorganisms in its potential degradation as a food source. The protein adsorption data also displays varied results within the group, PEGDB (1.37 ± 0.23 µg/mL) demonstrated the least protein attachment, whereas DPGDB (3.01 ± 0.44 µg/mL) demonstrated similar levels to the uPVC blank (3.45 ± 0.12 12 µg/mL) highlighting that this plasticizer could be attracting microorganism attachment and colonisation and growth exhibited in the fouling process.

3.2.2.5.1 LEACHING AND SURFACE ACTIVITY OF DIBENZOATE PLASTICIZERS

Table 3.9 details the plasticizer loss and thus surface activity for the dibenzoate plasticized PVC thin films

Table 3.9: Table showing total plasticizer loss for the dibenzoate doped PVC thin films given in %.

	DPGDB	PEGDB	DEGDB
Total Plasticizer Loss (%)	4.25	3.25	20.75

The level of migration gives an indication of the surface activity and thus biocidal activity of the plasticized PVC thin film coatings. DEGDB (4.25% loss) and DPGDB (3.25% loss) have migrated the least from the PVC matrix. This will have an impact on the level of surface activity these plasticizers are demonstrating from the matrix, as the level of migration in DEGDB and DPGDB suggests that the plasticizers are not going to be available upon the surface and any potential toxicity to microorganisms. In fact, what is being observed is an effect from PVC rather than the plasticizers themselves.

When analysing the slime adsorption for this group of plasticizers it can be seen that both the plasticizers with the lowest rates of plasticizer migration and loss from the matrix have seen elevated levels of slime production on their surfaces. PEGDB (0.034 ± 0.0017 AU), seen a smaller level of slime production perhaps because the plasticizer is leaching at a rate that benefits the PVC matrix as an antifouling agent. DPGDB (0.057 ± 0.0212 AU) demonstrated a similar slime response to that of the uPVC blank (0.056 ± 0.0003 AU), this indicates that the level of migration may not be significant in effectively acting as a biocidal agent for the PVC matrix. In a study by Azadeh Kermanshahi-pour *et al.*, biodegradation studies were performed using Rhodococcus rhodochrous where it was established that DPGDB and DEGDB were metabolised very slowly. [275] As DEGDB and DPGDB have leached at significantly lower rates

plasticizer availability is therefore lower in concentration, which in these cases led to more slime growth upon the surfaces, and thus offers a possible explanation to this group of results.

3.2.2.5.2 SUMMARY OF DIBENZOATE PLASTICIZERS

Across this group, DEGDB and DPGDB has leached significantly slower than DEGDB, this has been attributed to the molecular attributes as discussed throughout the chapter. PEGDB in particular is the best performing antifouling plasticized PVC thin film in this group, demonstrating least mass, slime, protein and carbohydrate adsorption throughout each of the assays.

3.2.2.6 SEBACATE PLASTICIZED PVC

Figure 3.25 shows results for slime, mass as well as protein and carbohydrate adsorption for the sebacate plasticized PVC thin films. The sebacate plasticizers showed a broad range of results in the group. DEHS demonstrated the highest antifouling activity of all the plasticizers used – showing least adsorption of slime, mass and least biochemical adsorption.
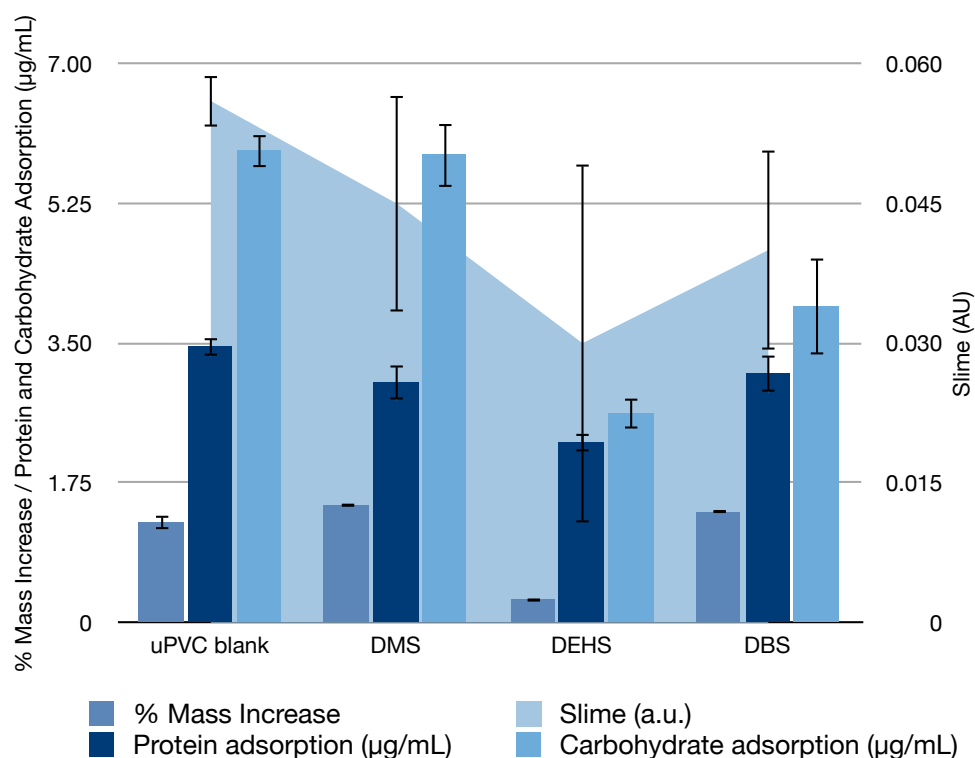
Figure 3.25: Chart showing all data series for mass, slime protein and carbohydrates for the sebacate doped PVC thin films.

DEHS (0.29 ± 0.13%) observed the least mass adhesion in the polymer coatings and is somewhat 4 times more effective in averting mass compared to the uPVC blank (1.26 ± 0.36%).

Mochida *et al.,* showed that growth inhibition of mammalian cells were more effective with higher doses of DBS when compared with ATBC (seen in the citrate plasticizer group), illustrating that the potency of DBS is less.[145] These results are similar to the findings in this work, where ATBC is more potent in the biofouling results when compared to DBS.

Interestingly, sebacic acid from which this plasticizer group is derived, is known to possess high potency towards some fungi. Melliou and Chinou performed MIC counts on Royal Jelly, of which sebacic acid is a major component; where it was found that sebacic acid exhibited the highest activity against the fungi used where concentrations of 0.15 – 0.20 µg/mL were used. [276] The effectiveness of succinic acid has been reproduced in this study, where all succinic acid esters doped in PVC have outperformed the uPVC blank.

Slime levels, demonstrated in Figure 3.24 show that DEHS (0.03 ± 0.020 AU) has demonstrated least slime adsorption when compared to the other sebacate plasticizers. DBS (0.040 ± 0.010 AU) and DMS (0.045 ± 0.013 AU) showed similar responses in this slime assay. All three plasticized PVC coatings showed decreased slime adsorption when comparing them to the uPVC blank (0.05 ±0.003 AU). When compared statistically using a 'student' t-test it was found that slime was a significant component in the overall mass showing p values <0.001. However, DMS had increased carbohydrate adsorption, suggesting that the content of the biofilm had higher carbohydrate concentrations. DMS also showed fastest leach rate from the PVC matrix, again highlighting that the level of surface activity on the DMS doped substrates were being used as a food source – and hence the level of carbohydrate adsorption increased.

The alkylation and substitution of alkyl branching on sebacate plasticizers has been discussed in Bonora *et al.,* where it was found that shorter chain sebacate plasticizers do not readily penetrate liposomes readily when compared to the longer chain sebacate plasticizers. [277] This could highlight a possible reason why DEHS has displayed less slime adsorption when compared to DMS. Two ester groups in the sebacate plasticizers are bound to a flexible chain favouring dipole-dipole electrostatic interactions. Consequently, the shorter chain sebacate plasticizers, for which the surface interactions are dominant, only perturb the inner surface of a cell membrane. The longer chains exhibit hydrophobic interactions and thus disturb the whole cell membrane highlighting the potency of molecular interactions with cells, which has also been discussed by Lee. [278]

DEHS protein adsorption (2.26 ± 0.12 µg/mL) was least when compared to the group, DES (3.01 µg/mL) and DBS (3.12 µg/mL) observed similar protein adsorption to the uPVC blanks. Tese results suggest that both DBS and DEHS have leached and the polymer is no longer active, and is therefore showing the same surface chemistry as the uPVC blank. The protein

adsorption assay presented herein was found to be reproducible and sensitive for the determination of proteins adsorbed on each of the test substrates, something that remains in many other author's work. [279,280]

Carbohydrate adsorption was assessed according to the Dubois method. It was found that DMS (5.86 ± 0.39 µg/mL) had demonstrated the greatest carbohydrate adsorption to its surface showing poor antifouling response, which when compared to the uPVC blank (5.91 ± 0.21 µg/mL) is very similar. However, DEHS (2.63 µg/mL) demonstrated least protein adsorption and is somewhat 50% superior to the uPVC blank. In the same manner, carbohydrates and proteins were determined in Strathmann *et al.,* [258] where it was found that protein was the predominant biomolecule contained in EPS. This is true of the results reported herein, where carbohydrates are in almost two-fold excess to proteins (in µg/mL) in some of the plasticized PVC thin films, this could be attributed to the microorganism interaction on the surface using the plasticizer as a food stuff and producing excess carbohydrate in this manner. Additionally, Lee *et al.* found that protein and carbohydrates in a reverse osmosis system adhered to filtration membranes in the ranges of 4.8 ± 0.8 and 7.7 ± 0.7 µg/mL respectively, highlighting again that carbohydrates are generally higher in concentration. In the same way, Aguilera *et al.,* used the same biochemical carbohydrate characterisation method where they found that carbohydrates were the predominant biomolecule in the EPS matrix, [281] something that is represented in this work.

3.2.2.6.1 LEACHING AND SURFACE ACTIVITY OF SEBACATE

In the same manner as the other plasticizers reported in this section of work, sebacate plasticizers doped in PVC have been analysed for their migration properties thus investigating the surface activity across the membranes. Both DEHS (19%) and DBS (10%) plasticized PVC experienced lower levels of migration when compared to DMS (29.25%) (Figure 3.26) that experienced almost one third of plasticizer migration from the PVC matrix.
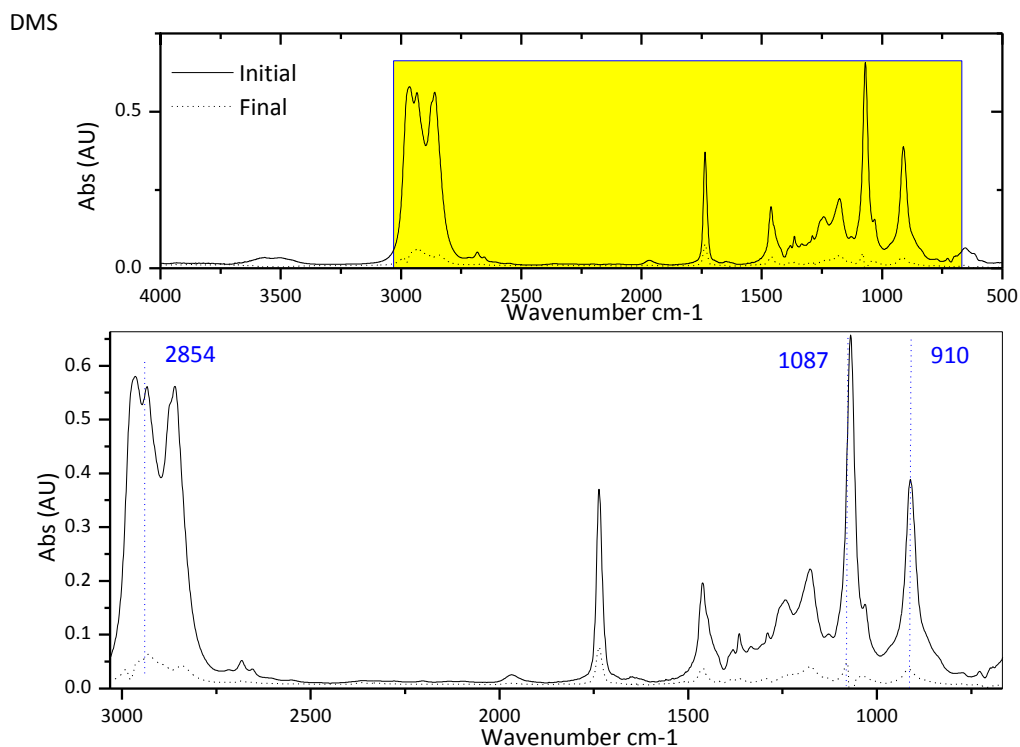
Figure 3.26: zoom of spectral region 3000 – 400 cm^{-1} showing 3 bands of interest. Absorbance measurements were obtained both before and after a pure water study, where change in absorbance and %RSD were calculated (n=3 ± 1SD).

As with phthalic acid esters, sebacic acid ester plasticizers are liquid plasticizers with low polarity [277] and thus their interaction at the PVC membrane outer surface plays a key role in their biological and toxicological effects which will be addressed within this section.

Plasticizers are generally not chemically bonded to the polymeric matrix and so have the ability to migrate through the matrix to the surface. In this case, this enables the polymeric matrix to deliver a compound release mechanism through the PVC. It has already been discussed that, as length and shape of ester chains increase the response for slime and mass is often reduced. Contrary to this, shorter alkyl chain plasticizers afford higher fouling levels as depicted in slime and mass results, *vide supra*. Sebacic acid ester derived plasticizers possess ester groups that are bound to a flexible chain and adhere to the surface of the PVC in a manner that gives a longer biocidal 'time-frame'. This is seen where the sebacate plasticizers showed improved antifouling results across some of the plasticizer groups, which could be attributed to dipole-dipole electrostatic interactions that are present between the plasticizer-polymer matrix. Consequently, the shorter chain sebacate plasticizers, for which surface interactions are dominant, have only demonstrated slight antifouling response and only slightly perturb microorganism interactions, whereas the longer chain sebacate plasticizers, where the

hydrophobic interactions are stronger than the electrostatic ones appear to have strong antifouling response.

3.2.2.6.2 SUMMARY OF SEBACATE PLASTICIZERS

Generally, a feature of the sebacic acid derived plasticizers used within this study showed good antifouling responses when compared to the other plasticizer groups. In similar work Bonora *et al.*, showed that migration of sebacic acid ester derived plasticizers were generally slower from the polymer matrix when branching within the molecule increased, they also attribute this migration rate to electrostatic interactions between the plasticizer molecule and polymer matrix. [277] In other work by Dugo *et al.*, it was found that sebacic acid derived plasticizers migrated at almost non-detectable limits when analysed using GCMS, this is a result not reflected in this body of work and as such, sebacate plasticizers showed detectable limits through the use of FTIR spectroscopy.

3.2.2.7 PALMITATE PLASTICIZED PVC

The palmitic acid derived plasticized PVC group also underwent the same testing as described previously for all other plasticizers in this chapter. Table 3.10 shows tabulated results for the different assays performed in the determination of the antifouling capability of the palmitate plasticized PVC material.

Table 3.10: Tabulated results for the palmitic acid derived plasticized PVC thin films.

	% Mass Increase	(SD)	Slime (AU)	(SD)	Protein adsorption (μg/mL)	(SD)	Carbohydrate adsorption (μg /mL)	(SD)
uPVC	1.26	0.095	0.056	0.0028	3.46	0.1231	5.912	0.213
IPP	0.56	0.2	0.053	0.00265	2.76	0.38	3.54	0.19
MP	0.54	0.3	0.05	0.0025	2.93	0.15	4.21	0.33

Clearly, the effects of the palmitate plasticizers result in decreased mass adhesion when compared to the uPVC blank by up to 50%, Figure 3.27. MP (0.54 ± 0.31%) has exhibited the best response in this assay and has reduced mass adhesion twofold when compared to the uPVC blank. This result is suggesting that the toxicity of this plasticizer is possibly showing less mass adsorption and duly less microorganism involvement upon the surface of these test coatings.
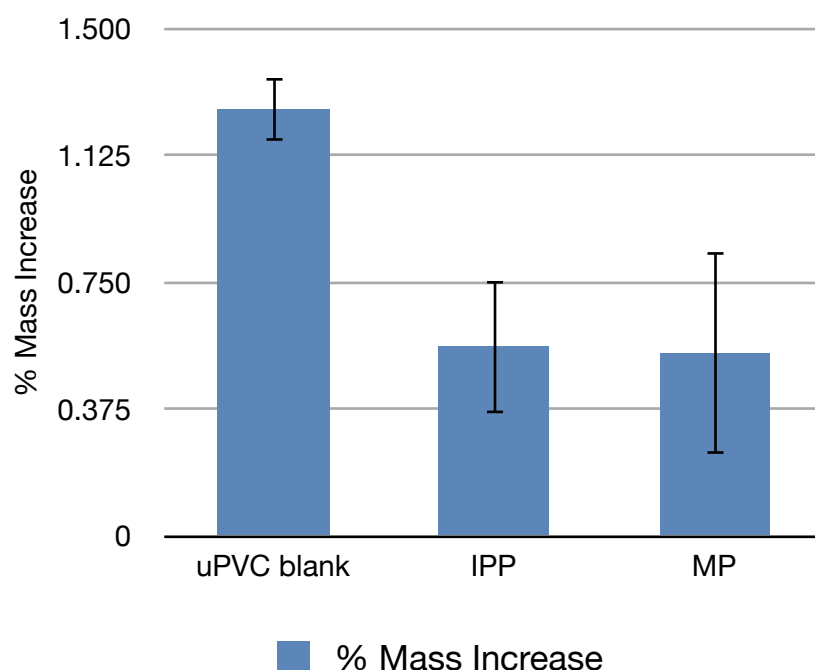
Figure 3.27: % Mass increase for palmitate plasticized PVC following a 7 d freshwater tank study (n=9 ± 1SD).

DMP has been reported to be toxic to brine shrimp by Huang *et al.*, where a brine shrimp lethality test (BST) revealed that MP was toxic in concentrations exceeding 100 µg/mL. [282] Furthermore, Gabel investigated an oviposition response of *Lobesia botrana* to MP. Egg laying was found to be weaker where palmitic acid was in abundance. [283] Although this test organism is outside of this study, it suggests an interesting concept; palmitic acid is somewhat poorer in allowing settlement that could be a theory as to why the palmitate plasticizers produced less mass adsorption.
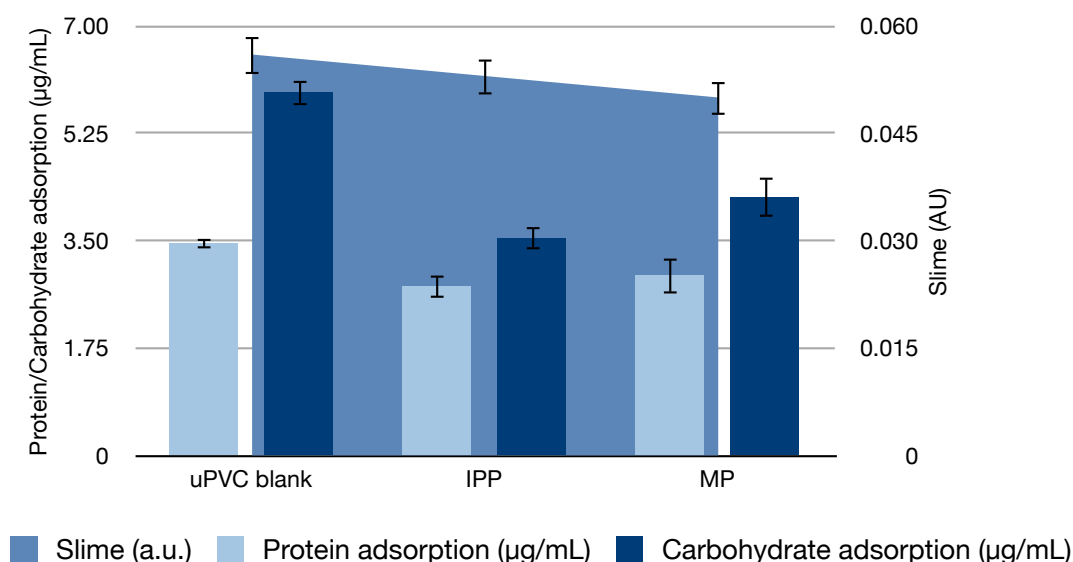
Figure 3.28: A comparison chart showing slime, protein and carbohydrate adsorption of the palmitate plasticized PVC coatings.

Slime was measured across PVC doped with palmitate plasticizers in the concentration range of 5% as discussed in Section 2.1.1.1, *vide infra*. Figure 3.28 shows the overall slime adhesion measured for IPP, MP and uPVC polymer coatings, showing that MP and IPP have adsorbed similar quantities of slime within the group.

There is also overlap of standard deviation across the plasticized PVC coatings, highlighting these polymers showed mixed responses in slime adsorption. The results demonstrate overlap between IPP, MP and even the uPVC polymer thin films showing that all three of these results are very similar. When a 'student' t-test was performed it was seen that statistical difference remains at $p < 0.0001$ showing that slime adsorption is still related to the level of overall mass accumulated on each of the test polymers. It is still important to note that overall mass of the two plasticized PVC polymer types; IPP and MP have adsorbed less mass when compared to the uPVC blank. This suggests that the content of the mass adsorbed to these plasticized PVC coatings pertains to slime.

For the carbohydrate adsorption assay, IPP (3.54 ± 0.19 µg/mL) has performed well and MP (4.21 ± 0.33 µg/mL) respectively. These results show that the response is 1.4 X more effective than the uPVC blank (5.91 ± 0.21 µg/mL). Similarly, the protein adsorption assay IPP (2.76 ± 0.38 µg/mL) and MP (2.93 ± 0.15 µg/mL) were outperforming the uPVC blank in the adsorption of protein to their surfaces. In a review by Hong Chen *et al.*, it was suggested that protein adsorption was dictated by not only surface charge or wettability, but also topography. [284] The topographical influence and wettability have shown throughout that this could influence the

level of the protein carbohydrate, mass and slime when carried out in the laboratory studies. One of the key findings in this work is that as plasticizers leach at slower rates, the level of fouling is reduced. This influence has been discussed in Unsworth *et al.*.[285]

3.2.2.7.1 LEACHING AND SURFACE ACTIVITY OF PALMITATE PLASTICIZED PVC

Leaching activity of the palmitate plasticized PVC thin films was obtained using FTIR absorbance measurements as summarised in Table 3.11.

Table 3.11: FTIR absorbance measurements illustrating plasticizer migration from the PVC matrix example data of both palmitate plasticizers.

IR band analysed	IPP		MP	
$2862\ cm^{-1}$	Initial	Final	Initial	Final
	0.74	0.71	1.03	0.05
Change in Absorbance	0.02		0.98	
% RSD	4.76		0.59	
$1462\ cm^{-1}$	Initial	Final	Initial	Final
	0.09	0.069	0.17	0.03
Change in Absorbance	0.021		0.14	
% RSD	3.14		8.66	
$1078\ cm^{-1}$	Initial	Final	Initial	Final
	1.41	1.32	1.67	0.02
Change in Absorbance	0.09		1.65	
% RSD	6.18		0.92	
$908\ cm^{-1}$	Initial	Final	Initial	Final
	0.47	0.457	0.64	0.1
Change in Absorbance	0.013		0.63	
% RSD	7.9		1.33	
Total Plasticizer Loss (%)	**3.6**		**85**	

MP plasticized PVC evidently displays high levels of plasticizer migration from the PVC matrix and a plasticizer loss of 85% was observed. IPP showed less plasticizer loss from the same matrix with a loss of 3.6%. As with previous plasticizers, the level of migration could be explained by the molecular structure of each palmitate. IPP has a branched alkyl system whereas MP displays a molecule that is smaller and has less branching, which showed higher plasticizer migration from the polymer matrix. In a study by Gan *et al.*, shorter chain palmoleic acid esters were found to migrate faster from the PVC matrix when compared to long(er) chained molecules,[286] stating that their volatility was an issue. The findings are similar to what is observed in the data, where MP has migrated from the PVC matrix in a 7-d period over 80% more than IPP. In a separate study by Macedo Cardoso *et al.,* it was found that IPP gave lower toxicity when tested against *Pseudomonas aeruginosa.* It was also established that IPP when

cleaned with an aluminium oxide column gave subsequent lower toxicity to this organism, [287] where IPP has performed most favourably in this work.

3.2.2.8 PHTHALATE PLASTICIZED PVC

Figure 3.29 demonstrates all parameters measured; slime, mass, protein and carbohydrate adsorption.
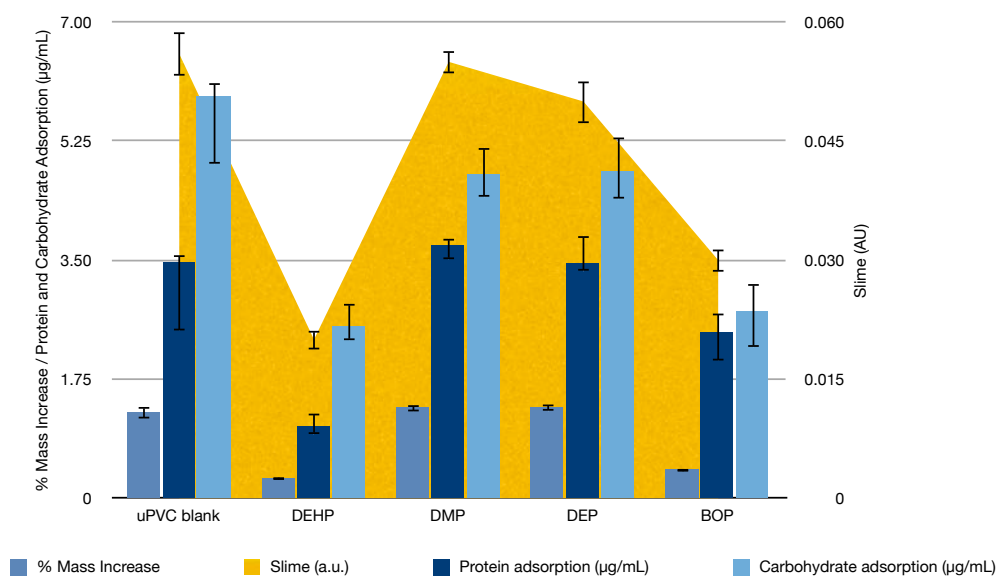
Figure 3.29: Phthalate doped PVC thin film results for slime, mass, protein and carbohydrate adsorption following a 7 d freshwater laboratory study.

This graph demonstrates that DEHP (0.29 ± 0.2%) and BOP (0.42 ± 0.21%) are outperforming DEP (1.34 ± 0.09%), DMP (1.33 ± 0.062%) and the uPVC control in all assays administered.

DEHP is already known to be toxic to a range of species of bacteria, [140] and indeed this is reflected thus far in the mass adhesion results seen in Figure 3.28. It proves that this plasticizer is indeed efficacious in delivering toxic responses to organisms that come in to contact with the compound. The mass result for DEHP is the lowest response seen throughout any of the plasticized PVC compounds already detailed in this body of work, and therefore presents itself as a good antifouling agent when doped into a PVC matrix.

Nalli *et al.*, had demonstrated that *Rhodococcus rhodochrous* was incapable of growing on phthalic acid when introduced as a sole carbon source, which although is not replicated in this study, demonstrates a good indication to the efficacy of the plasticizer group as an antimicrobial agent.[149] Furthermore, Amatya and Tuladhar showed that toxicity to invertebrates, in particular *Artemia salina* at LC_{50} was in the range of 538.15 mg/L. [288] In other

studies, Call *et al.*, showed that DEHP is toxic to the freshwater benthos *Chironomus tentans* in the concentration of 0.0477 mg/L,[143] which when the authors compared DEHP to Di-*n*-hexyl phthalate, no significant survival reductions were observed. This is not true of what is seen in this study, where mass changes have been observed on different phthalate plasticized PVC coatings.

Slime measurement has been used effectively to depict exopolymeric substances (EPS) in particular glycocalyx that some microorganisms secrete after settling on a substrate. [289]

In the cases of DEHP (0.02 ± 0.001 AU) and BOP (0.03 ± 0.002 AU) less slime has been detected in comparison to DEP (0.05 ± 0.004 AU) and DMP (0.055 ± 0.003 AU) respectively. DEHP and BOP both perform in a similar manner. Statistical analysis (ANOVA F = 44.74, p = 0.05) suggests that there is a clear difference between the levels of possible microorganism participation on the surface of DEHP and BOP when compared to the uPVC control. DEP and DMP both show values double to that of BOP and DEHP indicating that higher levels of slime have been produced upon these thin films. In the same manner, Van Pett *et al.*, showed that staining slime with the use of radiolabelled bacteria can show microorganism involvement upon a substrate. [290] This shows another method for slime adsorption upon on a given substrate; however, the cost of this method far exceeds the cost of the slime method employed in this thesis. Mass is clearly affected by the levels of slime produced across the plasticized PVC thin films and this is the first time slime and mass have been demonstrated in tandem to confirm mass linked to slime production upon plasticized materials. DEHP has displayed the least slime adsorption within this group of plasticized PVC polymers highlighting a candidacy as an antifouling coating, a polymer of which is already used in everyday life. [291] Similarly, Katano and Tsukatani found that when they added DEHP to PVC in the same concentration as this study, they too found that there was an antimicrobial activity when tested against *E. coli.* [139]

The phthalate plasticizer group demonstrates that DMP has a lower slime result compared to the mass. This is indicates mass has increased on the surface of DMP that has not been attributed to slime, but further analyses will validate this. Also in the case of DEP, the slime result shows a data point that is larger than the mass data point. This could indicate that slime is a major contributor to the biofouling exhibited across the plasticized PVC coatings. uPVC, DEHP, DEP and BOP all follow similar trends to each other, showing that as slime concentration increases, mass increase follows.

The carbohydrate adsorption levels for the branched and longer alkyl chain plasticizers (DEHP (2.53 ± 0.33 µg/mL)) and BOP (2.74 ± 0.42 µg/mL)) showed lesser amounts than the shorter least branched plasticizers (DMP (4.76 ± 0.41 µg/mL)) and DEP (4.81 ± 0.52 µg/mL) highlighting

that the latter of the two are displaying higher levels of microorganism activity. This of course can be related to the level of migration through the polymer, where, DMP and DEP leached from the PVC matrix at a faster rate, and therefore were not administering a potential biocidal effect over time. The biocidal activity for DEHP and BOP was slower and therefore the response for adsorption of carbohydrate to these plasticized PVC thin films could be attributed to the level of migration from the polymer matrix.

For protein adsorption assay, DEHP (1.06 ± 0.21 µg/mL) and BOP (2.44 ± 0.29 µg/mL) have again outperformed the remaining two plasticizers within the phthalate group. DEP (3.85 ± 0.42 µg/mL) and DMP (3.72 ± 0.11 µg/mL) showed increased quantities of protein adsorption especially when compared to the uPVC blank (3.45 ± 0.12 µg/mL).

3.2.2.8.1 LEACHING AND SURFACE ACTIVITY OF PHTHALATE DOPED PVC THIN FILMS

Figure 3.30 shows the typical data obtained for the leaching of phthalate acid ester derived plasticizers in PVC, in particular DEHP.
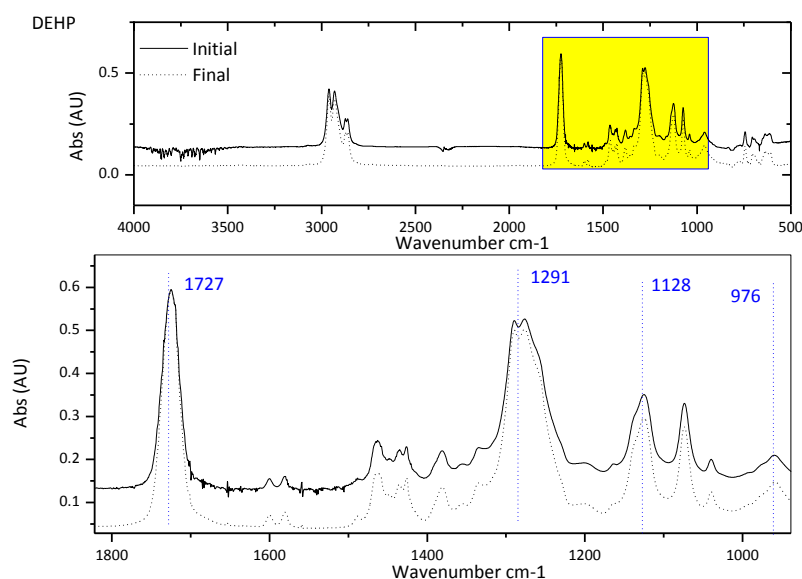
Figure 3.30: Whole spectra, (bottom) zoom of spectral region 1800 – 700 cm^{-1} showing 4 bands of interest.

Table 3.12: Tabulated plasticizer loss from the phthalate doped PVC thin films. Absorbance measurements were obtained both before and after a pure water study, where change in absorbance and %RSD was calculated (n=3 ± 1SD).

Plasticizer type	DEHP	DMP	DEP	BOP
Total Plasticizer Loss (%)	29.45	75.89	63.17	34.75

Data for migration of phthalate plasticized PVC is presented in Figure 3.29 and summarised in Table 3.12, where measurements were obtained both before and after a 7-d pure water leaching study. Each phthalate had the following IR-bands monitored ϑC$=\!=$O stretching (1727 cm^{-1}), CH$_2$CH$_3$ vibration (1291 cm^{-1}, 1128 cm^{-1}), C–Cl (1076 cm^{-1}, and 976 cm^{-1}) which relate to phthalic acid esters in the PVC matrix. [292]

DEHP (29.45%) leached significantly slower than the other plasticizers. This can be attributed to increased levels of branching within the molecule thus making it more difficult for the plasticizer to move through the polymer links. [252] From this study, it was found that DEP (63.17%) and DMP (75.89%) showed significantly more plasticizer loss from the matrix when exposed to water. It was also found that these membranes also showed significantly higher levels of biological activity of microorganisms in both the slime and mass results. Staples *et al.,* have reported that DMP and DEP showed significantly less toxicity in biological assays when compared to DEHP and BOP when using pure cultures of algae, protozoa and other microorganisms. [293] They determined that in order to get LC$_{50}$ for some microorganisms the following concentrations were required: DEP (137 mg/L), DMP (537 mg/L), BOP N/A and DEHP (25 mg/L). [294,295] DEHP and BOP have given greater antifouling impact on the levels observed in each assay. The PVC matrix offers a slow release biocidal matrix with each plasticizer in the PVC matrix, showing clear evidence that the phthalic acid esters are available to microorganisms that settle on the surface when compared to the undoped blank. Definitive proof lies with each plasticizer giving a range of biocidal effects from matrix to matrix.

3.3 CONCLUSIONS

The results presented herein have displayed varied outcomes across each of the plasticizer groups. Some showed good antifouling potential in the inhibition of mass, slime, protein and carbohydrate adsorption for each of the plasticized test polymers. Wettability, surface roughness and molecular features all seem to interlink with one another in forming some conclusions on why one plasticizer performs better than the other.

Within the adipate plasticizer group, DTDAd has performed inherently better than the other plasticizers within the group observing less mass, slime, protein and carbohydrate fouling responses. Indeed, surface roughness and plasticizer migration also play an important role in the investigation of the degree of fouling that has occurred. In the case of DTDAd, a high surface roughness value was observed which could be attributed to the molecular structure of the plasticizer molecule exhibiting high alkylation and branching. Literature is sparse in adipic acid ester derived plasticizers causing intrinsic PVC surface characteristic changes, such as surface roughness. The migration of a plasticizer from the polymer matrix will also affect its efficiency in biocidal release time, if any, from the material. This statement has been addressed within the plasticizer availability work; as the order of branching and alkylation in the plasticizer increases, leaching from the polymer matrix occurs at a slower rate. The choice of plasticizer is therefore important as its rate of migration from this matrix will govern its ability to be surface active for extended periods. Indeed, DTDAd reveals a high order of alkylation within the molecule and as such leaches from the PVC matrix at a slower rate. This suggests that we have an extended proliferation of surface activity and thus inhibition of mass, slime, protein and carbohydrates for extended periods of time. In the case of the shorter alkylated molecules in the adipate group, i.e. DIBA, leaching occurred at a faster rate and thus we have witnessed greater adsorption of biochemical such as proteins and carbohydrates along with slime and overall mass.

In the case of the azelate plasticizer group, the best performing plasticized thin films contained DIDAz showing a consistent fouling reduction in every assay used to interrogate the samples; slime, mass, carbohydrate and protein adsorption. Again, as with the best performing adipate plasticizer molecule, DIDAz has a high order of molecular alkylation giving rise to its ability to migrate at slower rates in the polymer matrix. Within the literature, it has been reported that azelaic acid has some antimicrobial properties when tested in pure culture studies. [144] This, with the slow leach rate enables for a slow antifouling release biocide from the polymer matrix and thus executes a promising answer as to what could be happening within the plasticized PVC coatings.

Within the citrate plasticizer group a mixed range of results in slime and mass fouling assays was observed. ATBC exhibited the slowest migration from the polymer matrix with lowest overall mass adsorption, however, slime was not consistent and protein and slime adsorption values were not conclusively lower than the rest of the group. This highlights that ATBC might not be of a conclusive antimicrobial nature, however further investigation is required. However, TEC leached at the fasted rate from the PVC matrix, and consequently saw an elevated overall mass value throughout this group of plasticizers further reinforcing the hypothesis that plasticizers indeed do have an effect on the rate of fouling.

The chloroparaffin doped PVC thin films has seen the best results in this group from the CLP_{70} which has consistently given the greatest reduction in mass, slime, protein and carbohydrate adsorption. The level of migration for this plasticizer was evidently far less than the other plasticizers and was attributed to the higher volume of substituted chlorine atoms upon the molecule, which gave rise to the CLP_{70} plasticizer leaching at a slower rate, and thus affording a more continuous release approach. It is also important to mention that chlorine in many aspects has a strong antimicrobial response and has been used for this property for decades. For instance, this has been aforementioned in Sverdrup's work where nitrifying bacteria were used as test organisms for this investigation. [266]

Dibenzoic acid ester derived plasticizers showed a range of varied results within the group. PEGDB performed the best in mass, slime, protein and carbohydrate fouling assays used within this thesis. The plasticizer consists of an ester moiety in the centre of the molecule and terminal dibenzoate substituted moieties. Interestingly, even though PEGDB leached at the greatest rate from the PVC matrix, the best antifouling response was observed. It could be suggested that the rate of migration for this plasticizer has offered an optimum migration and therefore optimum biocidal rate for this particular polymer. Further work would assist in dictating whether this statement would be correct. However, Kamaya *et al.,* reports the antimicrobial efficacy of dibenzoate compounds and thus the previous hypothesis could be correct. [296]

The sebacate group saw DEHS offering the best antifouling response throughout the assays of each plasticizer investigated within this group. It is already known that sebacic acid (from which these plasticizers are all derived) already holds known antifungal properties. [276] The higher order alkylation and branching that exists upon the DEHS molecule has been discussed in Bonora *et al.,* [277] where it was discovered that longer chained sebacate plasticizers were able to penetrate liposomes more readily than the shorter chained ones offering some discussion for the validity of this comment. Again, the higher branching and alkylation has

afforded a slower migration rate and has affected the level of fouling witnessed on the other sebacate plasticized thin film coatings.

The palmitic acid derived plasticizers have displayed similar findings with the other plasticizers already discussed within this conclusion. Indeed, the longer alkylated palmitate plasticizer showed a good response in each of the fouling assays for slime, mass, protein and carbohydrate adsorption. The level of migration through the PVC matrix had also seen MP migrate at the fastest rate of any of the other plasticizer groups. This proved interesting as the molecule is by no means the smallest molecule investigated within this study. However, it has been demonstrated in [286] that the volatility of this plasticizer is high in air and subsequently migrates from the matrix at a greater rate.

Of the phthalic acid esters, it was found that higher branching and longer alkyl chain moieties upon two of the plasticizer molecules (DEHP and BOP) gave opposite scale results in physical characterisation when compared to smaller chain length plasticizer molecules (DMP and DEP), and have consequently given interesting responses to the fouling assays herein. The work highlights that if more branched plasticizers are incorporated in the PVC matrix, different surface roughness values are achieved, when compared to the less branched molecules. It was found that DEHP and BOP changed the wettability (surface energy interaction with water) and thus presents a concept that organic, inorganic and microorganism involvement is somewhat different when comparing DMP and DEP plasticized PVC thin films. The level of leaching that was witnessed reflects the biocidal release hypothesis, where a slower rate of release and consequent antimicrobial response will indeed afford lower rates of fouling.

Plasticized PVC showed extremely positive results across some of the plasticizer groups, highlighting a potential low cost candidate as an optically clear transparent platform for biofouling resistance.

The results observed have displayed a range of outcomes for each of the plasticized PVC groups. Some showed good antifouling potential in the inhibition of biofilm development and overall resistance to biofouling - in the form of mass, slime, protein and carbohydrate adsorption assays.

The function of the plasticizer has been seen to intrinsically alter the fouling potential of the PVC matrix and has been observed within the plasticizer groups but also across the different groups of plasticizers. For instance, DTDAd performed inherently better than any of the other plasticizers within this group showing less biofilm adhesion and proliferation. DTDad has also demonstrated higher surface roughness values and wettability, which could be governed by

the molecular makeup of the molecule when introduced into PVC. Literature remains sparse in the adipic acid ester plasticizer group in detailing surface characteristics and surface roughness values. The migration of the plasticizer from the PVC matrix has also demonstrated an effect for the biofouling results, highlighting that migration could be related to the overall surface activity of the coating. This was addressed in the leaching studies performed where it was demonstrated that has molecular branching increased, migration from the matrix was slowed. Thus, this suggests that there has been an extension in the surface activity of the polymer – whereby inhibiting biofilm development and biofouling upon the surface.

Overall, the use of plasticized PVC showed some excellent antifouling results when investigated with a series of physical and biochemical tests. It was demonstrated that longer and branched molecules of plasticizers produced (generally) a rougher surface, more wettability and decreased levels of fouling. The level of plasticizer migration was also slowed resulting in a longer surface activity – which may or may not be related to a toxic effect for microorganisms.

4

Period 4 Metal Nanoparticle Synthesis

4.0 INTRODUCTION

Nanoparticles continue to be ever evolving in terms of interest for their chemistry and uses for novel research areas. This is due to the various unique properties exhibited from that of their bulk species. [297] They offer unique optical, catalytic and sensing properties as well as their potential use in a wide range of applications ranging from optical nanodevices to biosensing and antimicrobial agents. [298] It is the antimicrobial property that this thesis will pursue as a subject of interest. In order to prepare nanoparticles a series of synthetic steps are employed ranging from bottom-up to top-down syntheses. This chapter of work will describe the various research methods that are up-to-date with today's approaches to making the ideal nanoparticle.

4.1 AN INTRODUCTION TO NANOPARTICLES

Investigations into nanoparticles have been increasing over the past decade owing to their unique properties. Nanotechnology has progressed as the emerging science and in an important multidisciplinary area. [299] Specifically, this work will to focus on the antimicrobial effect of metal nanoparticles, stemming from the already well-established in silver nanotechnology. [170,171,300-303]

There is no absolute definition of the term nanoparticle, but more than often it is described as a particle with at least one diameter or facet less than 100 nm. [304] However, this broad term does not appreciate that some larger, metal nanoparticles in fact share properties with that of the smaller ones and it is not always seen in that of the bulk metal. One of the main differences is the localised surface plasmon band across the surface of the nanoparticle. Richard Feynman, in one of his articles published in 1960 entitled, "There is plenty of room at the bottom" discussed the idea of nanomaterials. His work pointed out that if one bit of information required only 100 atoms, then all the books ever written could be stored in a cube with dimensions of 1 cm long. [300,305] Reportedly, nanoparticles were first developed in the early nineteenth century for use in heterogeneous catalysis, followed by the use of silver halide nanoparticles in photography. [306] Properties of nanomaterials are often considered superior to their conventional counterparts in the polycrystalline form, as they are dependent on the microstructure, chemical composition, grain size, atomic structure, crystallographic orientation, coordination number and dimensionality, govern the microstructure. Nanoparticles, on the other hand, are smaller in size and possess a large surface area to

volume ratio, exhibiting novel properties, such as: increased mechanical strength, enhanced diffusivity, high heat capacity or magnetic behaviour and electrical resistivity. [307]

4.1.1 SURFACE PLASMON RESONANCE (SPR)

Surface plasmons (SP) are oscillations of electron density in the conduction band that occur at the metal/dielectric interface, exhibited by metal/water and metal/air interfaces. The metal/water interface is one that is directly linked to the thesis in the biofouling remit, where the effect of the metal nanoparticle will be involved in an aqueous environment. SP propagate evanescently in waveform, and any wave can have its amplitude enhanced with a wave of light with the same resonant wavelength applied to it. Excitation of SP with electromagnetic radiation is termed SPR. Stronger SP have been known to be associated with the roughness of the metal nanoparticle surface. [308] All of these properties are unique to the metal nanoparticle that can be brought about in synthesis.

4.1.2 SYNTHESIS OF NANOPARTICLES

Nanoscience and production of nanomaterials has experienced enormous development in the last decade. Preparation of nanoparticles with a controlled size, shape and composition, relies on fundamental scientific and technological advances. [309] Nanoparticle materials often exhibit different physical and chemical properties that can be both quantitatively and qualitatively different from the retrospective bulk material. Research has progressed in developing novel materials with improved properties, more functionality and of course, lower costs. Several physical, chemical and biological synthetic routes have been developed in order to handle this demand, obtaining improved control over size, distribution and morphologies. [306] Therefore, synthetic routes can often be quite challenging in order to get a full complement of these features. This work focuses on a 'polyol' synthesis that has been modified to suit a range of metal nanoparticles. Solution phase syntheses represent a promising route in terms of achieving low cost-throughput and high volume production. [310] The polyol method is a low temperature method (when compared to other methods) and has been used to synthesise noble metal nanoparticles extensively. [200,311] Other methods for preparation of nanoparticles include thermal reduction, [312] sono-chemical reduction, [313] metal vapour synthesis, [314] chemical reduction, [315] vacuum vapour deposition, [316] radiation methods, [317] micro-emulsion techniques, [318,319] or laser ablation. [320] One of the added advantages of the polyol method is that the reaction parameters can be controlled easily as demonstrated by Fievet *et al*.. [321,322] This section of the thesis will analyse many of the past and current synthetic routes in metal nanoparticle production. In September 2010 alone there were some 14,615 publications listed,

of which 8,964 were on synthesis related to the subject, showing that research in the area is colossal as given in Science Direct.

4.1.2.1 THERMAL REDUCTION SYNTHESIS

Thermal reduction is quite simply the reduction of metal salts into its constituent ions using thermal energy. This can be quite useful as thermal energy can be varied, which can be a parameter that brings about changes in rates of reactions and can therefore enable different nano-synthesis properties.

4.1.2.2 SONOCHEMICAL REDUCTION

Sonochemistry involves molecules undergoing a chemical reaction upon application of ultrasound radiation. The physical process by which the sonochemical process takes place is via acoustic cavitation. [323] Current theory has suggested that the mode by which acoustic radiation occurs is through breaking chemical bonds. Many theories seem to agree that the main scientific mode of action is the creation, growth and collapse of a bubble that is formed in a liquid matrix. [323] The growth of a bubble occurs through the diffusion of solute vapour into the volume of the bubble. The latter stage is the collapse of this bubble, which occurs when the bubble size reaches a maximum and is the point at which chemical bonds are modified. A bubble collapse occurs in less than a nanosecond, [324] with very high temperatures of 5000 - 25,000 K exhibited on the system during this collapse. This is accompanied with very high cooling rates of 10^{11} K/s. The high cooling rate eradicates the potential organisation of crystallisation products, this results in amorphous nanoparticles being produced and although explanation of the creation of amorphous products is well understood, nanostructured products is not.

In most cases sonochemical reactions yield nanosized products. [313] Sonochemical methods have certain advantages that other methods do not, these are:

- Nanoparticle mesoporous materials - Ultrasonic waves have the ability to insert amorphous nanosized catalysts into the mesopores, which enables a smooth homogenous coating on the surface. [325]
- Nanoparticles on polymeric and ceramic surfaces – Sonochemical deposition has been used extensively. [326,327] The nanoparticles are bonded to the surface through a chemical bond and/or a chemical interaction with the substrate and do not get removed by washing.

- Proteinacious addition of micro and nano spheres – demonstrations that any protein can be turned into a sphere can be found in Avivi *et al.*. [328] This has been further implanted in drug chemistry, where drugs are encapsulated in tetracycline, creating a biologically active species. [329]

4.1.2.3 CHEMICAL REDUCTION

A chemical reduction involves the oxidation state of an atom being changed in some way. In the synthesis of metal nanoparticles, the reduction of metal salts to their constituent metal particles is brought about by a nucleation and growth step. The reduction of metal ions to metallic particles is formed very early in the reaction stage, have short lifetimes and are sometimes extremely reactive. [330,331] The chemical reduction of a metal salt is therefore extremely dependant on solution conditions and even the nature of the reaction vessels. Thus, in order to produce particles of uniform size and shape a certain level of control is required over the nucleation and growth of a reaction, [332] Figure 4.1

Scandium chloride	Sc(III)	Sc^0
Titanium chloride	Ti(III)	Ti^0
Vanadium chloride	V(II)	V^0
Chromium nitrate	Cr(III)	Cr^0
Manganese chloride	Mn(II)	Mn^0
Iron chloride	Fe(III)	Fe^0
Cobalt chloride	Co(II)	Co^0
Nickel chloride	Ni(II)	Ni^0
Copper chloride	Cu(II)	Cu^0
Zinc chloride	Zn (II)	Zn^0
Gallium chloride	Ga(III)	Ga^0
Germanium chloride	Ge(II)	Ge^0
Selenium chloride	Se(IV)	Se^0
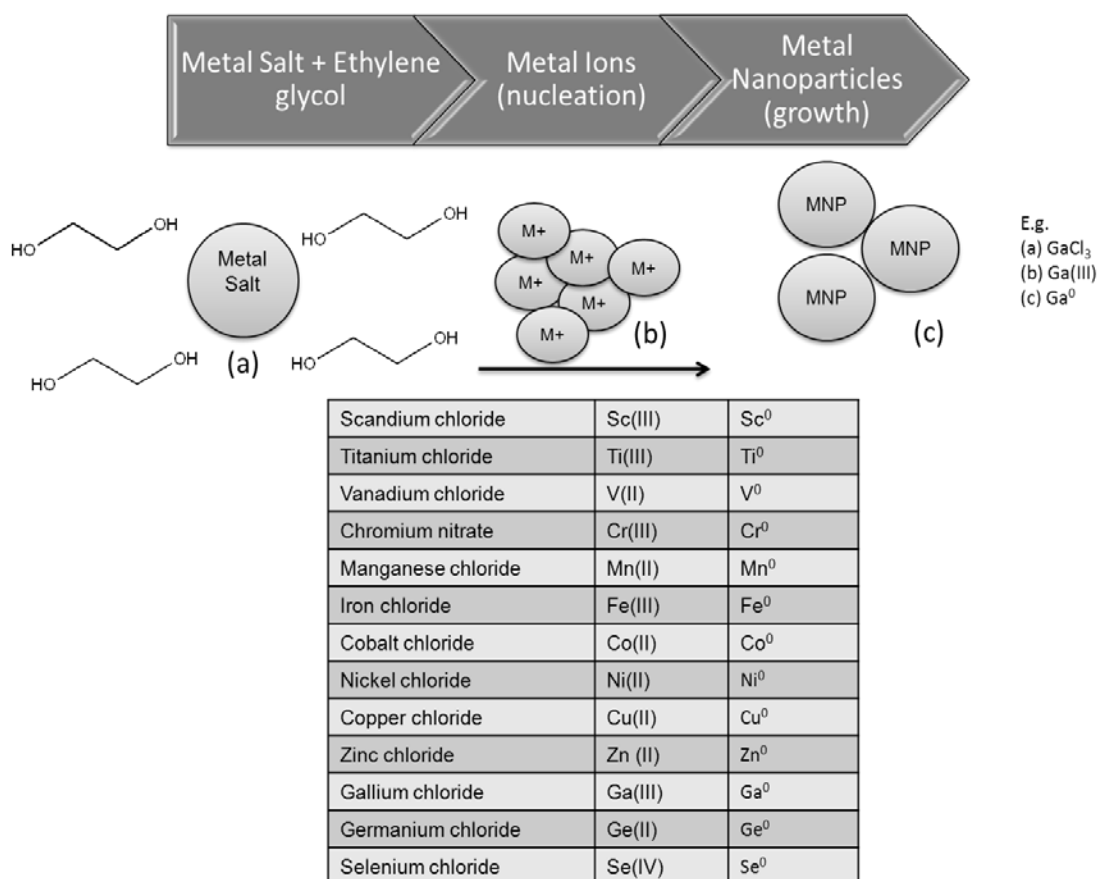
Figure 4.1: Schematic of metal nanoparticle growth steps.

4.1.2.4 METAL VAPOUR SYNTHESIS

In vapour-phase synthesis of nanoparticles, conditions are created where the vapour phase mixture is thermodynamically unstable, relative to the formation of solid material to be prepared in the nanoparticle form. [333] This includes the supersaturation vapour and what is commonly called the chemical supersaturation. This supersaturation is energetically favourable for a vapour-phase, causing molecules to react and form a condensed phase. If the supersaturation point is sufficient and the reaction condensation kinetics permits, particles will begin to nucleate. Once nucleation transpires, the remaining supersaturation is relieved and particle growth will occur rather than further nucleation. This process happens rapidly and is often relatively uncontrolled, leasing its own reaction into a continuous or quasi-continuous operation. In contrast to a colloidal system, the syntheses of nanoparticles are carried out in batches under well-controlled conditions. In most cases, once particles form in the gas phase, they begin to coagulate at a rate that is proportional to the square of their concentration number. This is only weakly dependant on their size. Swihart reports that on higher temperature gas vapour reactions, particles coalesce faster than they coagulate and more spherical morphological particles form. [333] Whereas at lower temperatures, they form more open structures due to coalescence being negligibly slower. In contrast to a liquid phase system, where the dispersion of particles can be stabilised with the use of capping agents or ligands, particles in the gas phase cannot cause agglomeration in every instant.

4.1.2.5 LASER ABLATION

In some respects, laser ablation is linked to gas vapour deposition synthesis of nanoparticles. Rather than a simple evaporation of material to produce a supersaturated vapour, a laser can be used to vaporise a plume of material. However, this method can generally only produce small volumes of nanoparticles. Gas-phase is not always a practical method for the syntheses of nanoparticles and some research groups [334] have harnessed a liquid colloidal system, where laser irradiation energy and the ablation process were carried out in an aqueous solution resulting in a colloidal system. However this only permits a relatively large size range (20 – 300 nm) and strongly dispersed (50 – 300 nm) nanoparticles. [320,335-338] This is thought to be mainly caused by the post-ablation of the nano-clusters that can be created in the ablation process. Due to the development of aqueous platform laser-ablation techniques, this agglomeration problem can be controlled with the introduction of protecting or capping agents into the aqueous system. [339]

4.1.2.6 POLYOL REDUCTION

To date, solution based synthesis of nanoparticles demonstrates the most successful route to obtaining new nanoparticles and morphologies. However, sometimes a mixture of shapes and sizes are obtained, making it difficult to investigate size and shape dependant features of nanoparticles. [340] Furthermore, reproducibility of many chemical methods can be greatly affected by trace amounts of contaminants such as ionic species. [200] This has been developed Section 2.2.1.3, *vide supra* where care has been taken in this investigation.

The polyol reduction of metal nanoparticles is a well-reported, versatile method in which precursor materials, in a multivalent high-boiling alcohol (e.g. glycol, polyethylene glycol, glycerin), at elevated temperatures (ranging from 150 – 300 °C), can readily synthesise nanomaterials. [341] It ensures dynamic liquid-phase synthesis giving rise to a range of features unique to the polyol method. Unique properties such as mesoscale to nanoscale size ranges can be obtained under the correct experimental conditions. The polyol method was initially used to describe the preparation of elemental metals and alloys, in which the joint reducing ability of the polyol towards a suitable metal precursor was driven. As a result, some of the more noble metals (Au, Pt, Pd, Cu) were realised. [342] Consequently, properties of polyol-mediated synthesis can be summarised in the following 5 points:

- The polarity of the polyols gives rise to pure inorganic and compound salts often being readily soluble; [341]
- The nucleation and growth process of nanoparticles can be performed at temperatures matching the boiling points of the polyol;
- The chelation of solid nuclei by the polyol, simultaneous in its formation, can serve as a joint particle growth and agglomeration prevention medium; [341,343,344]
- Since polyols possess low weight molecular attributes, they act as weak stabilisers which can be removed under certain experimental conditions;

4.2 AIMS AND OBJECTIVES

The aim of this chapter is to develop a series of metal nanoparticles for the investigation and potential use as an antifouling material – in the form of an agent suitable of being toxic to microorganisms when used as an antifouling material.

The objectives of the work are:

(1) The investigation of an entire series of metals. The synthesis of metal nanoparticles can often be inherently difficult to achieve and thus this chapter will aim at delivering a method which can be tailored to synthesise a range of metal nanoparticles in a reproducible manner – where period four in the periodic table has been selected as a point of interest.

(2) The characterisation of the metal nanoparticles with particular emphasis being directed in modern spectroscopic and microscopic techniques.

4.3 RESULTS

The initial part of this chapter deals with a method of optimisation for metal nanoparticle synthesis and some of the problems that were encountered illustrating any deviations from optimal conditions outlining any obstacles encountered. The remaining part of the chapter deals with a contemporary method that was optimised for the reproducibility of period four metal nanoparticles in which characterisation methods are dealt with.

4.3.1 NANOPARTICLE METHOD DEVELOPMENT

A simple aqueous metal nanoparticle synthesis was identified as a starting point by Solomon *et al.*, [345] for the work contained in this section, where a silver salt was reduced using sodium borohydride. An initial experiment for the synthesis of silver metal nanoparticles was replicated through the work given by Mock and co-workers. [346] Experimental parameters, such as concentrations of metal precursor ($AgNO_3$), molar ratios between the protecting agents (poly-(vinylpyrrolidone) (PVP)) and $AgNO_3$ and the strength of chemical interaction between the PVP were found to be essential to the outcome of the final product.

4.3.1.1 SYNTHESIS OF YELLOW COLLOIDAL SILVER

Multitudes of chemical reduction methods exist for the synthesis of silver nanoparticles. [347] The synthetic method for this experiment was optimised for reproducible, stable yellow, colloidal, silver solutions, are described in Section 2.2.1.1, *vide supra*. Here the method was used to produce stable, monodisperse, metal nanoparticles in order to transfer across to other metal salts contained in the periodic table. In order to achieve accurate monodisperse nanoparticles reaction conditions had to be maintained exclusively due to the fragility and sensitivity of the reaction.
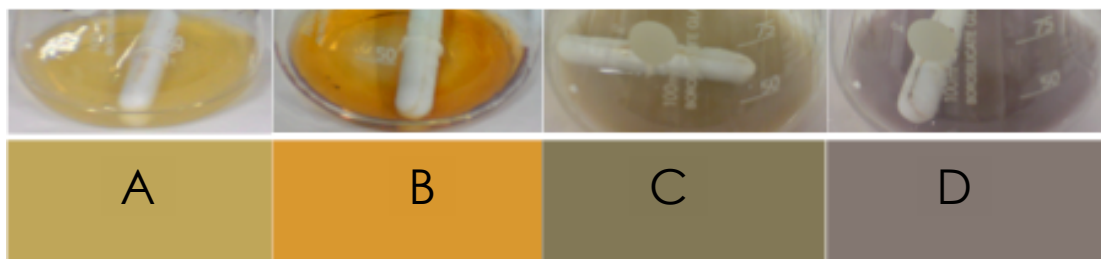
Figure 4.2: Colloidal silver at various stages of aggregation, (A) clear yellow sol (B) orange sol (C) grey sol (D) purple/grey sol (top) conical flasks with magnetic stirrer and solutions (bottom) colour stages.

The colours in Figure 4.2 illustrate the various stages of a typical silver nanoparticle synthesis. Reaction conditions including stirring, quantities of reagents (both numbers of moles and relative molarities) must be controlled in order to obtain a reproducible *stable* colloidal system. For instance, it was found that over time with constant heating and stirring, aggregation begins as the yellow sol (Figure 4.2 (A)) turns to orange (Figure 4.2 (B)), then to grey (Figure 4.2 (C)) and finally purple (Figure 4.2 (D)), after which it is noticeable that the colloid breaks down and particle aggregates settle out.

4.3.1.2 OPTICAL PROPERTIES

The colours associated with the colloids synthesised are due to a phenomenon known as plasmon absorbance. In short, incidence of UV-light creates an oscillation of conduction electrons on the surface of the nanoparticles and electromagnetic radiation is absorbed. The spectrum of the various solutions is shown in Figure 4.3, the experimental parameters of which can be found in Chapter 2, Section 2.2.2.1, *vide supra*.
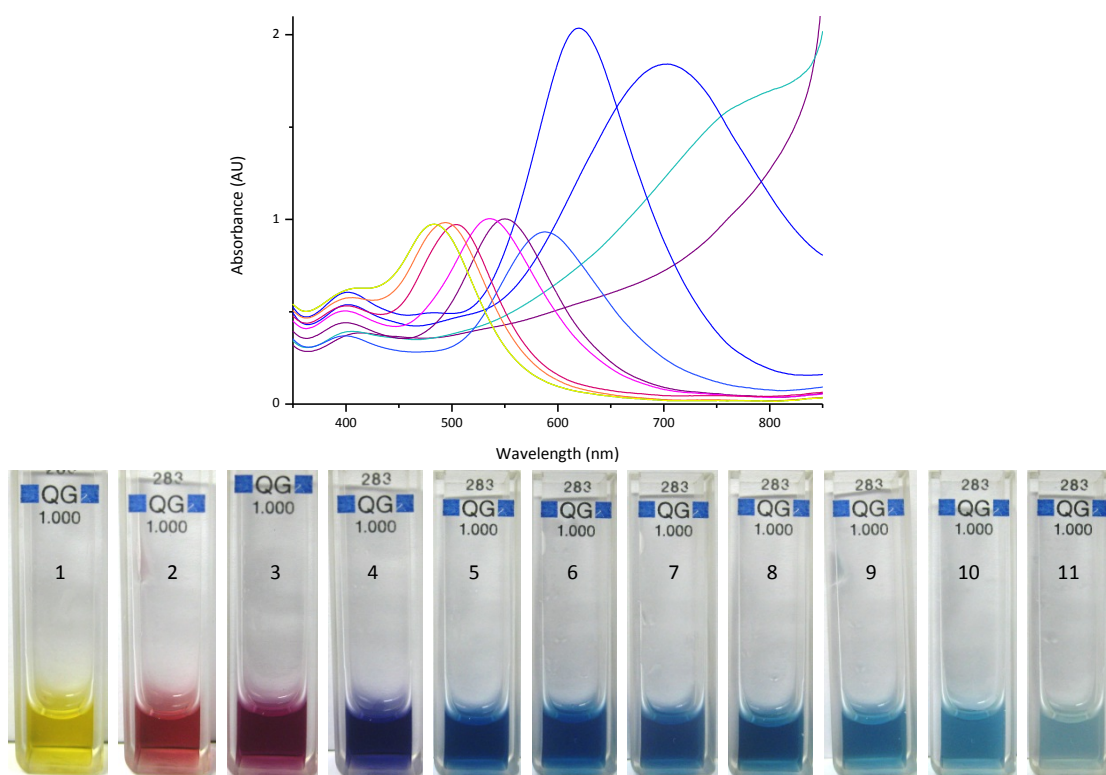
Figure 4.3: Photograph of a series of silver nanoparticle samples, illustrating range of colours obtained using different volumes of seed solution: 1) Seed, 2) 650 µL, 3) 500 µL, 4) 400 µL, 5) 260 µL , 6) 200 µL, 7) 120 µL, 8) 90 µL, 9) 60 µL, 10) 40 µL, 11) 20 µL.

The spectrum of this solution produces a band at ~400 nm, with the wavelength of the plasmon absorption maximum indicating a general size. The yellow colloidal solution was examined using a transmission electron microscope (TEM) mode scanning electron

microscope. Figure 4.4 shows the relative size of the silver nanoparticles using the SEM in TEM mode.
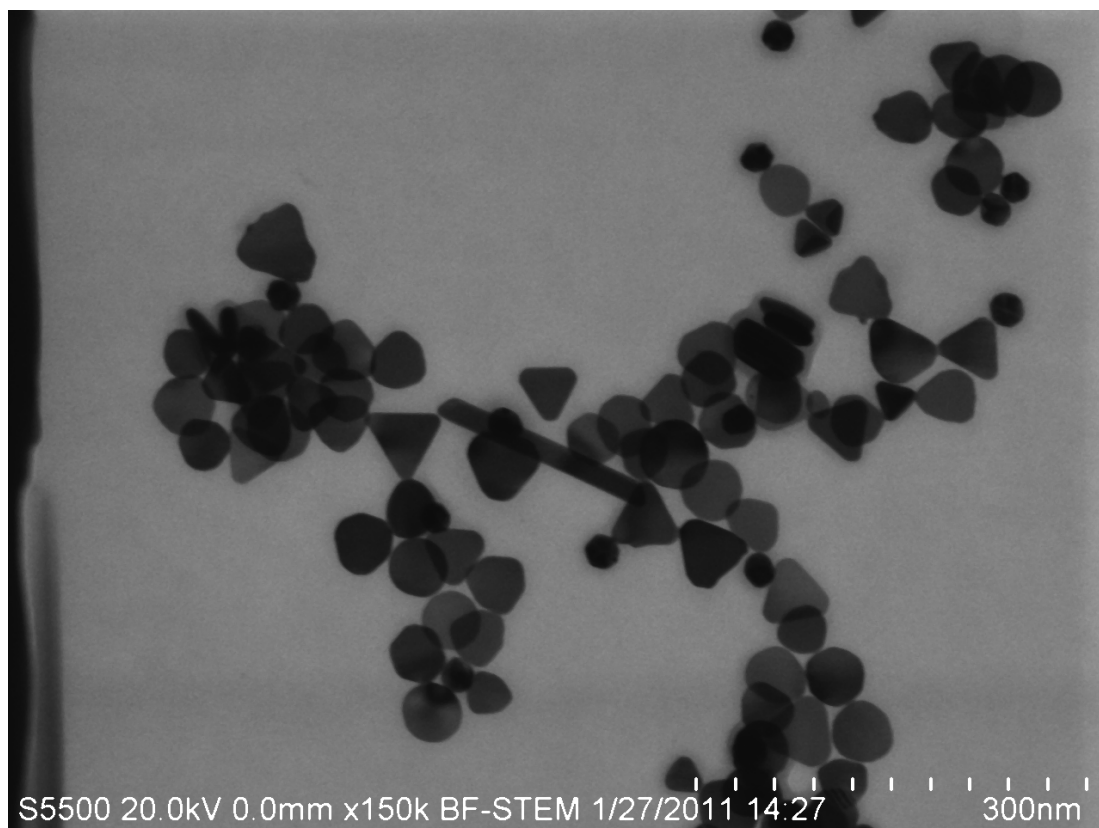
Figure 4.4: Scanning electron micrograph of silver nanoparticles produced via a seed mediated method for the polyol reduction.

It is important to note during each nanoparticle reaction, aggregation occurred over time if the solutions had not been stabilised effectively. In many cases, authors neglect to mention the problem of aggregation and so reproducibility of methods are often difficult. In this study a series of aggregation studies were performed to investigate the stability of a capping agent in this case, PVP.

Table 4.1 Particle size of silver nanoparticles compared with literature (n=3).

Data from	Particle Size (nm)	λ_{max} (nm)
(Figure 4.4)	43-53	400
(Lee *et al.*)	35-50	420
(Kamat *et al.*)	60-80	438

Table 4.1 took similar published works that have used the chemical reduction method and compared the values for particle and lambda max to the values obtained experimentally. The

results demonstrate that all values obtained for the silver nanoparticles exhibited broad size ranges – again illustrating the inherent difficulty in produced reproducible nanoparticle size ranges.

4.3.1.3 AGGREGATION STUDIES

Aggregation is a known problem throughout most nanoparticle syntheses. [348] Adsorption of the reducing agent plays a pivotal role in stabilising the growth of nanoparticles, in this case silver. There must be enough reducing agent to stabilise the reaction as it proceeds. If too much reducing agent is present, this too will cause an overall ionic effect and aggregation will commence. [349] In the case of the silver nanoparticles, the particles are kept in suspension by active repulsive forces between the particles thus any ionic fluctuations could present an aggregative property in the solution. A series of stability studies were performed in order to optimise the correct capping agents. In this case PVP was used (experimental can be found in Section 2.2.1.2, *vide supra*.)

Aggregation of samples
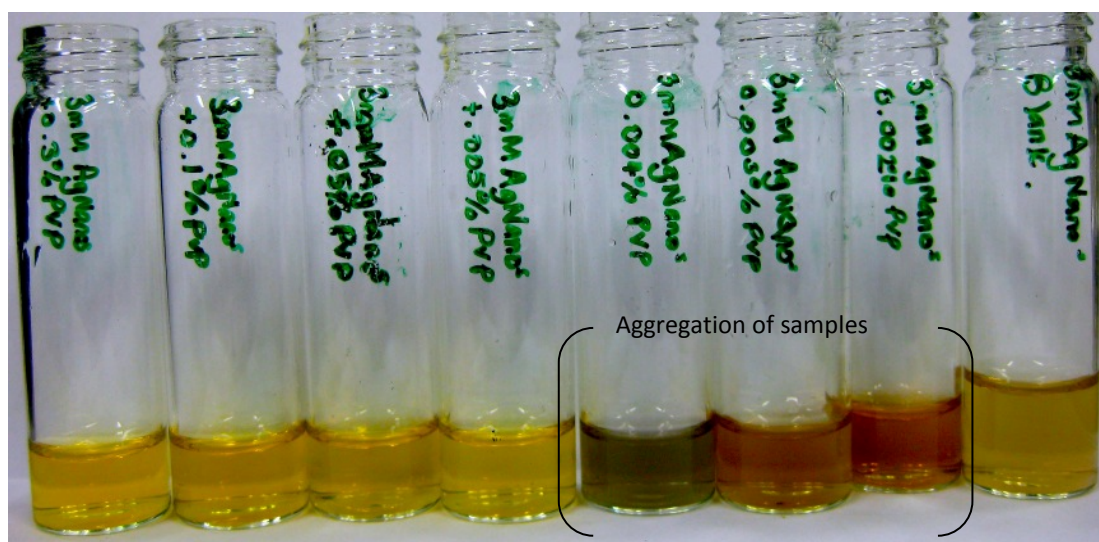
Figure 4.5: Photograph detailing the aggregation of silver nanoparticles due to the addition of sodium chloride in different concentrations as shown on vial labels.

An aggregation study using NaCl was carried out (experimental methods can be found in Chapter 2, Section 2.2.1.2). Different concentrations of PVP were added to each nanoparticle solution in order to establish the optimum capping level required in each of the colloidal solutions, thus preventing aggregation. The aggregation in this case was established through the addition of an electrolyte, NaCl. The salt causes a shielding effect of the charges and therefore aggregation occurs, as highlighted in Figure 4.5. The minimum concentration of PVP required, in this case, preventing aggregation and maintaining stability of the colloidal silver solutions was 0.005% (w/v) PVP.

Generally, the method gave a good indication to some of the problems that might be encountered when dealing with period four metal salts in producing metal nanoparticles. The method, once optimised, gave good reproducible results for colloidal stability and as suggested in other publications, sodium borohydride, [350] and PVP [351] are both suitable reagents for metal nanoparticle synthesis.

In theory, the stability of metal nanoparticles using an aqueous PVP and NaBH$_4$ reaction system should present reproducibility with the metal precursors used, which are discussed Section 2.2.1.3 *vide supra*. Experimentally, this was not always the case due to different metals having different properties from ionic radii, atomic packing to melting points and following recent publications a more practical synthesis was chosen, which was in the form of the polyol reduction.

As discussed Section 4.1.2.6 *vide supra*, a polyol reduction method offers a means of obtaining reproducible results using the same method for period four metal precursors. This happens for a number of reasons:

1. Temperatures can be controlled in the range of 150 – 250 °C, which are suitable for the laboratory fume-hood; [341]
2. Aqueous chemistry is still permitted; [352]
3. The polyol reduction offers a joint reduction and protecting agent solvent;
4. Possibility for microwave assisted preparation, which would reduce experimental times accordingly. [353]

All metal nanoparticles described here were prepared via a polyol-mediated synthesis with some deviations in temperature control being exploited only according to each metal precursor materials. By heating ethylene glycol (EG), colloidally stable solutions of each period four metal nanoparticle were obtained. The selection of a suitable precursor was found to affect the formation of the nanoparticle. In order to obtain particles with well-defined shape and size, each metal required optimisation. This was achieved by carefully adjusting the concentration of precursors, along with temperature and reaction duration, more details can be found in Chapter 2, Section 2.2 *vide supra*. Characterisation was performed after centrifugation, careful washing and drying, and in some results the re-suspension of the metal nanoparticles in a different solvent.

4.3.2 CHARACTERISATION OF THE NANOPARTICLES

Characterisation of the metal nanoparticles synthesised via the modified polyol reduction method are presented in this section of the chapter. The nanoparticles were characterised using a series of analytical techniques; ranging from spectroscopic and microscopic, and are discussed herein.

4.3.2.1 UV-VISIBLE ABSORPTION SPECTROSCOPY

Information on the optical properties of the metal nanoparticles was obtained using UV-visible (UV-vis) spectral absorption measurements. Figure 4.6 shows the absorption spectra of the products obtained through the polyol method for each of the metal nanoparticles. UV-vis is commonly used throughout nanoparticle synthesis to detect the presence of nanoparticles. [170,302,354-357]

It is well known that the observed wavelengths and absorbance of surface plasmon resonance bands depend on the size and shape of the metallic particles, causing relative band shifts with increasing particle size. [358] A sharp absorbance can illustrate a narrow size distribution of nanoparticles. [170] Nanoparticle shape will also cause changes to spectra, which can be highlighted with shoulders or band dips. [359,360]

MNP	Sc	Ti	V	Cr	Mn	Fe	Co	Ni	Cu	Zn	Ga	Ge	Se
Size (nm)	27	36	87	76	78	29	49	45	78	56	88	36	29
λmax	290	380	577	585	770	296	497	736	511	673	670	362	309
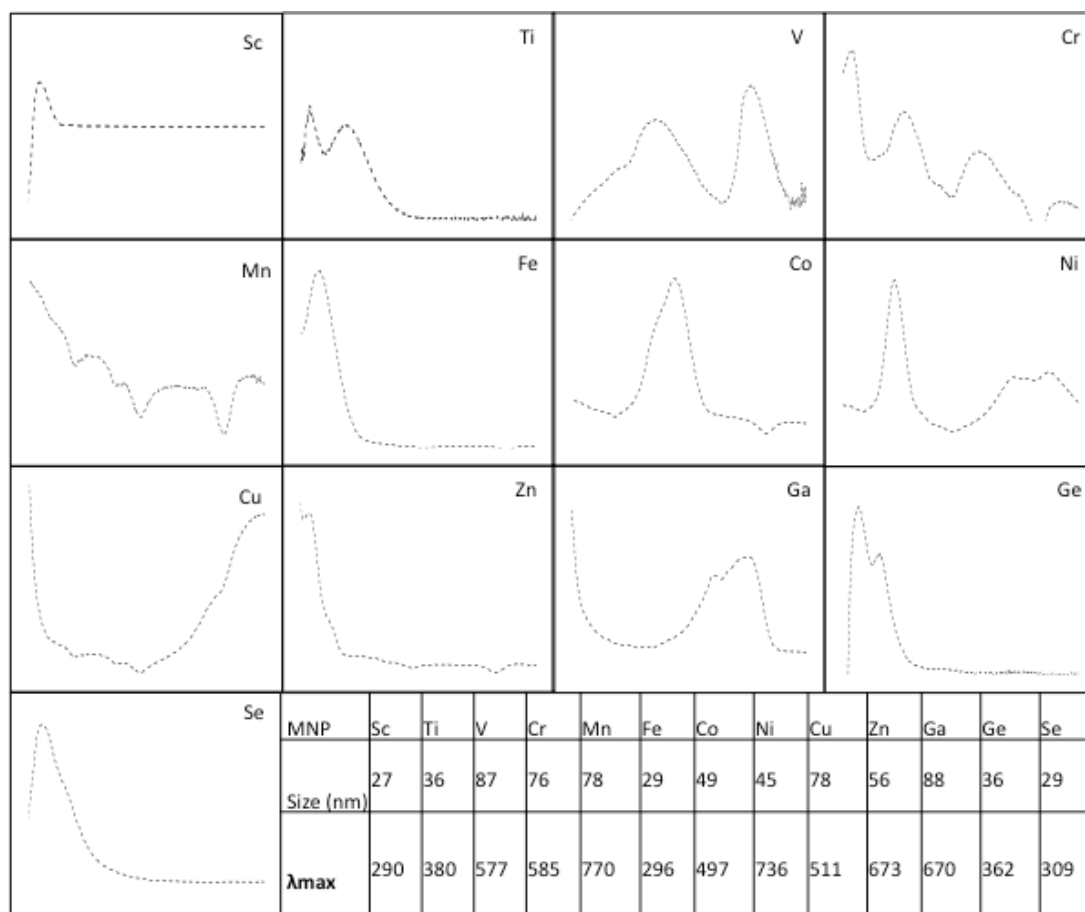
Figure 4.6: UV-visible spectra of synthesised metal nanoparticles from period four in the periodic table. (x-axis = wavelength (150 – 850 nm) and y-axis = absorbance (AU)).

The shape of nanoparticles can also be determined via imaging techniques such as FESEM or transmission electron microscopy (TEM). In most cases a characteristic band is obtained relating to the size and or shape of the metal nanoparticle. For example, silver nanoparticles tend to absorb in the region of 390 – 420 nm, [300] if the particle has spherical morphology.

Many of the spectra obtained in Figure 4.6 were found to show multiple resonance bands as opposed to one succinct plasmon band. Scandium for instance, has one band displayed in the spectra, with a maximum intensity at 290 nm. This is a characteristic band for an optical response of Sc^{3+}, which adopts an octahedral symmetry, given in the nanoparticle structure. Grosso and Serman also found this to be true of scandium nanoparticles they had synthesised with dimensions of <80 nm, [361] which is reflected in the absorbance values obtained in this work.

The spectra obtained for titanium in Figure 4.6 illustrates that the metal nanoparticles obtained in this synthesis possess multi-faceted morphologies as reported in Pal *et al.* [194] The maximum absorbance band at ~350 nm has been referred to as a characteristic metallic nanoparticle shift in Ghosh *et al.* [362] and has been reproduced in this spectra. No mention of

nanoparticle size was given in Ghosh *et al.,* but with similar spectra obtained herein, a prediction of ~50 nm could be suggested.

Vanadium's spectrum is a good example of having multi-facet morphological data portrayed within the spectral data. There are two distinct bands at (i) 577 nm (λ-max) and (ii) 416 nm, and could be explained by anisotropic particle definition as outlined in Baia *et al.*. [363] In a review by Lopez *et al.*, vanadium nanoparticles were characterised in the same manner confirming the nanoparticle existence, where metal salts and nanoparticle solutions were subtracted. [364] Chromium and manganese both represent anisotropic nanoparticles with a considerable amount of facets attributed to each nanoparticle. This illustrates that, as the number of SPR bands increases the symmetry of the nanoparticle decreases. [363,365] Chromium has attracted great attention due to its promising properties in catalysis, green pigmentation and industrial coatings. [366,367] For this reason uniform-sized nanospheres are sought in most research groups. [368] The results depicted show absorption peaks at 380, 460 and 585 nm, compared with the literature, these transition bands are blue shifted due to the nanoparticle size effect. An example of the triangular shaped of silver nanoparticles can be seen in Figure 4.4, *vide supra*, which formed part of the nanoparticle synthesis development. When a pronounced plasmon resonance is depicted (i.e. Co, Ni, Fe, Se) no other interferences are being detected, showing that free metal ions are not involved which is explained in Baia *et al.*. [363] According to Mie's theory, [369] only a single SPR band is exhibited on solutions containing spherical nanoparticles, which could also be affording the single pronounced SPR bands given in these spectra.

4.3.2.2 MORPHOLOGY OF PREPARED METAL NANOPARTICLES

Morphological data of the MNPs were obtained using FESEM to extract additional information of the size and shape of the nanoparticles synthesised using the polyol method. The FESEM used in this body of work has transmission electron microscope capabilities, which proves useful as many research groups utilise this instrument in the conformation of nanoparticle structure. [370-372]

Figure 4.7 – 4.19 shows FESEM images of particles synthesised using the modified polyol reduction method for metal nanoparticles originated from metal salts contained within period four of the periodic table.
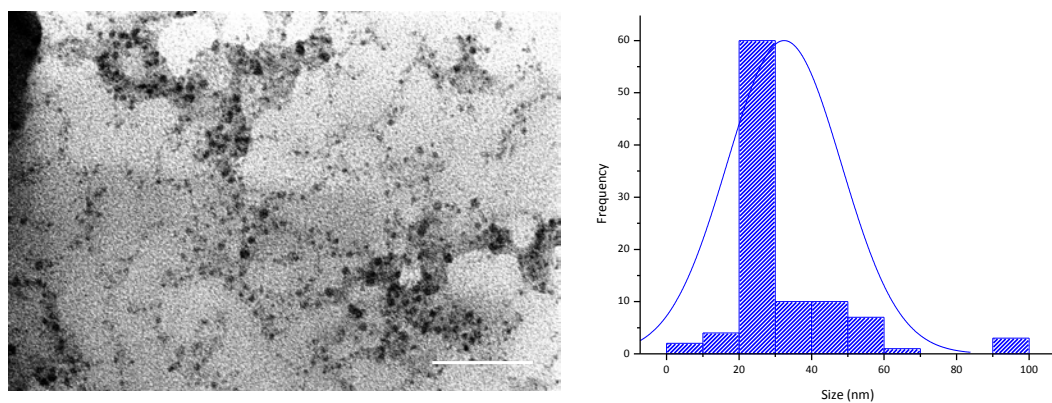
Figure 4.7: Scandium nanoparticles synthesised via the polyol reduction method scale bar = 500 nm (left) and size distributions of the nanoparticles (right).
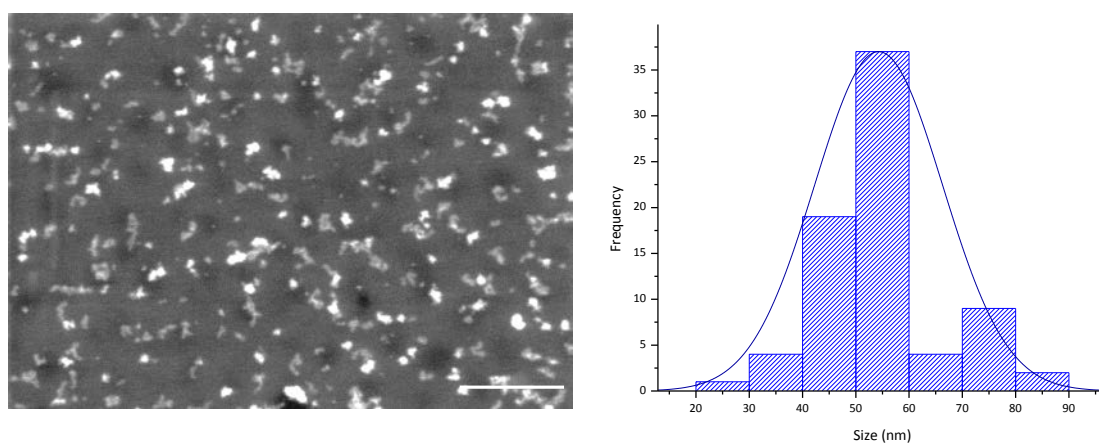
Figure 4.8: Titanium nanoparticles synthesised via the polyol reduction method scale bar = 500 nm (left) and size distributions of the nanoparticles (right).
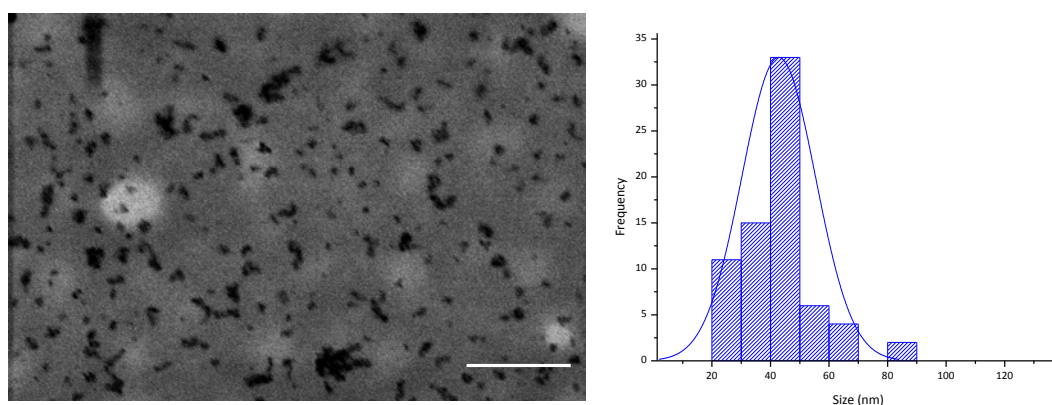
Figure 4.9: Vanadium nanoparticles synthesised via the polyol reduction method scale bar = 500 nm (left) and size distributions of the nanoparticles (right).
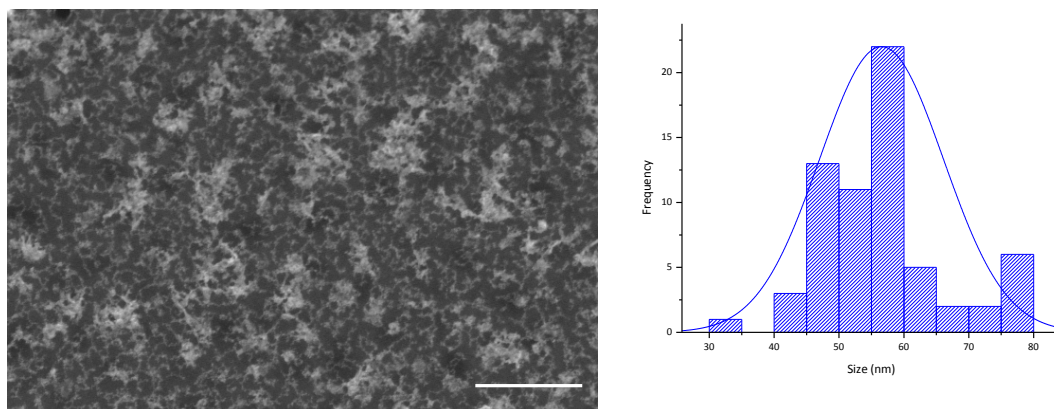
Figure 4.10: Chromium nanoparticles synthesised via the polyol reduction method scale bar = 500 nm (left) and size distributions of the nanoparticles (right).
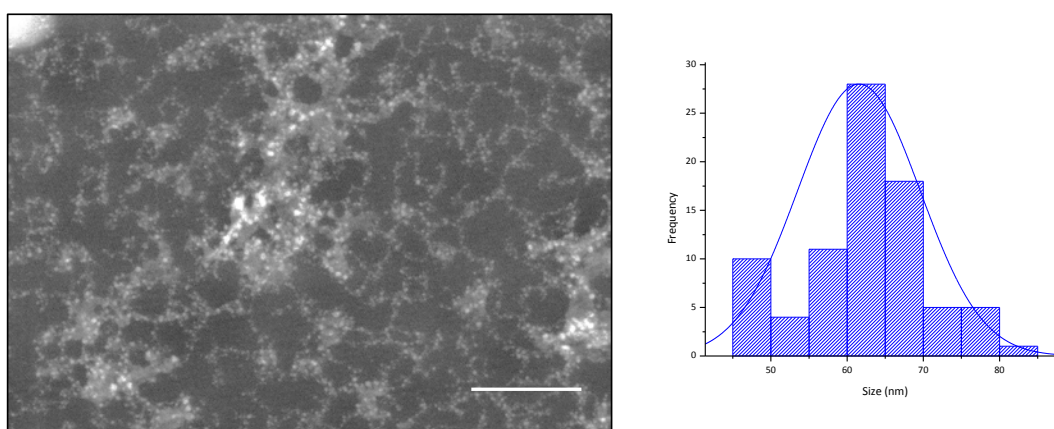
Figure 4.11: Manganese nanoparticles synthesised via the polyol reduction method scale bar = 500 nm (left) and size distributions of the nanoparticles (right).
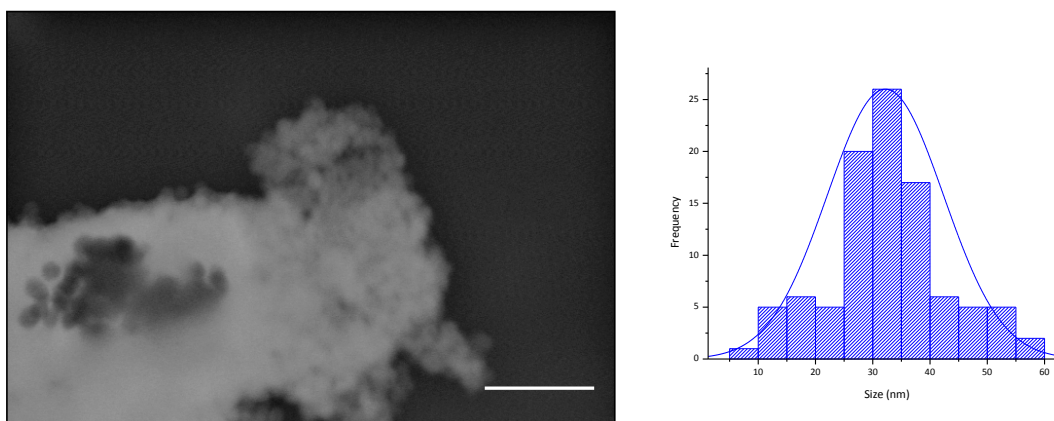
Figure 4.12: Iron nanoparticles synthesised via the polyol reduction method scale bar = 500 nm (left) and size distributions of the nanoparticles (right).
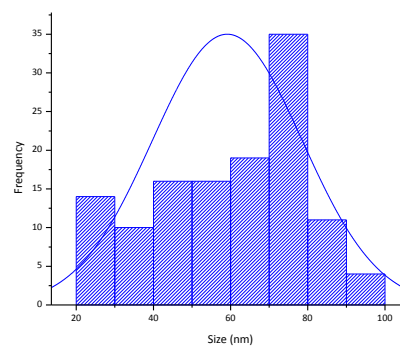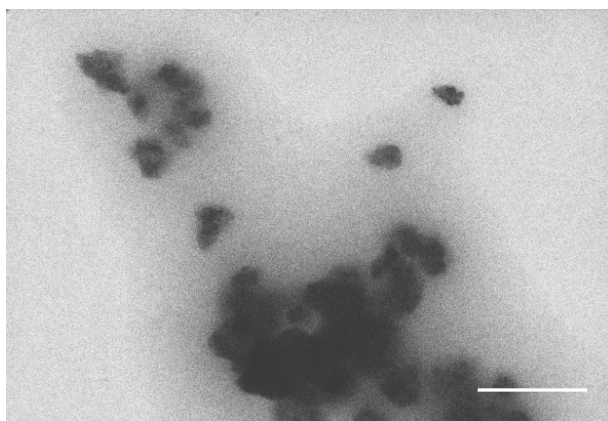
Figure 4.13: Cobalt nanoparticles synthesised via the polyol reduction method scale bar = 500 nm (left) and size distributions of the nanoparticles (right).
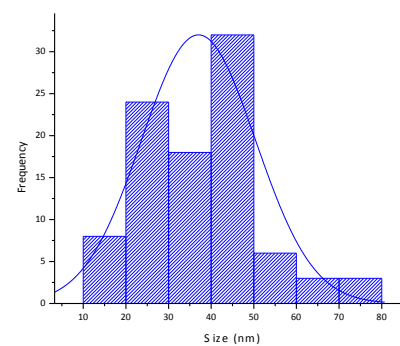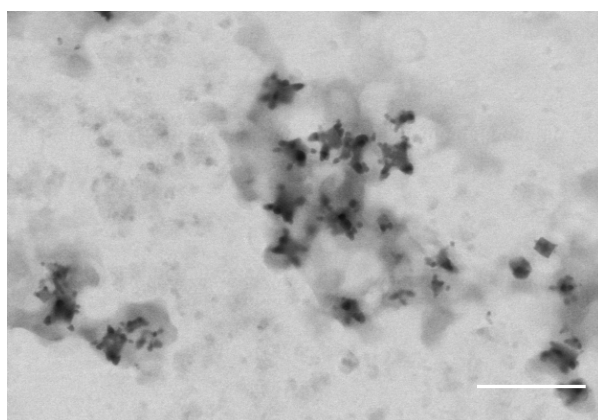
Figure 4.14: Nickel nanoparticles synthesised via the polyol reduction method scale bar = 500 nm (left) and size distributions of the nanoparticles (right).
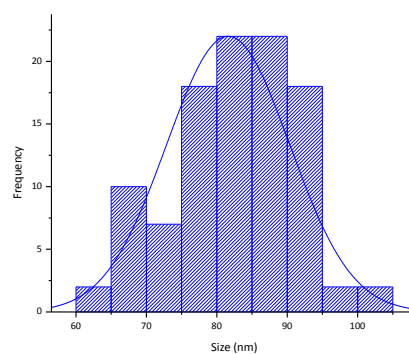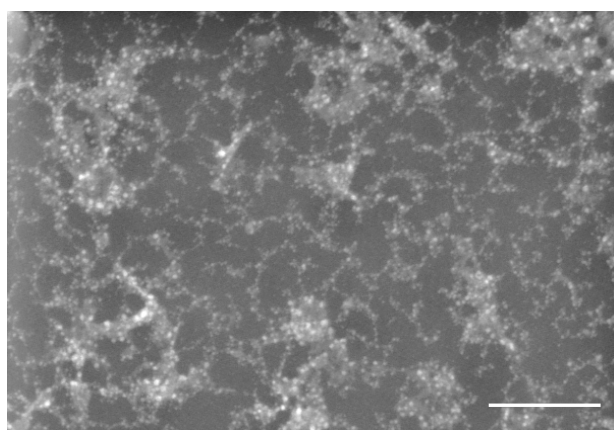
Figure 4.15 : Copper nanoparticles synthesised via the polyol reduction method scale bar = 500 nm (left) and size distributions of the nanoparticles (right).
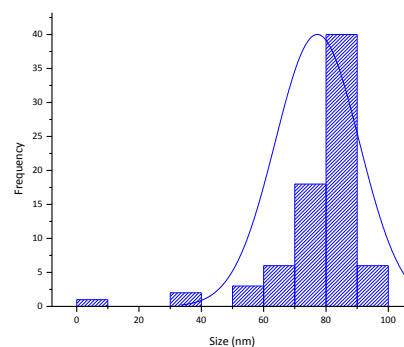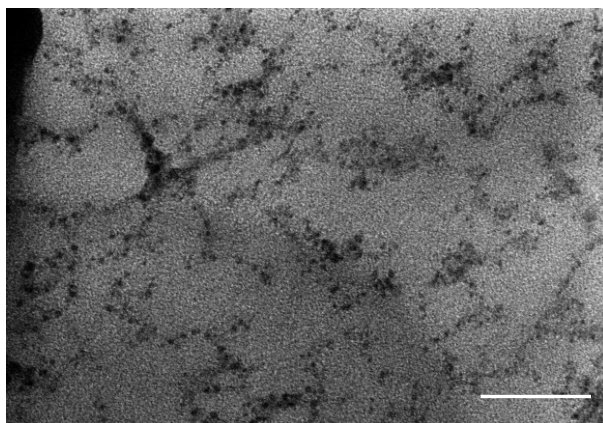
Figure 4.16 : Zinc nanoparticles synthesised via the polyol reduction method scale bar = 500 nm (left) and size distributions of the nanoparticles (right).
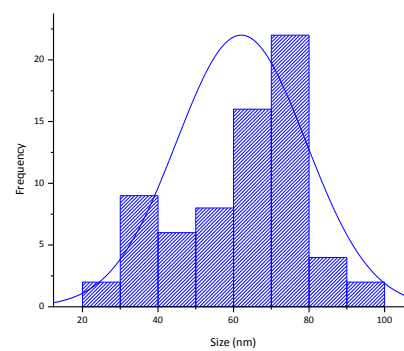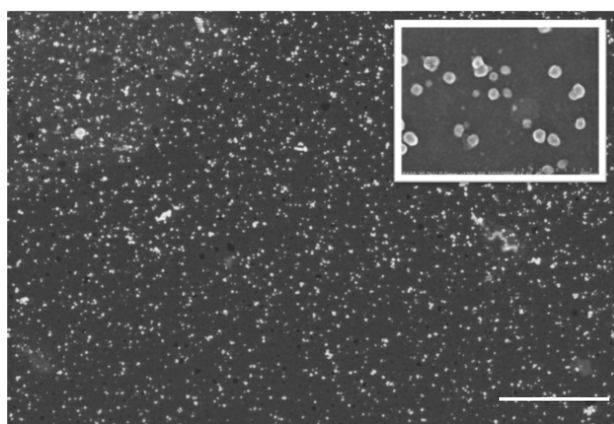
Figure 4.17: Gallium nanoparticles synthesised via the polyol reduction method scale bar = 500 nm (left) and size distributions of the nanoparticles (right).
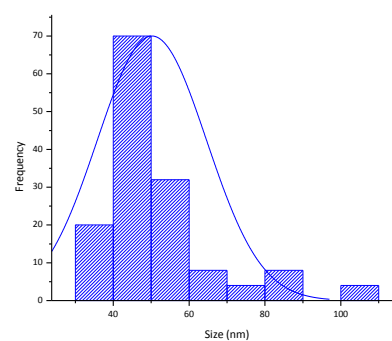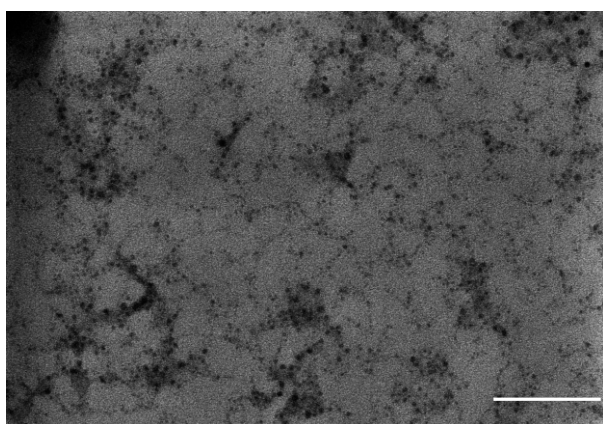
Figure 4.18: Germanium nanoparticles synthesised via the polyol reduction method scale bar = 500 nm (left) and size distributions of the nanoparticles (right).
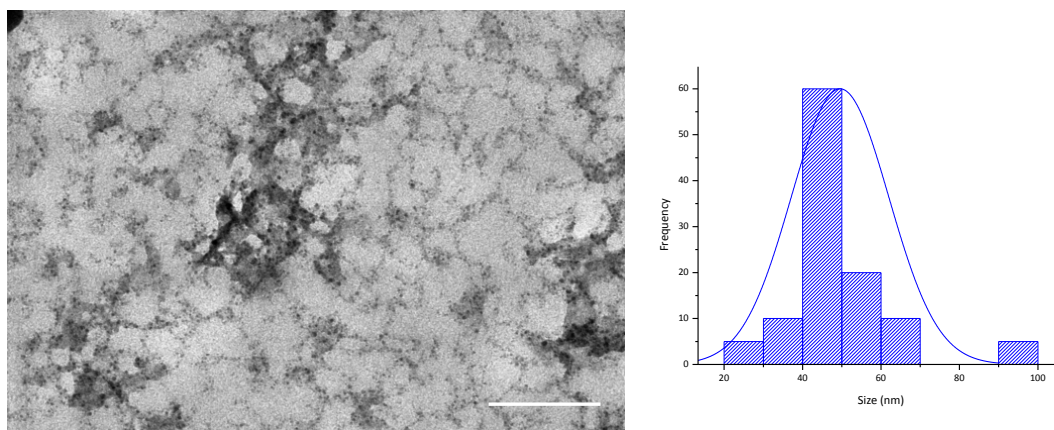
Figure 4.19: Selenium nanoparticles synthesised via the polyol reduction method scale bar = 500 nm (left) and size distributions of the nanoparticles (right).

Many of the metal nanoparticles synthesised exhibit sizes below 100 nm, illustrating that the polyol reduction method is transferable across each of the metals. The polyol method transpires, with other researchers to have good stability on a range of nanoparticles, indicating that the method is versatile. [373] Some of the data obtained in the UV-vis measurements (Figure 4.6) conflict with microscopic data obtained through microscopy (Figure 4.7 - 4.19). For instance, Baia *et al.* highlight that UV-vis and particle sizing are techniques that detect certain facets of the particle and consequently interferences can skew full depth of characterisation. [365] It becomes clear that within a given sample many other factors are introduced in each of the analytical techniques studied so far. Thus, ranges of techniques need to be selected to characterise nanoparticles in order to achieve conclusive information rather than speculative theory.

Selenium demonstrated a single absorption band when investigated under UV-vis. This suggests that the MNP would be of small size and high symmetry, as documented by Pal *et al.*. In fact, there is a small shoulder associated with the band depicted at ~315 nm, suggesting another dimension to the shape of the nanoparticle.

4.3.2.3 PARTICLE SIZE CHARACTERISATION

Particle size measurements were carried out using a Malvern nanosizer, which is based on a dynamic light scattering technique (experimental details can be found in Chapter 2, Section 2.2.2.5, *vide supra*. The diameter of the nanoparticle is taken in 3 measurements an example of which is demonstrated in Figure 4.20
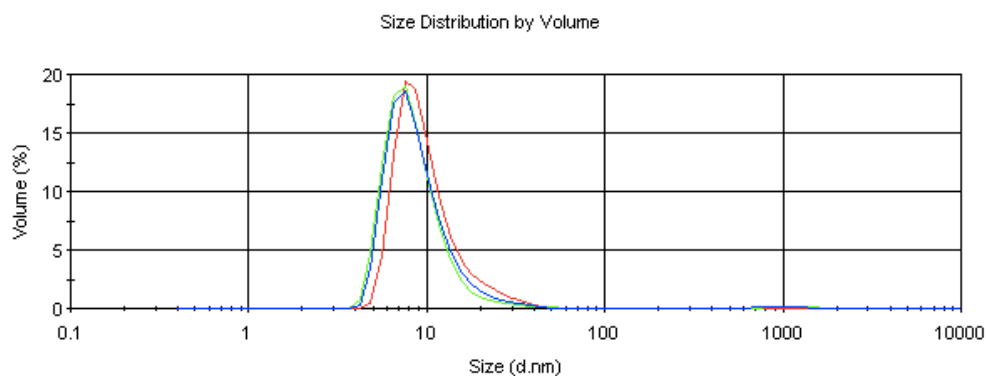
Figure 4.20: Graph of nanoparticle size distribution for scandium metal nanoparticles.

Although the nanoparticles were all washed and re-suspended, interference is a strong in this particularly sensitive technique, where temperature, gravity and light can all attribute to these fluctuations, results are shown in Table 4.2.

Particle size analysis, within this work, gave a range of results that were obtuse results. Results were often hindered by temperature fluctuations, [374] concentrations [375] and the types of nanoparticles within the solution. [376] The method is somewhat unreliable and is seldom reported in the literature. This would suggest that the method is not suitable for this type of work, or it is specific to certain types of nanoparticle analysis. However, the use of TEM and FESEM will give good analytical characterisation of nanoparticles that have been reported within this thesis.

Table 4.2: Metal nanoparticle size distribution data.

Metal Nanoparticle	Size Distribution (1) (nm)	Size Distribution (2) (nm)	Size Distribution (3) (nm)	Average d.(nm)	Polydispersity index (PDI)
Scandium	27.15	27.47	27.13	27	0.163
Titanium	55.21	54.91	56.07	55	0.221
Vanadium	44.66	44.30	43.19	43	0.155
Chromium	57.71	56.67	56.71	57	0.321
Manganese	60.5	60.64	60.81	61	0.121
Iron	33	32.51	36.33	34	0.812
Cobalt	76.01	76	76.27	76	0.224
Nickel	45.5	44.35	45.18	45	0.210
Copper	87.13	87.3	87.29	87	0.182
Zinc	81.32	81.8	80.91	81	0.170
Gallium	77.7	76.41	76.35	77	0.119
Germanium	43.02	42.82	42.11	42	0.200
Selenium	47.92	48.22	48.21	48	0.318

4.3.2.4 ENERGY DISPERSIVE X-RAY ANALYSIS (EDX)

A further technique used in the characterisation of the nanoparticles in this work was achieved using EDX. The technique confirmed the presence of the pure metal nanoparticle from SEM analysis. Other elemental confirmations have also been detected with carbon (attributed to the SEM carbon tab), which is set within the specifications of the instrument supplier data for the fixation tab. Yang *et al.,* synthesised metal nanoparticles of mesoporous silicates, EDX was used in the same way to characterise the surface of the material [377] and also highlighted carbon in the results attributed to the fixation tab. Other works include that of Klaus *et al.,* where EDAX has been used to characterise where the MNP entered the cells of bacteria. [378] The data obtained from Figure 4.21 was tabulated in Table 4.3, illustrating elemental composition of the examined spot on the sample, percentage relative standard deviation

(%RSD) has been calculated. An example of how the spot image is taken is given in Figure 4.21, where lists of elements are put in order of intensity from the sample spot.
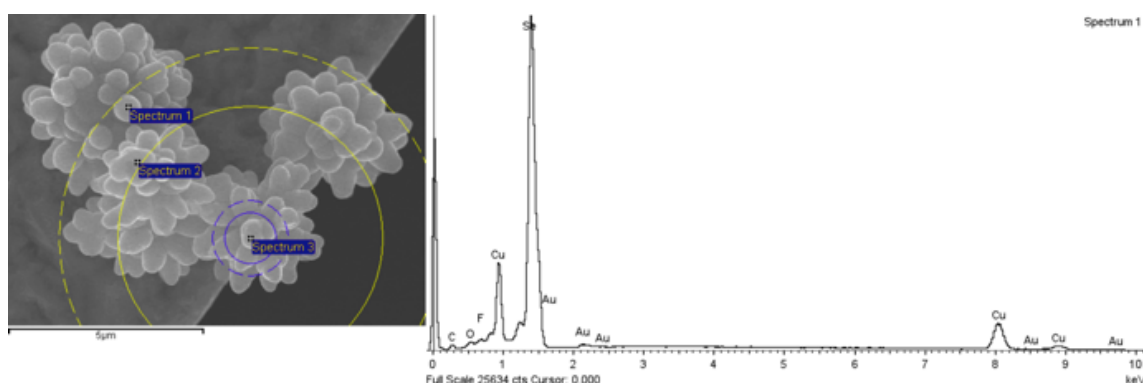
Figure 4.21: EDX data of selenium nanotree showing intensity peaks for elemental analysis of the sample spot.

The use of EDX confirms any quantitative information on the surface and has been performed routinely in many nanoparticle confirmatory papers. [312,379-382] Although the method gives good confirmatory data, it can often be subjective in other areas of analysis. The work portrayed in this chapter has relied on the calculation of %RSD (n=3) thus comparing the standard deviation from the mean. Table 4.3 shows that, in most cases composition is C.A. 40% with the exception of Ni, Cu & Zn (97.5, 99.67, 96.33%) respectively. Spot profiling of nanoparticles is a common method and has been reported in Couto *et al.,* with example compositional analysis conducted on Ni. The size of the nanoparticle and magnification at which the analysis is conducted all preferentially affect the data obtained. [375] Within these results, analysis was performed in the same manner with experimental details found in Chapter 2, Section 2.2.2.4, *vide supra*, thus maintaining sample linearity throughout the analysis and minimising any further subjective style sampling. One of the problems with quantifying the results in EDX is that samples are calculated from the relative sample composition, along with being somewhat subjective, the EDX instrument will also rely on high energy which can also denature the sample irreversibly.

Table 4.3: Mean % composition of metal contained in each spot sample with %RSD (n=3).

Metal Nanoparticle	Mean % Composition from original data	% RSD
Scandium	54.1	4.6
Titanium	65.52	3.63
Vanadium	49.08	2.47
Chromium	63.8	2.5
Manganese	62.73	1.4
Iron	40.37	8.4
Cobalt	74.29	3.4
Nickel	97.5	0.7
Copper	99.67	0.6
Zinc	96.33	3.9
Gallium	69.24	3
Germanium	46.65	2.77
Selenium	69.96	2.4

A small % RSD value indicates the results are of better quality, where standard deviation of the data is very close to the mean. Table 4.3 shows good % RSD values throughout the data, indicating that the method is able to obtain reproducible data with good limits, with all % RSD data being below 10%. % RSD enables data to be compared to the relative standard deviation and mean, it is used frequently to analyse data for reproducibility. [135,383-385]

4.4 CONCLUSIONS

The development and study of metal nanoparticles has been demonstrated in this chapter, as a starting point for their investigation as a potential candidate as antifouling agents.

It has been observed that the polyol reduction synthesis has been successfully used to produce a range of metal nanoparticles associated with period four in the periodic table, which has never been performed before this.

The reduction process has led to the formation of a range of nanoparticles estimated to be in the range of definition of a nanoparticle outlined previously in a reproducible manner.

UV-vis absorption data has enabled the investigation of surface plasmon resonance for the metal nanoparticles when produced in this synthesis method where a range of absorption peaks were realised.

Each metal nanoparticle had some similarity in sizes but the limitations in instrumentation could not resolve intrinsic morphology of the nanoparticles in every case. Further work in this field would require the use of transmission electron microscopy for this to be probed. Nonetheless, FESEM has characterised the size of each nanoparticle effectively and gives thorough information for the investigation of how nanoparticles potentially adsorb and penetrate a microorganism's cell membrane.

Although the method has induced nanoparticle sizes below 100 nm, which is a desirable attribute to most nanoparticle definitions, they are sometimes varied in size and structure. Contrastingly, this should not be the case if the method was reproduced and if reaction conditions remained the same for each metal synthesised. To answer this, each metal has rather contrasting properties when compared to each other, and if that were not the case then they would all be situated in the same position within the periodic table. Therefore each metal used has provided different atomic attributes and has given the varying characteristics observed throughout the body of synthetic work.

In summary, the polyol reduction method allows a suitable method for the successful reduction of metal salts for the nucleation and growth of the metal nanoparticles selected. The reaction is generally governed by changes in temperature, reaction concentrations and capping agents used, all of which can be controlled by the user. The method remains an ideal candidate for future synthetic approaches and further contributions to the literature will enable the polyol method to become the leading candidate for most metal nanoparticle synthetic approaches. The work performed for period four metal nanoparticles is novel to the polyol reduction method and shows that with optimisation metal nanoparticles can be synthesised accordingly.

5

Nanoparticle doped materials

5.0 INTRODUCTION

Chapter 4 details the synthesis of metal nanoparticles in preparation for the development of an efficacious antifouling material containing the synthesised nanoparticles, which will be examined within this chapter. Currently, a substantial amount of research has been documented regarding the use of silver nanoparticles as a microbiocide in antifouling materials. This forms an impetus for the work contained herein on the investigation of period four metal nanoparticles and their potential candidacy as an effective microbiocide in an antifouling capacity. The most successful nanoparticle has then been exploited in more biological assessments and has been compared to a market leading nanotechnology base.

5.1 METAL NANOPARTICLES

Metal nanoparticles have long been known to offer antimicrobial properties at a scientific investigatory level from as early as 1890, where Robert Koch successfully showed that gold inhibited microbial growth. [386] Currently, copper, [387] titanium, [201] silver, [300] and gold [386] are the most common metal nanoparticles employed as microbiocides doped in materials as antifoulants. They are already proven to be an effective toxin for microorganisms and their mode of action through cells is well documented. [300,301,386]

Other uses for metal nanoparticles in medicine are depicted by the Indians, where a solution of gold was prescribed for memory enhancement, or in ancient Egypt where dentists used gold in dentistry. In Alexandria, alchemists developed a powerful colloidal dispersion of gold to promote eternal youth, and throughout China gold was used to cook rice, to help replenish gold in the body. [388] These, although not proven remedies, are all examples of uses of metal nanoparticles through the ages to remedy a problem or ailment.

The success of new era metal nanoparticle application has erupted from, initially 1960, where Richard Feynman gave the famous lecture, "There's plenty of room at the bottom" through to the early 1990s where nanomaterial journals were first established. [389,390] The synthetic chemistry of metal colloids has now reached the degree of refinement necessary for the production of highly dispersed metals which can now be exploited for specific technological applications ranging from; photography, [391] catalysis, [392] electrochemistry, [393] and from this body of work, antifouling agents. [135]

The delivery of these potential agents will require a matrix or functional material to dope them within, providing a test material for their candidacy as an antifoulant or functional antifouling material. Material design will therefore be discussed in the next section of this chapter of work.

5.2 SURFACE COATINGS

A coating is defined as a material (usually a liquid) that is applied to a surface and appears as a continuous or discontinuous film after drying. [394] The need for coatings and materials for different applications will relate to what property the material or coating is desired. For example, a paint to prevent rusting, a coating to enhance cell growth, a material to enhance structural function or simply for decoration. These are all desirable attributes in the design of a material for this application, and consequently will be discussed in the following headings within.

5.2.1 METALLIC COATINGS

The use of metals to inhibit adverse effects to the useful substrate has been around for thousands of years. Aforementioned Chapter 3, *vide* supra, early Phoenicians and Carthaginians were said to have applied pitch and copper sheathing on ships while waxes, tars and asphaltum were used in other cultures. [395,396] Lead had also been used for the prevention of biofouling, with some reports of coatings containing arsenic in order to combat shipworms. [397] The Romans and Greeks both secured vast layers of lead sheathing on ship hulls using copper nails. [397]

Copper sheathing was used across some sea-faring cultures as reports mention, "the scraping of weeds, ooze and filth from the ship's sides to make them easily move through water". [395] In 1625, the first patent for fouling protection was introduced by William Beale, of which a probable copper compound and cement was passed, with intrinsic chemistry of copper being studied by Humphrey Davy some 100 years later. [395]

5.2.2 NEW TECHNOLOGICAL COATINGS

No new alternative seems to be able to reach the same level of effectiveness as the paints and metallic based coat systems that are already in place. This section of the chapter aims to deal with some of the 'newer' coating matrices that are currently in the research area.

5.2.2.1 NON-STICK FOUL RELEASE MATRICES

Non-stick coatings are a newer way of combatting the adhesion and fouling of organisms on a substrate. They work by providing a low-friction, ultra smooth surface on which it is hoped that organisms find it difficult to settle. So far this has been elucidated using the following two types of polymers:

- Fluoropolymers
- Silicones

Fluoropolymers are non-porous have a very low surface energy and possess good non-stick surface characteristics. [95] Meanwhile, silicone based polymers improve the non-stick efficiency of fluoropolymers. Poly (dimethylsiloxane) (PDMS)-based non-stick foul release coatings are used for their low-micro roughness, high elastic modulus and low glass transition temperatures. [398] The silicone-based polymers minimise the mechanical locking of biological based glues, which gives the polymer its foul release style asset.

The use of polysiloxanes substituted with fluorine also seems to attract suitable candidacy for surfaces with low bioadhesion. This would bring about a polymer with advantages such as low surface energies with elastic energies similar to silicones. [399-401]

5.2.2.2 DOPING MATRICES

Since the advent of polymer science, research has focused on creating a range of coatings suitable for replicating desirable properties outlined already in this chapter. Polymers as already mentioned have aligned themselves as new market leaders to create a novel non-toxic material suitable for specific roles and functions. For the purpose of this chapter, only antifouling based polymer matrices will be considered, where doping matrices will be discussed herein.

5.2.2.3 POLYMETHACRYLATE MATRICES

Methacrylic polymers are not new to the area of biofouling and until the ban of tributyltin (TBT), represented a large volume of successful matrix based coatings that were on the market. These well-known paints generally contained random methacrylic copolymers bearing the active biocide. The success of these coatings relied on the mechanism of action commonly referred to as 'self-polishing', defined by their constant release rate under stationary and dynamic conditions. [398]

Polymethacrylate polymers have been used as a doping matrix for candidate biocides because they can be chemically tailored to erode when dynamic flow is applied over the surface. Bressy *et al.*, demonstrated the tailoring of polymethacrylate coatings to stimulate a co-polishing feature as explained herein for use with biocidal compounds which are currently on the market. [402] The concept of tailored erosion could be of great interest for future methods in coating design and should not be disregarded. However, the coatings do have limitations and are applicable solely to certain dynamic conditions, which also should not be disregarded.

5.2.2.4 SOL-GEL MATRICES

Sol-gels are mentioned in the literature as a potential antifouling material suitable for the doping of biocidal agents within their matrix. The use of a sol-gel permits a multi-function coating/material rendering the coating an interactive nanomaterial coined in Corriu and Anh (2009), [403], which could present itself as an extremely desirable matrix for doping biocidal agents. They are generally of a hydrophilic nature owing to their silicon oxide structures, Figure 5.1 and therefore are of great interest as they have the possible function of being self-cleaning, [404] antifogging, [405] and extreme wettability. [406]
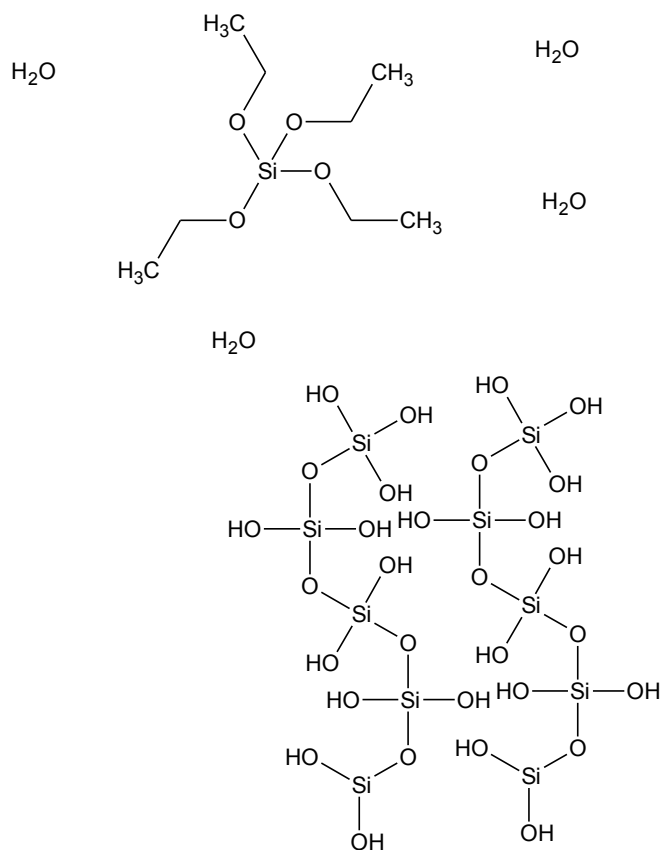
Figure 5.1: Structure of (top) tetraethoxysilane (TEOS) and water (bottom) polymerised TEOS sol-gel.

Sol-gels are quoted in the literature frequently for their 'potential' use as antifouling coatings, [407-409] but seldom are they implemented to test this claim of efficacy. Their surfaces characteristics can be tuned, such as surface composition, surface area and surface wettability. [21] The influence of these features has already been investigated in Rittschof *et al.*, [410] for invertebrate larvae and for algal zoospores.[411] This forms a promising basis for the investigation of doping biocidal agents into a tailorable sol-gel matrix as a possible antifouling coating.

5.3 AIMS AND OBJECTIVES

The aim of this work was to design an antifouling coating suitable of doping the metal nanoparticles already developed in Chapter 4. These nanoparticle-doped coatings were then assessed for their potential in a series of biofouling assays.

The objectives of the work were:

(1) To characterise of the nanoparticle-doped materials to investigate the effects of wettability, general morphology of the material and also investigate the stability of the nanoparticles within the matrix of the material.

(2) To measure the biofilm development for each of the metal nanoparticle-doped substrates through the use of mass, slime and more fundamentally the levels of protein and carbohydrate adsorption which is also attributed to microorganism proliferation on a given surface.

(3) In order to challenge the effectiveness of the material an environmental cell count will also be performed, and will be the first instance of enumerating the surface activity of the developed materials developed thus far in the thesis. Furthermore, a toxicity assay using *E. coli* will also substantiate the level of efficacy for the best performing nanoparticles.

(4) To assess the concentration of the metal nanoparticle in the material and determine how this affects the degree of fouling across the substrates.

(5) To determine if the nanoparticles influence the surface characteristic, morphology or surface activity of the nanoparticle doped material.

5.4 RESULTS

This section deals with the synthesis and characterisation of a range of nanoparticle doped sol-gels, carrying on from the work achieved in Chapter 4, *vide supra*. The sol-gels were doped with metal nanoparticles and then investigated for their antifouling potential using a series of biofouling based assays that have been developed within this thesis.

5.4.1 SOL-GEL CHARACTERISATION

The synthesised sol-gel was characterised using a range of techniques, thus investigating what surface properties the material exhibits when introduced into a water interface. Ranges of techniques have been used to achieve this goal including: SEM, EDX and contact angle and water uptake analysis, which have all been detailed herein.

5.4.1.1 SOL-GEL SURFACE MORPHOLOGY

The SEM morphology of the raw material surface is shown in Figure 5.2. The surface microstructure of both the undoped and doped sol-gels are displayed, which have been spin-coated on to carbon SEM tabs as detailed in the experimental Chapter 2, Section 2.3.1.4, *vide supra*.

It was found that the materials, once spin-coated, gave a 'smooth' morphological surface, the microstructure of the sol-gel blank can be seen in Figure 5.2, the smooth surface has been shown on Figure 5.2 (b). For brevity, only the cross-section morphologies of the membranes have been shown.
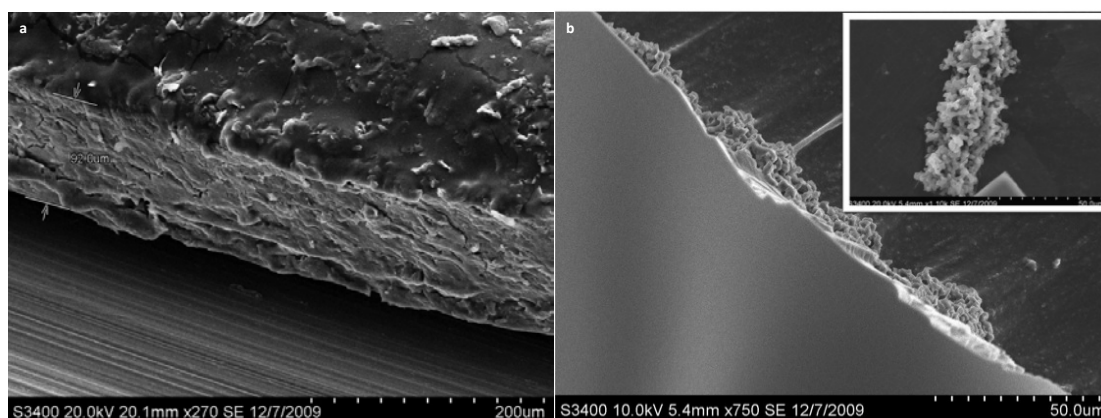
Figure 5.2: Electron micrographs of the surface characteristics of the sol-gel matrix - (a) side profile (b) top profile with mesoporous structural zoom.

The 'smooth' surface morphology presented in these results is also reported frequently within the literature. [403,412] However, the range of nanoparticles doped within these types of matrices is not prevalent. Silver nanoparticles has the most citations within the literature and SEM is frequently used to characterise such coatings. [413-417] Depending on the resolution of the SEM instrument, individual nanoparticles can often be difficult to resolve. [418]

5.4.1.2 CONTACT ANGLE

Surface energy analyses using contact angle measurements were performed on each of the nanoparticle-doped sol-gels in order determining the wettability of the material. Hydrophobic and super-hydrophilic surface coatings are considered to be the most suitable in the prevention of microbial adhesion. [120] Self-cleaning properties are also desirable and [419] reported hierarchical micro and nanostructuring could enables improved self-cleaning and therefore, antifouling properties. Sol-gels can be tailored to achieve varied wettability, and this is highly dependent on the mesoporous structure obtained through the synthetic conditions. For example Kontos and coworkers, [420] achieved varying degrees of wettability by the introduction of titanium dioxide, which is known to have antimicrobial properties. In a similar manner, the nanoparticles in this work have been doped into the matrix of the sol-gel. The measurement values are shown in Figure 5.3, where the nanoparticles were doped directly into the sol-gel matrix.
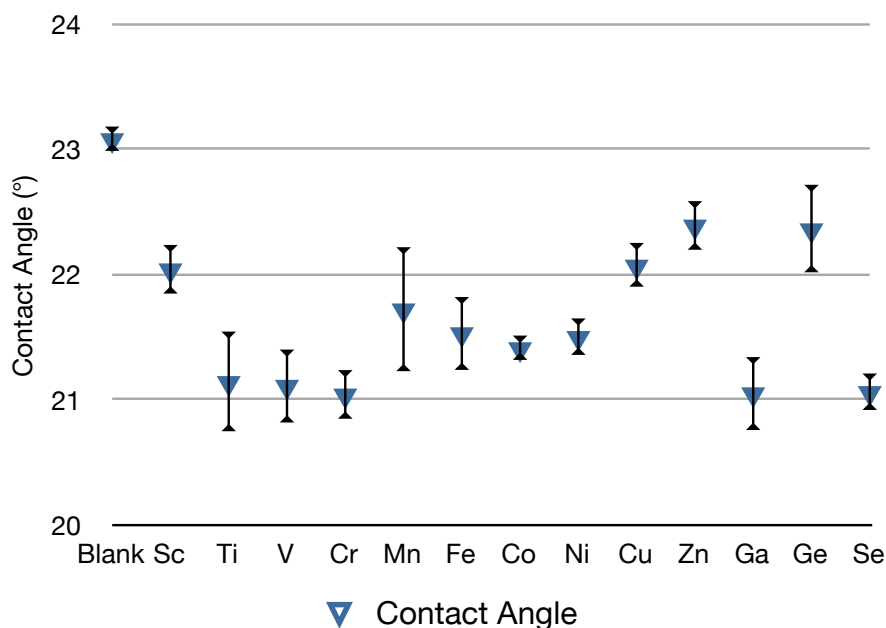
Figure 5.3: Scatter graph of contact angles of nanoparticle doped in sol-gel matrix (n=9 ± 1 SD).

The contact angles obtained show that the MNP-doped sol-gels have increased wettability, compared to the sol-gel blank. The values therefore show that the MNPs are having an effect on the surface energy in each of the doped sol-gel matrices. It has been suggested by Sharma *et al.*, that water spreading occurs when metallic species are introduced into a sol-gel matrix. [421] To enable the visualisation of this effect, a photographic comparison has been detailed in Figure 5.4, where the sol-gel blank is compared to iron doped nanoparticles in the same sol-gel matrix.
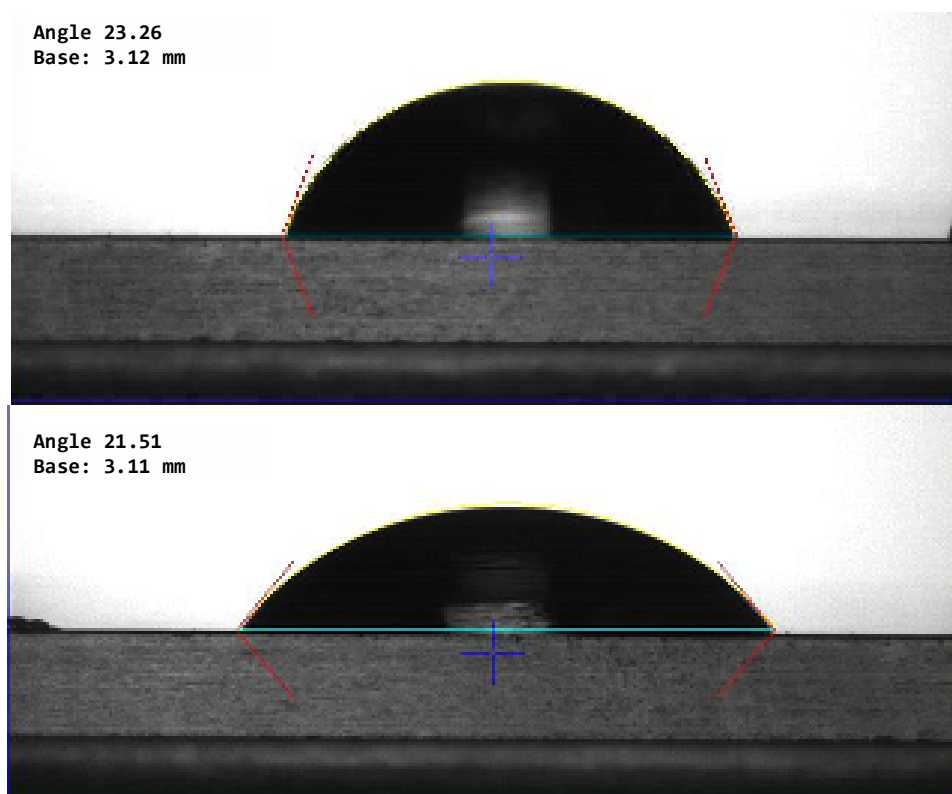
Figure 5.4: Photograph comparing wettability of (top) undoped sol-gel with (bottom) Fe-doped sol-gel.

It is evident that the addition of MNPs within the sol-gel changes the wetting characteristics of the surface. The interaction of metal species and protecting agents (in this case PVP) could present as the property of long-range electrostatic interactions between the sol-gel and the capillary property of the liquid.

In conclusion to the results obtained, that the metal nanoparticles, although do have a clear effect on the sol-gel wettability, this is not convincing experimentally. The sol-gel blank is negligible to the metal nanoparticle doped responses and will be discussed further in.

5.4.1.3 EDX ANALYSIS

EDX is another highly cited technique in the literature for the characterisation of sol-gels. It allows the surface to be characterised elementally, and is shown in Figure 5.5. Si and O were both found to be abundant within the matrix and is indicative of the formation of a sol-gel coating. This has been also detailed in Alias *et al.* where EDX was used accordingly to spot sample sol-gels, [422] this has been achieved in this chapter of work.
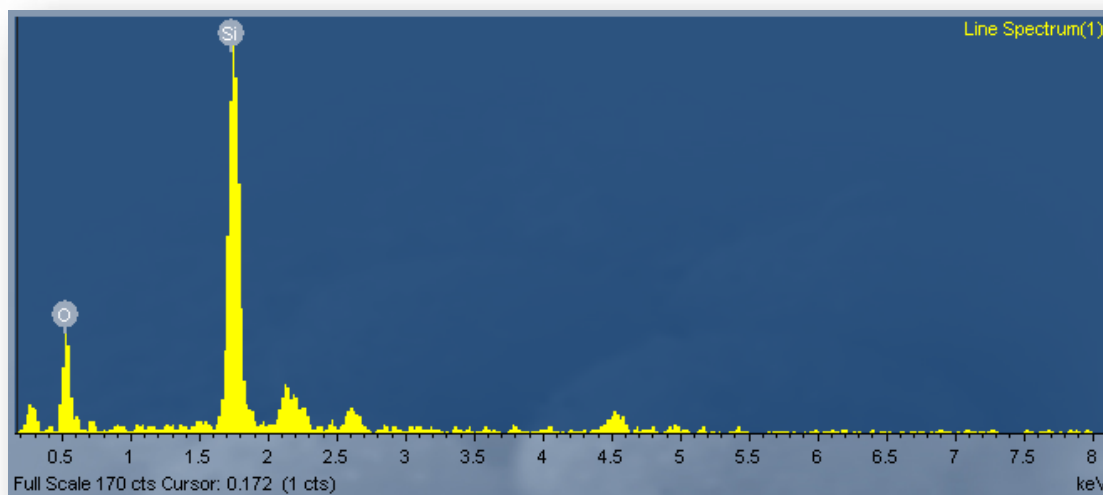
Figure 5.5 Typical EDX spectrum of the sol-gel blank used.

The EDX measurements were carried out on the sample to verify the chemical components of the local area. Measurements were then taken on each of the MNP-doped sol-gels to ascertain the level of surface activity that might be exemplified throughout the sol-gels. This was achieved using a 'freeze-fracture' method across the longitude of each of the MNP-doped sol-gels. It was intended that this would examine the dispersion of nanoparticles through each of the sol-gel matrices. This has been illustrated in Figure 5.6.

The data shows that despite the nature of the matrix of the sol-gel, nanoparticles could be found throughout the entire sol-gel's integral structure. This affirms that the sol-gel has a good homogenous dispersion of nanoparticles throughout the matrix; manual subtraction of the Si-elemental composition was carried out on each spectrum thus showing nanoparticle involvement in the sol-gel matrix.
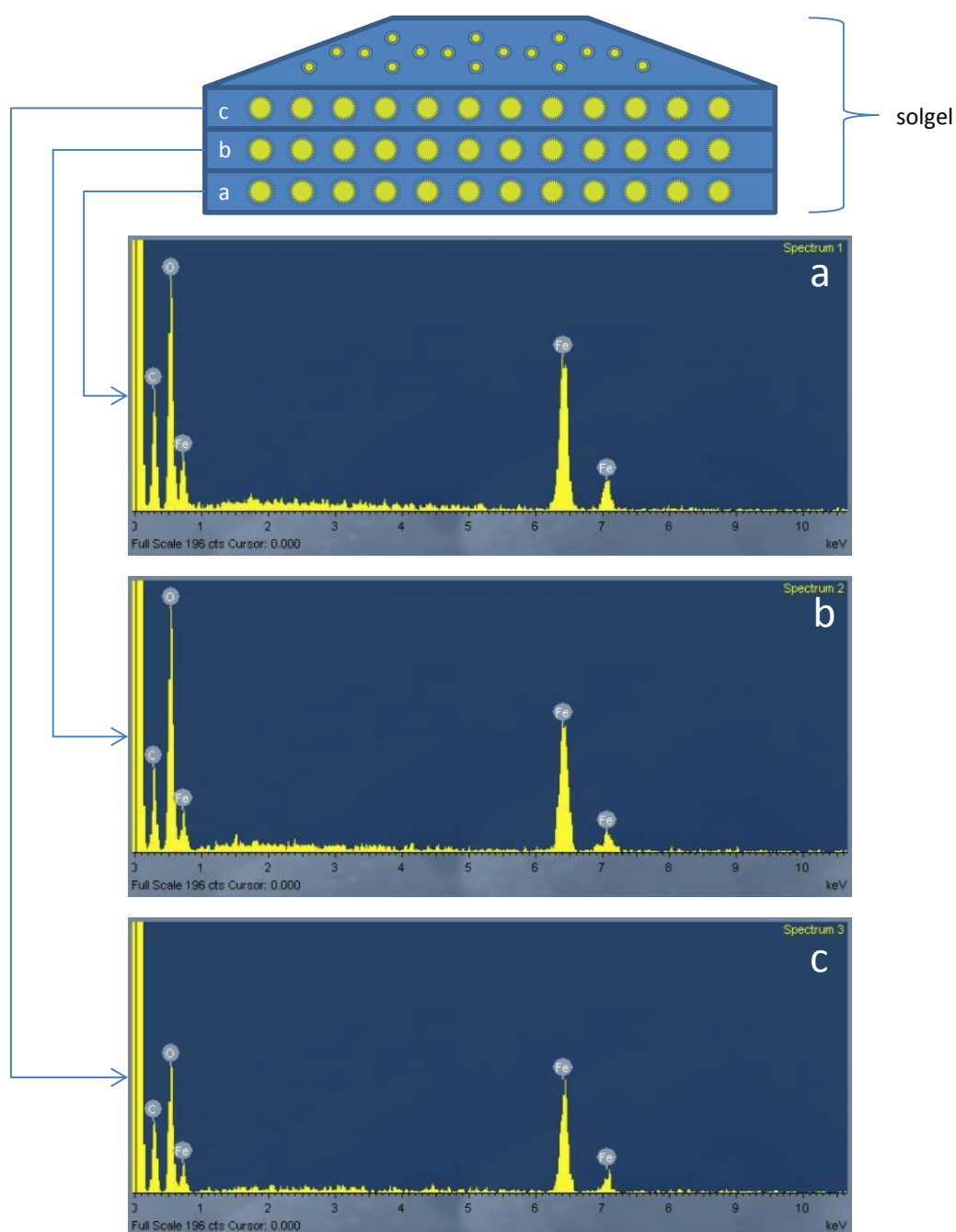
Figure 5.6 EDX spectra illustrating freeze fracture spot analysis of nanoparticle-doped sol-gel shown for iron.

Following characterisation of the sol-gel, the materials developed were then put through a series of laboratory-based assays outlined in Chapter 2. Assessment of slime, mass and a series of biochemical tests to quantify protein and carbohydrate adsorption to the test substrates has also been investigated.

5.4.2 AN ASSESSMENT OF FOULING

This section of the chapter deals with an inspection process of the developed materials. The nanoparticle doped sol-gels were subjected to a 7-day laboratory tank study where microfouling was assessed. Fouling occurs in many ways and so many techniques could be used to investigate the samples; the work presented here covers a range of adsorption characterisation and quantification techniques.

5.4.2.1 MASS ANALYSIS

The mass adsorbed to the surface of the test substrates pertains to the 'biofouling process', which takes into account the conditioning and adsorption of microorganisms, flora and other fauna with subsequent protective adhesive. A washing step was performed, described in Chapter 2, Section 2.3.2.1, *vide infra*, to remove particulate matter often referred to as 'geo-fouling' as this was not the remit of analysis as given by Jefferson (2004). [423] This gives the impression of microorganism involvement across each of the metal nanoparticle doped sol-gels, the results of which are displayed below in Figure 5.7, *vide supra*.
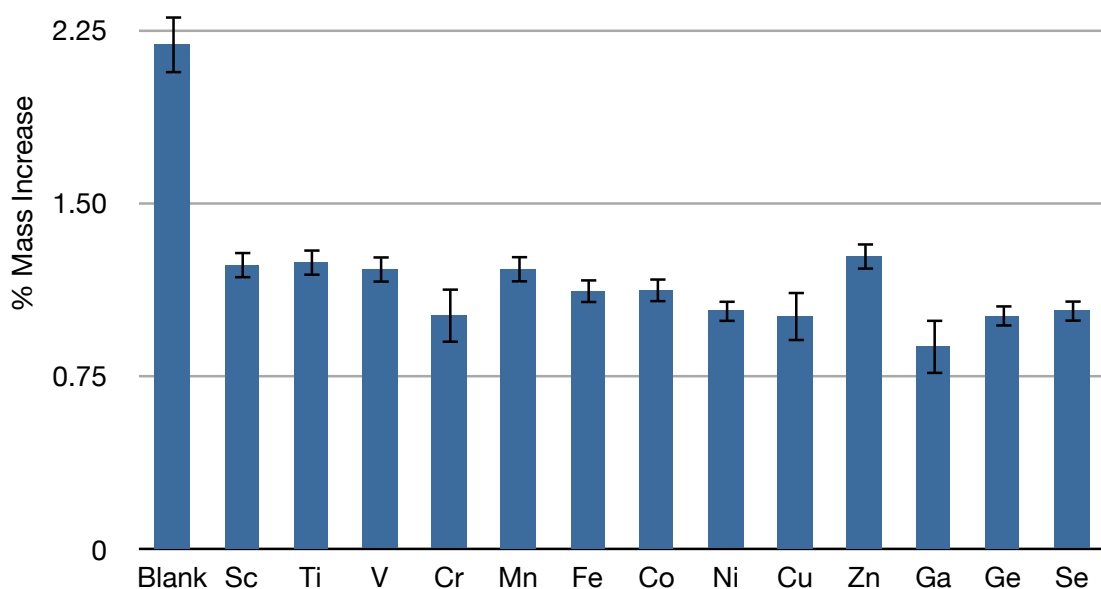
Figure 5.7: Scatter graph showing mass gain in percentage for each MNP-doped sol-gel (n=9, ±1SD).

The results depict that the MNP-doped sol-gels are influencing the overall mass gain that has occurred across each of the sol-gel matrices when compared to the blank. The blank is permitting higher levels of adsorption and thus greater degrees of biofouling. The results also

demonstrates that Ga, in particular, has shown least mass increase when compared to the rest of the group, presenting levels of up to 125% improved antifouling response to that of the undoped blank. Percentage mass increase is a simple parameter to quantify the levels of material adsorbed to each material. Alves *et al.*, quantified mass gain using a sonication method where adhered biomass was removed with a buffered NaOH solution proceeded by mass quantification. [40] The limitation to this method is that sonication is a powerful technique and can cause alterations in the already fragile biofilm or material, thus expanding the possibility of extra material (not attributed to biofouling) being introduced. Schooling *et al.,* used a matrix scraping method to analyse the biomass that adhered to the test substrate. [424] The method appears to introduce error with the scraping parameter, which would not be effective in removing the molecular level adsorption material, all of which are synergistic in attributing mass to the test substrates.

Although mass analysis is a very simple technique, it illustrates a versatile method in determining the level of adsorption of material on to the substrates surface, especially in the microfouling stage. Alone, mass analysis does not stand as a thorough probe into the level of biofouling on each of the substrates and so has been reinforced in this body of work with other fouling assays. The next screening technique that has been included in this chapter of work is the slime, which is described, in the next Section 5.3.2.2.

5.4.2.2 THE SLIME TEST (GLYCOCALYX)

This body of work measures the level of glycocalyx (slime) within the EPS matrix that has adhered to each of the test substrates.

Figure 5.8 shows the level of slime production on each of the different MNP-doped sol-gels after a series of fixation and staining steps had been applied, Chapter 2, Section 2.3.2.2 *vide supra*. The glycocalyx analysed represents a fraction of the slime layer adsorbed to the surface of the substrate, which in turn represents a fraction of the weight already achieved in Section 5.3.2.1.
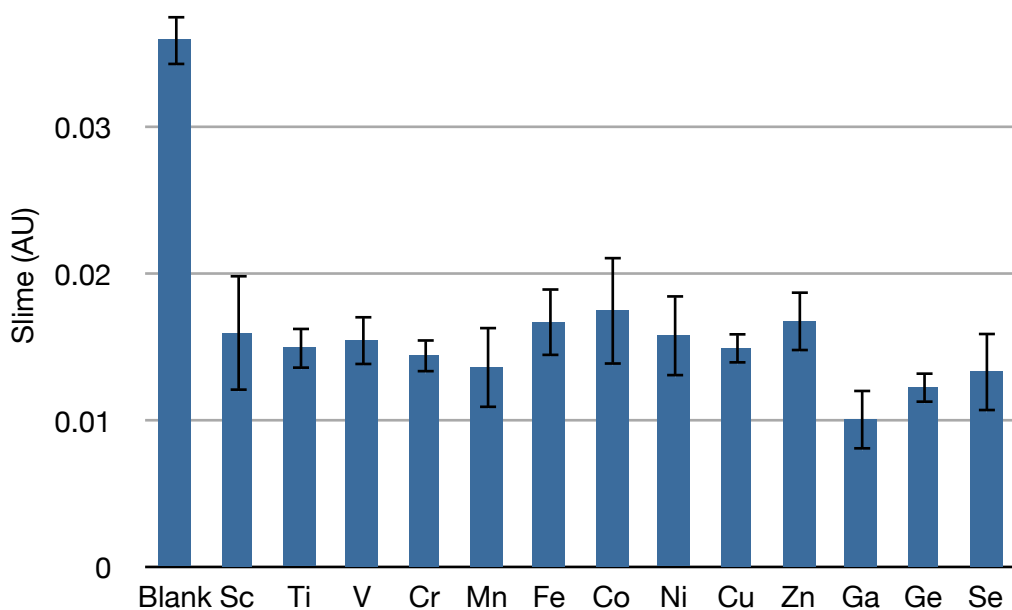
Figure 5.8: Bar chart showing slime test results for the period four metal nanoparticles doped within sol-gels (n=9, ±1SD), where slime is measured in AU.

EPS is known to play an important role in the accumulation of biofilms. [2,425-427] The quantification of slime adhered to the substrates, therefore represents the measurement of microorganism activity across each of the test substrates. In contrast to other slime tests presented in the literature, [199,428] mass analysis has been run in tandem with this assay. This gives an overall impression that slime can be attributed to percentage mass gain.

The level of adsorption of slime was observed to be much higher in the sol-gel blank when compared to the rest of the MNP-doped sol-gels. The Ga-doped sol-gel has given 130% better slime aversion when compared to the sol-gel blank, which is reflected with the mass result in Figure 5.7.

Figure 5.9 has been produced to analyse slime adsorption versus mass. The results shown illustrate that slime is attributed to mass across each of the MNP-doped sol-gels and, indeed, symmetry is replicated in these results. Slime and mass were observed to be similar when compared on an overlay chart shown in Figure 5.9.
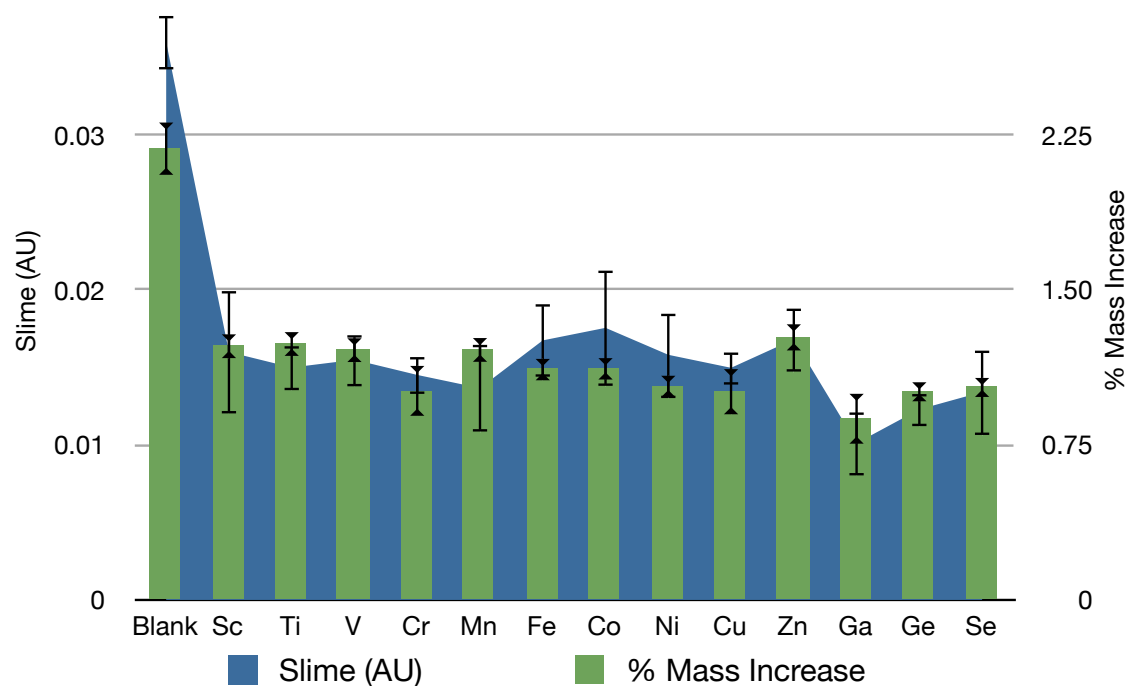
Figure 5.9: Dual graph showing mass increase plotted against slime (n=9 ± 1SD).

5.4.2.3 ENVIRONMENTAL BACTERIAL COUNTS

In this experiment, the sol-gel samples were subjected to a three-day environmental sample, where adhesion of microorganisms was enumerated on the substrate's surface. Each sol-gel was taken out and washed according to the experimental conditions outlined in Chapter 2 Section 2.3.2.2. The sol-gels then underwent a series of staining and enumeration steps using epifluorescence microscopy (performed by Emma Weir).

This work represents a 'real' sample study where the screening and enumeration of a broad range of microorganisms from an environmental system has been attempted. Many authors have established comprehensive adhesion and enumeration studies through the use of pure culture microorganism assays [429] this system contrastingly relates to a whole environmental system.
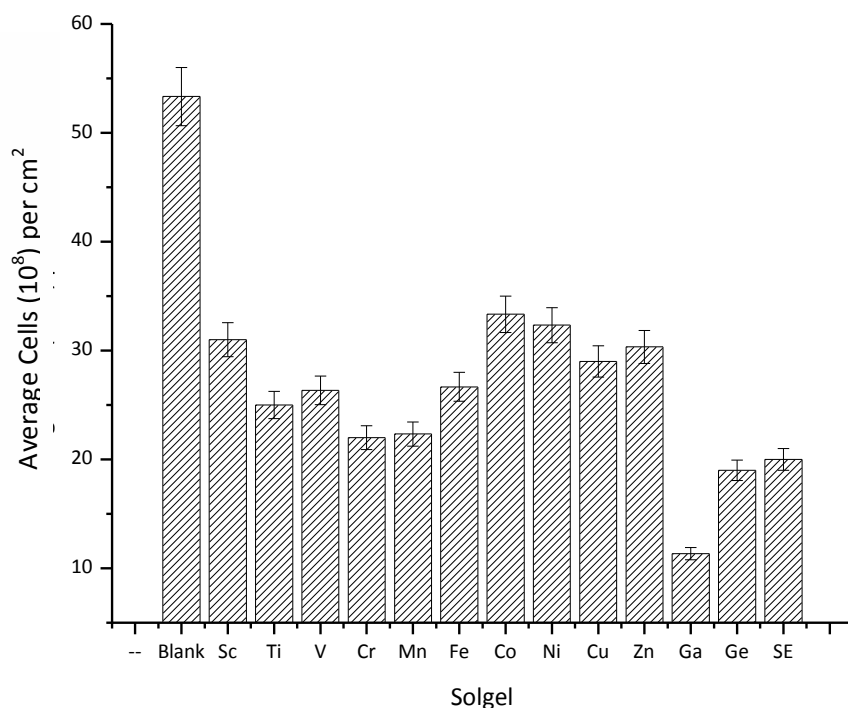
Figure 5.10: Bar chart showing microorganism count on MNP doped sol-gels from an environmental freshwater tank study, enumerated by epifluorescence where 5 separate independent samples (n=5 ± 1 SD) were counted for bacterial retention.

This 'real' sample adhesion study, Figure 5.10, differs from the literature, which generally involves pure culture assays, [429] the method of counting has been presented in Figure 5.11 (experimental details given in Chapter 2 Section 2.3.2.2). Azevedo *et al.,* exposed microorganisms to substrates to correlate a change in biofouling ability. The study was similar to this in the way of harnessing acridine orange with a three-day exposure time. [13]
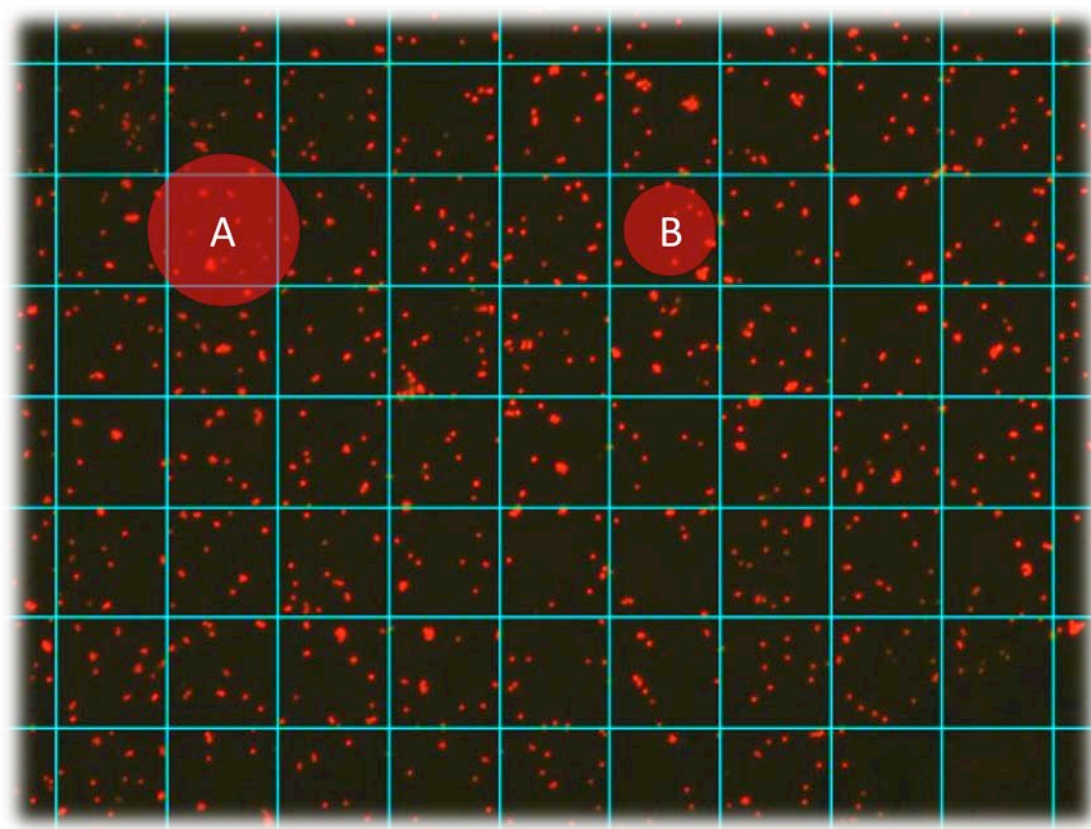
Figure 5.11: example of an epifluorecence image confirming bacterial numbers per square which were then enumerated for each substrate (A)=sample grid spot and (B)=bacteria within grid.

The results show that the MNP-doped sol-gels have all shown less microorganism adhesion when exposed to the freshwater system. The lower period four metals, Ga, Ge and Se have exhibited up to 15x bacterial retention compare to the undoped sol-gel. Upon inspection of the literature, Ga, Ge and Se all gave high spectrum antimicrobial, [133,430] bactericidal, [431] or fungicidal properties. [432] In view of the literature and retrospectively speaking, it is no wonder why these three nanoparticles have shown the best responses to this assay among the others *vide infra* Section 5.3.2.1 and 5.3.2.2.

5.4.2.4 MINIMUM INHIBITORY CONCENTRATION

Presented in this study, are the two most responsive MNPs, which were screened against a pure culture of *Escherichia coli*. The pure MNPs were taken and prepared as discussed in Section 2.3.2.1, *vide supra*. Following this, a 10 µL aliquot was taken, inoculated on the plates and incubated overnight. Figure 5.12 shows the results for the zones of inhibition on the MIC plates.

a
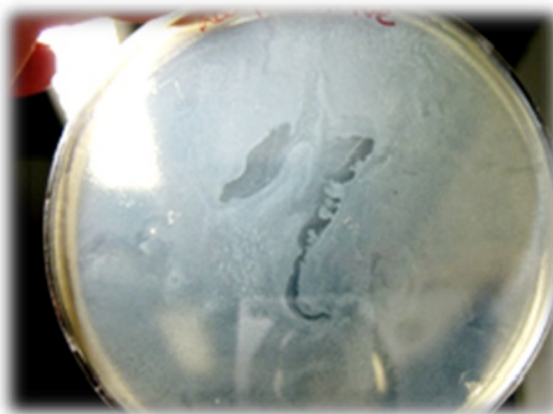
b
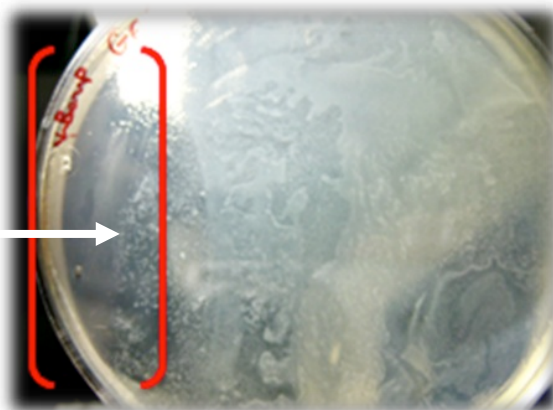
c
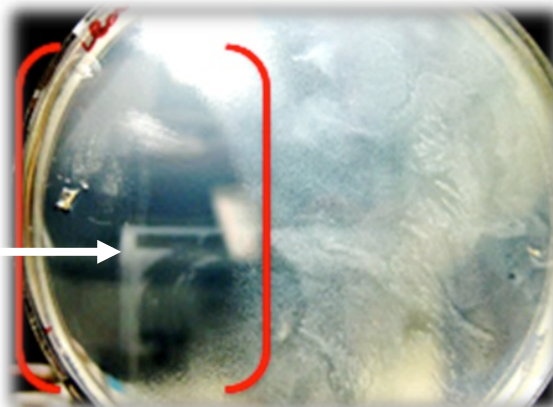
Figure 5.12: MIC plates of (a) positive control, (b) Ge-MNPs and (c) Ga-MNPs → = inoculation point.

Here the results show that the Ga-MNPs have delivered a potent reaction towards the *E. coli*. This is somewhat reflected in the literature, with rare antimicrobial properties reported in Eby (2008) [433] the results are exciting and promising and so will be discussed in further detail throughout the thesis.

5.5 CHALLENGING CONCENTRATION

The results obtained have shown that MNP-doped sol-gels show some efficacy for use as an antifouling material, further investigations were considered. One question that has to be asked is, did the materials show improved antifouling response from the effect of the nanoparticle, or was it a response seen from the material's wettability? The next stage of the work challenged the effect of concentration on wettability.

5.5.1 NANOPARTICLE CONCENTRATIONS

This section will aim at dealing with whether the nanoparticle concentrations, thus far are effective enough to cause an effect within the current sol-gel matrix.

Firstly, the average number of atoms per nanoparticle can be calculated from the data obtained from the FESEM analysis, shown Chapter 4, Section 4.2.2.2.2 *vide infra*. Assuming a spherical shape and uniform structure, the following considerations can be formulated. The average number of metal atoms (*N*) for each type of nanostructure was calculated using the following equation, where ρ is the density of the metal, *M* stands for the atomic weight and *D* is the diameter.

$$N = \frac{\pi}{6} \frac{\rho D^3}{M} \tag{3}$$

The next step was to calculate the molar concentration of the nanoparticle solutions, by the division of the total number of gold atoms (N_{total}, equivalent to the initial amount of metal salt added in the reaction solution) by the average number of metal atoms per nanoparticle (*N*) according to equation (3), where V is the volume of the reaction solution in litres and N_A is Avogadro's constant. A further assumption made was the reduction of metal salt to metal atoms was 100%. The concentration of each sample may then be calculated from the initial concentration according to the relative concentration as stated in Section 2.2.1.3.

$$C = \frac{N_{total}}{NVN_A} \tag{4}$$

The extinction coefficient of each metal nanoparticle can then be determined according to the Beer-Lambert law, Equation (5).

$$A = \varepsilon b C \tag{5}$$

The absorbance at the λmax was recorded for each sample and then plotted against the molar concentration of the solution. The extinction coefficient can be obtained from the slope of the

linear region of the absorbance-concentration curve. An example of the typical concentration spectra has been shown in Figure 5.13, which has been performed for silver nanoparticles. The metal nanoparticle spectra have been tabulated in Table 5.1.

(a)

(b)
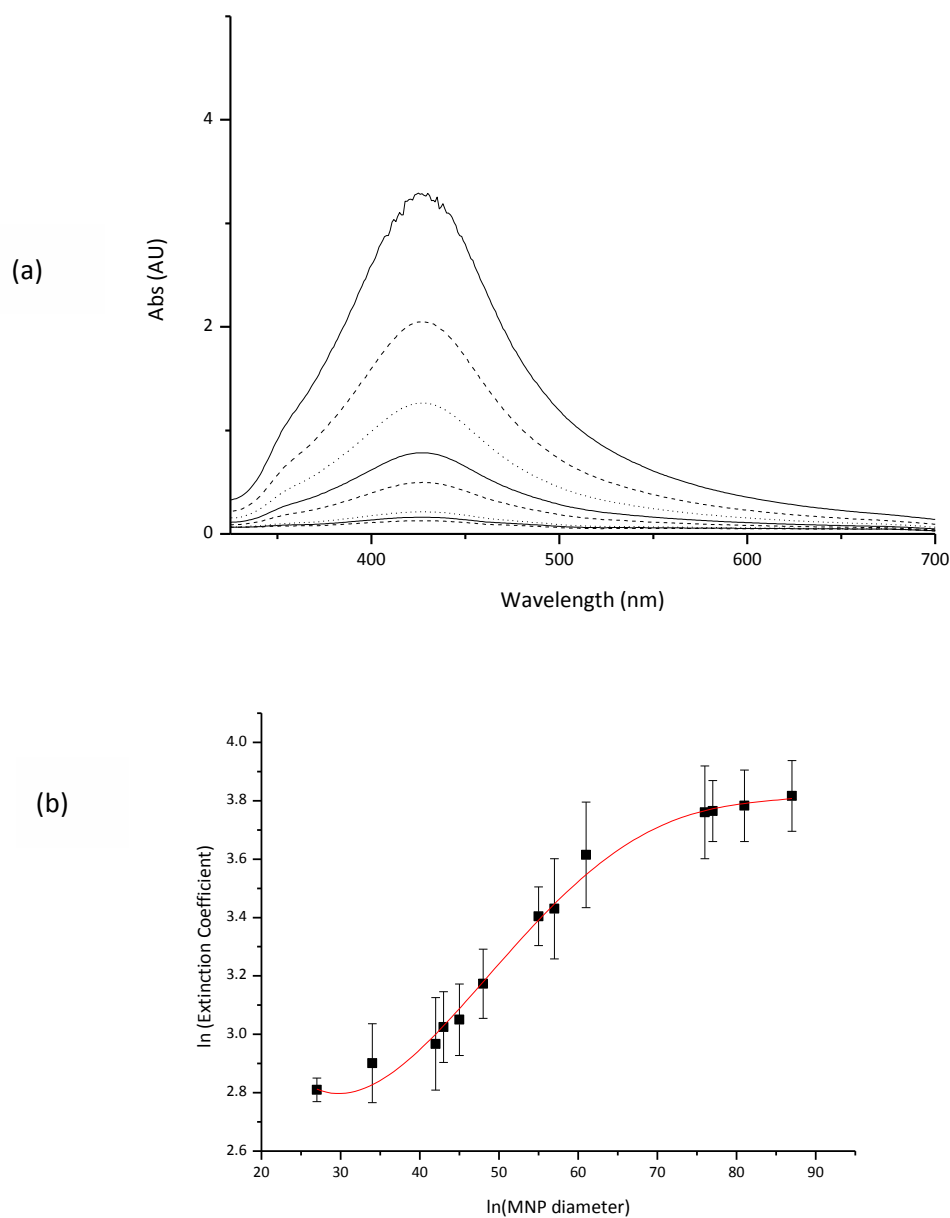
Figure 5.13: Absorption spectra (a) silver PVP-protected nanoparticles at varying concentrations and (b) plot of experimental data of maximum extinction at the surface plasmon resonance band vs. corresponding concentration.

Table 5.1: Table showing extinction coefficients (ε) of the synthesised MNPs with different sizes, solvent matrix water (dielectric constant 78.4 @ 25 °C) initial concentrations are at 5 mM.

MNP Sample	Nanoparticle size, d (nm)	ε (Mcm^{-1})
Sc	27	3.0874×10^{7}
Ti	55	4.8116×10^{10}
V	43	4.9012×10^{9}
Cr	57	4.7036×10^{10}
Mn	61	3.2244×10^{11}
Fe	34	3.6280×10^{9}
Co	76	6.4527×10^{11}
Ni	45	3.9762×10^{9}
Cu	87	7.9412×10^{11}
Zn	81	7.3182×10^{11}
Ga	77	6.4527×10^{11}
Ge	42	4.0511×10^{9}
Se	48	3.7064×10^{9}

The measured extinction coefficients of PVP protected metal nanoparticles have not been heavily reported in the literature. However, the more noble metals of silver, gold and aluminium have, thus, the relevant calculations have been applied in Equations 4 – 6. Jain *et al.,* report the characterisation of the extinction gold nanospheres, nanorods and nanoprisms. They found that as a nanoparticle exhibits larger size dimensions, larger extinction coefficients were achieved. This is reciprocated in this body of work where nanoparticle size would shift an order of magnitude in certain nanoparticles. [434] For example, Jain *et al.,* showed that the larger the nanoparticle, the higher the absorption wavelength maximum and the higher the extinction coefficient, all of which have been seen in the results of Chapter 4, *vide supra*. This finding is also in accordance with Mie's theory. [369] As nanoparticles have increased in size so to have the orders of magnitude for the extinction coefficients. For example, Sc MNPs had a mean size diameter of 27 nm, and ε of 3.09 x 10^{7} in comparison with Ti MNPs that have a mean diameter of 55 nm and an extinction coefficient of 3 orders of magnitude larger with a ε of 4.81 x 10^{10}, which corresponds with what has been reported in Jain *et al..* [434]
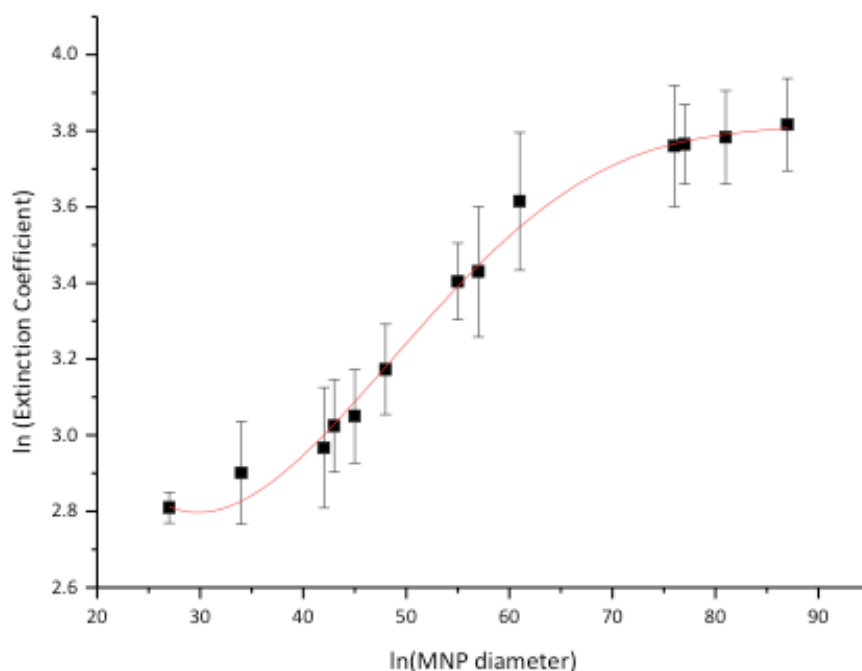
Figure 5.14: Experimental data and linear fitting curve of natural logarithm of extinction coefficient and logarithm of nanoparticle average diameter.

Figure 5.14 shows the double logarithmic plot of extinction coefficient and mean nanoparticle size, with the expression taken from equation (6), where ε is the extinction coefficient, D is the mean diameter of the metal nanoparticle and a is 10.81. This result is also in accordance with Mie's theory as well as the study. [435] The linear fitting of these experimental data was 0.995 and had a standard deviation of 0.0621.

$$\ln \varepsilon = k \ln D + a \qquad (6)$$

Link *et al.* obtained experimental values for *k* and *a* of 2.75 and 11.7 respectively from their experimental studies and 3.36 and 8.1 for theoretical values. The values obtained in this work show discrepancies, which could largely be owing to the difference in the average size and size dispersity of the metal nanoparticles and the protecting agent used in this study. [436] The result for the double logarithm of extinction coefficient versus metal nanoparticle size can be extended to most of the period four metals presented herein. The metal nanoparticles are presented within the same solvent, in this case water, and therefore are stabilised by the same dielectric constant (water = 78.4). The PVP protection or capping effect relies on electrostatic interactions between the ligand effect that is established between the metal nanoparticle and the protecting agent, and has created a stabilised network. Mie's theory indicates that SPR absorption of a nanoparticle is related to the dielectric constant and the media within which it

is contained (i.e. the solvent and protecting agent). In this study this has remained constant throughout each metal nanoparticle solution and has therefore not made significant contributions to the extinction coefficient of the SPR band. [437]

These results can therefore be used to calculate the nanoparticle concentration or average diameter of the nanoparticle solution. Thus, by determining the average size using a microscopic technique (i.e. TEM or FESEM), determination of the extinction coefficient can be extracted. Applying the use of UV-vis absorption spectra, the concentration of the sample can therefore be calculated.

5.5.2 NANOPARTICLE CONCENTRATION

The aim of this section of work deals with calculating concentrations of nanoparticles the sol-gels used in Section 5.3.1.1 *vide supra,* with more nanoparticles and thus investigating the overall effect of this feature. Here nanoparticles were synthesised in larger concentrations and then doped within the same sol-gel matrix as given in the experimental Chapter 2, *vide supra.*

5.5.2.1 CONCENTRATION OF NANOPARTICLES

As shown in Section 5.4.1 *vide supra*, the nanoparticle concentrations were calculated via UV-vis using the extinction coefficients and then plotting a double logarithm versus the average nanoparticle size. The results are shown in Table 5.2.

Table 5.2: Nanoparticle concentrations for each synthesised metal nanoparticle showing data of extinction coefficients and nanoparticle diameter, with re-ordered nanoparticle size showing extinction coefficient increases.

MNP Sample	Weak Solutions		Concentrated Solutions	
	Nanoparticle size, d (nm)	ε (Mcm^{-1})	Nanoparticle size, d (nm)	ε (Mcm^{-1})
Sc	27	3.0874×10^7	42	3.891×10^9
Ti	55	4.8116×10^{10}	57	5.0134×10^{10}
V	43	4.9012×10^9	51	4.992×10^9
Cr	57	4.7036×10^{10}	59	4.783×10^{10}
Mn	61	3.2244×10^{11}	71	4.342×10^{11}
Fe	34	3.6280×10^9	36	3.721×10^9
Co	76	6.4527×10^{11}	78	6.6654×10^{11}
Ni	45	3.9762×10^9	51	4.221×10^9
Cu	87	7.9412×10^{11}	91	8.016×10^{11}
Zn	81	7.3182×10^{11}	84	6.851×10^{11}
Ga	77	6.4527×10^{11}	79	5.865×10^{11}
Ge	42	4.0511×10^9	46	4.0123×10^9
Se	48	3.7064×10^9	50	3.923×10^9

Sc	27	3.0874×10^{7}	42	3.891×10^{9}
Fe	34	3.6280×10^{9}	36	3.721×10^{9}
Ge	42	4.0511×10^{9}	46	4.0123×10^{9}
V	43	4.9012×10^{9}	51	4.992×10^{9}
Ni	45	3.9762×10^{9}	51	4.221×10^{9}
Se	48	3.7064×10^{9}	50	3.923×10^{9}
Ti	55	4.8116×10^{10}	57	5.0134×10^{10}
Cr	57	4.7036×10^{10}	59	4.783×10^{10}
Mn	61	3.2244×10^{11}	71	4.342×10^{11}
Co	76	6.4527×10^{11}	78	6.6654×10^{11}
Ga	77	6.4527×10^{11}	79	5.865×10^{11}
Zn	81	7.3182×10^{11}	84	6.851×10^{11}
Cu	87	7.9412×10^{11}	91	8.016×10^{11}

The nanoparticles that were synthesised in large batches as depicted Section 2.2, *vide supra* were then taken and doped directly into the sol-gel matrix. A contrast in nanoparticle concentration can be seen in each of the spectra presented in Figure 5.15, here the nanoparticle doped sol-gels for the both the concentrated and normal doped solutions were run on UV-vis in order to confirm any concentration differences. A baseline correction was performed in order to remove the interference from the sol-gel solution thus giving the overall absorptions of each of the nanoparticles contained within the solutions. The data demonstrates clear absorption concentration shifts throughout all of the MNP-doped sol-gels, confirming overall that the nanoparticles were in greater concentrations seen.

MNP	Sc	Ti	V	Cr	Mn	Fe	Co	Ni	Cu	Zn	Ga	Ge	Se
Size (nm)	290	380	677	585	770	296	497	736	511	673	670	362	309
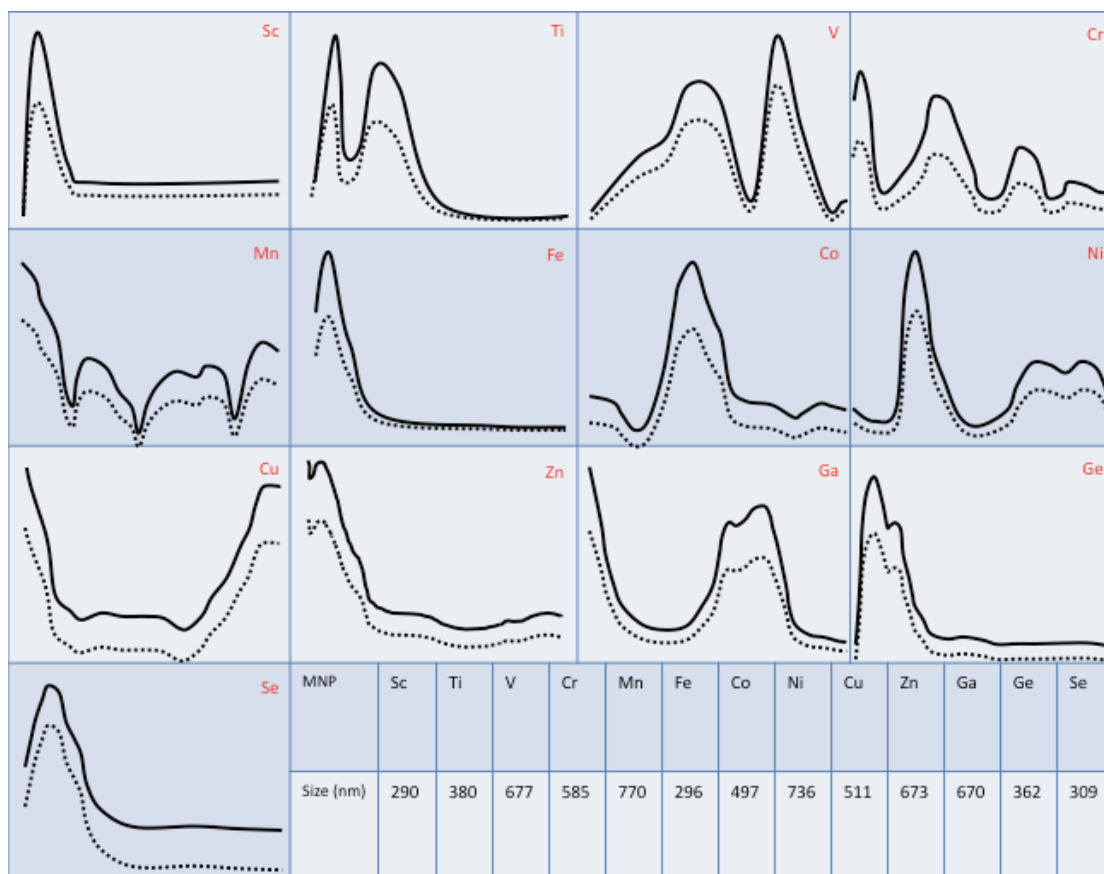
Figure 5.15: UV-vis spectra of concentrated nanoparticle solutions compared with initial concentration of nanoparticles depicted, x axis = 150 – 850 nm. The dotted line represents the un-concentrated samples whereas the solid line shows the concentrated nanoparticle samples.

The concentrated nanoparticle doped sol-gels underwent the same characterisations described in Section 5.3.1 *vide supra* and were then subjected to the biofouling screening assays.

5.5.3 CHARACTERISATION

In this section of work, characterisations of the concentrated metal nanoparticle sol-gel were performed, with further analysis being introduced using spectrophotometry in order to gain a solution concentration of the metal nanoparticles across period four.

5.5.3.1 SURFACE MORPHOLOGY

Surface morphology of the sol-gel has been characterised in Figure 5.16. The sol-gel remained porous; Figure 5.16 (a) and a small section of nanoparticles were resolved showing high concentrations of nanoparticles within the sample spot, Figure 5.16 (b).
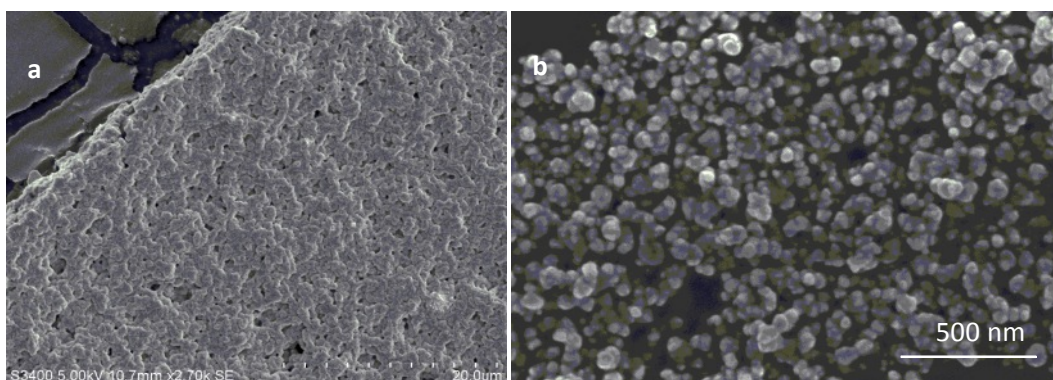
Figure 5.16: Electron micrographs showing concentrated nanoparticle doped sol-gel (a) morphology and (b) concentrated titanium MNP sol-gel.

Nanoparticle doped sol-gels have been characterised in this work using SEM which is well established as a technique for characterisation, with many other authors using the technique, to name but a few. [438,439] The sol-gel used remained constant for each of the metal nanoparticles that had been synthesised, thus maintaining sample reproducibility for each sol-gel. This principally analysed the nanoparticle effect as opposed to the effect of the sol-gel (if any effect at all). Once the MNP doped sol-gels had been spin coated on to the glass substrates and the same contact angle measurements were performed on each of the surfaces, as shown *vide infra 5.4.3.2.*

5.5.3.2 CONTACT ANGLE

A series of contact angle measurements were performed on each of the concentrated metal nanoparticle doped sol-gels. Each nanoparticle sol-gel had a sessile drop of water measured on the surface of the material. Figure 5.17, demonstrates a comparative graph of the concentrated sol-gels with the sol-gel contact angles presented in Figure 5.3, *vide supra*.
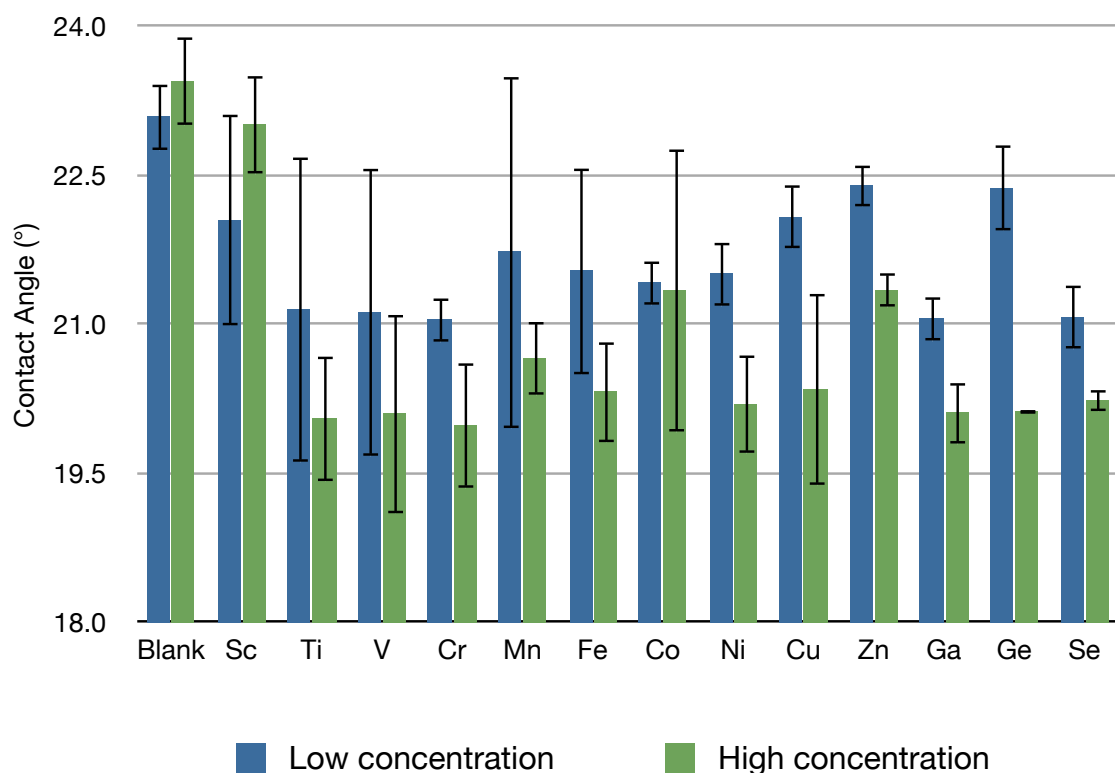
Figure 5.17: Line graph comparing the weakly and concentrated MNP-doped sol-gels for differences in contact angles for the (n=9 ±1SD).

The results shown above in Figure 5.17 show that there are some differences in contact angles across the concentrated and weakly doped MNP-sol-gels. The concentrated sol-gels show a small shift in overall angle reduced by roughly 2% when compared to the weakly doped sol-gels. This indicates that the metals contained within are exhibiting some preferential wettability in higher concentrations to those of the lesser concentrated sol-gels.

The metals are therefore causing some interaction with the solvent being applied, in this case water. It has been noted in an excellent review by Pask *et al.*, that glass mesoporous structures with metal included within the matrix causes the wettability to increase exhibiting lower contact angles. [440] This effect has been noted in both sets of contact angles results, whereby the sol-gel blank has a marginally higher contact angle value when compared to the MNP-doped ones. The larger concentration MNP-doped sol-gels have increased wettability when compared to the lower concentrated sol-gels. There are of course other considerations that would impose on some of these effects such as gravity, particle solid, particle-fluid and particle-particle interactions. The effect of gravity is expected to be negligible as temperatures and pressures remained the same throughout the measurements, as stated in Vafaei *et al.,* [156] thus achieving the reproducibility observed. In other literature, it has been reported that the protecting agent, in this case PVP, polarises in the water solution interface and causes long-

range electrostatic interactions between the MNPs and the capillary property of water. Meanwhile Shibuta *et al.,* have addressed wetting of metals using a molecular dynamic situation. They found that higher concentrations of metal atoms in the phase resulted in increased wettability, [441] which has also been observed in this study.

Although the contact angle is reduced, the effect of the nanoparticle concentrations in the sol-gel matrix has not greatly changed this function of wettability. Generally, throughout literature it is generally accepted that a superhydrophilic or superhydrophobic contact angle will influence the activity and morphological growth but also changes to cells. [406] It has therefore been established from this section of work that the nanoparticle contributes to the surface activity as an antifoulant.

5.5.4 BIOFOULING ASSESSMENT

The sol-gels with the larger metal nanoparticle concentrations were taken through the same series of screening techniques as seen *vide supra* 5.4.2. Presented within this body of results are mass, slime, protein and carbohydrate analyses.

5.5.4.1 MASS ANALYSIS

In this section, mass change was measured on the test surfaces. This was performed in the same manner as the results shown in the previous sol-gel section after a 7-day laboratory tank test.

The data presented in Figure 5.18 show that the mass adsorption from the effects of fouling in the laboratory tank test has been less excessive in the MNP-doped sol-gels. The sol-gel blank has shown clearly that more mass has again attached to this sample type. Also the results have mirrored some of the results obtained in Section 5.3.2.1 *vide supra* where the MNP-doped sol-gels have shown least mass accumulation on the test surface when compared to those that were undoped.
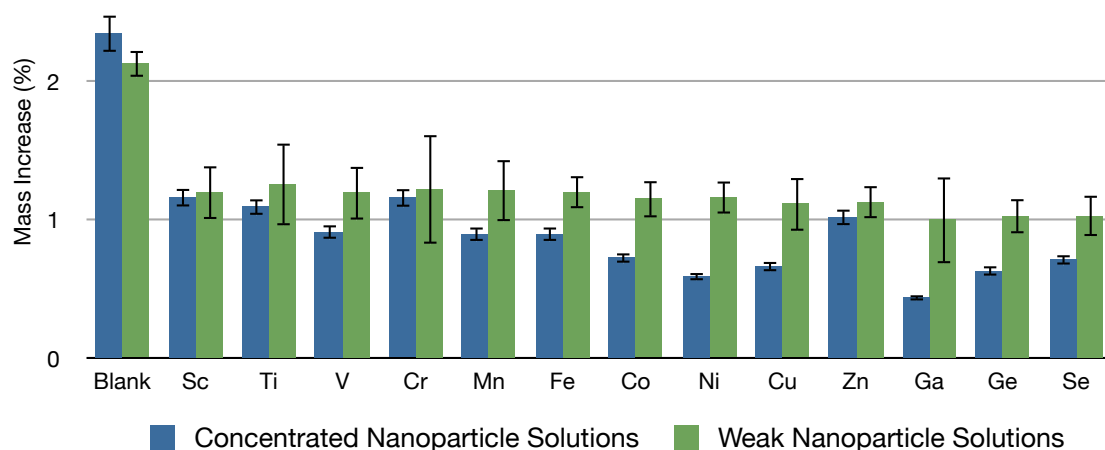
Figure 5.18: Comparative 3D Bar chart outlining the differences between mass adsorption of the original MNP-doped sol-gels and the concentrated MNP-doped sol-gels (n=9).

Here, the data have been compiled to show the effects of both the nanoparticle solutions compared to each other. The data demonstrates that the concentrated MNP-doped sol-gels have given improved responses to mass compared to the initial small doping of less concentrated MNPs in the initial experiments described. This demonstrates that the MNPs have an improved effect in higher concentrations. In some MNPs (i.e. Ga, Ni, Ge and Se), evidence of even greater effects have been seen, whereby mass aversion has been shown to be greater than 50% in the Ga results. The mass result is an initial screening method for the determination of a small element of biofouling and so other methods have been implemented to probe more thoroughly.

5.5.4.2 GLYCOCALYX (SLIME) TEST

As performed *vide supra* 5.3.2.2 the slime test measures a small aspect of the biofilm that has adsorbed on the surface of the test substrates, Figure 5.19.
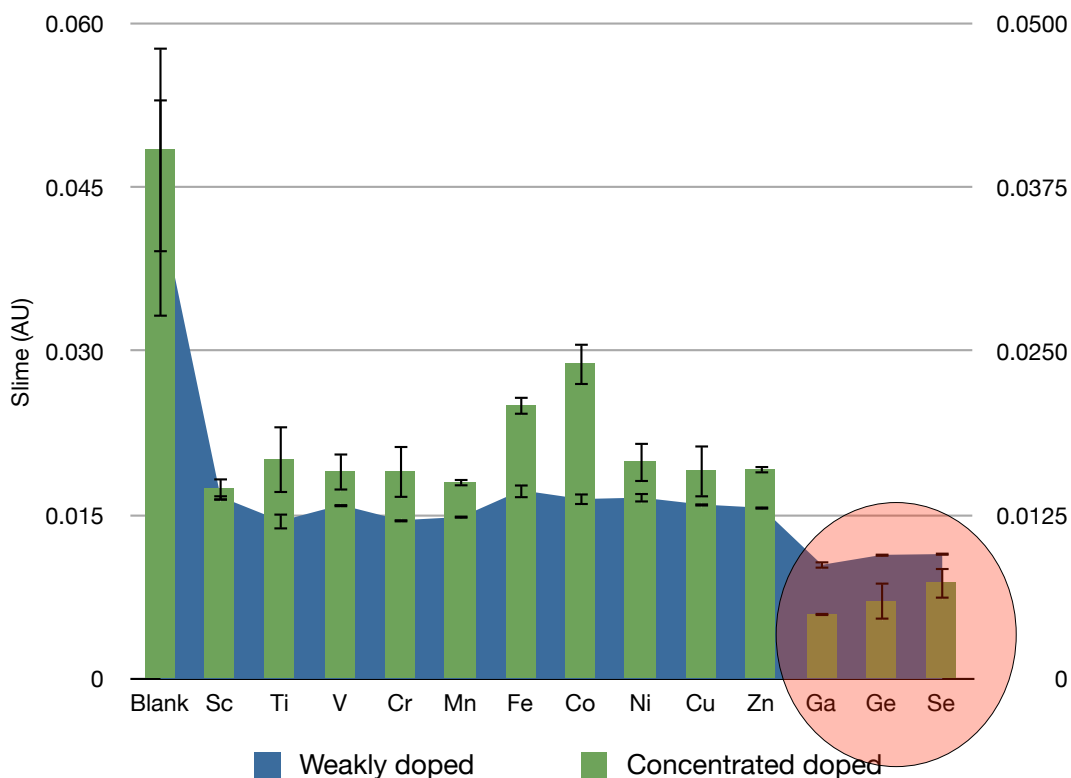
Figure 5.19: Chart showing slime test result for concentrated metal nanoparticle doped sol-gels (n=5 ±1SD) with red circle highlighting area of interest for Ga, Ge and Se metal nanoparticles.

The absorbance measurements for Ga, Ge and Se (0.00494, 0.00595 and 0.00793 AU) respectively have adsorbed less slime upon their surfaces. The level of slime measured for each of the MNP-doped sol-gels has shown significantly less adsorption when compared to the sol-gel blank (0.0437 AU). Gallium demonstrates an order of magnitude less than the sol-gel blank value and has shown least slime on its surface in this assay. This environmental measurement of slime is seldom reported in the literature as it was only optimised for pure culture study, particularly in the field of *E. coli.* [199] A method for the use of this staining technique was optimised and modified to suit the environmental field, published in the following work. [135,138]

Comparing the data of the weakly and concentrated metal nanoparticle sol-gels for the slime assays, some differences and similarities are observed for the period four metals. In some cases, slime elevated on the concentrated metal nanoparticles, which was not predictable –

working with a theory that as you increase biocide, the toxicity indeed increases. Iron and cobalt have both shown that this is not the case, and exhibit higher levels of slime adsorption upon the surfaces. Iron proves to be interesting, as it is already known that it is required for use in respiration of some cellular organisms. For example, Schwegmann *et al.,* [442] Fe-NPs were found to improve survival rates of bacteria in higher concentrations, and perhaps this is why slime has increased upon the surfaces of Fe-MNP doped sol-gels in this work, where microorganisms have produced more slime, especially when compared to the weakly concentrated Fe-MNP doped sol-gel. The concentrated Co-MNP doped sol-gels have also shown anomalous results when compared to the weakly concentrated MNPs. A difference in absorbance value of (0.014 AU) between the two data series was witnessed, which is significant. Literature suggests that cobalt is toxic to microorganisms in higher concentrations, something that is not reflected in this work. [443] The work by Gault *et al*. showed that Cobalt in its Co^{2+} state was extremely potent in cell viability experiments for some bacteria. In the same manner, Co (II) has been identified as a trace element required for microorganism growth, but in higher concentrations growth is inhibited as presented in Mergeay *et al..* [444] In a paper published by Mishra *et al.,* a series of toxic effects were seen with Co(III) across resistant strains of bacteria, but in elevated concentrations growth returned to normal levels, which could be a source of reason why slime has been elevated in the concentrated sol-gels presented herein. [445]

5.5.4.3 PROTEIN AND CARBOHYDRATE ADSORPTION ASSAY

Protein and carbohydrate adsorption measurements were taken in triplicate across each of the nanoparticle doped sol-gels, (both of normal and concentrated substrates) giving an indication of the level of fouling attributed to biochemical activity upon each of the test substrates. This was a 7 d freshwater tank study and measurements were taken immediately the 7 d exposure had lapsed.

5.5.4.3.1 PROTEIN ADSORPTION MEASUREMENTS

The results displayed in Figure 5.20 show the levels of protein that had adsorbed on each of the metal nanoparticle doped sol-gels, both in the concentrated and lightly concentrated sol-gel matrices.
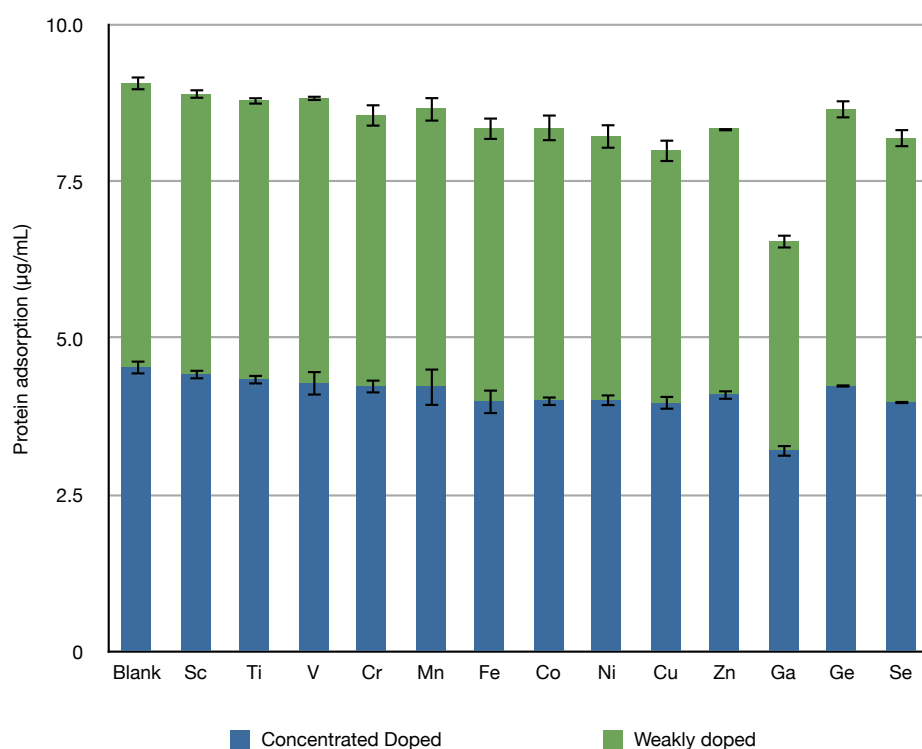
Figure 5.20: Protein adsorption measurements for both weak and concentrated doped sol-gels.

The gallium doped sol-gel matrix has the least protein adsorption to its surface of both MNP doped concentration sol-gel types, also highlighting that that the concentrated matrix demonstrates evidence of better efficacy in preventing protein adsorption in this result. Furthermore, across the metals used, the concentrated metal nanoparticle doped sol gels have all shown evidence of higher potency and thus lower protein adsorption within the group.

5.5.4.3.2 CARBOHYDRATE ADSORPTION MEASUREMENTS

The results displayed in Figure 5.21 shows the level of total carbohydrates that had been adsorbed to the nanoparticle doped sol-gels of both the concentrated and lower concentrated nanoparticle sol-gels.
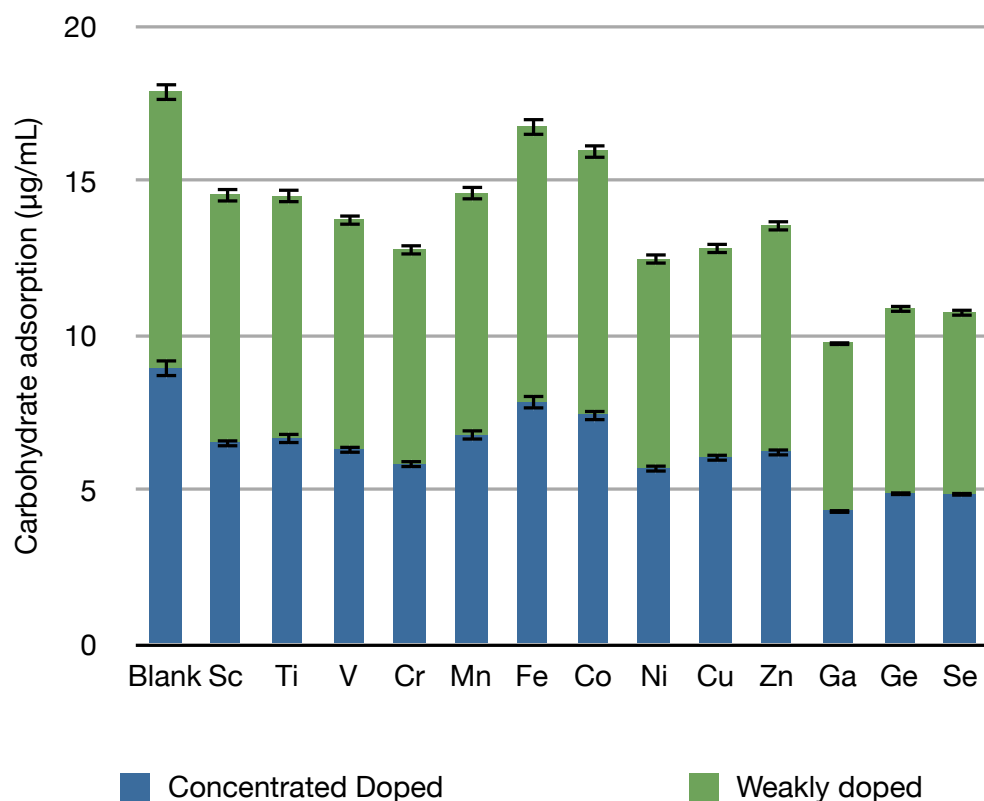
Figure 5.21: Total carbohydrate adsorption of nanoparticle doped sol-gels for concentrated and un-concentrated sol-gels.

Similar to Figure 5.20, carbohydrate adsorption has followed the same trend, where concentrated nanoparticle doped sol gels has shown least carbohydrate levels, with gallium out-performing any of the others.

5.6 GALLIUM VS. SILVER

This section of the thesis deals with a head-to-head examination of the intrinsic action of gallium in microorganisms and has been compared to the market leading metal, silver.

5.6.1 SILVER

Currently, the market leading metal nanoparticle is driven through silver nanotechnology. For instance, silver has been used for centuries to prevent and treat a variety of diseases, and through Davies and Etris it has been suggested that silver may be linked to man's earliest attempt to improve his environment. [122] Only now has it become known that silver has a positive influence towards the reduction of microbial activity. The mechanisms of which are still not fully understood, but postulations can be summarised in the following manner:

- Destruction of the organism by oxidation catalysed by silver;

- Disruption of the electron transfer in bacteria through the monovalent silver species, and preventing the unravelling of DNA in viruses through the substitution of hydrogen ions in the monovalent form;

- Destruction of bacteria and viruses through the bivalent and trivalent silver ion form;

- Destruction of algae and protozoa.

Silver holds unique properties over all the other metals, especially when introduced with oxygen. Oxygen in the air is adsorbed on to the surface of silver as atomic oxygen, and because atomic oxygen fits into the octahedral holes of silver,[446] oxygen accumulates within the bulk of silver. This stored octahedral oxygen significantly contributes to the catalytic activity and thus oxidative power of silver. It was not until 1986 that a filed patent in the USA covered the catalytic activity of silver in an aqueous media for sanitation of water. [74]

5.6.1.1 THE HISTORY OF SILVER AND ITS PRESENT USES

The use of silver has long been accounted for as a health regulatory material. Since ancient times, silver vessels have been used in Mexico (the world's largest producer of silver) to keep water and milk "sweet". Following this, Pliny the Elder, reported in is his book XXXIII, XXXV, that silver "…has healing properties as an ingredient in plasters, being extremely effective in causing wounds to heal…". [122] World War II saw a backward step in the use of silver as it was discovered that silver plates in the skull caused a toxic reaction to the blood-brain barrier.[446]

5.6.1.2 MONOVALENT SILVER

Silver in its monovalent state has a high affinity for sulfydryl group exposed to bacteria or viruses. This has been seen to inhibit hydrogen transfer in energy transfer systems. The medicinal value of silver has long been recognised where silver nitrate was mentioned in a Roman pharmacopoeia in 69 B.C. Silver nitrate, however, is corrosive to tissue and draws chloride ions out of the body's fluids. Thus, less corrosive silver compounds need to be discovered for medical value. Silver thiosulfate coated in silica gel microspheres were developed by Oka *et al..* [447] Here the authors incorporated silver in a silica gel, which in turn slowly releases silver over a long term without being immediately precipitated by any nearby chloride species and thus provides long lasting bactericidal action.

5.6.1.3 SILVER ORGANICS

The combination of silver with antibiotic compounds has already been explored. [448][449] Here, topical silver salts of sulfadiazine proved to be efficacious in reducing the development of early wound sepsis, showing that the combination was at least 50 times more active than sulfadiazine alone. Consequently, this has now become the treatment of choice for burn and wound therapy, allowing the wound to heal unhindered from bacteria.

Silver sulfadiazine is active against both gram positive and gram-negative organisms such as fungi, protozoa, and even viruses. It has also been shown to inhibit colony forming units of *Staphylococcus, Streptococcus, Pseudomonas* etc. [449] This should be used with some caution, as some bacteria are now developing resistance to silver compounds[301] thus new viable target biocides would prove to be beneficial.

5.6.1.4 EFFECTS OF NANO SILVER

Silver nanoparticles containing 20-15,000 silver atoms is generally smaller than 100 nm. [450] At the nanoscale, silver presents the most promising unusual physical, chemical and biological properties. However, as to the origin of these properties, seldom has clarification been related to the crystal structure of silver. Nanoparticles of silver are whole clusters of atoms and was summarised to be multiply twinned in papers by Ino and Ogawa. [451,452] Basically, the rationale suggested states that as a structure becomes smaller, the net gain in surface energy outweighs the strain energy cost and the total surface energy is lower than simple single structures owing to more low energy faces at expense of an internal strain. [453] For instance with silver (a face centred cubic, FCC metal), more {111} facets with the lowest surface energy of 1.172 Jm^{-2} for

the low index facets, [454] are preferential in surface planes when the size of the nanoparticle is decreased. However, the close packed {111} planes of the FCC crystal structure are of the highest atomic density within the unit cell. [455] Therefore silver nanoparticles may provide more active sites (silver atoms) that will facilitate broad-spectrum activity.

5.6.2 GALLIUM

Gallium is a semi-metallic element in group four of the periodic table and has shown efficacy in the treatment of various medical disorders. Gallium is already known to be effective in supressing bone resorption, hypercalcemia, [456] Paget's disease, [457] multiple myeloma, [456,458] bone metastases, and also in treating osteoporosis. [459] In addition, there is mounting evidence that gallium is effective at inhibiting T cell and macrophage activation, [460] activity against some cancers, [461] and some microorganisms, [462] the latter of which is of interest to this thesis.

Studies have already found that intra venous delivery of gallium tartrate was effective in treating syphilis in rabbits. [463] In a similar study gallium tartrate at 250 mg/kg eliminated *Trypanosoma evansi* parasites from infected mice. [462] Gallium nitrate has also been shown to be effective against drug resistant microorganisms and was used as an additive in other antimicrobial matrices. Yan *et al.* have shown that gallium could be effective in treatment of malarial parasites when used in tandem with organometallic compounds. [464]

Very little information exists for the exact mechanism for gallium's antimicrobial activity for microorganisms illustrating the need for research in this area, with some postulations made of the ability of gallium to enter through a microorganism's electron transport chain.

Results obtained already in this thesis have resulted in the drive to probe the efficacy of gallium as a potential candidate in the replacement of silver in the current market where silver currently is double in price compared to gallium (Ga = €43.8/100 g and Ag = €112/100 g; obtained on August 2011). This will be seen in the following results displayed in Section 5.6.3.

5.7 MIC RESULTS GA VS. AG

Presented in this section are the results of a series of nanoparticle-based experiments comparing gallium and silver nanoparticles in an MIC based experiment. The separate metals were inoculated into agar plates containing *E. coli* at varied concentrations.

5.7.1 SILVER ON *E. COLI*

Figure 5.22 reveals the plate results obtained for silver nanoparticles in concentrations of 0, 10, 50 and 100 µg/mL.
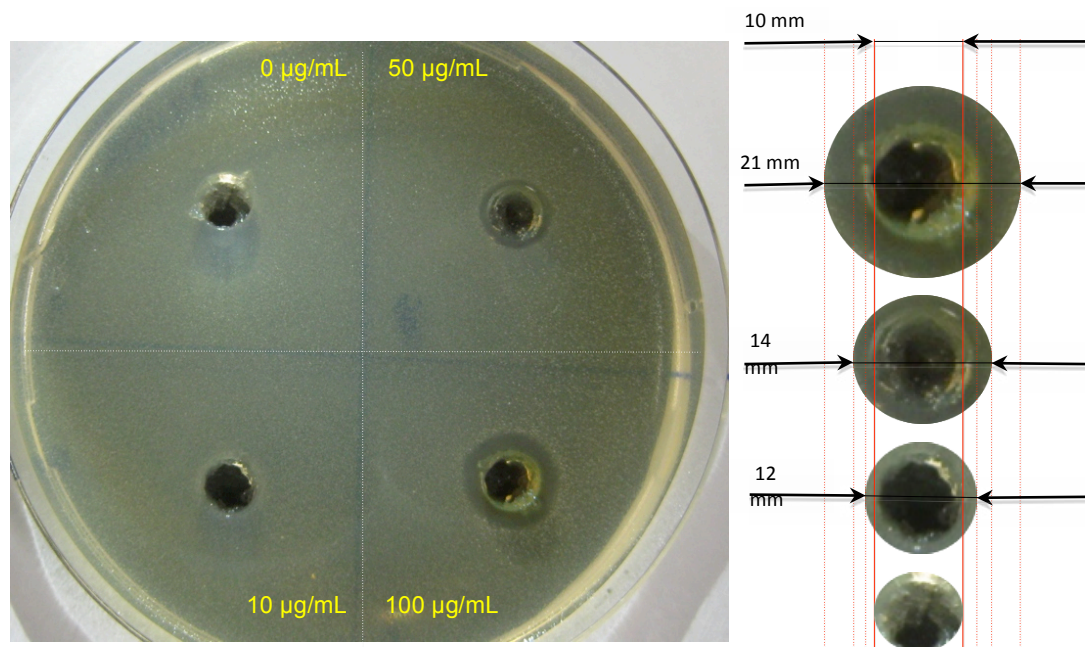
Figure 5.22: (L) Total MIC plate indicating the nanoparticle diffusion through the agar plate for silver nanoparticles tested against E. coli, which were then optimised to show the minimum amount required for toxicity. (R) indicates the level of inhibition per sample, top 100% to bottom 0%.

The synthesised silver nanoparticles showed effective antibacterial activity against the test organisms. MIC was recorded as the lowest concentration at which no visible growth of the organism was observed where 10 µg/mL afforded the minimum inhibitory concentration for *E. coli*. Many studies have demonstrated the antimicrobial activity of aqueous silver nanoparticles. Cho *et al.,* showed the antimicrobial activity of silver prepared using the same stabilising agent (PVP) and also found that the minimum inhibitory concentration against Gram negative bacteria (*E. coli*) and found the MIC value to be 10 µg/mL. [465]

5.7.2 GALLIUM ON *E. COLI*

Figure 5.23 shows the same experiment conducted for gallium following the same concentration range as given in silver.
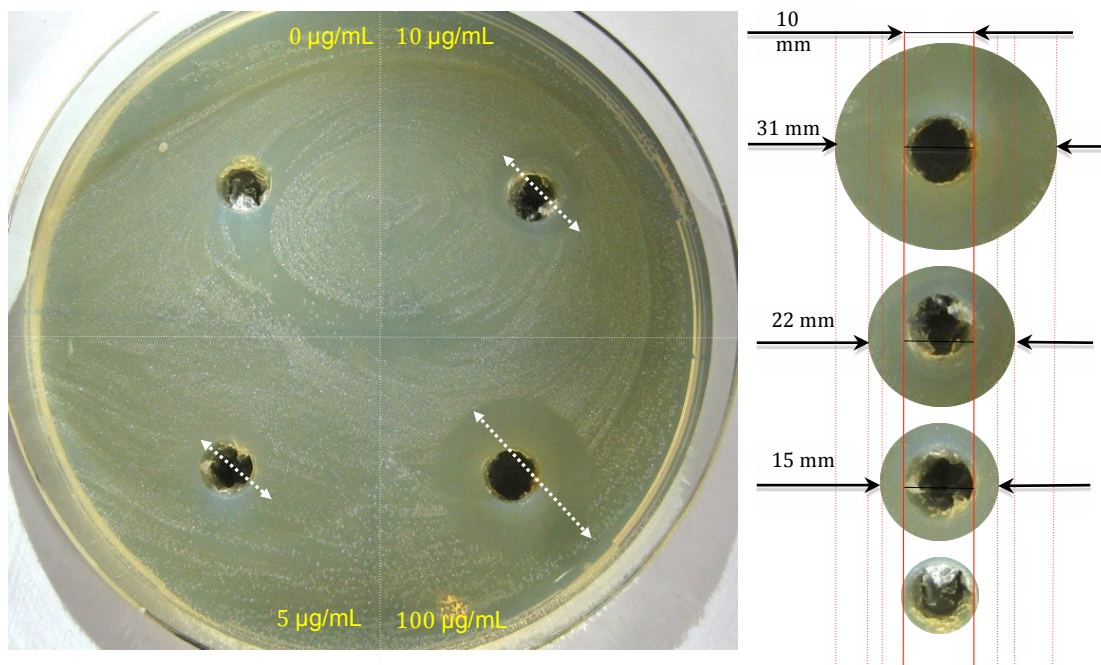
Figure 5.23: (L) Total MIC plate indicating the nanoparticle diffusion through the agar plate for gallium nanoparticles tested against *E. coli* which were then optimised to show the minimum amount required for toxicity (R) indicates the level of inhibition per sample, top 0 µg/mL to bottom 100 µg/mL.

As previously demonstrated, the results show toxicity towards the bacteria used. The effects of gallium have increased toxicity in each concentration when compared to silver in Figure 5.22 indicating that the antimicrobial activity of gallium is far higher than silver. The synthesised gallium nanoparticles, showed MIC of 5 µg/mL and a high toxicity at 100 µg/mL as demonstrated in Figure 5.23. In comparison to silver, gallium is somewhat twice as effective as silver in this assay. Gallium has certain unique properties that silver does not, and has been presented as being efficacious as an alternative antimicrobial agent to silver.

Gallium is thought to interrupt the iron transport system in microorganisms. [463] If this is true, then Fe is dependent in the function of a cells ability to metabolise, produce proteins and enable the smooth function of DNA replication. Research has shown that large amounts of iron are often responsible for pathogenic cells to grow[466] and multiply.[467]

If gallium is thought to be iron mimicking then, iron is also required to be investigated as a source for normal cellular activity. In Figure 5.24, iron nanoparticles were inoculated in the

same manner as gallium and silver . The results show that for every concentration of iron, the bacteria have grown normally, indicating that iron is indeed a precursor for normal cellular activity.
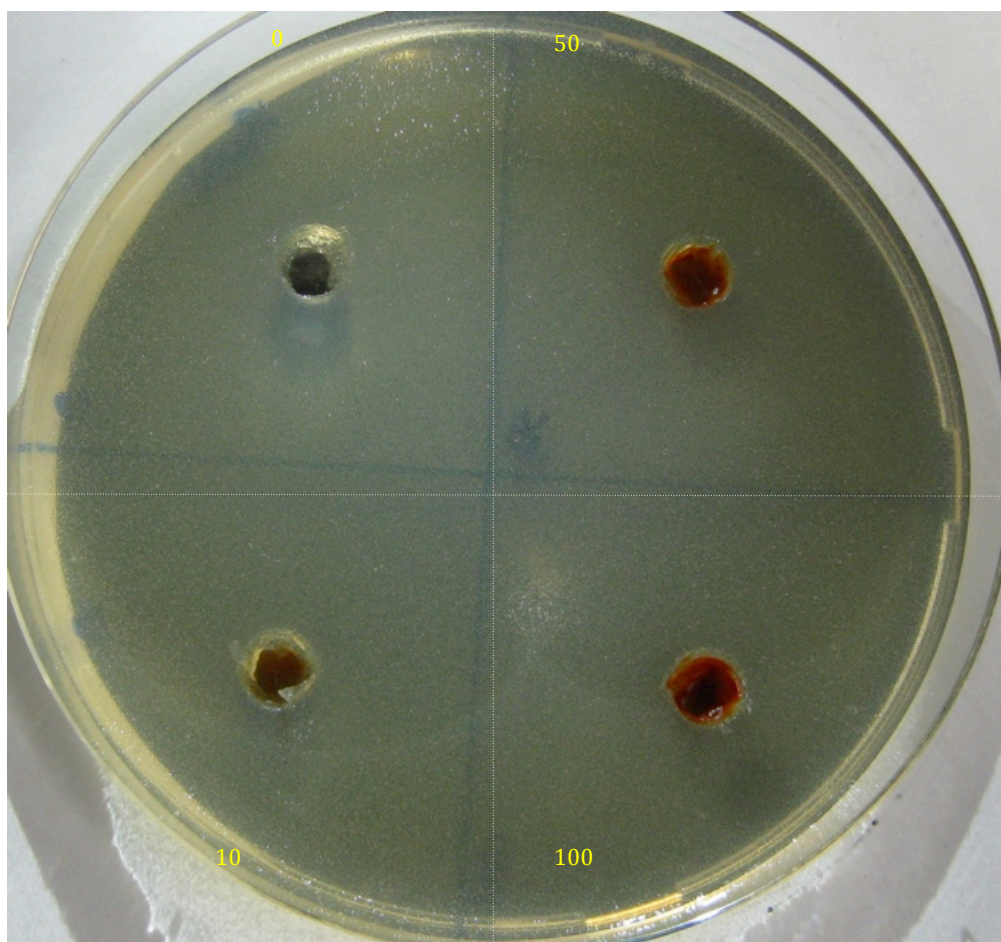
Figure 5.24: Total MIC plate indicating the nanoparticle diffusion through the agar plate for iron nanoparticles tested against *E. coli*.

Within this work, we have shown that gallium plays an important role in toxicity and cell function of a Gram-negative bacteria, *E. coli*. It has been known for some time that gallium resembles iron in certain respects. [468]

In order to understand the biochemistry as to a feature of why gallium has the capability of mimicking iron in cellular activity a summary has been presented in Table 5.3.

Table 5.3: Chemical comparisons of Ga and Fe.

Parameter	Unit	Ga^{3+}	Fe^{3+}
Ionic radius (octahedral)	Å	0.620	0.645
Ionic radius (tetrahedral)	Å	0.47	0.49
Ionisation potential (4th ionization potential)	eV	64	54.8
Electron affinity (3rd ionization potential)	eV	30.71	30.65
Absolute hardness (Pearson)	eV	17	12.08
Electronegativity (Pauling)	Pauling Units	1.81	1.83
Metal-oxygen bond dissociation energy	KJ/mol	353.5	390.4
Tendency to ionic bonding (H_A)	none	7.69	7.22

The coordination chemistry of gallium (Ga^{3+}) is very similar to that of Fe^{3+} as given in Table 5.3. As discussed *vide supra*, the biochemical similarities are associated between the two ions, in particular, protein and chelate binding – which are responsible for many of gallium's unique physiological activities. The high degree of similarity in chemical behaviour of Ga^{3+} and Fe^{3+} can be attributed largely to the values for ionic radii and measurements of ionic versus covalent bonding. In addition to the similarities it is important to show the differences, as this will give a potential reason in why gallium inhibits cellular activity once taken within a cell, these differences are:

1) Gallium is virtually irreducible under physiological conditions, whereas iron can be readily reduced, for example Fe^{3+} can be readily reduced to Fe^{2+} (and the re-oxidised). This property renders Ga in preventing it from entering the Fe^{2+} binding molecules such as heme and therefore prevents it in participating in any redox reactions; [469]

2) Iron is essentially unable to exist in aqueous solutions of pH systems close to neutral, resulting in the precipitation of Fe^{3+} to FeO(OH) limiting the Fe^{3+} and therefore narrowing the solubility to 10^{18} M. [470]

On the basis of the results obtained, gallium clearly mimics iron in this bacterial system showing that gallium has in fact caused inhibition in the gallium study and normal growth in the iron system. This potentially offers knowledge in defining the intrinsic value of gallium in the electron transport system.

5.8 CONCLUSIONS

The development of a nanoparticle-doped sol-gel has been demonstrated in this chapter as a highly successful material in the prevention and proliferation of biofouling. The results shown in this chapter have shown excellent potential as a future material in the prevention of biofouling especially in its initial stages.

The biofilm development in the form of mass, slime and biochemical adsorption assays have been successfully utilised in investigating the efficacy of the nanoparticle doped materials. Across the period, some metals have shown improved responses when compared to each other in the inhibition of biofilm development.

It was also seen that as nanoparticle concentration increased, wettability was affected in some of the materials, that wettability was not a contributing factor in the inhibition of biofouling on the test surfaces.

The most successful metal nanoparticle has been observed in gallium. The results for gallium are highly interesting and novel where, for the first time, the use of gallium metal nanoparticles have been used as agents for use in an antifouling capacity. Subsequently, further testing of such ground as an antimicrobial material (and toxic agent for use in antifouling materials) has been demonstrated in a series of MIC assays. Here it was observed that gallium nanoparticles were effective in preventing growth of *E. coli* and showed improved response to this species of microorganism when compared to the market leader, silver.

This level of research is of high novelty to the field of biofouling and represents a potential new route in targeting fouling organisms for application in antifouling materials. The intrinsic property of gallium acting as a "stealth" biocide which has the capability of moving through the cell wall unnoticed, where uptake is harmonious inside a cell, shows considerable impact for research in this area. Consequently, this would benefit from further research in a more appropriate discipline.

6

Theory into

practice

*Part of this chapter has been published in Chapman J. and Regan F. **Advanced biomaterials**, 2011

6.0 INTRODUCTION

This chapter focuses on the biofouling problem when presented in a natural and real environment. The aim is to detail the problems that are currently experienced in the sensing field and the subsequent need for antifouling measures owing to the fouling problem reducing data precision when deployed for extended periods of time.

6.1 OVERVIEW TO MONITORING

Typically, water quality can be assessed through monitoring parameters such as pH, conductivity, dissolved oxygen (DO), temperature, turbidity, along with nitrate and phosphate concentrations. Sensors are available for these purposes and consequently differences in construction means that many antifouling measures need to be employed to ensure that sensor performance is not compromised by the stages of biofouling and biofilm development. One traditional approach to the measurement of pH is the use of a proton selective glass membrane electrode. The core material of this sensor is glass, which has been constructed in an ultra-thin manner. Biofilm formation on glass electrodes subsequently impedes the readings delivered from the instrument. Similarly, dissolved oxygen is measured using a complete electrochemical cell consisting of a cathode, anode, electrolyte and gas-permeable membrane. [471] The major limiting factor of these types of sensor is in the design of the membrane that becomes readily fouled.

Turbidity and chlorophyll sensors attract fouling in a different manner. They require the use of an optical window within the sensor. Therefore an optical transparent platform is required in the coating of such devices so as not to inhibit the path of light. Usually, brush and wiper systems are employed in this application that remove the biological and fouled material from the sensor window site.

Indeed, while sensor surfaces require protection from biofouling, it is equally imperative to prevent the sensor housing from biofilm development. This is due to fouling upon this area creating an artificial environment around the housed sensors, and thus any measurements are not representative of the sample location. Sensor housings are often composed of a range of different materials from plastics to metals. Therefore a plethora of antifouling methods may need to be used in tandem to counteract this.

6.2 ENVIRONMENTAL MONITORING

Environmental monitoring is a significant driver for Wireless Sensor Network (WSN) research, promising dynamic, real-time data about monitored variables, enabling researchers to measure properties that have not previously been observable owing to their inaccessibility at appropriate spatial and temporal scales. [472,473]

A sensor network (SN) is comprised of a number of sensor nodes, designed to transmit data from an array of sensors to a data repository on a server. [472,474] Depending upon the required application, each sensor node is deployed in, or close to the object of interest and can be equipped with different types of sensors, allowing long-term, wide area, *in situ* multi-parameter monitoring. [474,475] At present, there are many challenges in the development of continuous long-term water-monitoring programmes in Europe. The success of a monitoring system that can provide real time data on a variety of water quality parameters over long periods of time will rely on the support of teams of researchers in the development of the building blocks of such systems. One of these obstacles is biofouling, which as previously mentioned, causes adverse effects to the sensor systems deployed in marine or fresh water matrices, and will be a focus in this chapter.

6.2.1 CURRENT STRATEGIES

One of the simplest methods in the treatment of fouling is through mechanical means. This usually involves the use of an energetic carrier, for instance a high-pressure water jet [476], which are already prevalent on the removal of biofouling from buoys. Although, this is not a suitable technique for delicate sensor suites. Alternatively, biocidal agents such as peracids, halogens or QUATS can be incorporated within materials [477] to prevent this without mechanical means. [471]

Superhydrophobic surfaces with contact angles greater than 150° are also attractive in fundamental research and industrial applications. Some papers suggest that the mechanism for this phenomenon is related to the double roughness of nano and micro structuring but also a low surface energy. [478] A range of methods have been used in the development for their fabrication including lithographic patterning, [479] chemical vapour deposition, [480] sol-gel methods, [481] among other methods. [232,482,483] Aforementioned superhydrophobic coatings are applicable to a range of fields from oil-water separation, fluidic drag reduction, biosurfaces and antifouling applications. Within these methods a great deal of research has focussed on

materials using self-assembled monolayers (SAMs) of thiols or layer by layer self-assembly multilayers which has been reported in Zhang *et al..* [484] More recently Bell *et al.,* obtained superhydrophobic and superhydrophilic surfaces through the use of heptadecafluoro-1-decanethiol and 1-mercaptohexanol with silver and gold metal affinity sites. [203]

6.2.2 SENSOR DESIGN

Currently, there are wide ranges of field deployable water quality instruments available that have the potential to measure a range of physico-chemical and environmental parameters. Many of these do not include antifouling based systems thus introducing the fouling problem to any system exposed. An example of data drift can be seen in Figure 6.1, whereby the sensors have had to be removed from the monitored site and periodically cleaned.
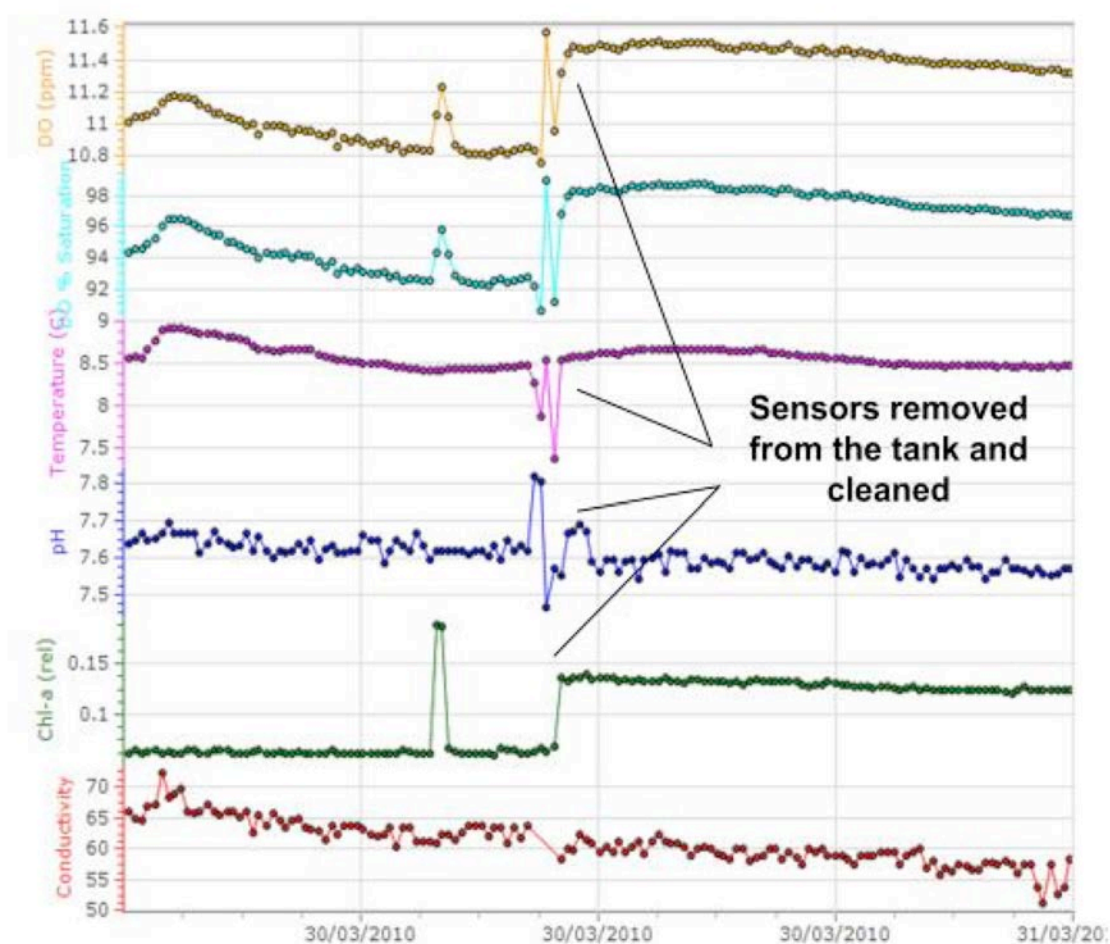
Figure 6.1: An example of data drift on a suite of sensors that had been deployed in a pump station, sensors have been removed and cleaned as shown in the figure. This data was taken from Regan *et al* – DEPLOY end of project report. [485]

What is being observed is that temperature, conductivity and pH readings are unaffected by biofouling whereas, the dissolved oxygen and chlorophyll-a readings are significantly affected. Biofouling interferes and blocks the optical paths, reducing and creating barriers to water flow through the pipes/hoses, adding weight to the instrumentation and inhibit the mechanical movement of certain sensor types thereby compromising the collected data. [486] Fouling by larger planktonic flora that becomes entangled with physical structures and instruments can inhibit the mechanical operation of pumps causing blockages in lines and proliferate as potential pressure fluctuations. [473]

Figure 6.2: Sensor coated in biofilm with evidence of geofouling deployed in a freshwater system.

Geofouling, Figure 6.2, occurs when sediment that has been suspended by tidal currents, collects on a substrate from the flow stream. This problem is predominant in estuaries, at the beds of fresh/marine sites, and during or after heavy rainfall when fresh sediment is washed into a water body. Over time these sediments attach, adhere and proliferate within heavy biofilms and this can cause further problems on any deployed sensor suite. [473] In addition further problems can incur (such as pump failure, equipment malfunction, sedimentation, electrical disruption, debris, ice or vandalism) which in turn affects the frequency of site visits. [487] When deployed unattended over an extended periods, *in-situ*, sensor readings become

unstable making drift, repeatability and accuracy of collected data critical issues for extended deployments as when intrinsic drift is combined with fouling, sensor data can quickly become imprecise. [488] Many potential antifouling solutions have been proposed including a variety of mechanical cleaning methods, applications of material types and chemical control methods as well as surface engineering concerning biomimetics. However, as biofouling can be specific to the geographical area and directly related to the hydrologic environmental conditions as well as the season, this choice of method will require empirical assessment in finding the most effective method for biofouling prevention.

Most commercially available sensors can be cleaned with water, a soft bristle and non-abrasive cloth. Heavily fouled material on sensors that resists such removal processes can often be soaked in detergent and water, but manufacturers recommend careful and specific cleaning procedures. Optical sensors are more sensitive to fouling requiring more frequent maintenance trips to ensure data integrity and quality. This forms the impetus of this chapter, whereby the already developed theory can be put into practice. Figure 6.3 shows various sensors that have been subjected to fouling and the sorts of problems encountered in such monitoring situations.

Figure 6.3: Examples of sensor fouling when introduced into an environmental system. Types of sensor include (a) turbidity, (b) pH, (c) fine filter, (d) conductivity and temperature, (e) turbidity, and (f) chlorophyll a.

6.3 AIMS AND OBJECTIVES

The aim of this chapter lies in the testing of materials developed from throughout the thesis in a real environment. The principle objective of the work is to develop a material suitable of application to a multi-facet substrate, in this case, an environmental monitoring device such as a sensor. These materials would therefore be capable of withstanding the detrimental effects of biofouling, offering a prolonged protection and thus reducing cost and maintenance in the long term. A number of objectives exist in achieving this which include:

Objective 1: To develop a series of field assays suitable of testing materials in fresh and marine water systems.

Objective 2: Take the most successful plasticized PVC and metal nanoparticles for testing in the field once these assays were developed.

Objective 3: Develop metal nanoparticles for combination material approaches as potential antifouling materials, taking lessons from nature.

Objective 4: Carry out continuous monitoring using an YSI sensor sonde to measure environmental changes in the test environment.

6.4 RESULTS

The results presented within this section of the thesis will be discussed in three succinct sections. The first is the development of a prototype-testing panel used in a freshwater system for the most successful plasticizers and metal nanoparticles doped in PVC. The second is in further improving materials as a combinatory approach, with particular emphasis on taking examples from nature. The third is a development of a second prototype for marine deployments for materials along with the combination of a continuous monitoring regime for these deployed materials.

6.4.1 FIELD DEPLOYMENT RIVER TOLKA, DUBLIN, IRELAND

Following on from the more successful results shown in previous chapters of this thesis, a more rigorous testing regime and also was representative of the true environment was required in determining the efficacy of such materials for their potential uses as an antifouling sensor material.

Consequently, a field deployment study was used to determine the antifouling potential of some of the better performing plasticizers and gallium metal nanoparticles when doped into a PVC matrix. The first prototype involved the use of a glass test panel, where the materials were coated directly – thus investigating a potential material for optical based antifouling sensor coatings.

6.4.1.1 THE GLASS PANEL

A one-month deployment study was carried out testing the best performing materials from the laboratory tanks tests, where some of the best performing materials were selected as given in Chapter 2, Section 2.5

A range of plasticizers and gallium metal nanoparticles of choice were doped into a PVC matrix and then drop coated on to the glass test panel. The materials were labelled in the order shown in Figure 6.4 and then left in the field for a 1-month study. The materials were unable to be analysed periodically and assays for testing could only be administered after the study had been completed.
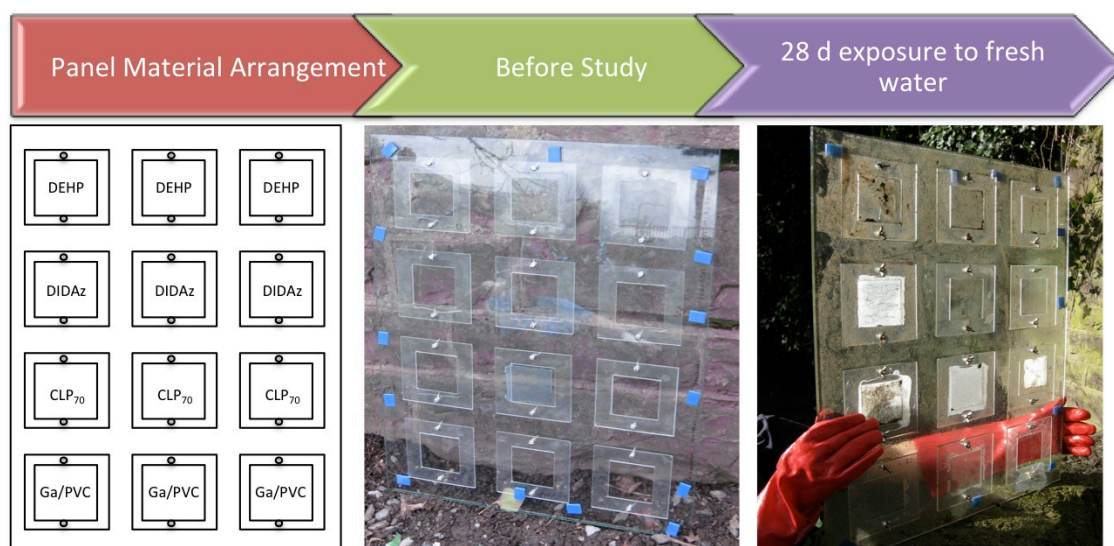
Figure 6.4: Schematic showing deployment study of materials coated to the test panel, a photograph of before and after the 28 d investigation. The panels relate to the areas of where the plasticized PVC and gallium-doped PVC was positioned.

Each of the PVC based materials following a 1-month deployment were tested for slime, protein and carbohydrate adsorption, and the results have been tabulated in Table 6.1.

6.4.1.2 FOULING RESULTS

Presented herein are the fouling results recorded for the glass test panel coated materials. The results have been tabulated for brevity.

Slime in the Ga/PVC material has shown lower levels of detection, highlighting it has been effective as an antifouling coating. DEHP (0.57 ±0.03 AU) has also shown a lower quantity of slime on its test surfaces especially when compared to CLP_{70} (1.21 ± 0.043 AU) and DIDAz (0.83 ± 0.05 AU). Slime again has proved to be useful tool in identifying the level of sorption of biomaterial and subsequent microorganism involvement across the test materials used within this deployment study. This has been routinely reported, and reinforces that microorganisms embed themselves in this protective layer, adding to the biofilm thickness. [489] It is also firmly accepted that EPS production, increased with attachment of bacteria to solid surfaces, is a multicomponent facet to the biofouling problem and thus other techniques need to be used for such characterisation. Subsequently, as mass was not performed, protein and carbohydrate adsorption were used to quantify the level of biofouling, of which are components in this slime matrix. [490]

Table 6.1: Tabulated results for slime, protein and carbohydrate adsorption following a 1-month field deployment in a freshwater system. (River Tolka, Dublin).

Analyte in PVC	Slime Test (AU)	Protein adsorption (µg/mL)	Carbohydrate adsorption (µg/mL)
DEHP	0.57 ± 0.03	6.72 ± 0.021	7.36 ± 0.056
DTDAz	0.83 ± 0.05	7.01 ± 0.032	8.32±0.079
CLP_{70}	1.21 ± 0.043	12.85 ± 0.64	17.44 ± 0.038
Ga-MNPS	0.45 ± 0.032	4.65 ± 0.23	7.31 ± 0.043

Protein adsorption was also lower in the gallium PVC material (4.65 ± 0.23 µg/mL) especially when compared to CLP_{70} which observed protein levels of 12.85 ± 0.64 µg/mL. The level of carbohydrate adsorption observed was also lower for gallium doped PVC than any of the other tested materials. Again, this highlights the potential use as an optically clear coating platform for sensors. Zhang *et al.*, also found that protein and carbohydrate adsorption was indicative of fouling when analysed for PVC membranes. They too, used a protein and carbohydrate assay in their findings, but also further confirmed the presence of characteristic protein and carbohydrate bands using FT-IR. [137]

Figure 6.5 shows the various levels of fouling shown in the photographs of the individual test materials. Clearly, levels of geofouling have been exhibited in all samples tested over this study. Images exhibiting less fouling are observed in Ga/PVC samples, where less fouling has been observed when compared to the other test materials. In a paper by Liu and Zhang a simulated sediment and fouling assay was established for an ultrafiltration membrane assay used in a banknote wastewater system. The authors report sedimentation as an contributer to additional fouling on the membranes. [491] This shows that sedimentation (geofouling) is also a positive factor when taking into account every aspect of fouling. However, this is a factor related to the system being tested, and may not exist in every system.

(a)

(b)

(c)

(d)
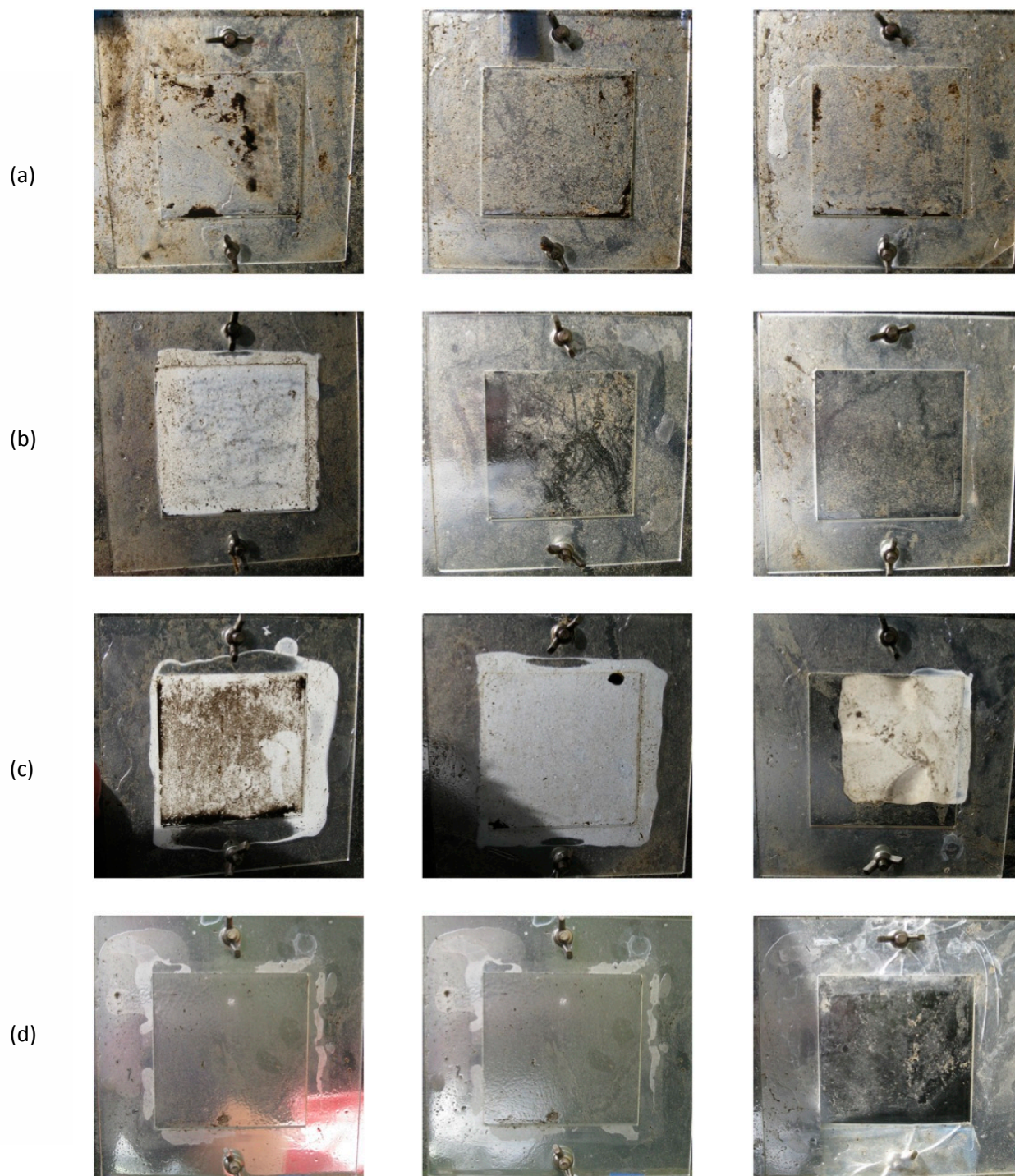
Figure 6.5: A series of photographs of each test material used in the glass panel test study. Performed in the river Tolka, Dublin Ireland on 20th April 2010 (a) DEHP, (b) DIDAz, (c) CLP$_{70}$ and (d) Ga/PVC.

The deployment of PVC doped materials has shown a breadth of results. The gallium nanoparticle doped materials have seemingly performed the best in this system, and visually this transparent material shows most promise. These materials show the capability of being used in a real test system, and the next phase of this work would be to coat them to real sensors.

6.5 FURTHER IMPROVEMENTS

The aim of this section is to create a material with a combination of properties suitable as an antifouling material coated to sensors. The use of nanoparticles has shown good potential as antifouling agents as shown in Section 6.4.1. To improve the use of such agents, combinational approaches could be of more use in creating a broad-spectrum antifouling material. Some natural sources have already evolved with such attributes, and thus biomimetics is an interesting route to further develop such a material.

6.5.1 THE LOTUS EFFECT

Controlling the wettability of a solid surface is of increasing interest from both a fundamental and practical perspective. [492-495] For a solid that possesses a contact angle greater than 150 ° of water on its surface is deemed to be superhydrophobic. The best-known example of this is in nature, is the lotus leaf, which shows the ability to reduce surface contamination through its self-cleaning mechanism, which has been on-going for thousands of years, Figure 6.6. It took some scientific development in SEM to resolve the mechanism behind this natural phenomenon. The lotus leaf was subsequently characterised to having protruding epicuticular protrusions of 20 – 40 μm apart, each covered with a waxy layer containing wax crystalloids only. [496]
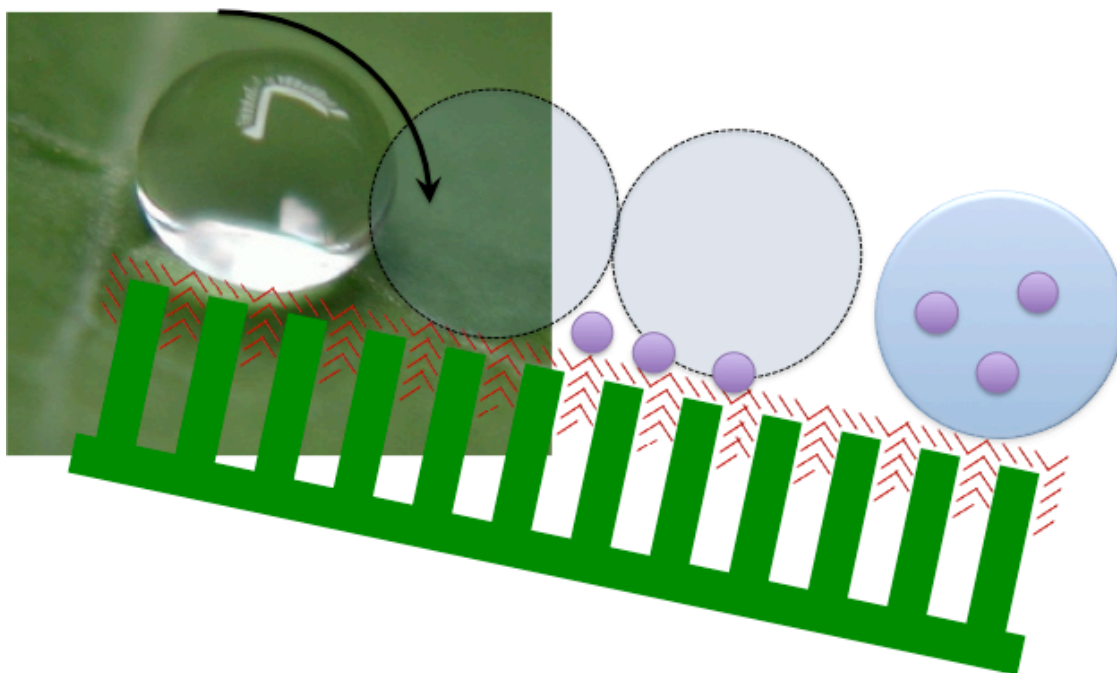
Figure 6.6: Schematic showing self-cleaning property of lotus leaf (*Nelumbo necifera*) the lines represent the waxy epicuticular layer where the purple circles represent the dirt particles, showing the roll-off effect of the water droplet.

Interest has therefore accumulated in designing surfaces with superhydrophobicity that can be used in applications such as antifouling, self-cleaning and water resistant coatings designed for a range of technologies; microfluidic channels, biosensors or antifouling coatings to name but a few. [497]

Recently Zheng *et al.* created a polyurethane/Pluronic ® surface with lotus-leaf like topography. They found that contact angles could be enhanced when lotus leaf modifications were fabricated. Protein adsorption was found to be significantly lower on the lotus leaf designed surfaces than the unmodified brought about by the increased superhydrophobicity. [498] Similarly Chen *et al.* found that micro texturing reduced protein adsorption, along with platelet and cell adhesion in PDMS surfaces. [499]

Owing to the unique properties of superhydrophobic coatings, their potential development for scientific and industrial applications is encouraging. In essence, high surface roughness is required for a superhydrophobic effect, as seen in the Lotus Leaf. Many non-abrasive applications can be envisioned where the superhydrophobic effects are significantly beneficial, i.e. creating a non-fouling surface. Naturally, these applications require a level of stability in maintaining the desired antifouling effects. This poses a question on durability of a material within a real environment where environmental stresses are not often considered when designing the material for the purpose it is required, an example of which, lies in antifouling sensor materials and coatings.

6.5.2 CHEMICAL BIOMIMICRY FOR SENSOR APPLICATIONS

In order to achieve the same surface property of the Lotus leaf, it is necessary to create (i) a highly rough surface and (ii) a waxy layer. [496] One way of achieving such properties are through the use of nanoparticles and self-assemblages of monolayers of a hydrophobic material. [500]

Therefore, the next stage of this chapter is to take an example from nature in the form of the Lotus Leaf with the use of nanoparticle technology to create a surface for antifouling purposes. This was achieved by taking already successful results and transferring them using inspiration from nature through chemical biomimicry. A series of characterisation methods are presented in this section and results for the superhydrophobic coatings in contact angle measurements and topographical data using SEM. A series of measurements of the already developed biofouling assays (protein, carbohydrates, slime and mass) were taken for gold and silver manufactured superhydrophobic copper surfaces. The materials were then exposed to the marine environment for an efficacious incite to the developed materials.

6.5.2.1 CONTACT ANGLE AND SEM MEASUREMENTS

Contact angle measurements for the superhydrophobic coatings were taken, following their production using silver particles. It was found that varying the concentrations of silver nitrate would cause different porous micro-nanostructures enabling varied attachment of the superhydrophobic molecules, as reported in Section 2.4. Similarly Song *et al.* reported 5 mM concentrations of the required metal salt achieving wetting degrees greater than 150 °[501] also observed in this body of work. Song also presented scanning electron micrographs illustrating the degree of micro and nano roughening of gold particles on the copper surface. Additionally, Bell *et al.* also characterised a superhydrophobic copper coating using roll and tilt angles of the water droplet.[203] This probes the interaction of wettability further than the work carried out in this thesis where only static contact angle analysis was performed

Electron microscopy was also performed on the materials to ascertain dimensions of the nanoparticle layers. An example of which can be seen in Figure 6.7, where nano and micro surface topography can be seen.
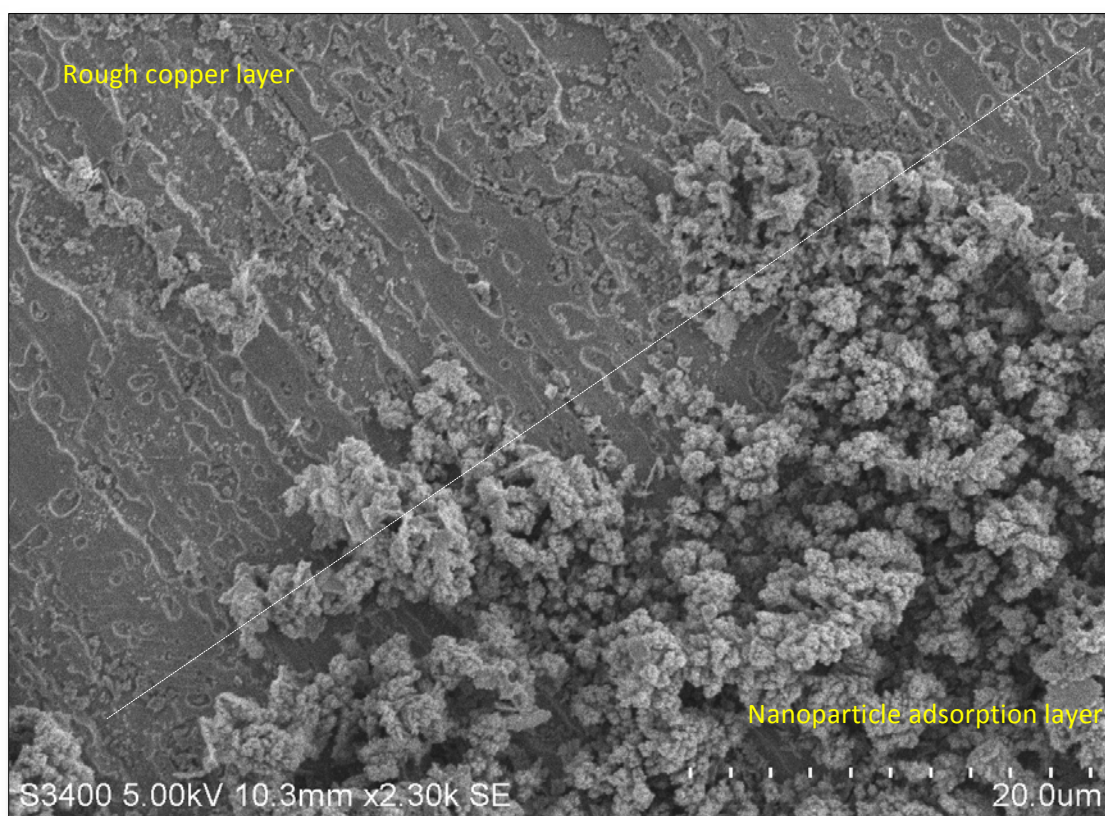
Figure 6.7: Scanning electron micrograph showing topography of metal particle layer adhered to a copper based substrate.

The copper layer has a raised parallel topography exhibiting peaks and troughs, whereas where the particle layer has formed, there is obvious nano and microtopography. The latter

results in a very inhomogeneous topography suitable for the attachment of a hydrophobic molecule, such as an alkanethiol. Zhang *et al.,* produced stable biomimetic (described as celery like structures) superhydrophobic surfaces which were realised using aluminium as a starting block for the fabrication of such surfaces where scanning electron micrographs similar to the one depicted in Figure 6.7 where nano and micro roughness was observed. [502]

6.5.2.2 ANTIFOULING RESPONSES FOR SILVER NANOPARTICLES ON A COPPER SUBSTRATE

The materials under investigation were analysed to determine their prevention of fouling over a 21 d period. Tests of mass, protein and carbohydrate adsorption all showed improved antifouling characteristics for the superhydrophobic material.
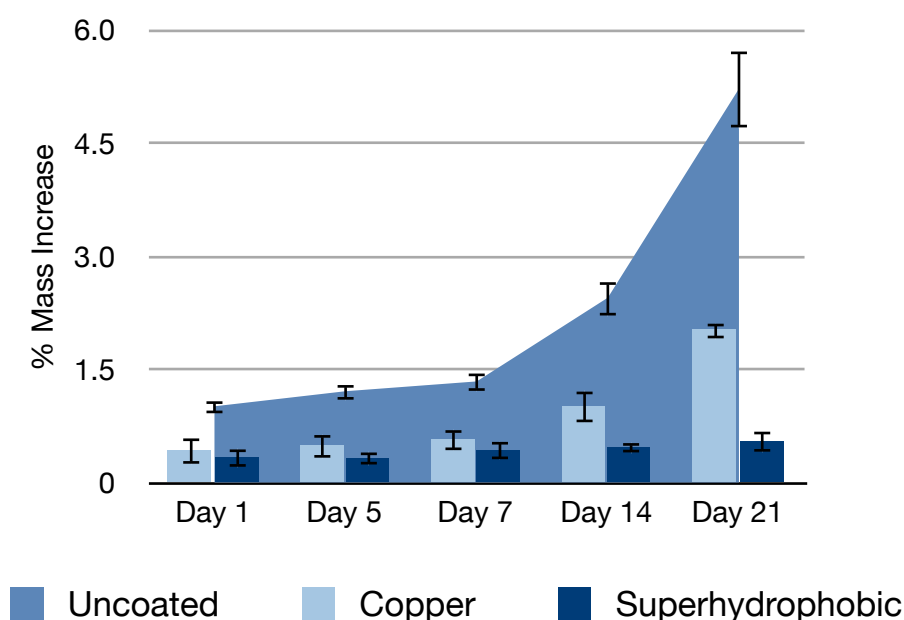
Figure 6.8: Chart showing percentage mass increase of three coated sensors (n=3 ± 1SD) when exposed to a marine system in Poolbeg Marina, Dublin, Ireland.

The results depicted in Figure 6.8 following a 21 d study the results show that the superhydrophobic coating shows least mass adhesion upon each of the substrates. The superhydrophobic coating after 21 d showed least mass increase (0.52 ± 0.12 %) compared to the copper coat which showed mass increase by up to 4 times (2.01 ± 0.11 %).

Figure 6.9 shows total protein adsorption of the three-coated sensors. The level of protein adhered to the sensor coated materials again favoured the superhydrophobic coated sensor over the other two materials.
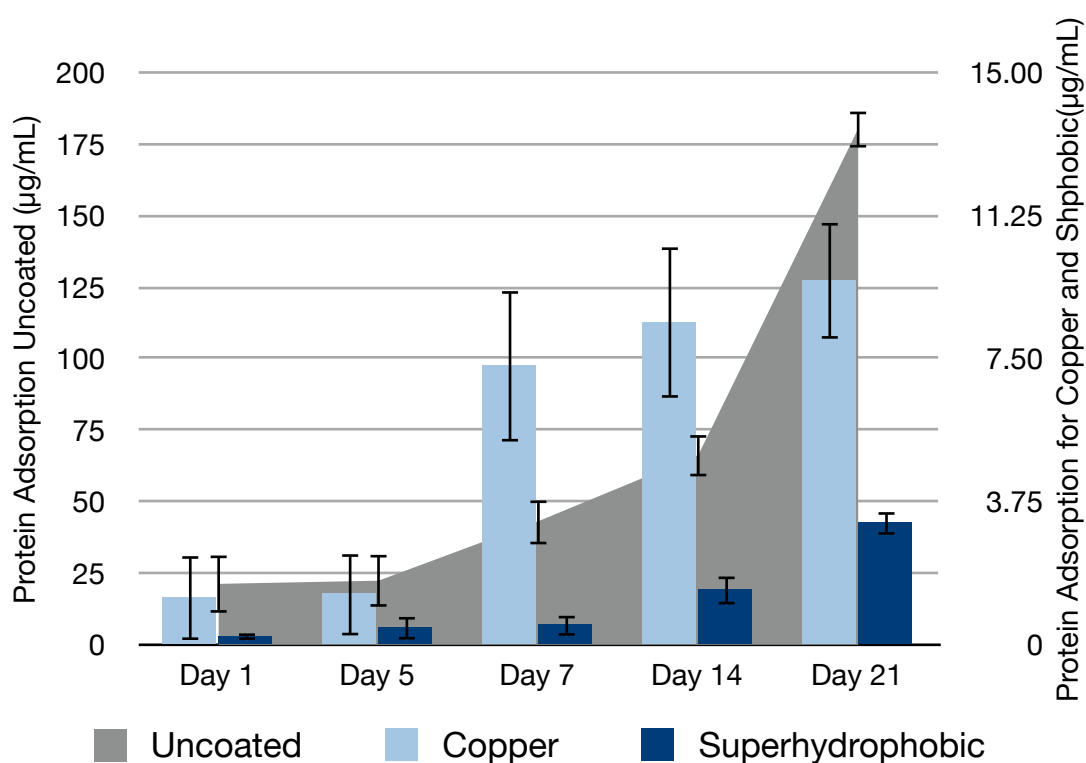
Figure 6.9: Chart showing total protein adsorption of the three-coated sensors of a 21 d study (n=3 ± 1SD) . The uncoated materials were plotted on the left y-axis as the level of adsorption was observably higher, when exposed to a marine system in Poolbeg Marina, Dublin, Ireland.

The results for the protein adsorption assay are convincing with both raw copper and superhydrophobic copper coated sensors resisting protein attachment by up to 12 times that of the uncoated sensor. As expected, and leading on from the biomass results obtained, the superhydrophobic coating has adsorbed least protein when compared to the raw copper substrate.

Protein adsorption was largely elevated upon the uncoated sensor showing adsorption levels of 181 ± 1.2 μg/mL with the superhydrophobic (1.3 ± 0.2 μg/mL) and copper coated (1.7 ± 0.3 μg/mL) sensors. It is generally accepted that superhydrophilic surfaces entice protein adsorption as outlined in some papers. [503] Patel *et al.,* report that superhydrophilic surfaces considerably increase protein adsorption when coated in polyester films and oxygen plasma treated. [406] Where the sensor is not superhydrophilic, it has shown increased wettability and therefore could be a factor in why increased levels of protein was observed in this assay. Contrastingly, the superhydrophobic-coated samples as protein levels were found to be lower in the superhydrophobic samples in contrast to Patel and co-workers results that were using superhydrophilic materials.

Figure 6.10 shows the level of carbohydrate adsorption detected for each of the coated sensors. The total carbohydrate adsorption indicates this biomolecule is a founding

component in the biofilm and in general biofouling, upon a substrate. [504] The results mirror the protein adsorption results, but also indicate that at 14 d the superhydrophobic coating (1.63 ± 0.37 μg/mL) is outperforming the raw copper alone that observed adsorption values of up to 5 times this value (8.01 ± 1.02 μg/mL). After this point at 21 d, the level of total carbohydrate increased by 3 times (5.2 ± 0.81 μg/mL), suggesting that the superhydrophobic has slower carbohydrate adsorption. Interestingly, Wang *et al.* also found that as a material's hydrophobicity changed, the level of biomolecule activity increased, as a material tended towards a hydrophilic value. [505] This has been attributed to polar groups and lower surface energies changing, subsequently forcing water molecules to adsorb to the surface increasing the attachment probability of the substrate. [505]
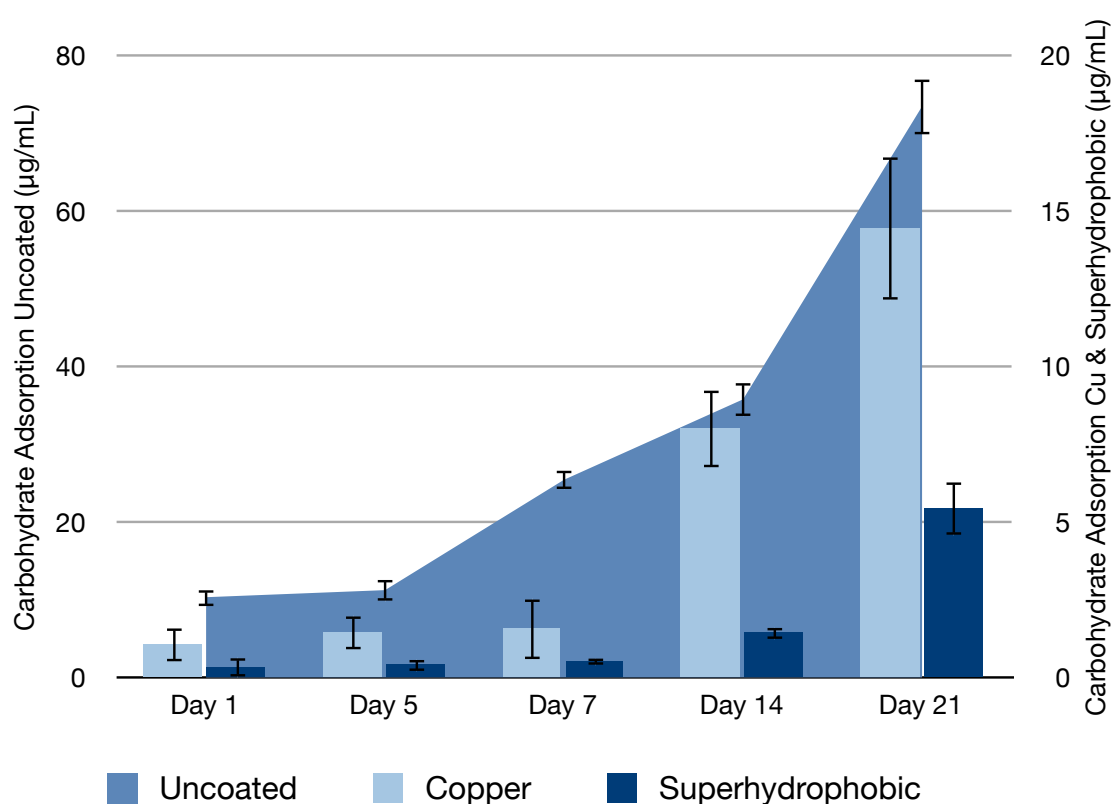
Figure 6.10: Total carbohydrate adsorption of the three-coated sensors of a 21 d study (n=3 ± 1SD) when exposed to a marine system in Poolbeg Marina, Dublin, Ireland.

Mass and slime were also compared for each of the coatings. Figure 6.11 shows the relationship between mass and slime for the three coatings. The mass increase has a similar trend to slime increase following the 21 d study. After 14 d the slime observed in (a), increased by 1.75 AU highlighting that microorganism interaction at this point could possibly be more abundant on the substrate. Mass increased as high as 0.129% ± 0.06 after 21 d, where the superhydrophobic substrate is still outperforming the others.
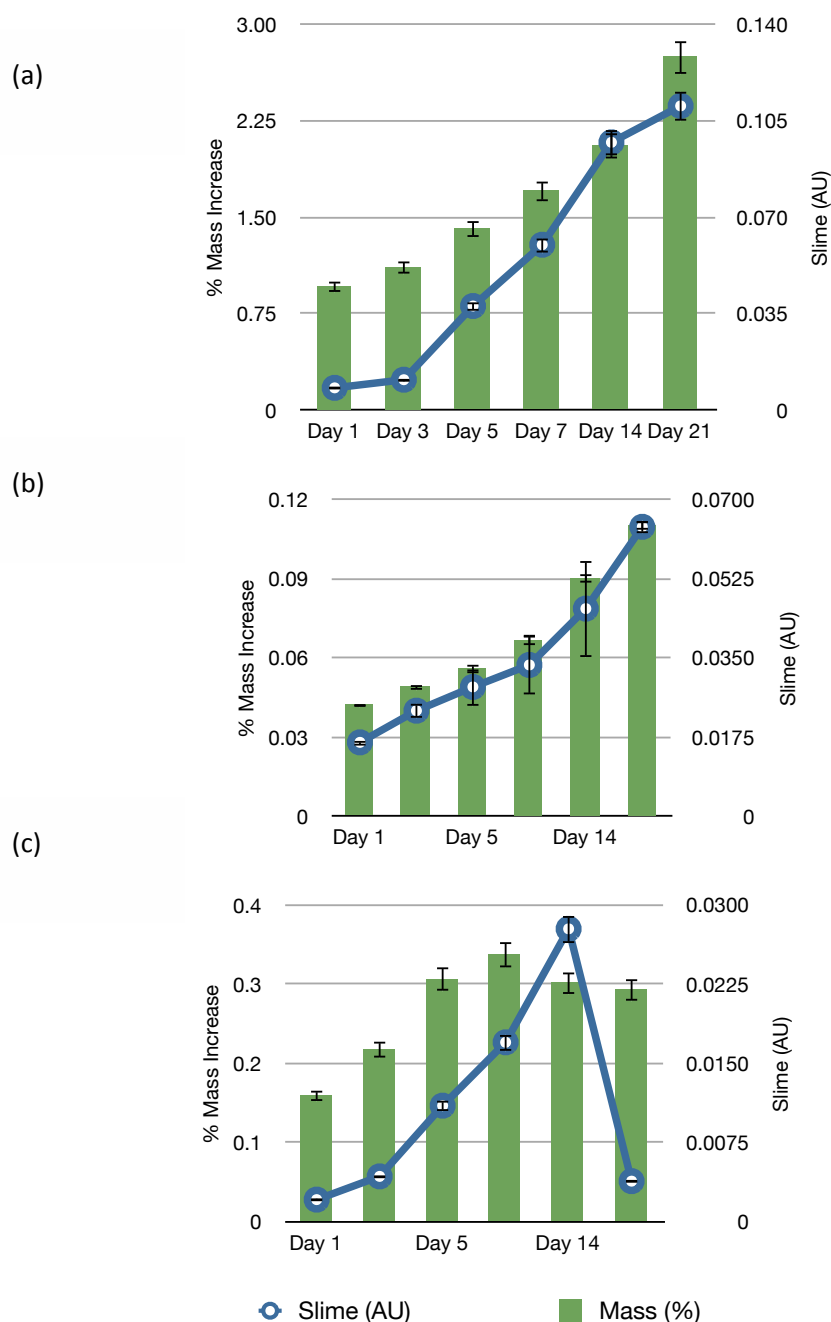
Figure 6.11: Comparison between slime and mass adsorption for each of the coatings tested. (a) uncoated, (b) copper coated and (c) superhydrophobic coated.

The trend between the two sets of data is apparent where slime increases with mass, which has been reported in Chapman *et al..* [138] Although EPS is known to contain carbohydrates, proteins, nucleic acids, lipids and humic substances, carbohydrates and proteins are the major constituents [506] and represent a mass to the adsorbed biofilm layer. This is evident in all results obtained in the Figures 6.11 a, b, c.

In Figure 6.11 (c) the superhydrophobic coating shows a gradual mass increase up until 14 d and then a decrease in mass has shown decrease at 21 d. Similarly, slime increased until 7 d and then began to decrease from the 14 – 21 d period. Also, detachment of biofilm and removal of particulate matter could be a contributing factor to these mass fluctuations observed. This could be evidence of material erosion and subsequent decrease in mass owing to this effect. This was then investigated through a series of contact angle measurements over time using the flow through tank system previously described in Section 2.4.2.2.

6.5.2.3 PERFORMANCE OF SUPERHYDROPHOBIC COATING

The mass and slime result showed it was necessary to investigate the materials ability to deliver the superhydrophobic characteristics over extended time periods. This was achieved through contact angle and mass analysis.

Contact angle measurements can be seen in Figure 6.12 following a 21 d study in a flow through test tank. From this study it was found the copper coat remained constant observed in the contact angle photographs displayed. The superhydrophobic coat begins to lose superhydrophobicity after 5 d where contact angles of >150° are observed. Nakajima *et al.* reported the lifetime of their superhydrophobic coatings to be 92 h when exposed to air using TiO_2 as a thin film photocatalyst. [483] Contrastingly, the lifetime of the superhydrophobic coating shown in this work appears to lose its 'superhydrophobicity' (>150 °) after 80 h following this coating becomes more hydrophilic for a 14 d period.
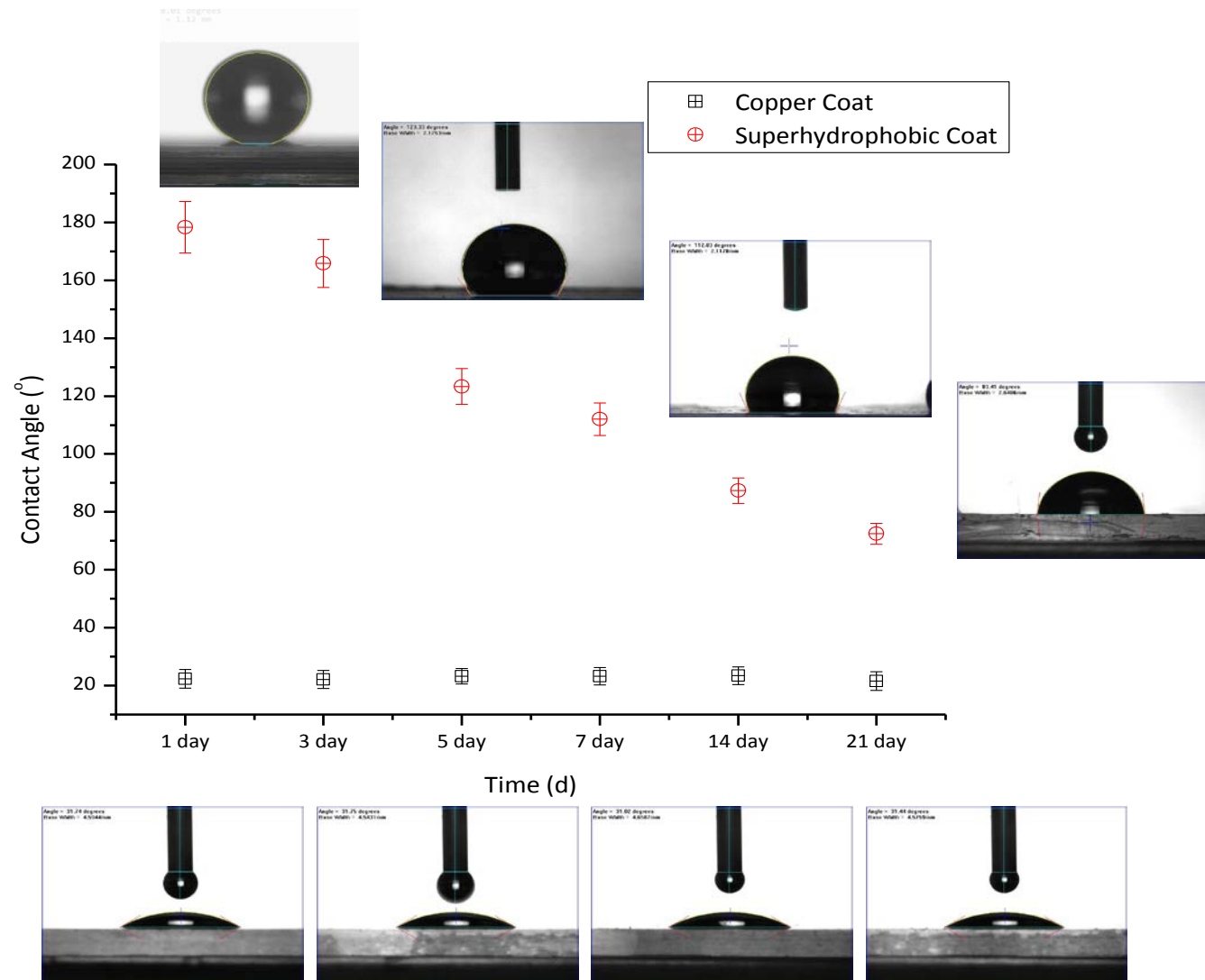
Figure 6.12: Contact angle measurements for copper and superhydrophobic coats following a 21 d pure water flow study. Contact angle images on top relate to superhydrophobic materials and below images relate to copper surfaces.

Mass was also taken into consideration and has been shown in Figure 6.13. Here, the coatings were investigated for mass change in a flow through tank system using Milli-Q water.
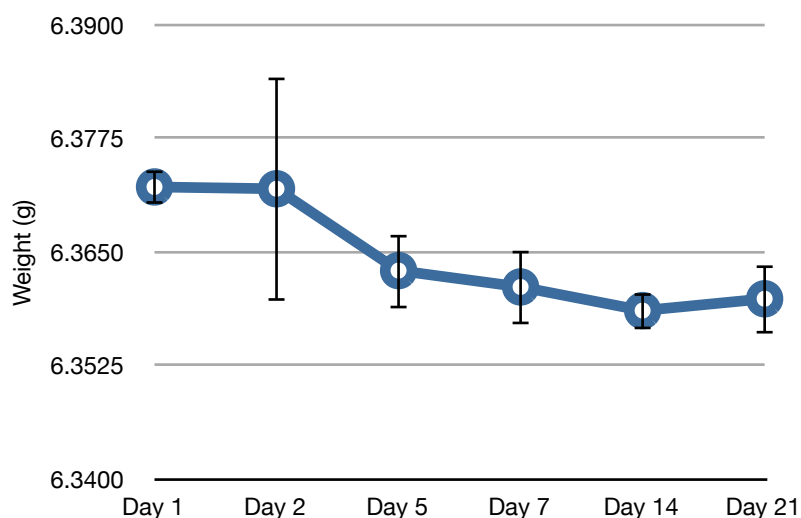
Figure 6.13: Mass change of the silver based superhydrophobic coating following 21 d in a Milli-Q flow through tank study where a flow rate of 8 L / min was administered.

The superhydrophobic coating shows evidence of erosion on the surface of the copper when introduced to a mild flow environment. Similarly Mahmud *et al.*, investigated the erosion of a superhydrophobic coating using static contact angles, which has also been reflected experimentally herein. However, they did not reinforce the result with any mass analysis, which is significant in attempting to investigate erosion with such claims. In conclusion, the change is mass is a direct result of the nanoparticle layer being eroded through the shear stresses of the environment – in this case the flow through tank system.

The results presented in this section, show promise in the assays carried out for the superhydrophobic coat and copper coated sensors. The superhydrophobic coating was found to be the better antifouling material compared to the uncoated and copper coated substrates this was demonstrated with least protein and carbohydrate adsorption in the relevant assays and has shown least mass and slime adsorption. The coating showed a mass change that was not similar to the other coatings and saw a decrease in mass. The superhydrophobic coating was investigated for its overall performance. Mass and contact angle were used to probe this, and indeed, it was found that the lifetime of the superhydrophobic coating was limited when exposed to an aquatic system. Consequently, improving the coatings performance would be beneficial to the antifouling material as it can be seen that the superhydrophobic coating

demonstrates positive antifouling response when compared to copper and the uncoated sensors.

6.5.3 GOLD NANOPARTICLES ON COPPER SUBSTRATES

Herein, the thesis will investigate gold on the copper base layer as a platform for attachment of the subsequent superhydrophobic molecular layer. The aim of this change in the particle base metal was to investigate the affinity and thus attempt to improve the lifetime of the superhydrophobicity, and thus antifouling protection as previously seen for the Ag superhydrophobic coated substrates.

6.5.3.1 ANTIFOULING RESPONSES FOR GOLD NANOPARTICLES ON A COPPER SUBSTRATE

The study for gold was extended as the previous silver study showed a decline in the material after 21 d. The impetus of this study was to observe if the metal nanoparticle (in this case gold) would prolong the superhydrophobic effect. Evidently, if the lifetime of the superhydrophobic coating could be improved, this could represent a positive result in reducing the cost of maintenance of a sensor suite but also the frequency of site visits, aforementioned.
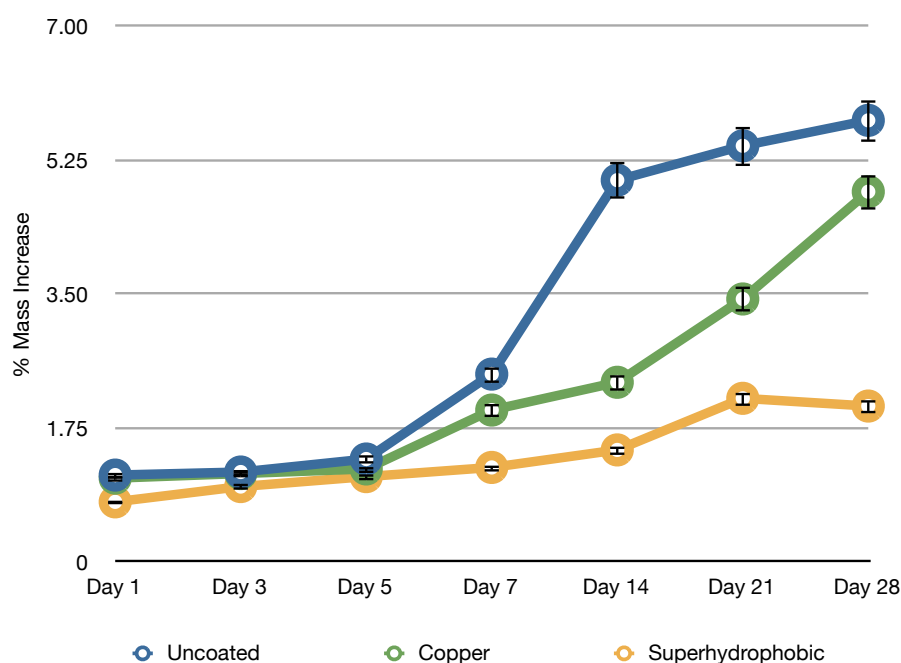
Figure 6.14: Mass adsorption measurements for uncoated, copper coated and superhydrophobic gold coated materials (n=3 ± 1 SD).

Figure 6.14 suggests that after 21 d the superhydrophobic gold-coated substrates continued to remain superhydrophobic. The measurement at 28 d shows that the coating had begun to erode and mass loss was being seen in the superhydrophobic gold samples. This again shows that the affinity for the superhydrophobic molecule has improved by 7 d for gold than silver. The following results show that the affinity for the superhydrophobic molecule is stronger for gold than that of silver. This has been explained extensively in Sellers *et al.,* who have explained the relationship for the affinity of alkanethiolates with gold and silver surfaces [507] highlighting the understanding of the chemisorption of alkanthiolates on both gold and silver.

Furthermore, Figure 6.15 compares protein adsorption for after a 28 d study for gold and 21 d silver coated copper substrates with the superhydrophobic molecular layer. The data shows that up to 14 d the gold superhydrophobic (0.72 ± 0.27 µg/mL) coating had less protein adsorption than the silver superhydrophobic coating (0.67 ± 0.23 µg/mL). Following the 28 d exposure, the level of protein on the Au-superhydrophobic substrates increased (4.23 ± 0.34 µg/mL) whereas adsorption on the Ag-superhydrophobic substrates remained less (3.21 ± 0.15 µg/mL).
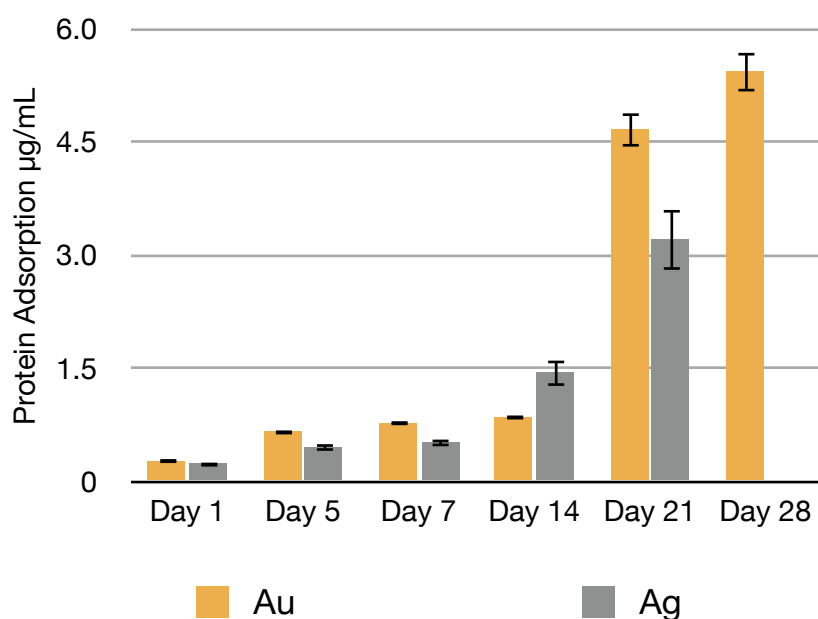
Figure 6.15: Protein adsorption chart comparing Ag and Au superhydrophobic coatings.

Interestingly, the preferential adsorption of proteins to gold and silver has been reported in Sheardown *et al.*. It was found that protein adsorption was higher on gold surfaces rather than

silver for both fibrinogen and albumin based experiments, which has indeed been reflected with this work where gold experienced higher protein adsorption over silver. [508]

This phenomenon has only been realised once the superhydrophobic coating has eroded, where it can be seen in day 14 for the Ag (1.41 ± 0.02 µg/mL) base layer protein adsorption remained higher than in the Au (0.53 ± 0.04 µg/mL) base layer. Whereas, once the superhydrophobic characteristic diminished, both raw gold and copper was exposed to the surrounding environment, and an observed increase in protein was experienced due to the affinity of the metals for protein attraction.[509]

Figure 6.16 details total carbohydrate adsorption for the gold and silver superhydrophobic substrates.
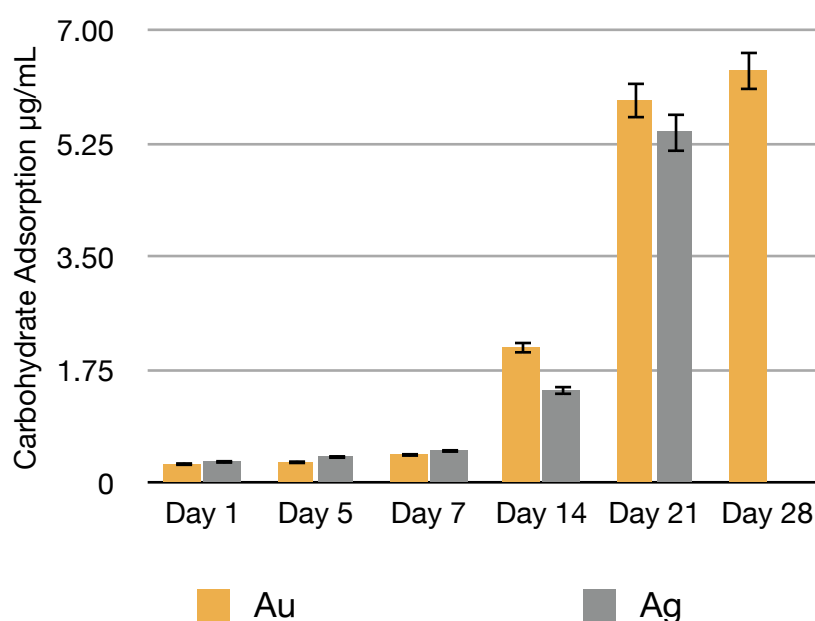
Figure 6.16: Bar chart comparing carbohydrate adsorption of gold and silver superhydrophobic coatings over a 28 d period.

The Ag superhydrophobic substrates have shown least carbohydrate adsorption following a 21 d study mirrored with the protein results already obtained. Silver coated superhydrophobic copper substrates (1.25 ± 0.32 µg/mL) display an aversion to carbohydrate adsorption at 14 d, which is less than that of the gold-coated substrates (1.56 ± 0.22 µg/mL). This shows that the alkanethiol molecule potentially stronger affinities for different metal species as shown in Sellers *et al..* The lifetime of the superhydrophobic coating shows less carbohydrate adsorption for both metal substrates up to 14 d where carbohydrate adsorption is similar. Following this,

when the superhydrophobic characteristic has diminished, the silver base metal shows less carbohydrate adsorption over gold particle substrates. Indeed, some authors have also found that gold entices carbohydrate adsorption and this can be seen in Min *et al.,* where carbohydrate adsorption was found to be higher on gold than on silver metals through a developed bio sensing technique by up to 50 %, [509] which too has been reflected in this study.

General toxicity of silver and gold could also be causing improved antifouling results following the erosion of the superhydrophobic layer at the 14 d timeframe. For example, in work by Farkas *et al.*, silver and gold nanoparticles were tested for their toxicity against *Oncorhynchus mykiss* and found Ag to be extremely cytotoxic to this particular species, [510] thus, this could be a reason for carbohydrate levels to be less in the Ag coated copper substrates when compared to the Au substrates, once the superhydrophobic layer has diminished the surface active silver or gold remains.
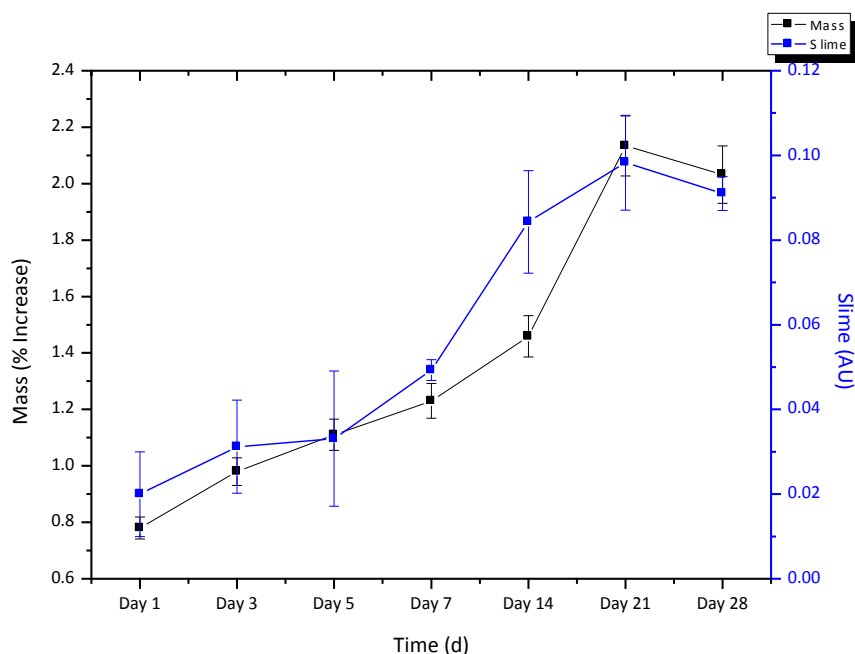
Figure 6.17: Double y-plot of slime vs. mass adsorption for the gold-coated copper superhydrophobic substrates (n=3 ± 1SD).

It was found that after 21 d, slime and mass decreased, Figure 6.17. This has already been attributed to the lifetime of the coating diminishing as seen in Section 6.4.2.4, *vide supra*, where the level of slime and mass decrease due to the effects of erosion from the copper substrate. Again, this work is merely a tool to suggest that slime levels are linked to level of

mass adhered to the surface of the substrates and has been something carried out to show this throughout the thesis.

In conclusion, to the work carried out so far in this chapter, silver and gold both have strong advantages and disadvantages when introduced into these antifouling assays. Firstly, the silver has a shorter superhydrophobic lifetime than that of the gold-based copper coat. The silver coating has then showed a more antimicrobial and subsequent antifouling characteristic than that of gold. The gold-coated substrates, although the superhydrophobic lifetime was improved by 7 d showed after this point observed elevated levels of protein and carbohydrates associated with biofilm development and subsequent biofouling.

6.6 DEPLOYMENT 2 – POOLBEG MARINA, DUBLIN

In this section, superhydrophobic materials for gold and silver based copper coated substrates were deployed for a 6 w study in Poolbeg Marina, Dublin, Ireland. The materials were monitored for their efficacy in preventing the effects of fouling, these studies were carried out in parallel to constant monitoring of pH, turbidity, conductivity, depth, salinity and temperature to see if normal environmental conditions would affect the level of fouling. The samples were deployed in engineered Perspex frames as shown in Figure 6.18, sonde and location details can be found in Chapter 2, Section 2.5.3, *vide supra*.

Figure 6.18: Superhydrophobic gold copper coated substrates and sensors used in the long term deployment study at Poolbeg Marina, Dublin, Ireland.

6.6.1 ASSESSMENT OF FOULING

Mass increase for silver and gold copper coated substrates following a 6-week exposure time in a marine environment is shown in Figure 6.19. The levels of mass for silver and gold have shown similar trends for both sample types.
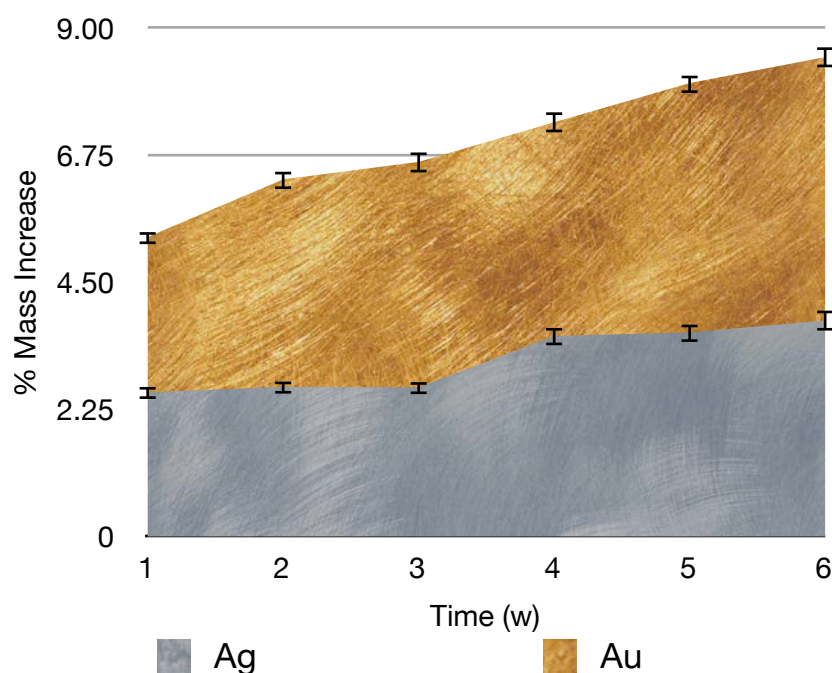
Figure 6.19: Mass adsorption for gold and silver superhydrophobic coated copper substrates.

It was found that Ag (3.82% ± 0.191) showed the least mass adsorption to the copper substrates after the 6 w exposure time when compared to the Au coated substrates (4.66 ±0.192 %). Interestingly, at 3 w the level of mass for Ag decreased, suggesting a point when the superhydrophobic and metal layer began to erode from the copper surface, thus providing further antifouling combinational approaches.

Figure 6.20 details the total protein adsorption measured for Ag and Au superhydrophobic metal-coated copper substrates following a 6 w exposure. The Ag superhydrophobic coating has outperformed the Au coating convincingly in this protein adsorption assay.
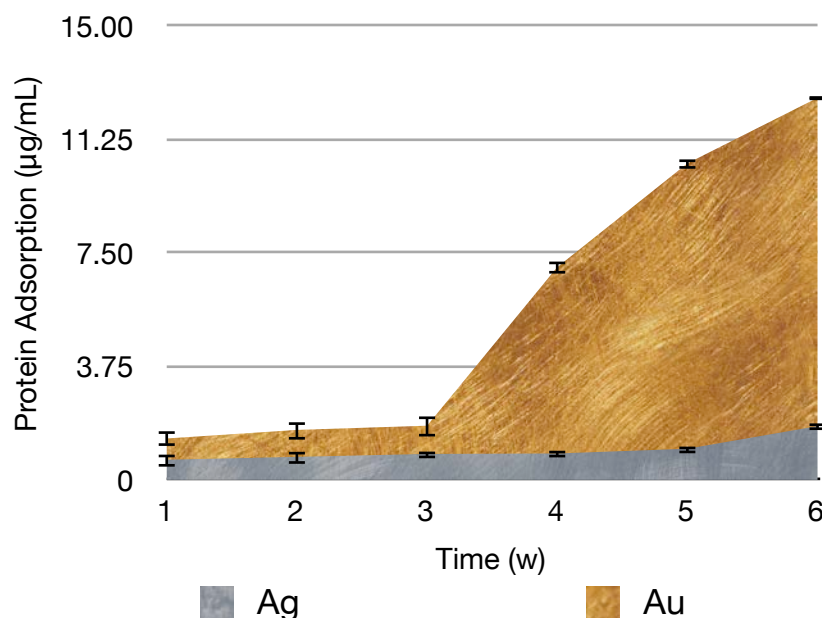
Figure 6.20: Shows total protein adsorption for Ag and Au metal superhydrophobic-coated substrates following a 6 w exposure (n=3 ± 1SD).

A trend remained for both Ag and Au superhydrophobic substrates for the first 3 weeks of the marine deployment. The values of which remained below 1 µg/mL for both Ag and Au. Following this period, the level of protein for Au coated copper substrates increased at an extremely high rate (6.16 ± 0.23 µg/mL) whereas the silver coated copper substrates saw protein levels of 0.87 ±15 µg/mL which is some 7 times less than the Au substrates. Interestingly, the Au protein adsorption then increased at an exponential rate in the last 2 w of the marine deployment reaching a final value of 10.85 ± 0.10 µg/mL, which was 10 times more than what was adsorbed to the Ag coated substrates. This extreme level of protein adsorption can be attributed to a localised plasmon resonance (LPR) effect where gold has been reported to have a stronger affinity for certain proteins than silver. [511,512] This is due to the electrostatic interaction with the wave of oscillations of electrons on the surface of the metal interacting preferentially with some biochemical.

Figure 6.21 shows the total carbohydrate adsorption that was observed for the 6 w marine deployment study for the same superhydrophobic samples aforementioned in Section 6.4.3
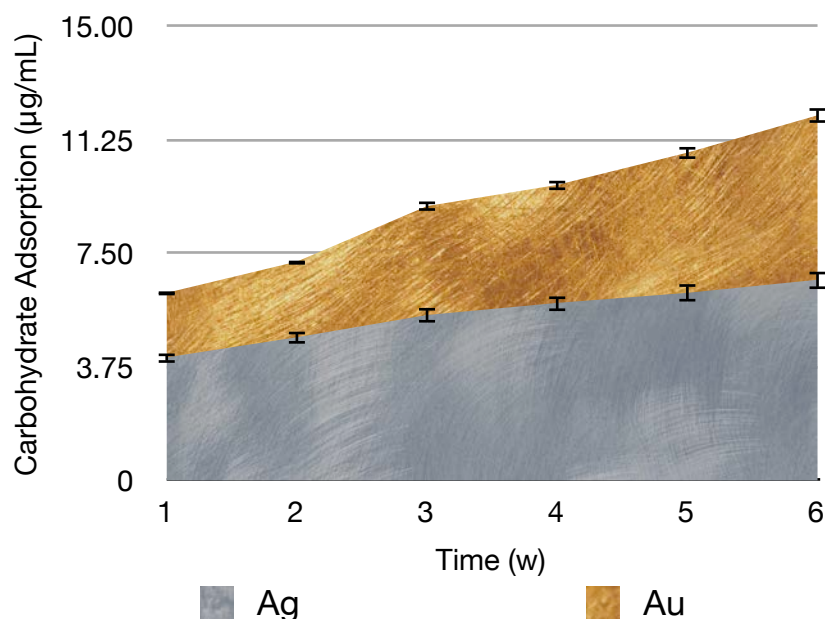
Figure 6.21: Total carbohydrate adsorption for silver and gold superhydrophobic copper coated substrates for the 6 w Poolbeg Marine study.

During the 6 w study it was observed that Au copper coated superhydrophobic substrates adsorbed higher carbohydrate quantities than that of Ag. After the 6 w period Au (6.63 µg/mL ± 0.33) was observed and in Ag (5.43 µg/mL ± 0.27) illustrating that Ag has been more successful in all biofouling assays. Environmental factors can also be controlling the level of adsorption and subsequent biofouling levels and will be discussed accordingly in section 6.4.4.2, *vide infra*.

6.6.2 ENVIRONMENTAL CONDITIONS AND FOULING MEASUREMENTS

In this section, the live real-time data that was acquired alongside the sample testing was used to correlate environmental cues with attributed fouling. Live data was acquired for turbidity, dissolved oxygen, salinity and temperature were all recorded. Spikes in data points were seen as environmental events on the autonomous telemetry for sonde data was acquire. Following sample removal in six weeks the following data was obtained shown in Table 6.2.

Table 6.2: Showing average data points of the six week marine field study for temperature, salinity, dissolved oxygen and turbidity for the sensors sonde.

Week Number	Temperature (°C)	Salinity (ppt)	Dissolved Oxygen (mg/L)	Turbidity (NTU)
1	8.46 ± 0.12	20.44 + 0.98	9.75 ± 0.23	3.41 ± 0.2
2	8.63 ± 0.27	20.528 ± 1.27	10.01 ± 0.34	2.56 ± 0.4
3	9.21 ± 0.26	20.13 ± 0.54	11.03 ± 0.11	2.33 ± 0.2
4	9.18 + 0.32	20.17 ± 0.63	10.49 ± 0.71	10.32 ± 0.4
5	10.23 ± 0.22	20.84 ± 1.33	10.51 + 0.49	8.32 ± 0.3
6	10.61 ± 0.16	20.73 ± 0.44	10.48 ± 0.67	3.54 ± 0.3

Figure 6.22 illustrates the overall fluctuations that were seen over the course of the 6 w study with the superhydrophobic materials. Over the course of the study, it was observed that the temperature increased due seasonal warming from 8 to 10.5 °C that is representative of that time of year and has been reported previously in Goodtale *et al..* [513] It was also found that the values obtained for conductivity, DO and turbidity were all expected to be within these ranges presented in Table 6.2. [514] Turbidity increased in week 4 at this point due to increased rainfall and storms – the port is also very busy and coating could also be attributed to this spike.

6.6.3 ENVIRONMENTAL TEMPERATURE AND OBSERVATIONS OF FOULING

The use of the sensor sondes enabled real-time data to be collected from the Poolbeg Marina site for temperature, salinity, DO and turbidity. These parameters were then examined against the level of fouling observed when samples were removed. Figure 6.22 shows double-y plots for silver and gold superhydrophobic substrates plotted against temperature and time.
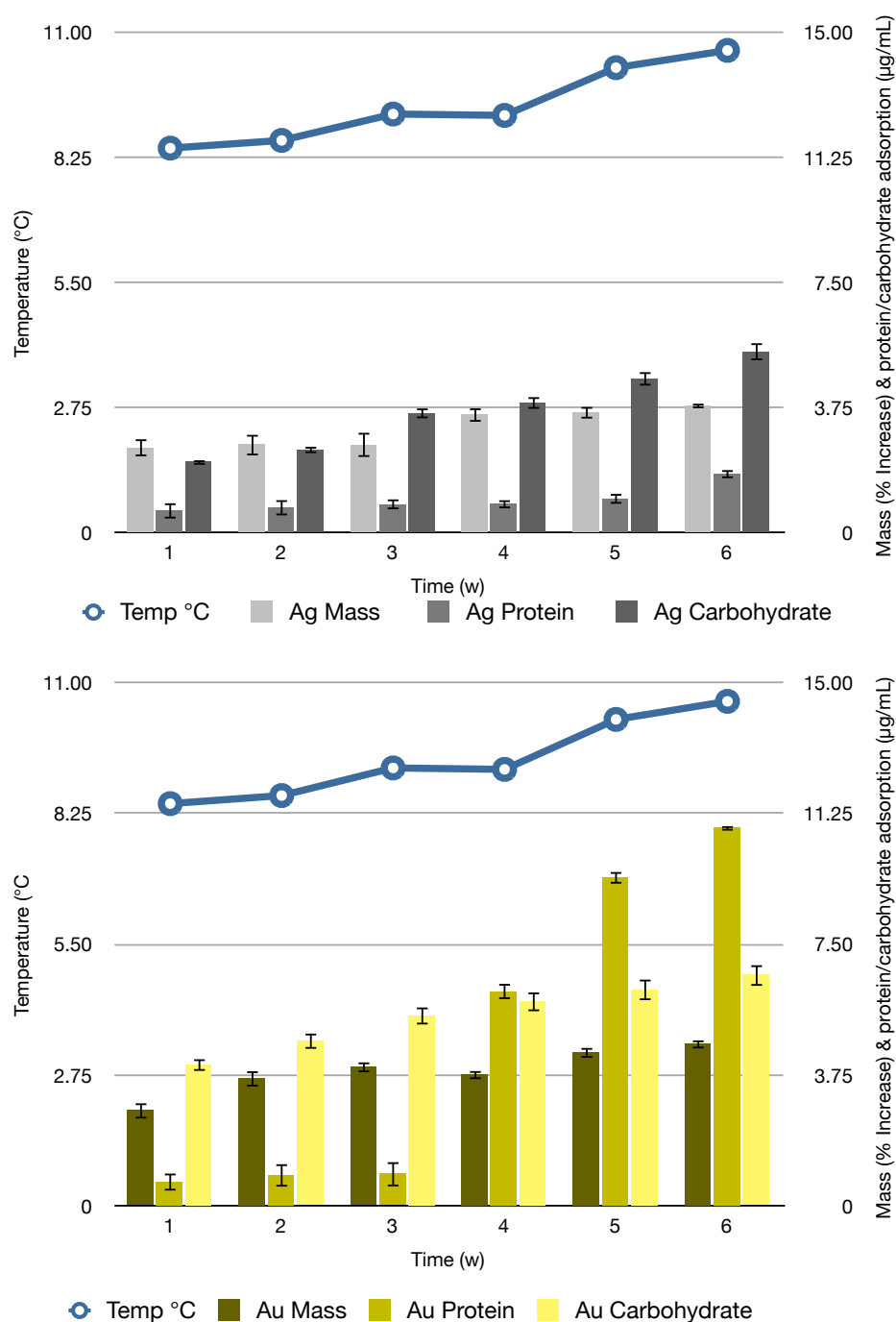
Figure 6.22: Double y-plot for silver and old superhydrophobic substrates showing the effect of temperature over the course of the deployment (n=3 ± 1SD).

In both cases for Ag and Au superhydrophobic substrates for temperature, the level of mass also increased periodically over the 6 w study. This elevated temperature incline, could be beneficial to some microorganisms as it presents a more suitable reproduction environment and can encourage growth due to more favourable conditions. It was reported by Lewis *et al.,* that cell density of the marine stalk forming diatom *Achnanthes longipes* increased in higher

temperature ranges between 14 and 26 °C, they also report that increasing the intensity of light did not produce any further growth effect. Generally, the level of mass has increased across the silver and gold superhydrophobic materials in this assay. Furthermore, the temperature has also increased, making temperature fluctuation a possible reason for increased mass on the substrates. In other work from Alexander *et al.* it was found that as temperature increased the zebra mussels, *Dreissena polymorpha* rate of respiration also increased (directly). [515] However, as turbidity increased, the level of respiration decreased, indicating that turbidity may affect species in growth, which will be discussed, *vide infra*. After performing a one-way ANOVA for silver and gold mass was not significant in comparing the mean values of turbidity and temperature in a Tukey Test ($p<0.01$). For the silver superhydrophobic coatings analysis of variance was performed for protein adsorption against turbidity and temperature where it was observed that there was significance in turbidity ($p<0.01$) but not temperature. This is suggesting that turbidity affects the overall level of fouling, whereas temperature did not. Additionally, the same analysis was performed for carbohydrate adsorption for silver and gold surfaces where it was concluded that carbohydrate adsorption had no significance for turbidity results, but significance was realised for temperature ($p<0.01$), for gold substrates carbohydrate adsorption when compared to temperature showed significance ($p<0.05$).

6.6.4 EFFECT OF TURBIDITY IN THE ENVIRONMENT

The effect of turbidity was also compared to the level of mass, protein and carbohydrate adsorption results and hence a picture of the overall biofilm and biofouling rates. Following the 6 w deployment of the silver and gold superhydrophobic materials, turbidity showed no further effects to the level of biofilm formation or biofouling, Figure 6.23.
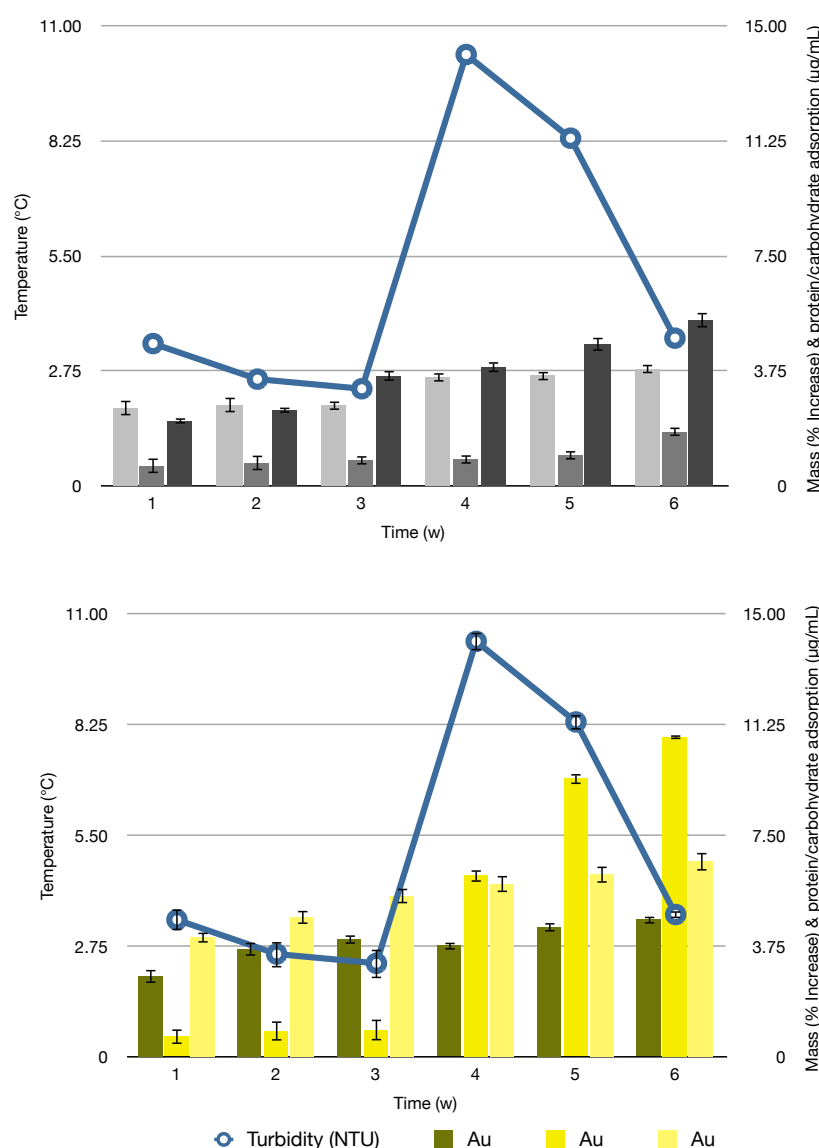
Figure 6.23: Double axis plots showing the effect of turbidity in the Poolbeg deployment for gold and silver superhydrophobic substrates over a 6 w deployment (n=3 ± 1SD).

Turbidity does not affect the level of fouling observed for gold and silver substrates. The level of turbidity decreases in week 1 – 3 of which we observe an increase in overall biofilm formation. Week 4 saw a turbidity spike in the data, where no further fouling effects was

observed. Again, this highlights the fact that turbidity did not impact the level of fouling observed for the gold or silver superhydrophobic substrates. When an analysis of variance was performed for the whole data of turbidity and biofilm formation for both silver and gold substrates, no significance was observed between any means of the data sets, therefore a Tukey test did not present any statistical significance. Although these results do not present any definitive observed effects in terms of turbidity affecting biofilm formation, it is important to mention that turbidity does appear to affect optical sensors when introduced into a system because this adds to total suspended solid and geofouling upon a substrate and is therefore of importance in this type of consideration. [516] Furthermore, it is accepted that turbidity contributes to the overall biofouling process, highlighting significance to the overall problem. [517]

6.7 CONCLUSIONS

Superhydrophobic surfaces affect the level of biofouling, which has been observed in many of the results shown within this chapter. The surfaces were found to resist elevated levels of fouling observed from the assays linked to biofilm development in the mass, slime, protein and carbohydrate adsorption assays. Obvious signs of diminished lifetimes had been incurred when introduced into the real environment yet success was still observed.

It was found that silver and gold have advantages and disadvantages when used as metal interfaces for the adhesion of the superhydrophobic monolayer. Where, when silver is used as the metal layer, the lifetime of the superhydrophobic layer is reduced by approximately 1 week in contrast to the gold coating. However, although gold has an improved superhydrophobic lifetime over silver, it does not perform as well in the fouling assays. Consequently, it was found that silver remained the suitable antifouling material owing to the pronounced level of biocidal activity within a limited period of time confirmed in the biofouling results.

The use of a field assay enables a true snapshot of the processes that envelope when testing the effects of biofouling on substrates. This can be seen in the initial deployment platform where geofouling was pronounced in the sample site – a property that might not be incurred when testing materials in the laboratory. This has proved a vital facet to the work, as the result is more representative to the overall fouling problem.

During the field studies, the materials have been deployed and subsequently exposed to a more complex environment previously detailed in the laboratory studies. The use of copper tape has provided a novel approach in the application of superhydrophobic materials for sensors, which can undergo prolific volumes of fouling and biofilm development. The environmental results also demonstrate that in order to effectively measure a material for antifouling application, environmental fluctuations can also be influential based on the environmental results observed through the use of the sensor suite. Consequently, the most successful plasticized PVC materials used in earlier stages of the thesis have undergone a more thorough 'test' which has also been observed in the gallium doped PVC which too has seen different responses to what was obtained in previous chapters.

The real benefits of these materials enable the end user to apply these developed materials as antifouling platforms in environmental monitoring, which could be applied in the following contexts, Figure 6.24.
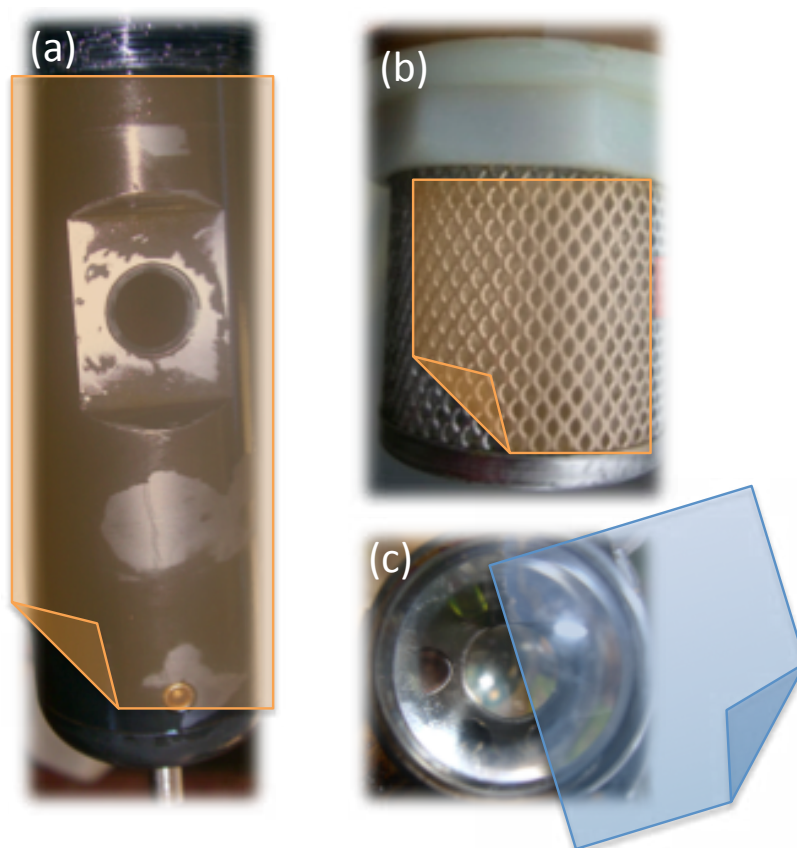
Figure 6.24: Figure showing potential antifouling material sites employed on a suite of sensor areas. (a) superhydrophobic copper coating for sensor house, (b) superhydrophobic copper mesh for fine filters and (c) plasticized/nanoparticle doped PVC for optical windows.

The real benefit of using such coatings enables the improvement of lifetimes and overall performance of the sensor suite. This can be in the form of data remaining stable for longer, reduction in maintenance, reduction in frequency of visits and overall reduced costs of ownership.

7

Conclusions & Recommendations

7.0 INTRODUCTION

This chapter features the conclusions and positive results from the work carried out. A summary of the novelty of the research is discussed with future aims, directions and recommendations for further work presented.

7.1 CONCLUSIONS AND RECOMMENDATIONS

The focus of this thesis has been the development and characterisation of antifouling coatings for application in the environmental and sensing field. The importance of developing an alternative material that has the ability to withstand the impact of biofouling over extended periods of time is desirable for sensing platforms and in further any environmentally deployed substrate. This was driven by the fresh and marine water fields following the outright ban of TBT in January 2008, where novel alternatives are required.

It has been shown in Chapters 3 and 5 that optically clear based coatings can be manufactured for subsequent doping of 'antifouling' agents. The results demonstrate that when plasticizers were incorporated into PVC a range of physical and chemical antifouling properties were induced. Gallium nanoparticles when concentrated and doped into sol-gels provided excellent antifouling results for optically clear applications. These developments would be suitable for optical based protection of sensing systems. Current technologies rely on mechanical cleaning systems that are energy withdrawing and increase cost of ownership. Furthermore, if these optically clear-based coatings were developed further a movement in the state-of-the-art technology could transpire.

Future work in the plasticization of PVC would benefit through the investigation of concentrations of plasticizers in different polymers. The deployment of these materials in the real environment is the real test and true to life experiment that can be carried out in this field of research. Therefore, the coating of these materials to live sensors would consequently benefit the work greatly.

Chapter 4 dealt with synthesis of a series of metal nanoparticles that could then be doped into materials for their use as an antifouling material. It was shown that the polyol reduction method could be extended to create a series of transition metal nanoparticles for their investigation as potential candidates in preventing biofouling. It was found that the polyol

method is versatile for this purpose and through careful synthesis nanometre dimension nanoparticles could be made.

Future work could involve fine-tuning the most successful metals, in particular to this thesis, gallium, germanium and selenium. The investigation of these metals for their size and shapes could prove to be of vital importance and novelty to this research area. If these metals were effectively characterised and either doped or immobilised onto surfaces then another state-of-the-art technology could develop for a range of applications not only in environmental sensing but also further afield.

Chapter 6 was of most interest as it involved the development of materials from previous nanotechnology findings. The superhydrophobic materials showed real promise as an antifouling material, particularly that they had been tested in the real environment. These developed materials were shown to coat sensors and substrates and enhance their performance in the field.

Future work would be to create meshes and filters made of the superhydrophobic material for their uses in antifouling materials. These could then be used as a primary protection in initial filtration treatments and also in sensor design. The final stage of this work would be to make the superhydrophobic material completely transparent. In doing so, this could then be applied to substrates that require transparent functionability.

8

Bibliography and Publications

8.0 BIBLIOGRAPHY

1.   Watnick P, Kolter R. *Journal of Bacteriology* **2000**;*182*:2675.

2.   Costerton J. *International journal of antimicrobial agents* **1999**;*11*:217-221.

3.   Costerton J, Cheng K, Geesey G, Ladd T, Nickel J, Dasgupta M, Marrie T. *Annual Reviews in Microbiology* **1987**;*41*:435-464.

4.   Staudigel H, Furnes H, McLoughlin N, Banerjee NR, Connell LB, Templeton A. *Earth-Science Reviews* **2008**;*89*:156-176.

5.   Altermann W, Kazmierczak J, Oren A, Wright D. *Geobiology* **2006**;*4*:147-166.

6.   Hall-Stoodley L, Costerton JW, Stoodley P. *Nature reviews.Microbiology* **2004**;*2*:95-108.

7.   The biofilm life cycle in three steps: attachment, growth of colonies, swarming phenomenon and detachment in clumps or "seeding dispersal." **2003** *2009 23/9* http://www.biofilm.montana.edu/.

8.   Jain DK. *Water research* **1995**;*29*:1869-1876.

9.   Cooksey K. *Biofilms: Science and Technology, pp137-147, Dordrecht, Kluwer Academic Press* **1992**.

10.   Busscher HJ, Norde W. *Journal of Biomedical Materials Research* **2000**;*50*:463-464.

11.   Hermansson M. *Colloids and Surfaces B: Biointerfaces,* **1999**;*14*:105-119.

12.   Castonguay MH, Van der Schaaf S, Koester W, Krooneman J, Van der Meer W, Harmsen H, Landini P. *Research in microbiology* **2006**;*157*:471-478.

13.   Azevedo N, Pacheco A, Keevil C, Vieira M. *Journal of applied microbiology* **2006**.

14.   Ma H, Winslow CJ, Logan BE. *Colloids and Surfaces B: Biointerfaces,* **2008**;*62*:232-237.

15.   Rasmussen TB, Givskov M. *Microbiology* **2006**;*152*:895.

16.   Fuqua WC, Winans SC, Greenberg EP. *Journal of Bacteriology* **1994**;*176*:269-275.

17.   Gorey C, Escobar IC, Gruden CL, Cai G. *Desalination* **2009**;*248*:99-105.

18.   Dobretsov S, Dahms HU, Yili H, Wahl M, Qian PY. *FEMS microbiology ecology* **2007**;*60*:177-188.

19.   Sintim HO, Smith JAI, Wang J, Nakayama S, Yan L. *Future Med.Chem.* **2010**;*2*:1005-1035.

20. Barraud N, Schleheck D, Klebensberger J, Webb JS, Hassett DJ, Rice SA, Kjelleberg S. *Journal of Bacteriology* **2009**;*191*:7333.

21. Finlay JA, Callow ME, Ista LK, Lopez GP, Callow JA. *Integrative and Comparative Biology* **2002**;*42*:1116.

22. Callow ME, Callow JE. *Biologist (London, England)* **2002**;*49*:10-14.

23. Callow M. *Biofouling(Print)* **1993**;*7*:313-327.

24. Molino P, Wetherbee R. *Biofouling* **2008**;*24*:365-379.

25. Sutherland I. *Microbiology* **2001**;*147*:3-9.

26. Stoodley P, Dodds I, Boyle J, Lappin-Scott H. *Journal of applied microbiology* **1999**;*85*:19S-28S.

27. Flemming H. *Biodeterioration and Biodegradation, DECHEMA Monographien* **1996**;*133*:311–317.

28. Flemming HC, Schaule G, Griebe T, Schmitt J, Tamachkiarowa A. *Desalination* **1997**;*113*:215-225.

29. Costerton JW, Geesey GG, Cheng KJ. *Scientific American* **1978**;*238*:86-95.

30. Costerton J, Marrie T, Cheng K. *Bacterial adhesion.Plenum Publishing Corp., New York* **1985**:3-43.

31. Characklis W, Turakhia M, Zelver N. *Biofilms* **1990**:265–340.

32. Characklis W. *Biofouling and Biocorrosion in Industrial Water Systems* **1991**:7–28.

33. Characklis W. *Biotechnology and bioengineering* **1981**;*23*:1923-1960.

34. William G. Characklis and P.A. Wilderer. Structure and function of biofilms. : John Wiley & Sons**, 1990**.

35. Mayer C, Moritz R, Kirschner C, Borchard W, Maibaum R, Wingender J, Flemming HC. *International journal of biological macromolecules* **1999**;*26*:3-16.

36. Cullimore DR. Microbiology of well biofouling. Ney York: CRC**, 1999**.

37. Sutherland IW. *Biotechnology Advances* **1994**;*12*:393-448.

38. Zhang X, Bishop P, Kupferle M. *Water Science & Technology* **1998**;*37*:345-348.

39. Malic S, Hill KE, Hayes A, Percival SL, Thomas DW, Williams DW. *Microbiology* **2009**;*155*:2603-2611.

40.   Alves M, Mota Vieira J, Álvares Pereira R, Pereira M, Mota M. *Water research* **2001***;35*:255-263.

41.   Butterfield PW, Camper AK, Biederman JA, Bargmeyer AM. *Water research* **2002***;36*:3898-3910.

42.   Flemming RG, Proctor RA, Cooper SL. *Journal of Biomaterials Science, Polymer Edition* **1999***;10*:679-697.

43.   Peter W. Atkins. Atkins: Physical chemistry, sixth and seventh edition. : Oxford University Press**, 1998**.

44.   Robinson D. *Naturwissenschaften* **1978***;65*:438-439.

45.   Fux C, Costerton J, Stewart P, Stoodley P. *Trends in microbiology* **2005***;13*:34-40.

46.   Chen X, Stewart P. *Applied Microbiology and Biotechnology* **2002***;59*:718-720.

47.   Atkins PW. Physical chemistry. : Oxford University Press Oxford**, 1998**.

48.   Kim I, Stabnikova E, Ivanov V. *Bioprocess and Biosystems Engineering* **2000***;22*:285-290.

49.   Kujundzic E, Cristina Fonseca A, Evans EA, Peterson M, Greenberg AR, Hernandez M. *Journal of microbiological methods* **2007***;68*:458-467.

50.   Schmitt J, Nivens D, White DC, Flemming HC. *Water Science and Technology* **1995***;32*:149-156.

51.   Taylor SW, Jaffé PR. *Water Resources Research ;26*.

52.   Christensen B. *Journal of Biotechnology* **1989***;10*:181-202.

53.   Christensen BE, Characklis WG. *Biofilms* **1990**:93-130.

54.   Potts M. *Microbiology and Molecular Biology Reviews* **1994***;58*:755.

55.   Roberson EB, Firestone MK. *Applied and Environmental Microbiology* **1992***;58*:1284.

56.   Fierer N, Schimel JP. *Soil Biology and Biochemistry* **2002***;34*:777-787.

57.   Ophir T, Gutnick DL. *Applied and Environmental Microbiology* **1994***;60*:740.

58.   A. H. Chamberlain. *Matrix polymers: the key to biofilm processes* **1997** .

59.   Kennedy A, Sutherland I. *Biotechnology and applied biochemistry* **1987***;9*:12-19.

60.   Harvey R. *Dissertation Abstracts International Part B: Science and Engineering.* **1981***;42*:1981.

61.   Kaplan D, Christiaen D, Arad SM. *Applied and Environmental Microbiology* **1987**;*53*:2953.

62.   Geesey GG, Lewandowski Z, Flemming HC. Biofouling and biocorrosion in industrial water systems. : CRC Press**, 1991**.

63.   Les A, Walker RW. *Water, Air, & Soil Pollution* **1984**;*23*:129-139.

64.   Jang LK, Nguyen DV, Kolostyak K, Geesey GG. *Water research* **1995**;*29*:2525-2529.

65.   Turakhia M, Cooksey K, Characklis W. *Applied and Environmental Microbiology* **1983**;*46*:1236.

66.   Higgins MJ, Novak JT. *Journal of Environmental Engineering* **1997**;*123*:479-485.

67.   Cameron S, Levin L, Zoller M, Wigler M. *Cell* **1988**;*53*:555-566.

68.   Dohse DM, Lion LW. *Environmental science & technology* **1994**;*28*:541-548.

69.   Evans L. Biofilms: Recent advances in their study and control. : CRC**, 2000**.

70.   Wolfaardt G, Lawrence J, Headley J, Robarts R, Caldwell D. *Microbial ecology* **1994**;*27*:279-291.

71.   Wolfaardt G, Lawrence J, Robarts R, Caldwell D. *Microbial ecology* **1998**;*35*:213-223.

72.   Späth R, Flemming H, Wuertz S. *Water Science & Technology* **1998**;*37*:207-210.

73.   Curtis A, Wilkinson C. *Materials Today* **2001**;*4*:22-28.

74.   Kerr A, Beveridge C, Cowling M, Hodgkiess T, Parr A, Smith M. *Journal of the Marine Biological Association of the UK* **2001**;*79*:357-359.

75.   Kerr A, Smith MJ, Cowling MJ, Hodgkiess T. *Materials & Design* **2001**;*22*:383-392.

76.   Curtis A, Wilkinson C. *Materials Today* **2001**;*4*:22-28.

77.   Lotz MM, Burdsal CA, Erickson HP, McClay DR. *The Journal of cell biology* **1989**;*109*:1795.

78.   Scheuerman TR, Camper AK, Hamilton MA. *Journal of colloid and interface science* **1998**;*208*:23-33.

79.   Wilkerson WR, Seegert C, Feinberg AW, Zhao LC, Callow JA, Callow ME, Brennan AB. *Polymer Preprints(USA)* **2001**;*42*:147-148.

80.   Grozea CM, Walker GC. *Soft Matter* **2009**;*5*:4088-4100.

81.   Fletcher MM. Bacterial adhesion: Molecular and ecological diversity. : Wiley-Liss**, 1996**.

82. Aldred N, Clare AS. *Functional surfaces in biology* **2009**:43-65.

83. Thompson R, Norton T, Hawkins S. *Hydrobiologia* **1998***;375*:203-216.

84. Schumacher JF, Carman ML, Estes TG, Feinberg AW, Wilson LH, Callow ME, Callow JA, Finlay JA, Brennan AB. *Biofouling* **2007***;23*:55-62.

85. Bers AV, Prendergast G, Zürn C, Hansson L, Head R, Thomason J. *Biology letters* **2006***;2*:88.

86. Bers AV, Wahl M. *Biofouling* **2004***;20*:43-51.

87. Efimenko K, Rackaitis M, Manias E, Vaziri A, Mahadevan L, Genzer J. *Nature materials* **2005***;4*:293-297.

88. Scardinoa A, Zhangc H, Cooksonc D, Lambc R, de Nysb R. *Biofouling* **2009***;25*:757-767.

89. Marmur A. *Angew.Chem* **2003***;115*:824-826.

90. Cassie A, Baxter S. *Transactions of the Faraday Society* **1944***;40*:546-551.

91. Neinhuis C, Barthlott W. *Annals of Botany* **1997***;79*:667.

92. Omae I. *Chemical reviews* **2003***;103*:3431-3448.

93. Turner GPA. Introduction to paint chemistry and principles of paint technology. : Chapman and Hall New York**, 1988**.

94. Chambers L, Stokes K, Walsh F, Wood R. *Surface & Coatings Technology* **2006***;201*:3642-3652.

95. Brady R. *International Coatings Expo and Technology Conference 1999(ICE'99)* **1999***;77*.

96. Berglin M, Lonn N, Gatenholm P. *Biofouling* **2003***;19 Suppl*:63-69.

97. Sarikaya M, Tamerler C, Jen AKY, Schulten K, Baneyx F. *Nature materials* **2003***;2*:577-585.

98. Wahl M. *Marine ecology progress series.Oldendorf* **1989***;58*:175-189.

99. Bi H, Zhong W, Meng S, Kong J, Yang P, Liu B. *Anal.Chem* **2006***;78*:3399-3405.

100. Davis AR, Targett NM, McConnell OJ, Young CM. *Bioorganic marine chemistry* **1989***;3*:85–114.

101. Ralston E, Swain G. *Bioinspiration & Biomimetics* **2009***;4*:015007.

102. Dalsin JL, Messersmith PB. *Materials Today* **2005***;8*:38-46.

103. Finlay JA, Krishnan S, Callow ME, Callow JA, Dong R, Asgill N, Wong K, Kramer EJ, Ober CK. *Langmuir* **2008***;24*:503-510.

104. Matsui Y, Nagaya K, Funahashi G, Goto Y, Yuasa A, Yamamoto H, Ohkawa K, Magara Y. *Biofouling* **2002***;18*:137-148.

105. TD Race and MA Kelly. *A comparison of metal leachate rate and zebra mussel control efficacy for coatings and materials* **1994** .

106. A. Skaja. Ecological Requirements of developing Dreissena polymorpha eggs **2009** *79:69-8 Arch. Hydrobiol. (Suppl.)*.

107. Beer D, Srinivasan R, Stewart PS. *Applied and Environmental Microbiology* **1994***;60*:4339-4344.

108. Park H, Hung Y, Chung D. *International journal of food microbiology* **2004***;91*:13-18.

109. Verween A, Vincx M, Degraer S. *International Biodeterioration & Biodegradation* **2009***;63*:523-528.

110. Roosenburg W, Rhoderick J, Block R, Kennedy V, Gullans S, Vreenegoor S, Rosenkranz A, Collette C. *Mar.Ecol.Prog.Ser* **1980***;3*:93-96.

111. Vosmaer A. Ozone, its manufacture, properties and uses. : D. Van Nostrand Co.**, 1916**.

112. Rafoth A, Gabriel S, Sacher F, Brauch H. *Journal of Chromatography A,* **2007***;1164*:74-81.

113. Schmid T, Panne U, Adams J, Niessner R. *Water research* **2004***;38*:1189-1196.

114. Rakotonirainy MS, Caillat L, Héraud C, Memet J, Tran QK. *Journal of Cultural Heritage* **2007***;8*:160-169.

115. Hastrup ACS, Green III F, Clausen CA, Jensen B. *International Biodeterioration & Biodegradation* **2005***;56*:173-177.

116. Tiller JC, Sprich C, Hartmann L. *Journal of Controlled Release* **2005***;103*:355-367.

117. Deng J, Wang L, Liu L, Yang W. *Progress in Polymer Science* **2009***;34*:156-193.

118. Nalli S, Cooper DG, Nicell JA. *Chemosphere* **2006***;65*:1510-1517.

119. Davda J, Labhasetwar V. *International Journal of Pharmaceutics,* **2002***;233*:51-59.

120. Speranza G, Gottardi G, Pederzolli C, Lunelli L, Canteri R, Pasquardini L, Carli E, Lui A, Maniglio D, Brugnara M, Anderle M. *Biomaterials* **2004***;25*:2029-2037.

121. Kerr A, Smith MJ, Cowling MJ. *Materials & Design,* **2003***;24*:247-253.

122. Corrosion Doctors **2007** *2008 01/23* *www.corrosiondoctors.org*.

123.   Steinberg PD, De Nys R, Kjelleberg S. *Journal of chemical ecology* **2002**;*28*:1935-1951.

124.   Goto R, Kado R, Muramoto K, Kamiya H. *Biofouling* **1992**;*6*:61-68.

125.   Cueto M, Darias J, San-Martin A, Rovirosa J. *Journal of natural products* **1997**;*60*:279–281.

126.   De Nys R, Steinberg P, Willemsen P, Dworjanyn S, Gabelish C, King R. *Biofouling* **1995**;*8*:259-271.

127.   Manefield M, de Nys R, Kumar N, Read R, Givskov M, Steinberg P, Kjelleberg S. *Microbiology (Reading, England)* **1999**;*145 (Pt 2)*:283-291.

128.   Shimizu Y. *Chemical reviews* **1993**;*93*:1685-1698.

129.   Yasumoto T, Murata M. *Chemical reviews* **1993**;*93*:1897-1909.

130.   Murata M, Naoki H, Matsunaga S, Satake M, Yasumoto T. *Journal of the American Chemical Society* **1994**;*116*:7098-7107.

131.   Okano K, Shimizu K, Satuito C, Fusetani N. *The Journal of experimental biology* **1996**;*199*:2131-2137.

132.   Murugan E, Vimala G. *Journal of colloid and interface science* **2011**;*357*:354-365.

133.   Valappil SP, Ready D, Neel E, Pickup DM, Chrzanowski W, ODell LA, Newport RJ, Smith ME, Wilson M, Knowles JC. *Advanced Functional Materials* **2008**;*18*:732.

134.   Williams A, Sugandhi E, Macri R, Falkinham J,III, Gandour R. *Journal of Antimicrobial Chemotherapy* **2007**;*59*:451-458.

135.   Chapman J, Weir E, Regan F. *Colloids and Surfaces B: Biointerfaces* **2010**;*78*:208-216.

136.   Kim M, Byun JW, Shin DS, Lee YS. *Materials Research Bulletin* **2009**;*44*:334-338.

137.   Zhang Y, Tian J, Liang H, Nan J, Chen Z, Li G. *Journal of Environmental Sciences* **2011**;*23*:529-536.

138.   Chapman J, Lawlor A, Weir E, Quilty B, Regan F. *Journal of Membrane Science* **2010**;*365*:180-187.

139.   Katano H, Tsukatani T. *Bulletin of the Chemical Society of Japan* **2010**;*83*:190-194.

140.   Roh JY, Jung IH, Lee JY, Choi J. *Toxicology* **2007**;*237*:126-133.

141.   Kapanen A, Stephen J, Brueggemann J, Kiviranta A, White D, Itävaara M. *Chemosphere* **2007**;*67*:2201-2209.

142.   Yan H, Pan G. *Chemosphere* **2004**;*55*:1281-1285.

143. Call DJ, Markee TP, Geiger DL, Brooke LT, VandeVenter FA, Cox DA, Genisot KI, Robillard KA, Gorsuch JW, Parkerton TF. *Environmental Toxicology and Chemistry* **2001**;*20*:1798-1804.

144. Narasimhan B, Ohlan S, Ohlan R, Judge V, Narang R. *European journal of medicinal chemistry* **2009**;*44*:689-700.

145. Mochida K, Gomyoda M, Fujita T. *Bulletin of environmental contamination and toxicology* **1996**;*56*:635-637.

146. Whitehead K, Mitragotri S. *Pharmaceutical research* **2008**;*25*:1412-1419.

147. Liu J, Shimizu K, Kondo R. *Chemistry & Biodiversity* **2009**;*6*:503-512.

148. Basse N, Papapostolou D, Pagano M, Reboud-Ravaux M, Bernard E, Felten AS, Vanderesse R. *Bioorganic & medicinal chemistry letters* **2006**;*16*:3277-3281.

149. Nalli S, Cooper DG, Nicell JA. *Science of the Total Environment* **2006**;*366*:286-294.

150. Kim H, Park BS, Lee KG, Choi CY, Jang SS, Kim YH, Lee SE. *J.Agric.Food Chem* **2005**;*53*:8537-8541.

151. Azenha M, Vasconcelos MT, Cabral JPS. *Environmental Toxicology and Chemistry* **1995**;*14*:369-373.

152. Bayoudh S, Othmane A, Bettaieb F, Bakhrouf A, Ouada HB, Ponsonnet L. *Materials Science & Engineering C* **2006**;*26*:300-305.

153. Adkins J, Mera A, Roe-Short M, Pawlikowski G, Brady R. *Progress in Organic Coatings* **1996**;*29*:1-5.

154. Bae TH, Tak TM. *Journal of Membrane Science* **2005**;*249*:1-8.

155. Bayoudh S, Othmane A, Bettaieb F, Bakhrouf A, Ouada HB, Ponsonnet L. *Materials Science and Engineering: C* **2006**;*26*:300-305.

156. Vafaei S, Borca-Tasciuc T, Podowski M, Purkayastha A, Ramanath G, Ajayan P. *Nanotechnology* **2006**;*17*:2523-2527.

157. DJW Moriarty. *Methodology for determining biomass and productivity of microorganisms in detrital food webs* **1987** .

158. Vrouwenvelder HS, van Paassen JAM, Folmer HC, Hofman JAMH, Nederlof MM, van der Kooij D. *Desalination* **1998**;*118*:157-166.

159. Chandra J, Patel JD, Li J, Zhou G, Mukherjee PK, McCormick TS, Anderson JM, Ghannoum MA. *Applied and Environmental Microbiology* **2005**;*71*:8795.

160. Lee J, Kim IS. *Desalination* **2011**;*273*:118-126.

161.   Little B, Wagner P, Ray R, Pope R, Scheetz R. *Journal of Industrial Microbiology and Biotechnology* **1991**;*8*:213-221.

162.   Callow JA, Osborne MP, Callow ME, Baker F, Donald AM. *Colloids and Surfaces B: Biointerfaces* **2003**;*27*:315-321.

163.   Dempsey M. *Marine Biology* **1981**;*61*:305-315.

164.   Holt KB, Bard AJ. *Biochemistry* **2005**;*44*:13214-13223.

165.   Ikada E. *Journal of Polymers and the Environment* **1999**;*7*:197-201.

166.   Lazarova V, Manem J. *Water research* **1995**;*29*:2227-2245.

167.   Lee WF, Tsao KT. *Journal of Applied Polymer Science* **2006**;*100*:3653-3661.

168.   Stewart PS, Murga R, Srinivasan R, de Beer D. *Water research* **1995**;*29*:2006-2009.

169.   Beech IB, Smith JR, Steele AA, Penegar I, Campbell SA. *Colloids and Surfaces B: Biointerfaces* **2002**;*23*:231-247.

170.   Shrivastava S, Bera T, Roy A, Singh G, Ramachandrarao P, Dash D. *Nanotechnology* **2007**;*18*:225103.

171.   Morones JR, Elechiguerra JL, Camacho A, Holt K, Kouri JB, Ramirez JT, Yacaman MJ. *Nanotechnology* **2005**;*16*:2346-2353.

172.   Dynes JJ, Tyliszczak T, Araki T, Lawrence JR, Swerhone GDW, Leppard GG, Hitchcock AP. *Environ.Sci.Technol* **2006**;*40*:1556-1565.

173.   Denkhaus E, Meisen S, Telgheder U, Wingender J. *Microchimica Acta* **2007**;*158*:1-27.

174.   Trainor TP, Templeton AS, Eng PJ. *Journal of Electron Spectroscopy and Related Phenomena* **2006**;*150*:66-85.

175.   Al-Bataineh SA, Britcher LG, Griesser HJ. *Surface Science* **2006**;*600*:952-962.

176.   Hansma HG, Pietrasanta LI, Auerbach ID, Sorenson C, Golan R, Holden PA. *Journal of Biomaterials Science, Polymer Edition* **2000**;*11*:675-683.

177.   van der Aa BC, Michel RM, Asther M, Zamora MT, Rouxhet PG, Dufrêne YF. *Langmuir* **2001**;*17*:3116-3119.

178.   Whitehead KA, Deisenroth T, Preuss A, Liauw CM, Verran J. *Colloids and Surfaces B: Biointerfaces* **2011**;*82*:483-489.

179.   Beech IB, Sunner JA, Hiraoka K. *International microbiology* **2005**;*8*:157.

180.   Pradier C, Rubio C, Poleunis C, Bertrand P, Marcus P, Compère C. *J.Phys.Chem.B* **2005**;*109*:9540-9549.

181.   Christensen BE. *Journal of Biotechnology* **1989***;10*:181-202.

182.   Guan Y, Kisaalita W. *Colloids and Surfaces B: Biointerfaces* **2011***;84*:35-43.

183.   Visick KL, Fuqua C. *Journal of Bacteriology* **2005***;187*:5507.

184.   Wells DA, Weil DA. *Pharma Genomics* **2003***;21*:522-538.

185.   Peterson GL. *Analytical Biochemistry* **1977***;83*:346-356.

186.   Oosthuizen MC, Steyn B, Theron J, Cosette P, Lindsay D, von Holy A, Brozel VS. *Applied and Environmental Microbiology* **2002***;68*:2770.

187.   Lahm HW, Langen H. *Electrophoresis* **2000***;21*:2105-2114.

188.   Singh RP, Shukla MK, Mishra A, Kumari P, Reddy CRK, Jha B. *Carbohydrate Polymers* **2011***;84*:1019-1026.

189.   Wiegand I, Hilpert K, Hancock REW. *Nature Protocols* **2008***;3*:163-175.

190.   Sambhy V, MacBride MM, Peterson BR, Sen A. *Journal of the American Chemical Society* **2006***;128*:9798-9808.

191.   Lok CN, Ho CM, Chen R, He QY, Yu WY, Sun H, Tam PKH, Chiu JF, Che CM. *J.Proteome Res* **2006***;5*:916-924.

192.   Zeng F, Hou C, Wu S, Liu X, Tong Z, Yu S. *Nanotechnology* **2007***;18*:055605.

193.   Qi L, Xu Z, Jiang X, Hu C, Zou X. *Carbohydrate research* **2004***;339*:2693-2700.

194.   Pal S, Tak YK, Song JM. *Applied and Environmental Microbiology* **2007***;73*:1712-1720.

195.   Herrero M, Quemener E, Ulve S, Reinecke H, Mijangos C, Grohens Y. *Journal of Adhesion Science and Technology* **2006***;20*:183-195.

196.   Voccia S, Jerome C, Detrembleur C, Leclere P, Gouttebaron R, Hecq M, Gilbert B, Lazzaroni R, Jerome R. *Chem.Mater* **2003***;15*:923-927.

197.   Cioffi N, Ditaranto N, Torsi L, Picca RA, De Giglio E, Sabbatini L, Novello L, Tantillo G, Bleve-Zacheo T, Zambonin PG. *Analytical and bioanalytical chemistry* **2005***;382*:1912-1918.

198.   Image J **2011** *24.01.2009* ***http://rsbweb.nih.gov/ij/***.

199.   Tsai CL, Schurman DJ, Smith RL. *Journal of Orthopaedic Research* **1988***;6*.

200.   Wiley B, Herricks T, Sun Y, Xia Y. *Nano Letters* **2004***;4*:2057.

201.   Peltonen LI, Kinnari TJ, Aarnisalo AA, Kuusela P, Jero J. *Acta Oto-Laryngologica* **2007***;127*:587-593.

202.   Dubois M, Gilles K, Hamilton J, Rebers P, Smith F. *Analytical Chemistry* **1956**;*28*:350-356.

203.   Larmour IA, Bell SEJ, Saunders GC. *Angewandte Chemie* **2007**;*119*:1740-1742.

204.   Castritsi-Catharios J, Bourdaniotis N, Persoone G. *Chemosphere* **2007**;*67*:1127-1132.

205.   Mirabedini SM, Pazoki S, Esfandeh M, Mohseni M, Akbari Z. *Progress in Organic Coatings* **2006**;*57*:421-429.

206.   Yoldas B, O'Keeffe T. *Applied Optics* **1979**;*18*:3133-3138.

207.   Berto D, Giani M, Covelli S, Boscolo R, Cornello M, Macchia S, Massironi M. *Science of The Total Environment* **2006**;*368*:298-305.

208.   Wilkes CE, Summers JW, Daniels CA, Berard MT. PVC handbook. : Hanser Gardner Pubns**, 2005**.

209.   Rahman M, Brazel CS. *Polymer Degradation and Stability* **2006**;*91*:3371-3382.

210.   Pfaendner R. *Polymer Degradation and Stability* **2006**;*91*:2249-2256.

211.   Krauskopf L. *Marcel Dekker, Encyclopedia of PVC.* **1988**;*2*:143-261.

212.   Akovali G, Feldman D, Banerjee B. *Polymers in construction* **2005**:35.

213.   Murphy J. Additives for plastics handbook. : Elsevier Science Ltd**, 2001**.

214.   Määttä J, Koponen H-, Kuisma R, Kymäläinen H-, Pesonen-Leinonen E, Uusi-Rauva A, Hurme K-, Sjöberg A-, Suvanto M, Pakkanen TA. *Applied Surface Science* **2007**;*253*:5003-5010.

215.   Burgos N, Jiménez A. *Polymer Degradation and Stability* **2009**;*94*:1473-1478.

216.   Li W, Yuan M, Yang M. *European Polymer Journal* **2006**;*42*:1396-1402.

217.   Yang C, Wu GM. *Materials Chemistry and Physics* **2009**;*114*:948-955.

218.   Karal O, Elif Hamurcu E, Baysal BM. *Polymer* **1997**;*38*:6071-6078.

219.   Sanchez AC, Popineau Y, Mangavel C, Larre C, Gueguen J. *J.Agric.Food Chem* **1998**;*46*:4539-4544.

220.   Haishima Y, Seshimo F, Higuchi T, Yamazaki H, Hasegawa C, Izumi S, Makino T, Nakahashi K, Ito R, Inoue K, Yoshimura Y, Saito K, Yagami T, Tsuchiya T, Nakazawa H. *International journal of pharmaceutics* **2005**;*298*:126-142.

221.   Giovambattista N, Debenedetti PG, Rossky PJ. *Proceedings of the National Academy of Sciences* **2009**;*106*:15181.

222. Kiso Y, Kon T, Kitao T, Nishimura K. *Journal of Membrane Science* **2001**;*182*:205-214.

223. Marchal F, Nardello-Rataj V, Chailloux N, Aubry J, Tiddy GJT. *Journal of colloid and interface science* **2008**;*321*:177-185.

224. Tsao YH, Yang S, Evans DF, Wennerstroem H. *Langmuir* **1991**;*7*:3154-3159.

225. Seguchi M. *Cereal Chem* **1985**;*62*:166-169.

226. Ellison A, Zisman W. *The Journal of physical chemistry* **1954**;*58*:260-265.

227. Marmur A. *Langmuir* **2006**;*22*:1400-1402.

228. Miwa M, Nakajima A, Fujishima A, Hashimoto K, Watanabe T. *Langmuir* **2000**;*16*:5754-5760.

229. Triandafillu K, Balazs DJ, Aronsson B-, Descouts P, Tu Quoc P, van Delden C, Mathieu HJ, Harms H. *Biomaterials* **2003**;*24*:1507-1518.

230. Boussu K, Van der Bruggen B, Volodin A, Snauwaert J, Van Haesendonck C, Vandecasteele C. *Journal of colloid and interface science* **2005**;*286*:632-638.

231. Rahmawan Y, Jang KJ, Moon MW, Lee KR, Suh KY.

232. Nakajima A, Hashimoto K, Watanabe T. *Monatshefte für Chemie/Chemical Monthly* **2001**;*132*:31-41.

233. Yoshimitsu Z, Nakajima A, Watanabe T, Hashimoto K. *Langmuir* **2002**;*18*:5818-5822.

234. Costa L, Luda MP, Trossarelli L. *Polymer Degradation and Stability* **2000**;*68*:67-74.

235. Costa L, Camino G. *Polymer Degradation and Stability* **1985**;*12*:125-129.

236. Costa L, Camino G, Trossarelli L. *Polymer Degradation and Stability* **1983**;*5*:267-273.

237. Gusev MN, Kissin YV, Voronovitskii MM, Berlin AA. *Petroleum Chemistry U.S.S.R.* **1968**;*8*:138-145.

238. Razumovskii LP, Aseyeva TM, Kulikova ZK, Khokhlova LL, Zaikov GY. *Polymer Science U.S.S.R.* **1987**;*29*:1009-1014.

239. Regan F, Meaney M, Vos JG, MacCraith BD, Walsh JE. *Analytica Chimica Acta* **1996**;*334*:85-92.

240. Meiron TS, Marmur A, Saguy IS. *Journal of colloid and interface science* **2004**;*274*:637-644.

241. Pries A, Secomb T, Gaehtgens P. *Pflügers Archiv European Journal of Physiology* **2000**;*440*:653-666.

242.   Vink H, Duling BR. *Circulation research* **1996***;79*:581.

243.   Smith ML, Long DS, Damiano ER, Ley K. *Biophysical journal* **2003***;85*:637-645.

244.   Squire JM, Chew M, Nneji G, Neal C, Barry J, Michel C. *Journal of structural biology* **2001***;136*:239-255.

245.   Naruhashi K, Tamai I, Sai Y, Suzuki N, Tsuji A. *Journal of Pharmacy and Pharmacology* **2001***;53*:73-81.

246.   Bhasin C, Panchal DG. *Phosphorus, Sulfur, and Silicon and the Related Elements* **2004***;179*:1545-1568.

247.   Tarbell J, Pahakis M. *Journal of internal medicine* **2006***;259*:339-350.

248.   Novak AF, Solar JM, Mod RR, Magne FC, Skau EL. *Applied and Environmental Microbiology* **1969***;18*:1050.

249.   Iconomopoulou SM, Andreopoulou AK, Soto A, Kallitsis JK, Voyiatzis GA. *Journal of Controlled Release* **2005***;102*:223-233.

250.   Buchardt CN, Johnsson JE, Kiil S. *Fuel* **2006***;85*:725-735.

251.   Su W, Chen Y, Lin F. *Acta Biomaterialia* **2010***;6*:3044-3055.

252.   Faouzi MA, Dine T, Luyckx M, Gressier B, Goudaliez F, Mallevais ML, Brunet C, Cazin M, Cazin JC. *International journal of pharmaceutics* **1994***;105*:89-93.

253.   Thiboutot D, Thieroff-Ekerdt R, Graupe K. *Journal of the American Academy of Dermatology* **2003***;48*:836-845.

254.   Matthies C, Schink B. *FEMS microbiology letters* **1993***;111*:177-182.

255.   Sivakumar PM, Balaji S, Prabhawathi V, Neelakandan R, Manoharan PT, Doble M. *Carbohydrate Polymers* **2010***;79*:717-723.

256.   Charnock C, Brudeli B, Klaveness J. *European Journal of Pharmaceutical Sciences* **2004***;21*:589-596.

257.   Ishihara K, Nomura H, Mihara T, Kurita K, Iwasaki Y, Nakabayashi N. *Journal of Biomedical Materials Research Part A* **1998***;39*:323-330.

258.   Strathmann M, Wingender J, Flemming H. *Journal of microbiological methods* **2002***;50*:237-248.

259.   Yang Y, Sreenivasan PK, Subramanyam R, Cummins D. *Applied and Environmental Microbiology* **2006***;72*:6734.

260.   Volatility and solvent extractability of plasticizers **1997** *2010 12*.

261. Lee County Mosquito Control District. Controlled delivery compositions and processes for treating organisms in a column of water or land US Patent No. US6337078 B, 2002.

262. Thomsen L. *Marine ecology progress series.Oldendorf* **1991***;71*:301-306.

263. Gruetzmann R, Wagner KG. *European Journal of Pharmaceutics and Biopharmaceutics* **2005***;60*:159-162.

264. Bando H, McGinity JW. *International journal of pharmaceutics* **2006***;323*:11-17.

265. Fisk AT, Tomy GT, Muir DCG. *Environmental Toxicology and Chemistry* **1999***;18*:2894-2902.

266. Sverdrup LE, Hartnik T, Mariussen E, Jensen J. *Chemosphere* **2006***;64*:96-103.

267. Tang WZ, Wang F. *Chemosphere* **2010***;78*:914-921.

268. Wang P, Udeani GO, Johnston TP. *International journal of pharmaceutics* **1995***;114*:177-184.

269. Kang Y, Meyerhoff ME. *Analytica Chimica Acta* **2006***;565*:1-9.

270. Ertan-Lamontagne MC, Parthum KA, Seitz WR, Tomellini SA. *Applied Spectroscopy* **1994***;48*:1539-1544.

271. Fankhauser-Noti A, Grob K. *Trends in Food Science & Technology* **2006***;17*:105-112.

272. Demssie G, Belay SM. Method and compound for the prophylaxis or treatment of an immunodeficiency condition, such as AIDS. US Patent No. US2003/22159 A1, 2003.

273. Middleton AJ, Smith EB. *Proceedings of the Royal Society of London.Series B, Biological Sciences* **1976***;193*:173-190.

274. Jennings VLK, Rayner-Brandes MH, Bird DJ. *Water research* **2001***;35*:3448-3456.

275. Kermanshahi pour A, Cooper DG, Mamer OA, Maric M, Nicell JA. *Chemosphere* **2009***;77*:258-263.

276. Melliou E, Chinou I. *J.Agric.Food Chem* **2005***;53*:8987-8992.

277. Bonora S, Ercoli L, Torreggiani A, Fini G. *Thermochimica Acta* **2002***;385*:51-61.

278. Lee AG. *Biochimica et biophysica acta* **1977***;472*:285-344.

279. Raunkjær K, Hvitved-Jacobsen T, Nielsen PH. *Water research* **1994***;28*:251-262.

280. Sapan C, Lundblad R, Price N. *Biotechnology and applied biochemistry* **1999***;29*:99-108.

281. Aguilera A, Souza-Egipsy V, San Martín-Úriz P, Amils R. *Aquatic Toxicology* **2008***;88*:257-266.

282. Huang JM, Nakade K, Kondo M, Yang CS, Fukuyama Y. *Chemical & pharmaceutical bulletin* **2002**;*50*:133-136.

283. Gabel B, Thiéry D. *Journal of chemical ecology* **1996**;*22*:161-171.

284. Chen H, Yuan L, Song W, Wu Z, Li D. *Progress in Polymer Science* **2008**;*33*:1059-1087.

285. Unsworth LD, Tun Z, Sheardown H, Brash JL. *Journal of colloid and interface science* **2006**;*296*:520-526.

286. Gan LH, Ooi KS, Goh SH, Gan LM, Leong YC. *European Polymer Journal* **1995**;*31*:719-724.

287. Cardoso VM, Solano AGR, Prado MAF, Nunan EdA. *Journal of pharmaceutical and biomedical analysis* **2006**;*42*:630-634.

288. Amatya, S, and Tuladhar S. M. *Pakistan Journal of Scientific and Industrial Research* **2005**;*48*:212-215.

289. Neyens E, Baeyens J, Dewil R, Deheyder B. *Journal of Hazardous Materials* **2004**;*106*:83-92.

290. Van Pett K, Schurman D, Smith RL. *Journal of Orthopaedic Research* **1990**;*8*.

291. Meek M, Chan P. *Journal of Environmental Science and Health, Part C* **1994**;*12*:179-194.

292. Chawla A, Hinberg I. *Artificial Cells, Blood Substitutes and Biotechnology* **1991**;*19*:761-783.

293. Staples CA, Adams WJ, Parkerton TF, Gorsuch JW, Biddinger GR, Reinert KH. *Environmental Toxicology and Chemistry* **1997**;*16*:875-891.

294. Hoffman DJ. Handbook of ecotoxicology. : CRC**, 2003**.

295. Brewer RH. *Biological Bulletin* **1984**;*166*:11-21.

296. Kamaya Y, Tsuboi S, Takada T, Suzuki K. *Archives of Environmental Contamination and Toxicology* **2006**;*51*:537-541.

297. Reddy KR, Sin BC, Ryu KS, Kim J, Chung H, Lee Y. *Synthetic Metals* **2009**;*159*:595-603.

298. Barnes WL, Dereux A, Ebbesen TW. *Nature* **2003**;*424*:824-830.

299. Lane N. *Journal of Nanoparticle Research* **2001**;*3*:95-103.

300. Sharma VK, Yngard RA, Lin Y. *Advances in Colloid and Interface Science* **2009**;*145*:83-96.

301. Chen X, Schluesener HJ. *Toxicology letters* **2008**;*176*:1-12.

302. Shahverdi AR, Fakhimi A, Shahverdi HR, Minaian S. *Nanomedicine: nanotechnology, biology, and medicine* **2007**;*3*:168-171.

303. Zhang W, Qiao X, Chen J. *Colloids and Surfaces A: Physicochemical and Engineering Aspects* **2007**;*299*:22-28.

304. Cushing BL, Kolesnichenko VL, O'Connor CJ. *Chemical reviews* **2004**;*104*:3893-3946.

305. R. P. Feynman. *Plenty of Room at the Bottom* **1960** .

306. Shankar SS, Ahmad A, Sastry M. *Biotechnology progress* **2003**;*19*:1627-1631.

307. Hahn H, Padmanabhan K. *Nanostructured materials* **1995**;*6*:191-200.

308. H. Y. Lin and YF Chen. *An alternative mechanism for surface enhanced spectroscopy: second harmonic surface plasmon resonance* **2005** .

309. Hyeon T, Lee SS, Park J, Chung Y, Na HB. *J.Am.Chem.Soc* **2001**;*123*:12798-12801.

310. Alivisatos A. *Science* **1996**;*271*:933.

311. Komarneni S, Li D, Newalkar B, Katsuki H, Bhalla AS. *Langmuir* **2002**;*18*:5959-5962.

312. Dhas NA, Raj CP, Gedanken A. *Chem.Mater* **1998**;*10*:1446-1452.

313. Kumar RV, Mastai Y, Diamant Y, Gedanken A. *Journal of Materials Chemistry* **2001**;*11*:1209-1213.

314. Vitulli G, Bernini M, Bertozzi S, Pitzalis E, Salvadori P, Coluccia S, Martra G. *Chem.Mater* **2002**;*14*:1183-1186.

315. Huang H, Yan F, Kek Y, Chew C, Xu G, Ji W, Oh P, Tang S. *Langmuir* **1997**;*13*:172-175.

316. Liu Z, Bando Y, Tang C. *Chemical Physics Letters* **2003**;*372*:179-182.

317. Casella IG, Cataldi TRI, Guerrieri A, Desimoni E. *Analytica Chimica Acta* **1996**;*335*:217-225.

318.   Lisiecki I, Filankembo A, Sack-Kongehl H, Weiss K, Pileni MP, Urban J. *Physical Review B* **2000**;*61*:4968-4974.

319. Pileni M, Ninham B, Gulik-Krzywicki T, Tanori J, Lisiecki I, Filankembo A. *Advanced Materials* **1999**;*11*:1358-1362.

320. Yeh MS, Yang YS, Lee YP, Lee HF, Yeh YH, Yeh CS. *J.Phys.Chem.B* **1999**;*103*:6851-6857.

321. Mercier D, Lévy JCS, Viau G, Fievet-Vincent F, Fievet F, Toneguzzo P, Acher O. *Physical Review B* **2000**;*62*:532-544.

322. Fievet F, Fievet-Vincent F, Lagier JP, Dumont B, Figlarz M. *Journal of Materials Chemistry* **1993**;*3*:627-632.

323. Gedanken A. *Ultrasonics sonochemistry* **2004**;*11*:47-55.

324. Grinstaff M, Cichowlas A, Choe SB, Suslick K. *Ultrasonics* **1992**;*30*:168-172.

325. Landau M, Vradman L, Herskowitz M, Koltypin Y, Gedanken A. *Journal of Catalysis* **2001**;*201*:22-36.

326. Suslick KS, Hammerton DA, Cline RE. *Journal of the American Chemical Society* **1986**;*108*:5641-5642.

327. Pol V, Reisfeld R, Gedanken A. *Chem.Mater* **2002**;*14*:3920-3924.

328. Avivi Levi S, Gedanken A. *Ultrasonics sonochemistry* **2005**;*12*:405-409.

329. Avivi S, Nitzan Y, Dror R, Gedanken A. *J.Am.Chem.Soc* **2003**;*125*:15712-15713.

330. Henglein A. *Chemical reviews* **1989**;*89*:1861-1873.

331. Belloni J. *Current Opinion in Colloid & Interface Science* **1996**;*1*:184-196.

332. Jana NR, Gearheart L, Murphy CJ. *Langmuir* **2001**;*17*:6782-6786.

333. Swihart MT. *Current Opinion in Colloid & Interface Science* **2003**;*8*:127-133.

334. Sibbald MS, Chumanov G, Cotton TM. *J.Phys.Chem* **1996**;*100*:4672-4678.

335. Sylvestre JP, Kabashin AV, Sacher E, Meunier M, Luong JHT. *J.Am.Chem.Soc* **2004**;*126*:7176-7177.

336. Dolgaev SI, Simakin AV, Voronov VV, Shafeev GA, Bozon-Verduraz F. *Applied Surface Science* **2002**;*186*:546-551.

337. Kabashin AV, Meunier M, Kingston C, Luong JHT. *J.Phys.Chem.B* **2003**;*107*:4527-4531.

338. Tsuji T, Kakita T, Tsuji M. *Applied Surface Science* **2003**;*206*:314-320.

339. Mafune F, Kohno J, Takeda Y, Kondow T, Sawabe H. *J.Phys.Chem.B* **2000**;*104*:9111-9117.

340. Wang L, Chen X, Zhan J, Chai Y, Yang C, Xu L, Zhuang W, Jing B. *J.Phys.Chem.B* **2005**;*109*:3189-3194.

341. Feldmann C. *Solid State Sciences* **2005**;*7*:868-873.

342. Andrade Sales E, Benhamida B, Caizergues V, Lagier JP, Fiévet F, Bozon-Verduraz F. *Applied Catalysis A: General* **1998**;*172*:273-283.

343. Feldmann C. *Advanced Materials* **2001**;*13*:1301-1303.

344. Feldmann C, Jungk HO. *Angewandte Chemie International Edition* **2001**;*40*:359-362.

345. Solomon SD, Bahadory M, Jeyarajasingam AV, Rutkowsky SA, Bortiz C, Mulfinger L. *Journal of chemical education* **2007**;*84*:322.

346. Mock J, Barbic M, Smith D, Schultz D, Schultz S. *The Journal of chemical physics* **2002**;*116*:6755.

347. Sivaraman SK, Elango I, Kumar S, Santhanam V. *Current science* **2009**;*97*:1055.

348. Radomski A, Jurasz P, Alonso-Escolano D, Drews M, Morandi M, Malinski T, Radomski MW. *British journal of pharmacology* **2005**;*146*:882-893.

349. Van Hyning DL, Klemperer WG, Zukoski CF. *Langmuir* **2001**;*17*:3120-3127.

350. Osby JO, Heinzman SW, Ganem B. *Journal of the American Chemical Society* **1986**;*108*:67-72.

351. Law M, Goldberger J, Yang P. **2004**.

352. Yu K, Kim DJ, Chung HS, Liang H. *Materials Letters* **2003**;*57*:3992-3997.

353. Zhu H, Lin Y, Yin Y. *Journal of colloid and interface science* **2004**;*277*:100-103.

354. Jain P, Pradeep T. *Biotechnology and bioengineering* **2005**;*90*:59-63.

355. Sondi I, Salopek-Sondi B. *Journal of colloid and interface science* **2004**;*275*:177-182.

356. Xu J, Han X, Liu H, Hu Y. *Colloids and Surfaces A: Physicochemical and Engineering Aspects* **2006**;*273*:179-183.

357. Seitz O, Chehimi MM, Cabet-Deliry E, Truong S, Felidj N, Perruchot C, Greaves SJ, Watts JF. *Colloids and Surfaces A: Physicochemical and Engineering Aspects* **2003**;*218*:225-239.

358. Brause R, Moeltgen H, Kleinermanns K. *Applied Physics B: Lasers and Optics* **2002**;*75*:711-716.

359. Li C, Cai W, Li Y, Hu J, Liu P. *J.Phys.Chem.B* **2006**;*110*:1546-1552.

360. Cobley CM, Rycenga M, Zhou F, Li ZY, Xia Y. *Angewandte Chemie* **2009**;*121*:4918-4921.

361. Grosso D, Sermon PA. *Journal of Materials Chemistry* **2000**;*10*:359-363.

362. Ghosh D, Pradhan S, Chen W, Chen S. *Chem.Mater* **2008**;*20*:1248-1250.

363. Baia L, Simon S. **2007**.

364.   Lopez R, Feldman L, Haglund Jr R. *Physical Review Letters* **2004**;*93*:177403.

365.   Baia M, Toderas F, Baia L, Popp J, Astilean S. *Chemical Physics Letters* **2006**;*422*:127-132.

366.   Hakuli A, Harlin M, Backman L, Krause A. *Journal of Catalysis* **1999**;*184*:349-356.

367.   Wang S, Murata K, Hayakawa T, Hamakawa S, Suzuki K. *Applied Catalysis A: General* **2000**;*196*:1-8.

368.   Xu H, Lou T, Li Y. *Inorganic Chemistry Communications* **2004**;*7*:666-668.

369.   Mie G. **1908**;*25*:377-445.

370.   Xu X, Yang Q, Wang Y, Yu H, Chen X, Jing X. *European polymer journal* **2006**;*42*:2081-2087.

371.   Ng C, Schadler L, Siegel R. *Nanostructured Materials* **1999**;*12*:507-510.

372.   Cui H, Xu Y, Zhang ZF. *Anal.Chem* **2004**;*76*:4002-4010.

373.   Gao Y, Jiang P, Song L, Liu L, Yan X, Zhou Z, Liu D, Wang J, Yuan H, Zhang Z. *Journal of Physics D: Applied Physics* **2005**;*38*:1061-1067.

374.   Uchino K, Sadanaga E, Hirose T. *J.Am.Ceram.Soc.* **1989**;*72*:1555-1558.

375.   Couto GG, Klein JJ, Schreiner WH, Mosca DH, de Oliveira AJA, Zarbin AJG. *Journal of colloid and interface science* **2007**;*311*:461-468.

376.   Zhang F, Chan SW, Spanier JE, Apak E, Jin Q, Robinson RD, Herman IP. *Applied Physics Letters* **2002**;*80*:127.

377.   Yang C, Liu P, Ho Y, Chiu C, Chao K. *Chem.Mater* **2003**;*15*:275-280.

378.   Klaus T, Joerger R, Olsson E, Granqvist CG. *Proceedings of the National Academy of Sciences of the United States of America* **1999**;*96*:13611.

379.   Sosa IO, Noguez C, Barrera RG. *J.Phys.Chem.B* **2003**;*107*:6269-6275.

380.   Zhao M, Crooks RM. *Chem.Mater* **1999**;*11*:3379-3385.

381.   Kang S, Cui Z, Xu Z, Mu J. *Colloids and Surfaces A: Physicochemical and Engineering Aspects* **2008**;*315*:44-46.

382.   Tseng C, Chang C, Sung Y, Ou J, Ger M. *Colloids and Surfaces A: Physicochemical and Engineering Aspects* **2009**;*333*:138-144.

383.   Razmi H, Habibi E. *Electrochimica Acta ;In Press, Corrected Proof*.

384. Zheng D, Hu C, Gan T, Dang X, Hu S. *Sensors and Actuators B: Chemical* **2010**;*148*:247-252.

385. Sparks CM, Fittschen UEA, Havrilla GJ. *Spectrochimica Acta Part B: Atomic Spectroscopy ;In Press, Corrected Proof*.

386. Leibfarth JH, Persellin RH. *Inflammation Research* **1981**;*11*:458-472.

387. Calle GR, Vargas IT, Alsina MA, Pasten PA, Pizarro GE. *Environ.Sci.Technol* **2007**;*41*:7430-7436.

388. Pradeep T. Nano the essentials. : Tata McGraw-Hill**, 2007**.

389. Sergeev GB. Nanochemistry. : Elsevier Science Ltd**, 2006**.

390. Sergeev GB. *Russian Chemical Reviews* **2001**;*70*:809-825.

391. M M. Photography: A cultural history. : Laurence King Publishing**, 2006**.

392. Więckowski A. Catalysis and electrocatalysis at nanoparticle surfaces. : Marcel Dekker**, 2003**.

393. Ogle K, Baeyens J, Swiatowska J, Volovitch P. *Electrochimica Acta* **2009**;*54*:5163-5170.

394. Ghosh SK. Functional coatings: By polymer microencapsulation. : Vch Verlagsgesellschaft Mbh**, 2006**.

395. Woods Hole Oceanographic Institution (WHOI). *COD* **1952**.

396. Callow ME, Fletcher RL. *International Biodeterioration & Biodegradation* **1994**;*34*:333-348.

397. Yebra DM, Kiil S, Dam-Johansen K. *Progress in Organic Coatings,* **2004**;*50*:75-104.

398. Kiil S, Weinell CE, Yebra DM, Dam-Johansen K. Chapter 7 marine biofouling protection: Design of controlled release antifouling paints. In: Ka M. Ng,Rafiqul Gani and Kim Dam-Johansen, editor. Computer Aided Chemical Engineering: Elsevier**, 2007**. p. 181-238.

399. Owen MJ. *Industrial and Engineering Chemistry Product Research and Development* **1980**;*19*:97-103.

400. Watermann BT, Daehne B, Sievers S, Dannenberg R, Overbeke JC, Klijnstra JW, Heemken O. *Chemosphere* **2005**;*60*:1530-1541.

401. Watermann B, Berger H-, Sönnichsen H, Willemsen P. *Biofouling* **1997**;*11*:101-118.

402. Bressy C, Margaillan A. *Progress in Organic Coatings* **2009**;*66*:400-405.

403. Corriu R, Anh NT. Molecular chemistry of sol-gel derived nanomaterials. : John Wiley & Sons Inc**, 2009**.

404. Asatekin A, Kang S, Elimelech M, Mayes AM. *Journal of Membrane Science* **2007**;*298*:136-146.

405. Nie M, Patel P, Sun K, Meng DD. *Proceedings of the Nano/Micro Engineered and Molecular Systems, January* **2009**:1017–1020.

406. Patel P, Choi CK, Meng DD. *Journal of the Association for Laboratory Automation* **2010**;*15*:114-119.

407. Tarimala S, Kothari N, Abidi N, Hequet E, Fralick J, Dai LL. *Journal of Applied Polymer Science* **2006**;*101*:2938-2943.

408. Liu X, Yang J, Wang L, Yang X, Lu L, Wang X. *Materials Science and Engineering A,* **2000**;*289*:241-245.

409. Kim SS, Choi SY, Park CG, Jin HW. *Thin Solid Films* **1999**;*347*:155-160.

410. Rittschof D, Forward R, Cannon G, Welch J, McClary M, Holm E, Clare A, Conova S, McKelvey L, Bryan P. *Biofouling* **1998**;*12*:31-44.

411. Callow ME, Jennings AR, Brennan A, Seegert C, Gibson A, Wilson L, Feinberg A, Baney R, Callow J. *Biofouling* **2002**;*18*:229-236.

412. Brinker CJ, Scherer GW. Sol-gel science: The physics and chemistry of sol-gel processing. : Academic Pr**, 1990**.

413. Stobie N, Duffy B, Hinder SJ, McHale P, McCormack DE. *Colloids and Surfaces B: Biointerfaces* **2009**;*72*:62-67.

414. Kobayashi Y, Katakami H, Mine E, Nagao D, Konno M, Liz-Marzán LM. *Journal of colloid and interface science* **2005**;*283*:392-396.

415. Tsuji H, Sakai N, Sugahara H, Gotoh Y, Ishikawa J. *Nuclear Instruments and Methods in Physics Research Section B: Beam Interactions with Materials and Atoms* **2005**;*237*:433-437.

416. Villegas MA, García MA, Paje SE, LLopis J. *Materials Research Bulletin* **2005**;*40*:1210-1222.

417. Yliniemi K, Ebbinghaus P, Keil P, Kontturi K, Grundmeier G. *Surface and Coatings Technology* **2007**;*201*:7865-7872.

418. Hwang B, Santhanam R, Liu D. *Journal of Power Sources* **2001**;*97*:443-446.

419. Sun T, Feng L, Gao X, Jiang L. *Accounts of Chemical Research* **2005**;*38*:644-652.

420. Kontos AI, Kontos AG, Tsoukleris DS, Vlachos GD, Falaras P. *Thin Solid Films* **2007**;*515*:7370-7375.

421. Sharma SD, Singh D, Saini K, Kant C, Sharma V, Jain S, Sharma C. *Applied Catalysis A, General* **2006**;*314*:40-46.

422. Alias SS, Ismail AB, Mohamad AA. *Journal of Alloys and Compounds* **2010**;*499*:231-237.

423. Jefferson B, Brookes A, Le Clech P, Judd S. *Scaling and Corrosion in Water and Wastewater Systems* **2004**;*49*:237-244.

424. Schooling, SR and Beveridge, TJ. *Journal of bacteriology* **2006**.

425. Costerton J, Stewart PS, Greenberg E. *Blood* **1998**;*91*:4020.

426. Costerton JW, Lewandowski Z, Caldwell DE, Korber DR, Lappin-Scott HM. *Annual Review of Microbiology* **1995**;*49*:711-745.

427. Wilcox MH. *Journal of Hospital Infection* **1998**;*40*:160-162.

428. Hoyle BD, Jass J, Costerton JW. *The Journal of antimicrobial chemotherapy* **1990**;*26*:1-5.

429. Roszak D, Colwell R. *Microbiology and Molecular Biology Reviews* **1987**;*51*:365.

430. Valappil SP, Ready D, Abou Neel EA, Pickup DM, O'Dell LA, Chrzanowski W, Pratten J, Newport RJ, Smith ME, Wilson M, Knowles JC. *Acta Biomaterialia* **2009**;*5*:1198-1210.

431. Amtul Z, Follmer C, Mahboob S, Atta-Ur-Rahman, Mazhar M, Khan KM, Siddiqui RA, Muhammad S, Kazmi SA, Choudhary MI. *Biochemical and biophysical research communications* **2007**;*356*:457-463.

432. Goodman S. *Medical hypotheses* **1988**;*26*:207-215.

433. Eby GA. *Medical hypotheses* **2008**;*71*:584-590.

434. Jain PK, Lee KS, El-Sayed IH, El-Sayed MA. *J.Phys.Chem.B* **2006**;*110*:7238-7248.

435. Liu X, Atwater M, Wang J, Huo Q. *Colloids and Surfaces B: Biointerfaces* **2007**;*58*:3-7.

436. Link S, El-Sayed MA. *J.Phys.Chem.B* **1999**;*103*:4212-4217.

437. Klar T, Perner M, Grosse S, Von Plessen G, Spirkl W, Feldmann J. *Physical Review Letters* **1998**;*80*:4249-4252.

438. Wang J, Pamidi PVA. *Anal.Chem* **1997**;*69*:4490-4494.

439. Iskandar F, Okuyama K, Shi F. *Journal of Applied Physics* **2001**;*89*:6431.

440. PASK JA, FULRATH RM. *Journal of the American Ceramic Society* **1962**;*45*:592-596.

441. Shibuta Y, Suzuki T. *Chemical Physics Letters* **2010**;*486*:137-143.

442. Schwegmann H, Feitz AJ, Frimmel FH. *Journal of colloid and interface science* **2010***;347*:43-48.

443. Gault N, Sandre C, Poncy J-, Moulin C, Lefaix J-, Bresson C. *Toxicology in Vitro* **2010***;24*:92-98.

444. Mergeay M, Nies D, Schlegel HG. *Journal of Bacteriology* **1985***;162*:328-334.

445. Mishra A, Kaushik NK, Verma AK, Gupta R. *European journal of medicinal chemistry* **2008***;43*:2189-2196.

446. Davies RL, Etris SF. *Catalysis Today* **1997***;36*:107-114.

447. Oka H, Tomioka T, Tomita K, Nishino A, Ueda S. *Metal-Based Drugs* **1994***;1*:511.

448. Hoffmann S. *Scandinavian Journal of Plastic and Reconstructive Surgery and Hand Surgery* **1984***;18*:119-126.

449. Fox Jr CL. *Archives of Surgery* **1968***;96*:184.

450. Chen X, Schluesener H. *Toxicology letters* **2008***;176*:1-12.

451. Shozo I. *Journal of the Physical Society of Japan* **1966***;21*.

452. Ino S, Ogawa S. *J.Phys.Soc.Japan* **1967***;22*:1365-1374.

453. Ajayan P, Marks L. *Physical Review Letters* **1988***;60*:585-587.

454. Vitos L, Ruban A, Skriver HL, Kollar J. *Surface Science* **1998***;411*:186-202.

455. Giorgio S, Urban J. *Applied Physics Letters* **1988***;52*:1467-1468.

456. Warrell Jr R, Bockman R, Coonley C, Isaacs M, Staszewski H. *Journal of Clinical Investigation* **1984***;73*:1487.

457. Bockman R, Boskey A, Blumenthal N, Alcock N, Warrell R. *Calcified tissue international* **1986***;39*:376-381.

458. Warrell R, Alcock NW, Bockman RS. *Journal of Clinical Oncology* **1987***;5*:292.

459. Warrell R, Lovett D, Dilmanian FA, Schneider R, Heelan RT. *Journal of clinical oncology* **1993***;11*:2443.

460. Whitacre C, Apseloff G, Cox K, Matkovic V, Jewell S, Gerber N. *Journal of neuroimmunology* **1992***;39*:175-181.

461. Adamson RH, Canellos GP, Sieber SM. *Cancer chemotherapy reports.Part 1* **1975***;59*:599-610.

462. Olakanmi O, Britigan BE, Schlesinger LS. *Infection and immunity* **2000***;68*:5619.

463.   Bernstein LR. *Pharmacological reviews* **1998**;*50*:665.

464.   Yan GH, Wang GJ, Li YC. *Zhongguo yao li xue bao = Acta pharmacologica Sinica* **1991**;*12*:530-533.

465.   Cho KH, Park JE, Osaka T, Park SG. *Electrochimica Acta* **2005**;*51*:956-960.

466.   Cazzola M, Bergamaschi G, Dezza L, Arosio P. *Blood* **1990**;*75*:1903.

467.   Schaible UE, Kaufmann SHE. *Nature Reviews Microbiology* **2004**;*2*:946-953.

468.   Chitambar CR, Wereley JP. *Journal of Biological Chemistry* **1997**;*272*:12151.

469.   Logan K, Ng P, Turner C, Schmidt R, Terner U, Scott J, Lentle B, Noujaim A. *International journal of nuclear medicine and biology* **1981**;*8*:271-276.

470.   Weiner R. *Nuclear medicine and biology* **1996**;*23*:745-751.

471.   Whelan A, Regan F. *Journal of environmental monitoring : JEM* **2006**;*8*:880-886.

472.   Hart JK, Martinez K. *Earth-Science Reviews* **2006**;*78*:177-191.

473.   Jannasch HW, Coletti LJ, Johnson KS, Fitzwater SE, Needoba JA, Plant JN. *Limnol.Oceanogr.Methods* **2008**;*6*:263-276.

474.   Akyildiz IF, Su W, Sankarasubramaniam Y, Cayirci E. *Computer networks* **2002**;*38*:393-422.

475.   Yang X, Ong KG, Dreschel WR, Zeng K, Mungle CS, Grimes CA. *Sensors* **2002**;*2*:455-472.

476.   Granhag L, Finlay J, Jonsson PR, Callow J, Callow M. *Biofouling* **2004**;*20*:117-122.

477.   Tachikawa M, Tezuka M, Morita M, Isogai K, Okada S. *Water research* **2005**;*39*:4126-4132.

478.   Jiang L, Wang R, Yang B, Li T, Tryk D, Fujishima A, Hashimoto K, Zhu D. *Pure and applied chemistry* **2000**;*72*:73-82.

479.   Öner D, McCarthy TJ. *Langmuir* **2000**;*16*:7777-7782.

480.   Lau KKS, Bico J, Teo KBK, Chhowalla M, Amaratunga GAJ, Milne WI, McKinley GH, Gleason KK. *Nano Letters* **2003**;*3*:1701-1705.

481.   Tadanaga K, Katata N, Minami T. *Journal of the American Ceramic Society* **1997**;*80*:3213-3216.

482.   Erbil HY, Demirel AL, Avcı Y, Mert O. *Science* **2003**;*299*:1377.

483.   Nakajima A, Fujishima A, Hashimoto K, Watanabe T. *Advanced Materials* **1999**;*11*:1365-1368.

484. Yu X, Wang Z, Jiang Y, Shi F, Zhang X. *Advanced Materials* **2005**;*17*:1289-1293.

485. F. Regan, A. Lawlor, B. O. Flynn, et al. *A demonstration of wireless sensing for long term monitoring of water quality* **2009** .

486. Manov DV, Chang GC, Dickey TD. **2010**.

487. Wagner RJ, Geological Survey (US). Guidelines and standard procedures for continuous water-quality monitors: Site selection, field operation, calibration, record computation, and reporting. : US Dept. of the Interior, US Geological Survey**, 2000**.

488. P. Arzberger, J. Bonner, D. Fries and A. Sanderson. *Sensors for environmental observatories* **2004** .

489. Bryers JD. *Biotechnology and bioengineering* **1984**;*26*:948-958.

490. Maruyama T, Matsushita H, Shimada Y, Kamata I, Hanaki M, Sonokawa S, Kamiya N, Goto M. *Environmental science & technology* **2007**;*41*:1359-1364.

491. Zhang G, Liu Z. *Journal of Membrane Science* **2003**;*211*:235-249.

492. Wang R, Hashimoto K, Fujishima A, Chikuni M, Kojima E, Kitamura A, Shimohigoshi M, Watanabe T. *Nature* **1997**;*388*:431-432.

493. Blossey R. *Nature materials* **2003**;*2*:301-306.

494. Gao X, Jiang L. *Nature* **2004**;*432*:36-36.

495. Lafuma A, Quéré D. *Nature materials* **2003**;*2*:457-460.

496. Barthlott W, Neinhuis C. *Planta* **1997**;*202*:1-8.

497. La D, Nguyen TA, Lee S, Kim JW, Kim YS. *Applied Surface Science* **2011**;*257*:5705-5710.

498. Zheng J, Song W, Huang H, Chen H. *Colloids and Surfaces B: Biointerfaces* **2010**;*77*:234-239.

499. Chen H, Song W, Zhou F, Wu Z, Huang H, Zhang J, Lin Q, Yang B. *Colloids and Surfaces B: Biointerfaces* **2009**;*71*:275-281.

500. Brenier R, Ramos SMM, Montchanin M. *Applied Surface Science* **2009**;*255*:7439-7445.

501. Song W, Zhang J, Xie Y, Cong Q, Zhao B. *Journal of colloid and interface science* **2009**;*329*:208-211.

502. Guo Z, Zhou F, Hao J, Liu W. *Journal of the American Chemical Society* **2005**;*127*:15670-15671.

503. Minarik L, Rapp J. *Eye & Contact Lens* **1989**;*15*:185.

504. Cowling MJ, Hodgkiess T, Parr ACS, Smith MJ, Marrs SJ. *The Science of The Total Environment* **2000**;*258*:129-137.

505. Wang C, Yang F, Meng F, Zhang H, Xue Y, Fu G. *Bioresource technology* **2010**;*101*:5469-5474.

506. Comte S, Guibaud G, Baudu M. *Process Biochemistry* **2006**;*41*:815-823.

507. Sellers H, Ulman A, Shnidman Y, Eilers JE. *Journal of the American Chemical Society* **1993**;*115*:9389-9401.

508. Sheardown H, Cornelius RM, Brash JL. *Colloids and Surfaces B: Biointerfaces* **1997**;*10*:29-33.

509. Min I, Choi L, Ahn K, Kim BK, Lee BY, Kim KS, Choi HN, Lee W. *Biosensors and Bioelectronics* **2010**;*26*:1326-1331.

510. Farkas J, Christian P, Urrea JAG, Roos N, Hassellöv M, Tollefsen KE, Thomas KV. *Aquatic Toxicology* **2010**;*96*:44-52.

511. Khlebtsov NG. *Journal of Quantitative Spectroscopy and Radiative Transfer* **2004**;*89*:143-153.

512. Ostuni E, Yan L, Whitesides GM. *Colloids and Surfaces B: Biointerfaces* **1999**;*15*:3-30.

513. Goodale CL, Aber JD, Ollinger SV. *Climate Research* **1998**;*10*:35-49.

514. Eaton AD, Franson MAH. Standard methods for the examination of water & wastewater. : Amer Public Health Assn**, 2005**.

515. Alexander Jr JE, Thorp JH, Fell RD. *Canadian Journal of Fisheries and Aquatic Sciences* **1994**;*51*:179-184.

516. Schoellhamer DH. *Marine Geology* **1993**;*110*:303-313.

517. Klahre J, Flemming H. *Water research* **2000**;*34*:3657-3665.

8.1 PUBLICATIONS

* Period four metal nanoparticles on the inhibition of biofouling.

Colloids Surf B Biointerfaces. 2010 Jul 1;78(2):208-16.

Chapman J, Weir E, Regan F.

* Phthalate doped PVC membranes for the inhibition of fouling in its initial stages.

Membrane Science, 2010 Sept 3; 365;1-2: 180-187

Chapman J, Lawlor A, Weir E, Quilty B, Regan F

* Sebaccic and succinic acid derived esters doped in PVC for the inhibition of biofouling

Applied Biomaterials and Biomechanics, *accepted*

Chapman J, Regan F

* Nanofunctionalised Superhydrophobic Antifouling Coatings for Environmental Sensor Applications – Advancing Deployment with Answers from Nature.

Advanced Biomaterials, 2011 October 1*; in press*

Chapman J, Regan F